UNIVERSITY OF SOUTHAMPTON

FACULTY OF ENGINEERING, SCIENCE & MATHEMATICS

OPTOELECTRONICS RESEARCH CENTRE

CLADDING-PUMPED RAMAN FIBRE LASER SOURCES

by

Junhua Ji

Thesis for the degree of Doctor of Philosophy

MARCH 2011

University of Southampton

ABSTRACT

FACULTY OF ENGINEERING AND APPLIED SCIENCE

OPTOELECTRONICS RESEARCH CENTRE

Doctor of Philosophy

CLADDING-PUMPED RAMAN FIBRE LASER SOURCES

by Junhua Ji

In this thesis, I investigate cladding-pumped Raman fibre lasers and amplifiers. Such devices, offering a novel way to generate Raman gain, combine the advantages of the hugely successful cladding-pumped rare-earth doped fibre lasers with those of stimulated Raman scattering. They not only inherit most advantages of conventional fibre devices, such as flexibility, high efficiency, compactness, and robustness, but also provide their own advantages and distinct properties relative to conventional fibre sources, i.e., wavelength flexibility and nearly instantaneous gain without energy storage.

Cladding-pumped Raman fibre laser sources utilise double-clad Raman fibres as the gain medium. These are similar to a rare-earth doped double-clad fibre except that there is no laser-ion doping of the core. With double-clad fibres, the high-power output from low-cost multimode pump sources can be converted into diffraction-limited signal beams, e.g., through stimulated Raman scattering. Thus, cladding-pumped Raman fibre laser sources are a kind of brightness enhancers. In the beginning of this thesis, I theoretically analyse various factors that limit the brightness enhancement of such devices. One of the limits is unwanted 2^{nd}-Stokes generation, which restricts the area ratio between the inner cladding and core. By designing a new DCRF with a W-type core, I successfully relax this restriction by nearly five times. Combined with other factors, i.e., core damage threshold, walk-off, numerical aperture, and background loss, a brightness enhancement of more than 3500 for the designed fibre could be achieved in such devices shown by a model with right pump sources and parameters.

Secondly, I focus on the conversion efficiency of such devices. A well-designed fibre with inner-cladding-to-core area ratio around six was used as a double-clad Raman fibre, pumped by a source with nearly rectangular pulse shapes. The nearly rectangular pulses were obtained from an erbium and ytterbium co-doped master optical power oscillator through pre-pulse shaping. A sufficiently short piece was chosen to reduce the background loss and walk-off. The highest peak power conversion into the 1^{st} Stokes was 75% and the energy conversion efficiency was over 60% in a pulsed cladding-pumped Raman fibre amplifier.

Thirdly, I study the power scalability. Theoretically, I analyse the achievable power of such devices. The core size turns out to be a critical factor in most cases. The ultimately output power is limited to around 24 kW by thermal lensing if the core is large enough and enough pump power available. Experimentally, in collaboration with co-workers, a 100 W cladding-pumped Raman fibre laser was demonstrated at 1116 nm. The output beam was nearly diffraction-limited. It shows the potential of power scalability of such devices and the ability of generating high power diffraction-limited sources at wavelengths outside the conventional range that rare-earth doped fibres offer.

Since a large core size is a critical factor for power scaling, new double-clad Raman fibres with large-mode areas were introduced. They were experimentally demonstrated to work as efficiently as the previous fibre. An Nd:YAG laser was used to pump one of these fibres, and a 1 mJ Raman fibre source with good beam quality was thus demonstrated. This shows that double-clad Raman fibres offer another approach to obtaining high-brightness high-energy sources. In addition, based on a cladding-pumped Raman fibre converter, a simple and efficient method was proposed to generate supercontinuum sources.

List of Contents

List of Figures

List of Tables

List of Abbreviation

AOM	Acousto-Optic Modulator
AWG	Arbitrary Waveform Generator
BPP	Beam Parameter Product
CP	Cladding Pumped
CW or cw	Continuous Wave
DCF	Double Clad Fibre
DCRF	Double Clad Raman Fibre
DM	Dichroic Mirror
EDFA	Erbium-Doped Fibre Amplifier
EYDFA	Erbium:Ytterbium co-Doped Fibre Amplifier
FBG	Fibre Bragg Grating
FWHM	Full Width at Half Maximum
FWM	Four-Wave Mixing
HNLF	Highly Non-Linear Fibre
HPFL	High Power Fibre Laser
HR	High Reflection
HT	High Transmission
LD	Laser Diode
LP	Linearly Polarised
LIDAR	LIght Detection And Ranging
MCVD	Modified Chemical Vapour Deposition
MM	Multi-Mode
MMF	Multi-Mode Fibre
MOPA	Master Oscillator – Power Amplifier
NA	Numerical Aperture
OPD	Optical Path Difference
ORC	Optoelectronics Research Centre
OSA	Optical Spectrum Analyser
PBGF	Photonic BandGap Fibre
PRF	Pulse Repetition Frequency
RE	Rare-Earth
RFA	Raman Fibre Amplifier
RFL	Raman Fibre Laser
RIP	Refractive Index Profile
SBS	Stimulated Brillouin Scattering
SFM	Self Phase Modulation
SMF	Single Mode Fibre
SRS	Stimulated Raman Scattering
SC	Supercontinuum
TDF	Thulium-Doped Fibre
TFB	Tapered Fibre Bundle
TLS	Tuneable Laser Source
WDM	Wavelength Division Multiplexing
WLS	White-Light Source
YDF	Ytterbium-Doped Fibre
YDFA	Ytterbium-Doped Fibre Amplifier
YDFL	Ytterbium-Doped Fibre Laser
ZDW	Zero Dispersion Wavelength

DECLARATION OF AUTHORSHIP

I, …….Junhua JI……

declare that the thesis entitled

….CLADDING-PUMPED RAMAN FIBRE LASER SOURCES……

and the work presented in the thesis are both my own, and have been generated by me as the result of my own original research. I confirm that:

- this work was done wholly or mainly while in candidature for a research degree at this University;
- where any part of this thesis has previously been submitted for a degree or any other qualification at this University or any other institution, this has been clearly stated;
- where I have consulted the published work of others, this is always clearly attributed;
- where I have quoted from the work of others, the source is always given. With the exception of such quotations, this thesis is entirely my own work;
- I have acknowledged all main sources of help;
- where the thesis is based on work done by myself jointly with others, I have made clear exactly what was done by others and what I have contributed myself;
- none of this work has been published before submission, **or** [delete as appropriate] parts of this work have been published as: [please list references]

Signed: ……Junhua JI……..

Date:……2011-03-20…….

Acknowledgements

First of all, I would like to take this opportunity to thank my supervisor Prof. Johan Nilsson for giving me the chance to study at ORC, and being patient through my whole study. He continues to direct me in the right way when I have troubles in my study and to encourage me all the time. I am also grateful to my co-supervisor Dr. Christophe A. Codemard. He sets a good example for me to show how a good scientist should be.

I am also grateful to Dr. J. K. Sahu and other members at Silica Fibre Fabrication group for drawing excellent fibres used in this thesis. I would like to thank Dr. Seongwoo Yoo for helping me characterise various fibres, such as, measure background loss with an OTDR, take facet images from time to time, Mr. Robert Standish for helping measure refractive index profiles of different fibres, and Mr. Andrew Webb to help me rewind a very long fibre. Thank Dr. Seongwoo Yoo for other helps during my study. I also would like to thank Dr. Morten Ibsen for his FBG used in this thesis. My thanks also go to current and previous members of High Power Fibre Laser group: Dr. Yoonchen Jeong, Dr. Daniel B. S. Soh, Dr. Jean-Noel Maran, Dr. Carl Farrell, Mr. Luis Vazquez-Zuniga, and Mr. Gysbert van der Westhuizen for, discussion, sharing labs and equipments.

I would like to thank Simon Butler and Fadzilah Lotffe for practical help in the lab, and Eve Smith for her help during my study. I would like to extend my gratitude to all the staff and students of the ORC for their advices, supports, and help from time to time.

I would like to acknowledge ORC for providing me the scholarship. Also, I would like to thank my supervisor Prof. Johan Nilsson to sponsor me in the last three months of my study.

Last but not the least I am indebted to my wife's and my own parents for their endless love and constant support. Special thanks go to my wife, Weili XU, for her love and support from the beginning to the end during my PhD. Without her, I cannot make it.

Chapter 1 Introduction

This chapter will provide an introduction into the area of research undertaken throughout my PhD studies. The history of fibre lasers is briefly reviewed in the first section. This is followed by an overview of the development of cladding-pumped Raman fibre sources in section 1.2. After that, motivations for studying cladding-pumped Raman fibre devices are given. Finally, in section 1.4, the layout of this thesis is presented.

1.1 Overview of fibre lasers

In 1964, Snitzer and Koester reported the first rare-earth (RE) doped fibre laser. It consisted of a coiled neodymium (Nd)-doped glass fibre transversally side-pumped by a flash-lamp [1]. It was just four years after T. Maiman demonstrated the first laser, a ruby rod emitting at a wavelength of 694 nm [2]. In 1973, Stone and Burrus longitudinally pumped an Nd-doped fibre [3]. Compared to transverse pumping, longitudinal pumping improved the pumping efficiency. In the following year, they demonstrated the first fibre laser pumped by a laser diode (LD) [4]. Diode-pumping allows for much better performance than lamp-pumping does, but the lack of reliable LDs still prevented fibre lasers from being an attractive proposition at the time. The advent of the low-loss single-mode RE-doped silica fibre in 1985 re-ignited the developments in this field [5]. Poole and co-workers from the University of Southampton incorporated RE ions into preforms by solution doping during modified chemical vapour deposition (MCVD). In the next year, Mears, Reekie, Jauncey, and Payne experimentally reported the first low-loss, high gain erbium-doped fibre amplifier (EDFA) in the world [6]. In contrast to alternative configurations, the fibre provided the confinement and low loss necessary for efficient operation at levels of pump powers realistic for diode-pumping. The EDFA is a milestone in the field of telecommunication. However, it not only brought a revolution in optical communication,

but also promoted the development of laser diodes and other optical components. In the early 1990's, commercial EDFAs started to appear on the market.

In recent years, high power fibre amplifiers and lasers have been extensively studied and rapidly developed. At first, this owes to the steady progress of laser diodes which can offer sufficient pump power. Besides, a special fibre design, the double-clad fibre (DCF), cleverly solves the problem that the available pump power is limited to the relatively small amount of pump power that can be launched into the small fibre core. The double-clad fibre was first proposed by Maurer [7] and demonstrated by Snitzer and co-workers in 1988 [8]. They used laser diodes for pumping, as proposed by Kafka in the late 1980s [9]. Since then, the output power of fibre lasers has increased very rapidly, reaching 1 kW with good beam quality [10]-[13] in 2004. This can be compared to the watt-level of power possible with fibres diode-pumped in the core. The highest reported diffraction-limited output power from fibre lasers is now 10 kW [14] while kW-level ytterbium-doped fibre lasers (YDFLs) are available commercially, together with many other types of high-power fibre sources [15]. The power scaling of fibre lasers has been demonstrated by several research groups around the world, such as High Power Fibre Laser (HPFL) group and others at Optoelectronics Research Centre (ORC), University of Southampton, and other groups at the Friedrich Schiller University of Jena, University of the Michigan, SPI Lasers, and IPG Photonics. In Figure 1.1, the power evolution of continuous wave (CW) fibre lasers with good beam quality is given in the last 14 years based on the achievements mostly from the groups mentioned above. The power of fibre lasers has seen an enormous and exponential increase since 2003. It is possible to further increase the output power of fibre lasers with diffraction-limited beam, however, the potential scalability will be challenging and ultimately limited by several factors, i.e., thermal effects, nonlinear effects, and material damage [16]. Thermal effects, e.g., thermal fracture, thermal melting and thermal lensing, limit the maximum heat power that can be deposited in an optical fibre core for a given length. The maximum extractable power is then proportional to the maximum deposited heat. In addition, for optical signals with narrow bandwidth, the output power will be limited by a nonlinear effect, i.e., stimulated Brillouin scattering (SBS). The output power will be limited by nonlinearities also when the signal bandwidth is broad compared to the Brillouin linewidth, typically by stimulated Raman scattering (SRS), which can convert a significant fraction of the signal power to longer wavelengths. For a detailed analysis,

please see reference [16]. However, as far as I am aware, the principal limiting factor in Figure 1.1 has been the available pump power.

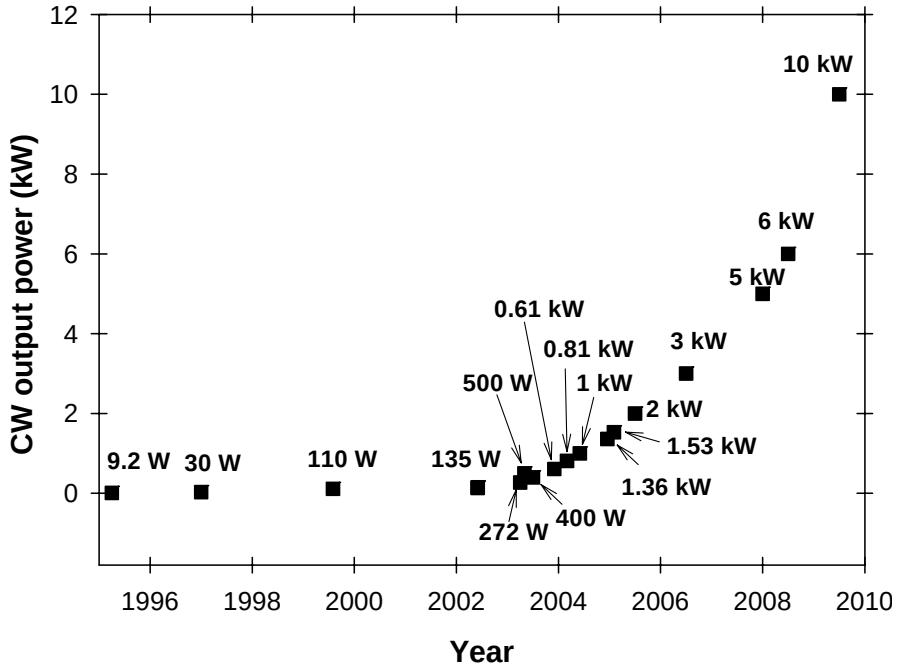

Figure 1.1: Power evolution of CW double-clad fibre lasers with diffraction-limited beam quality over the last 14 years.

1.2 Development of cladding-pumped Raman fibre sources

Besides RE-doped fibre devices, Raman fibre devices were another type of active fibre devices attracting the attention of researchers due to the potential benefits of the wide Raman gain bandwidth in telecommunications first pointed out by Ippen, Patel, and Stolen [17]. Later on, most Raman work was carried out with single-mode fibres (SMFs) because their relatively small cores benefited stimulated Raman scattering and also because of the requirements of optical fibre communications (see [18] and references therein). As it comes to the output power, the current record power of Raman fibre sources is 150 W, set in 2009 with a SMF-based laser [19]. On the other hand, SMFs require pump sources with good beam quality. In terms of enhancement of the (spatial) brightness, Raman fibre devices based on SMFs are severely limited and can at most approach a doubling of the brightness of the pump, through double-ended pumping. Brightness is an important term in the field of lasers. It determines the power density achievable in a beam focused on a target. Brightness itself is determined by the optical power and the beam quality factor. Whereas SMF-based Raman devices do produce diffraction-limited output beams, they still look limited in brightness compared to

cladding-pumed devices, since the more challenging pumping makes power-scaling more challenging. I will further discuss brightness and beam quality in section 2.3.

Cladding-pumped (CP) Raman fibre lasers (RFLs) and amplifiers (RFAs) follow the approach of CP RE-doped fibre sources. They combine the cladding-pumping technology and advantages of SRS [20]-[21] and were first demonstrated in 2002 [21] by Nilsson and co-workers in the HPFL group at ORC, University of Southampton. Cladding-pumped Raman fibre devices utilise so-called double clad Raman fibres (DCRFs), which are similar to conventional RE-doped double clad fibres except that the cores are not doped with RE ions. Inside such fibres, multimode (MM) pump sources, launched into the inner cladding can be converted through SRS into a nearly diffraction-limited output beam that propagates in the core at the Stokes wavelength. Therefore, DCRFs act as brightness enhancers. This effect is also known as "beam clean-up" [22]-[23]. By contrast to other work [24]-[25] where a graded-index fibre is used, the waveguide structure of DCRFs allows for robust single-mode propagation and ready selection of the fundamental mode, for example, by using a piece of SMF [26] or a fibre Bragg grating (FBG) written specifically for the fundamental mode [27].

In the following several years, experiments on CP Raman fibre devices have been carried out in both CW [26]-[27]and pulsed [28]-[29] regimes. Although CP Raman fibre devices have been studied for some years, there are still several aspects that either remained unexplored or needed to be improved. Especially the output average power and energy of such devices have been limited to levels that would often be inadequate. In the CW regime, the highest average power reported was up to 10 W [26]. In the pulsed regime, the highest energy reported was ~ 10 μJ [29]. My colleagues and I increased the output power of the CW RFLs to 100 W [30] with good beam quality. We also demonstrated a high brightness pulsed CP Raman fibre source with 210 μJ output energy [31]. Later, I also used an Nd:YAG laser to pump a DCRF, generating over 1 mJ of pulse energy distributed over several Stokes orders with good beam quality.

The conversion efficiency is invariably a concern. Together with colleagues, I theoretically and experimentally analysed the limitations set on the conversion efficiency into the 1st Stokes in CP Raman fibre devices [32]. Before the work presented in this thesis, the brightness enhancement was limited to ~ 10. We theoretically investigated the achievable brightness enhancement with pulsed CP RFAs based on a designed fibre [33] and showed that much higher brightness enhancement is possible

with CP Raman fibre devices. Recently, new DCRFs with large-mode areas have been fabricated by the Silica Fibre Fabrication group at ORC. We have experimentally demonstrated that the new fibres with large-mode areas can work as efficiently as the previous, much smaller, DCRFs [34]. Moreover, the DCRFs with large-mode area increase the core damage threshold, and are more promising for the generation of higher power and energy in diffraction limited output beams. With such fibres, we also demonstrated a nearly diffraction-limited supercontinuum (SC) source [35].

1.3 Motivations

So why are we working on CP Raman fibre devices? For one thing, they inherit most advantages of the hugely successful cladding-pumped RE-doped fibre sources. At the same time, they bring their own features, which may be advantageous in certain situations.

RE-doped fibre devices have been applied in many areas already. For example, fibre amplifiers have been widely used in communications [36], particularly extensively in telecommunications. With the increase of output power and energy, fibre laser sources are utilised in a variety of industries for tasks such as laser cutting, laser welding, laser marking, and laser drilling. Also, fibre lasers are used or considered for defence and aerospace applications such as remote missile defence, remote sensing, and range-finding, including light detection and ranging (LIDAR). Fibre lasers play an important role in the scientific research as well, including sensing, atom cooling, spectroscopy, and nonlinear optical conversion. The development of the CP Raman fibre sources makes them a potential replacement of RE-doped fibre devices in many applications.

1.3.1 Properties and advantages of fibre sources

CP Raman fibre devices retain many advantages of RE-doped fibre devices such as high average power, high efficiency, large gain bandwidth, versatility, robustness, reliability, and simplicity. In this section, I will address some properties and advantages of fibre sources.

First of all, in contrast to bulk-optic lasers, fibre lasers can tightly confine the beam, offering a long intense interaction between pump and signal. This leads to a

lower threshold and higher gain efficiency. For example, Ref. [37] compares the Raman gain efficiencies between bulk and fibre Raman amplifiers. For a bulk Raman amplifier,

$$\begin{aligned} G_{Np}/P_p &= g_R \int A_{eff}^{-1}(z)dz = g_R \int \{\pi\omega_0^2[1+(\lambda z)^2/(\pi\omega_0^2 n)^2]\}^{-1} dz \\ &= g_R \pi n/\lambda = 0.43\times10^{-6}\, W^{-1} = 1.9\, dB/MW \end{aligned} \tag{1.1}$$

where G_{Np} is the gain in nepers, P_p is the pump power, the Raman gain coefficient g_R is 10^{-13} m/W, A_{eff} is the effective area, the refractive index n is 1.45, and the wavelength λ is 1060 nm. Strictly, this assumes that the bulk length infinite, but most of the gain occurs within the Rayleigh length of the focus. For a Raman fibre amplifier, with some typical parameter values, the gain efficiency becomes,

$$G_{Np}/P_p = g_R L_{eff}/A_{eff} = 14\, W^{-1} = 60.8\ dB/W \tag{1.2}$$

with the same g_R as in the bulk laser and effective area 30 μm^2. The effective length L_{eff} equals to (1-exp(-αL))/α, which is close to α^{-1} if the fibre length L is 10 km or longer while the background loss α is set to 1 dB/km. The gain efficiency is improved by 7.5 orders of magnitude! Therefore, it is much easier to amplify light through SRS in a fibre than in a bulk. Although the Raman gain coefficient is significantly larger in materials used for bulk Raman amplifiers and lasers, this example still clearly illustrates the attractions of fibre for Raman amplifiers and lasers.

Normally, only SMFs have a core size as small as 30 μm^2, which more or less rules out brightness improvement. However, thanks to the long interaction length and the resulting high gain efficiency, it is reasonable to scale up the area significantly and an increase by three orders of magnitude still leads to gain efficiencies that are realistic with pulsed and even cw pumping. This opens up the possibility of cladding-pumping, in which an inner cladding guides the pump light. Inside the inner cladding, a core structure can be defined, in which the signal can propagate. Fibres with such a structure are referred to as DCFs. Figure 1.2 illustrates a transverse cross section and refractive index profile (RIP) of a conventional DCF. Based on DCFs, pump sources with poor beam quality can be converted into the signal with good beam quality. Our DCRFs are one kind of DCFs and can as such enhance the brightness.

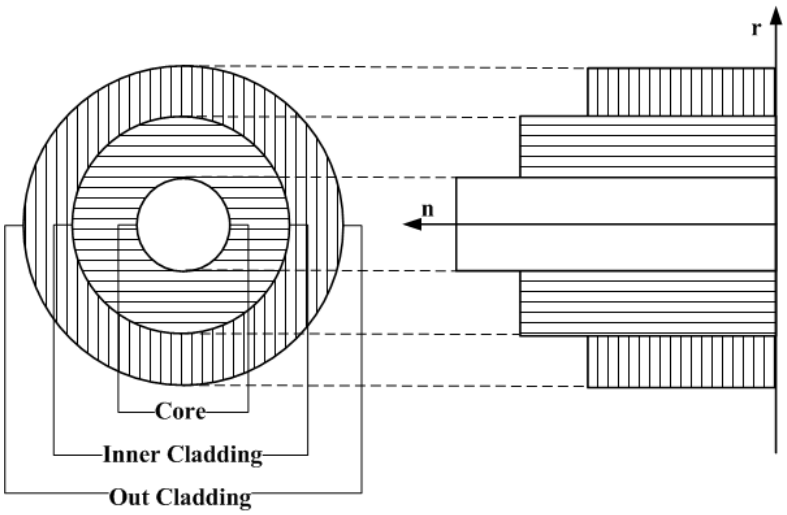

Figure 1.2: Cross section and refractive index distribution of a DCF.

Moreover, through designing the RIP, desired fibre characteristics can be obtained, such as large-mode area fibre for power scaling, a specific cut-off wavelength, etc. For example, a W-type fibre can control the transmission spectrum [38]. This will be particularly useful in a RFL or RFA if high conversion efficiency is required into the 1st Stokes by suppressing the 2nd-Stokes generation.

Furthermore, thanks to the thin active medium and long interaction length, fibres have good thermal properties. The high damage temperature of silica, together with a number of other favourable properties, makes silica-based fibre particularly suitable for high-power fibre lasers (including amplifiers). Active thermal management like air cooling and water cooling can also be applied, e.g., to make lasers or other fibre-based devices stable over long periods. Besides, fibre is easy to handle and install, e.g., in a compactly coiled spool, thanks to its flexibility.

Fibres can also be spliced together into “all-fibre” systems (e.g., lasers) comprising several components. This makes them easy to integrate with other fibre devices and systems. It also eliminates alignment problems and improves the robustness, which is very attractive and several all-fibre devices are available on the market. For example, with a FBG or through the fibre design, wavelength filters or reflectors can be made. There are also many other fiberised components like modulators, isolators, and couplers, which allow for compact all-fibre laser systems with high functionality. In an experiment on a CP RFA described in Chapter 4, I used an FBG to choose the core modes of the signal instead. In addition, using an all-fibre configuration, a compact CP Raman fibre source has been reported by others [39].

1.3.2 Comparison of CP Raman fibre devices and RE-doped fibre devices

Besides keeping most advantages of RE-doped fibre devices, CP Raman fibre devices provide some exciting advantages and differences compared to CP RE-doped fibre devices.

Firstly, SRS is ubiquitous and wavelength-agile. It will occur in any optical fibre at any wavelength (provided the loss is sufficiently low), determined only by the pump wavelength and fibre material [17]. This is a key advantage over RE-doped fibre devices, which despite a number of transitions in different host materials still exhibit large spectral gaps [40], in particular at high powers in silica hosts [41]. Figure 1.3, shows emission bands for some RE ions in silica glass, i.e., Nd, ytterbium (Yb), erbium (Er), thulium (Tm), and holmium (Ho). The emission bands of RE ions are finite and for high-power operation, even more restricted than Figure 1.3 suggests. By contrast, through SRS process, amplification is possible over the whole fibre transmission band.

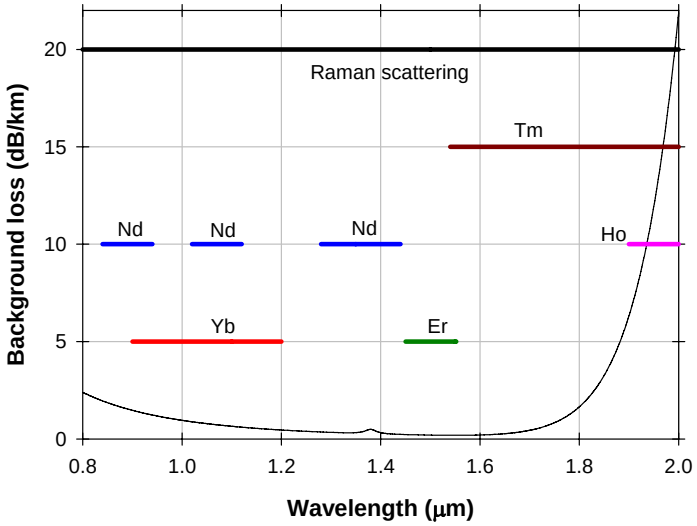

Figure 1.3: Silica background loss and emission bands of some RE ions in silica fibre up to 2 μm.

The nearly instantaneous nature of SRS is another difference. It allows us to directly transfer energy from a pump pulse to a signal pulse, without the intermediate energy storage that occurs in RE-doped gain media, and without the need to store energy to create gain. This instantaneity is useful for brightness-enhancement of pulses as well as for high quasi-unidirectional gain. Temporally, the gain follows the profile of a pump pulse, in a "gain wave" that travels with the pump pulse. For pulse lengths shorter than the fibre, the gain in the counter-propagation direction is much reduced,

despite the intrinsically bi-directional nature of the Raman gain. This can eliminate the need for an optical isolator. By contrast, most RE-doped fibre lasers and amplifiers operate at a high gain that is "always on" and with a significant stored energy. This makes them sensitive to feedback and necessitates the use of isolators to prevent catastrophic events such as self-Q-switching. In the high-power regime, isolators are expensive, bulky, components that often degrade the brightness of the beam and limit the output power. A short-lived, instantaneous, travelling gain also makes it easier to reach a high gain, which is useful for many applications.

In addition, pulses are in some respects a weak point of RE-doped fibre lasers, because of limits in energy storage and damage threshold. For example, in a pulsed fibre laser, higher peak power and output energy are obtained with large-core fibres because of the higher energy storage and higher damage threshold those fibres offer. As there are some practical limits on the numerical aperture (NA) and core size of single mode fibre, multimode cores, e.g. [42], are also used. CP Raman fibre lasers offer a radically different approach to high-energy pulses. They would not store the energy, but instead improve the brightness of high-energy multimode pulses, which are much easier to produce.

Furthermore, in the ultra-high power regime, another essential advantage is the lower background loss. It may allow the heat to be distributed over a longer interaction length, which reduces the impact of the heating on the waveguide. A further attraction over RE-doped fibres, is a relative freedom from photo-darkening (especially important at short wavelengths) and a greater freedom in choice of materials. These fibres are not known to photo-darkening in the infrared region.

Finally, a very large range of materials can be used with Raman fibre devices, including pure silica. There may be some materials that have higher damage thresholds than conventional RE-doped silica [43]. Furthermore, the freedom in materials allows for improved control of the refractive index profile, which is also very important in the high power and pulsed regimes, with the large cores they necessitate. While many of these advantages hold for core-pumped RFLs, too, cladding-pumping facilitates scaling to high average powers. Thus, the output beam quality of any multimode laser source can be improved through SRS in a simple add-on consisting of a section of "passive" multimode fibre. In addition, this cheap and simple solution allows spectral, spatial and polarization combination of several pump sources into a single RFL [25], [44], for

further power scaling. Again, thanks to the wavelength flexibility, the CP Raman fibre devices can use multimode RE-doped fibre devices as their pump. It is generally easier to build a MM source rather than a diffraction limited source with the same output power. There are also other options for pump sources, such as solid state lasers, which offer high energy. This makes such pump sources attractive for the generation of high-energy diffraction-limited pulses in DCRFs.

1.3.3 Comparison of Core-pumped and CP Raman fibre devices

As mentioned in section 1.2, most Raman work has been carried out with SMFs due to the relatively low threshold. Another benefit of such devices is their compatible with highly developed fibre components such as WDMs and isolators. Furhtermore, the output beam is usually diffraction-limited. Also, in theory, core-pumped Raman fibre devices can achieve slightly higher conversion efficiency of the pump into the 1st Stokes. I will discuss this in section 4.3.4. On the other hand, the small core of a SMF requires pump sources with good beam quality. Compared to multimode pump sources, single-mode pump sources are more difficult to power-scale. Cladding-pumped Raman fibre devices are therefore more promising for the generation of high power and high energy. Furthermore, a CP Raman fibre device can provide a brightness which exceeds that of the pump source. With a well-designed core structures, the output beam can be diffraction limited or nearly diffraction limited.

1.4 Outline

The structure of this thesis is organised as follows.

1) In Chapter 2, background material relevant for this thesis is introduced, such as mode selection, walk-off, beam quality, and Raman scattering.

2) In Chapter 3, I theoretically analyse the achievable brightness enhancement from CP Raman fibre devices by considering different factors, i.e., 2nd-Stokes generation, background loss, walk-off and material damage. To prevent the 2nd Stokes from building up, a novel DCRF with a W-type core is designed. The achievable brightness enhancement is calculated for pulse-pumped CP RFAs based on the designed fibre. The calculated results show that a brightness enhancement of up to 3500 can be possible although it depends on the pump pulse duration and pump intensity.

3) Work described in both Chapter 4 and Chapter 5 is based on a DCRF with fibre number F71-LF11 made in house. In Chapter 4, the DCRF F71-LF11 is investigated in terms of achievable conversion efficiency into the 1st Stokes with a pulsed fibre laser pump source. Special attention is paid to different factors limiting the conversion efficiency, i.e., inner-cladding-to-core area ratio, background loss, pump pulse shapes, and inner-cladding shapes. A peak power conversion over 70% was experimentally obtained while the energy conversion efficiency into the 1st Stokes exceeded 60%.

4) In Chapter 5, I focus on the power scalability of CP Raman fibre devices. A 100 W CW CP RFL with nearly diffraction-limited output was experimentally demonstrated with the DCRF F71-LF11. In addition, I also theoretically analyse factors limiting the ultimate output power and find that the core size is the key for the power scaling most of the time.

5) For the power scaling, three DCRFs with large-mode areas are introduced in Chapter 6. The new fibres were also fabricated at ORC. At the beginning, the new fibres were investigated with a pulsed fibre source, and the experimental results proved that these new fibres can also work efficiently. In order to generate high energy sources, a Q-switched multimode Nd:YAG laser was utilised for pumping. High-brightness pulses with 1 mJ of energy were obtained from one of the new fibres. Besides, in a novel approach, SC is generated in a CP Raman fibre converter. Experimentally, a SC source was demonstrated covering wavelengths from 1 μm to beyond 1.75 μm .

6) Finally, Chapter 7 summarises the works described in the thesis and outlines possible future work related to CP Raman fibre devices.

1.5 Reference

[1] C. J. Koester, and E. Snitzer, "Amplification in a fiber laser", Appl. Optics, **3**(10), 1182 (1964).

[2] T. H. Maiman, "Stimulated optical radiation in ruby masters", Nature, **187**(4736), 493 (1960).

[3] J. Stone, and C. A. Rurrus, "Neodymium-doped silica lasers in end-pumped fiber geometry", Appl. Phys. Lett., **23**(7), 388 (1973).

[4] J. Stone and C. A. Burrus, "Neodymium-doped fiber lasers: room temperature CW operation with an injection laser pump", Appl. Optics, **13**(6), 1256 (1974).

[5] S. B. Poole, D. N. Payne, and M. E. Fermann, "Fabrication of low loss optical fibres containing rare-earth ions", Electron. Lett., **21**(17), 737 (1985).

[6] R. J. Mears, L. Reekie, I. M. Jauncey and D. N. Payne, "Low-noise erbium-doped fibre amplifier operating at 1.54 μm", Electron. Lett., **23**(19), 1026 (1987).

[7] R. D. Maurer, "Optical waveguide light source", US patent no. 3,808,549 (1974).
[8] E. Snitzer, H. Po, F. Hakimi, R. Tumminelli, and B. C. McCollum, "Double-clad, offset core Nd fiber laser", in Proc. of Opt. Fiber Sensors, New Orleans 1988, paper PD5 (Postdeadline).
[9] J. Kafka, "Laser diode pumped fiber laser with pump cavity", US patent no. 4,829,529 (1989).
[10] Y. Jeong, J. K. Sahu, D. N. Payne, and J. Nilsson, "Ytterbium-doped large-core fiber laser with 1 kW continuous-wave output power", in Proc. of Advanced Solid-State Photonics (ASSP), New Mexico 1-4 Feb. 2004, paper PD1 (Postdeadline).
[11] A. Liem, J. Limpert, H. Zellmer, A. Tünnermann, V. Reichel, K. Mörl, S. Jetschke, S. Unger, H. R. Müller, J. Kirchhof, T. Sandrock, and A. Harschak, "1.3 kW Yb-doped fiber laser with excellent beam quality", in Proc. of Conference on Lasers and Electro-Optics/IQEC, San Francisco 16-21 May 2004, paper CPDD2 (Postdeadline).
[12] Y. Jeong, J. K. Sahu, D. N. Payne, and J. Nilsson, "Ytterbium-doped large-core fiber laser with 1.36 kW continuous-wave output power", Opt. Express, **12**(25), 6088 (2004).
[13] V. P. Gapontsev, D. V. Gapontsev, N. S. Platonov, O. Shkurihin, V. Fomin, A. Mashkin, M. Abramov and S. Ferin, "2 kW CW ytterbium fiber laser with record diffraction-limited brightness", in Proc. of Conf. Lasers and Electro-Optics/Europe, Munich 12-17 Jun. 2005, paper CJ1-1-THU.
[14] E. Stiles, "New developments in IPG fiber laser technology", in Proc. of 5th Int. Workshop Fiber Lasers, Dresden Germany October 2009.
[15] Information available from IPG Photonics: www.ipgphotonics.com and SPI Lasers: www.spilasers.com.
[16] J. W. Dawson, M. J. Messerly, R. J. Beach, M. Y. Shverdin, E. A. Stappaerts, A. K. Sridharan, P. H. Pax, J. E. Heebner, C. W. Siders, and C. P. J. Barty, "Analysis of the scalability of diffraction-limited fiber lasers and amplifiers to high average power", Opt. Express, **16**(17), 13240 (2008).
[17] E. P. Ippen, C. K. N. Patel, and R. H. Stolen, "Broadband tunable Raman-effect devices in optical fibers", US patent no. 3,705,992 (1972).
[18] J. Bromage, "Raman amplification for fiber communications systems", J. Lightwave Technol., **22**(1), 79 (2004).
[19] Y. Feng, L. R. Taylor, and D. B. Calia, "150 W highly-efficient Raman fiber laser", Opt. Express, **17**(26), 23678 (2009).
[20] R. Rice, "Multimode Raman fiber amplifier and method", US patent no. 6,353,087 (2002).
[21] J. Nilsson, J. K. Sahu, J. N. Jang, R. Selvas, D. C. Hanna, and A. B. Grudinin, "Cladding-pumped Raman fiber amplifier", in Proc. of Optical Amplifiers and Their Applications (OAA 2002), Vancouver Canada 14-17 Jul. 2002, paper PD2-1/2/3 (Postdeadline).
[22] R. S. F. Chang, R. H. Lehmberg, M. T. Duiganan, and N. Djeu, "Raman beam cleanup of a severely aberrated pump laser", IEEE J. Quantum Electron., **21**(5), 477 (1985).
[23] J. T. Murray, W. L Austin, and R. C. Powell, "Intracavity Raman conversion and Raman beam clean up", Opt. Mater., **11**(4), 353 (1999).
[24] S. H. Baek, and W. B. Roh, "Single-mode Raman fiber laser based on a multimode fiber", Opt. Lett., **29**(2), 153 (2004).

[25] N. B. Terry, K. T. Engel, T. G. Alley, and T. H. Russell, "Use of a continuous wave Raman fiber laser in graded-index multimode fiber for SRS beam combination", Opt. Express, **15**(2), 602 (2007).
[26] C. A. Codemard, P. Dupriez, Y. Jeong, J. K. Sahu, M. Ibsen, and J. Nilsson, "High-power continuous-wave cladding-pumped Raman fiber laser", Opt. Lett., **31**(15), 2290 (2006).
[27] J. Jang, Y. Jeong, J. K. Sahu, M. Ibsen, C. A. Codemard, R. Selvas, D. C. Hanna, and J. Nilsson, "Cladding-pumped continuous-wave Raman fiber laser", in Proc. of Conf. Lasers and Electro-Optics/QELS, Baltimore 3-5 Jun 2003, paper CWL1.
[28] C. A. Codemard, J. K. Sahu, and J. Nilsson, "Cladding-pumped Raman fiber amplifier for high-gain high-energy single-stage amplification", in Proc. of OFC, Anaheim USA 6-11 March 2005, paper OutF5.
[29] C. A. Codemard, J. K. Sahu, and J. Nilsson, "High-brightness pulsed cladding-pumped Raman fiber source at 1660 nm", in Proc. of Conf. Lasers and Electro-Optics /QELS, Baltimore 6-11 May 2007, paper CTuN3.
[30] C. A. Codemard, J. Ji, J. K. Sahu, and J. Nilsson, "100 W CW cladding-pumped Raman fiber laser at 1120 nm", in Proc. of Photonics West, San Francisco Jan. 2010, paper 7580-58.
[31] A. Shirakawa, C. A. Codemard, J. Ji, K. K. Chen, A. Malinowski, D. J. Richardson, J. K. Sahu, and J. Nilsson, "High-brightness 210 μJ pulsed Raman fiber source", in Proc. of Conf. Lasers and Electro-Optics /QELS, San Jose 4-9 May 2008, paper CTuL1.
[32] J. Ji, C. A. Codemard, M. Ibsen, J. K. Sahu, and J. Nilsson, "Analysis of the conversion to the first stokes in cladding-pumped fiber Raman amplifiers", IEEE J. Sel. Top. Quantum Electron., **15**(1), 129 (2009).
[33] J. Ji, C. A. Codemard, and J. Nilsson, "Brightness enhancement limits in pulsed cladding pumped fibre Raman amplifiers", in Proc. of Photonics West, San Francisco Jan. 2010, paper 7580-56.
[34] J. Ji, C. A. Codemard, J. K. Sahu, and J. Nilsson, "Pulsed cladding-pumped large mode area fiber Raman amplifier", in Proc. of Photonics West, San Francisco Jan. 2010, paper 7580-47.
[35] J. Ji, C. A. Codemard, A. S. Webb, J. K. Sahu, and J. Nilsson, "Near-diffraction-limited supercontinuum generation in a cladding-pumped nonlinear fiber converter", in Proc. of Conf. Lasers and Electro-Optics/QELS, San Jose May 2010, paper CMMM5.
[36] H. Hemmati, *Near-earth Lasers Communications*, 1st Ed., CRC Press (2008).
[37] J. Nilsson, "Laser physics", ORC postgraduate lecture (2006).
[38] K. Mikoshiba and H. Kajika, "Transmission characteristics of multimode W-type optical fiber experimental study of the effect of the intermediate layer", Appl. Optics, **17**(17), 2836 (1978).
[39] A. K. Sridharan, J. E. Heebner, M. J. Messerly, J. W. Dawson, R. J. Beach, and C. P. J. Barty, "Brightness enhancement in a high-peak-power cladding-pumped Raman fiber amplifier", Opt. Lett., **34**(4), 2234 (2009).
[40] M. J. F. Digonnet, *Rare-earth Doped Fiber Laser and Amplifiers*, 2nd Ed., New York: Marcel Dekker (2001).
[41] J. Nilsson, W. A. Clarkson, R. Selvas, J. K. Sahu, P. W. Turner, S.-U. Alam, and A. B. Grudinin, "High-power wavelength-tunable cladding-pumped rare-earth-doped silica fiber lasers", Opt. Fiber Technol., **10**(1), 5 (2004).
[42] Y. Jeong, J. K. Sahu, M. Laroche, W. A. Clarkson, K. Furusawa, D. J. Richardson, and J. Nilsson, "120-W Q-switched cladding-pumped Yb-

doped fiber laser", in Proc. of Conf. Lasers and Electro-Optics/Europe-EQEC, Munich 23-27 June 2003, paper CL5-4.

[43] J. K. Sahu, P. Dupriez, J. Kim, A. J. Boyland, C. A. Codemard, J. Nilsson, and D. N. Payne, "New Yb:Hf-doped silica fiber for high-power fiber lasers", in Proc. of Conf. Lasers and Electro-Optics/QELS, Baltimore 22-27 May 2005, paper CTuK1.

[44] B. M. Flusche, T. G. Alley, T. H. Russell, and W. B. Roh, "Multi-port beam combination and cleanup in large multimode fiber using stimulated Raman scattering", Opt. Express, **14**(24), 11748 (2006).

Chapter 2 Background

This chapter introduces the background knowledge and theory related to this thesis, and will be helpful to understand subsequent chapters. In section 2.1, mode selection is discussed, which is important since the Raman gain is not restricted to the core in case of cladding-pumping. Furthermore, with pulsed pumping, walk-off and dispersion are critical as explained in section 2.2. Beam quality is an important factor, and it is defined in section 2.3. After this, I discuss the Raman scattering process with a focus on Raman gain and threshold, and introduce models to simulate SRS in fibres in the quasi-CW regime. Following this, the conversion efficiency will be calculated in a single-stage co-pumped CP RFA.

2.1 Mode selection

In a multimode Raman fibre, the transverse power distribution of the pump primarily determines the Raman gain profile in a transverse section and thus which (spatial) Stokes-mode can be amplified through SRS [1]. By contrast, the dopant distribution is normally less important, and certainly for the fibres I have used. The transverse pump distribution in the fibre is given by the incident pump distribution (in case of end-pumping), and the details of the pump propagation in the fibre. This in turn depends on mode coupling, longitudinal coherence, and pump depletion. If the longitudinal coherence is poor so that modal interference can be neglected, then the transverse pump power distribution is given by the sum of the power distributions of the excited modes. In the absence of mode coupling, the power in each pump mode and thus the transverse pump power distribution is determined by the modes excited at the launch end together with the depletion of individual modes. The modal excitation in turn depends on several factors such as spot size, offset, and incident angle of the incident pump beam. Theoretically, the modal power distribution among the excited pump modes at the launch end can be calculated in several ways, for example, with the mode matching method, plane wave expansion [2], and direct phase vector [3]. In reality, the modal

power distribution is very difficult and complicated to measure in fibre and it is practically cumbersome [4]. A further complication is that mode coupling between modes with similar propagation constant is normally not negligible. However it may still be possible to treat modes that are sufficiently strongly coupled as a single group, or quasi-mode, with some particular intensity profile that stays constant along the fibre [5]. Thus, a modal, or quasi-modal, description of the pump propagation can be helpful both for qualitative understanding and quantitative analysis.

According to the mode matching method, the excitation coefficient $\eta_{m,n}$ of a mode $F_{m,n}(x, y)$ (where m and n are the azimuthal number and the radial mode number respectively) for an incident input field $F_i(x, y)$ is calculated according to [6],

$$\eta_{m,n} = \frac{\int_{-\infty}^{+\infty}\int_{-\infty}^{+\infty} F_i(x,y)F_{m,n}(x,y)dxdy}{\sqrt{\int_{-\infty}^{+\infty}\int_{-\infty}^{+\infty}\left|F_i(x,y)\right|^2 dxdy \times \int_{-\infty}^{+\infty}\int_{-\infty}^{+\infty}\left|F_{m,n}(x,y)\right|^2 dxdy}}. \tag{2.1}$$

Here x and y are transverse orthogonal coordinates.

For pump sources with poor beam quality, i.e., which are heavily multimode and cannot be tightly focussed, it may be necessary to fill the inner cladding to achieve a good pump launch. In this case all pump modes will be equally excited, largely. However I have normally used pump sources of much better beam quality. It is then possible to excite a subset of the pump modes, and the Raman conversion will vary accordingly. In particular, lower order modes can then be selected and excited on purpose in a MMF [7]. Normally for DCRFs, lower order pump-modes overlap well with core-modes at the signal wavelength and assist in the 1st-Stokes generation in the core. Thus, the ability of a pump source with high beam quality to excite only lower-order pump modes can help with signal mode selection. This has been demonstrated in a MMF without a double-clad structure, with lower order modes at the Stokes wavelength being generated under appropriate launching conditions [1]. An alternative method to restrict the generation of the 1st Stokes to core-modes in a DCRF with its well defined core structure and core mode(s), is to seed the core through a selective launch in case of an amplifier [8] or through mode-selective feedback in case of a laser, e.g., as provided by a FBG written either in the core of a DCRF or in a separate SMF that is spliced to the DCRF [9]. In this approach, the Stokes power will build up primarily in the core even if the Raman gain is not higher in the core than in the inner cladding.

2.2 Walk-off length in a MMF

Stimulated Raman is nearly instantaneous, and the energy is converted from a pump into a Stokes wave without intermediate energy storage. Thus, the Raman gain is temporally and spatially overlapped with the pump pulses. As soon as the Stokes wave no long overlaps the pump, the SRS power transfer ends. In case of pulsed co-pumping, the pulse energy is launched into different modes, which travel at different group velocities, v_g. This is modal dispersion. The signal propagates in a different group velocity too. In addition, the pump and signal are at different wavelengths. Thus, they travel at different velocities due to chromatic dispersion. The difference in group velocities between the pump and signal leads to a walk-off in temporal and thus restrict SRS. Finally, the energy transfer between different parts of pump modes and Stokes mode can be concentrated at different locations along the fibre [10]. In such cases, the walk-off length determines the effective fibre length, over which the pump and signal can interact effectively with each other and can be defined as [11],

$$L_{walk-off} = \left| \frac{v_p v_s}{v_p - v_s} \right| \Delta T \tag{2.2}$$

where v_s and v_p are the group velocities at the signal and pump wavelength, respectively, and ΔT is the launched pump pulse duration. In silica glass, the walk-off parameter due to the chromatic dispersion is ~ 20 ps/m both at 1 μm and 1.5 μm [11], although with positive and negative differences, respectively, between the group velocities of the Stokes and pump waves. In my pulsed experiments, a typical pump duration is ~ 20 ns, and the fibre length is normally ~ 100 m or shorter. The walk-off length induced by the material is around 1 km, much longer than the fibre length. So in most cases, chromatic dispersion does not have to be taken into account with nanosecond pulses.

The walk-off length due to modal dispersion can be calculated as [12],

$$L_{walk-off} \approx c \frac{n_{oc}}{n_{co}} \frac{1}{n_{co} - n_{oc}} \Delta T \tag{2.3}$$

where n_{co} and n_{oc} are the refractive index of the core and outer cladding, respectively. For the DCRF with fibre number LF11-F71 used in my experiment, the walk-off length due to modal dispersion is 250 m for a pulse with 20 ns duration, which is comparable to the fibre length normally used in the experiments, i.e., ~ 100 m. Note that this is the worst case of the modal dispersion. Normally the walk-off length is longer than that

given by Eq. (2.3) and the walk-off effect can be reduced by adjusting launching conditions to excite lower order pump modes. Nevertheless, for pulsed CP Raman fibre devices, the walk-off effect is important. It can determine the conversion efficiency and fibre length should be chosen carefully to avoid it.

This walk-off length applies for co-propagating pump and Stokes pulses, and generally I will reserve the term "walk-off" for this case. Nevertheless, for counter-propagating pulses one may well take the view that also these experience walk-off. This is very fast, occurring at the sum rather than the difference of the group velocities of pump and Stokes pulse, and as a result the interaction is much reduced for the counter-propagating case. Thus, in the unseeded case with pulsed pumping, forward SRS dominates. The Raman gain and SRS in the backward is much smaller. For example, when the pump pulse repetition frequency (PRF) is sufficiently high to have a large number of pump pulses in the fibre at the same time, the counter-propagating Raman gain equals the co-propagating gain multiplied by the duty cycle of the pump pulses.

2.3 Beam quality and brightness enhancement

The concepts of brightness and beam quality are generally well known and have already been used above. In this section, I will define and quantify them.

The beam quality can be described by the M^2 factor:

$$M^2 = \frac{\Theta W_0}{\lambda / \pi} \tag{2.4}$$

where Θ is the divergence half-angle of the far field and W_0 is the beam radius at the waist of the light beam [13]. The M^2 factor is also known as beam quality factor or beam propagation factor (or parameter). The beam parameter product (BPP) is another quantity used to describe the beam quality:

$$BPP = \Theta W_0 = M^2 \frac{\lambda}{\pi}. \tag{2.5}$$

For a diffraction-limited Gaussian beam, the beam parameter product equals λ / π. The M^2 factor equals the ratio between BPPs for a certain laser source and a diffraction-limited Gaussian beam with the same wavelength. Thus, the M^2 factor equals unity for a diffraction-limited beam.

The beam quality of a laser corresponds to the degree to which the beam can be focused for a given beam divergence (or convergence) angle. Together with the optical

power, the M^2 factor determines the brightness, which is another important term in the field of lasers. It is arguably even more important than its constituents, beam quality and power, since it, rather than the power, determines the power density achievable in a beam focused on a target, and thus often the effect of the beam. Nevertheless, there is no strict definition of this term. It can be understood as being equivalent to radiance, defined by [14]:

$$L = \frac{d^2 P}{d\Omega dA \cos\theta} \approx \frac{P}{\Omega A \cos\theta} \tag{2.6}$$

where the approximation holds for small A and Ω. In Eq. (2.6), L is the radiance ($W \cdot m^{-2}$ sr^{-1}), P is the radiant flux or power (W), θ is the angle between the surface normal and the light flux, A is the area of the source (m^2), and Ω is the solid angle (sr). However, the quantity usually depends on which part of the beam is measured (in the far field). When the quantity is a constant independent of the angle θ, the source is called Lambertian source. However, the laser source is not a Lambertian source so the brightness (or radiance) must be averaged, somehow, to come up with a quantity that applies to the source as a whole. One possibility is to use the approximation in Eq. (2.6), but arguably a more correct expression is:

$$L = B = P/(\lambda^2 M_x^2 M_y^2) \tag{2.7}$$

where M_x^2 and M_y^2 are beam propagation factors in orthogonal planes.

Compared to the approximation in Eq. (2.6), Eq. (2.7) is preferable since M^2 is strictly defined with integral expressions, and is an invariant quantity through an imaging optical system without loss or aberrations [15]. In the case of a beam of radius a emerging from a fibre, according to Eq. (2.4) and Eq. (2.7), the brightness can be expressed as,

$$B = \frac{P}{\lambda^2 M_x^2 M_y^2} = \frac{P}{\pi^2 \Theta^2 W_0^2} \approx \frac{P}{\pi^2 NA^2 a^2}. \tag{2.8}$$

Above, the beam distribution is assumed to be circular.

Many types of lasers can be thought as brightness converters, including CP fibre lasers. In these devices, a multimode pump source with lower brightness is converted to a signal with higher brightness. In a recent paper, a state-of-the-art Yb-doped DCF was used to generate 2.1 kW output power in a diffraction-limited beam [16]. The fibre has a 0.06 NA, 50 μm diameter core and a 0.48 NA, 850 μm diameter inner cladding. The

power conversion efficiency is around 71% for the Yb-doped fibre (YDF) laser. The brightness enhancement η_B can be easily calculated based on Eq. (2.8):

$$\eta_B = \frac{B_s}{B_p} \approx \frac{P_s}{P_p}\left(\frac{NA_{cl}a_{cl}}{NA_{co}a_{co}}\right)^2 . \tag{2.9}$$

In Eq. (2.9), the subscripts *cl* and *co* stand for inner cladding and core respectively while subscripts *s* and *p* are for signal and pump respectively. For the case above, the brightness enhancement can be 13,200. It does however assume that all modes of the inner cladding are excited by the pump and all modes of the cores are excited by the signal. However, since the output beam was diffraction-limited the quantity $NA_{co}\,a_{co}$ = 1.5 μm should rather be replaced by λ_s/π = 0.35 μm. The brightness enhancement then becomes 19 times larger, or 246,000. This assumes that the pump beam filled the inner cladding, but this was nearly the case [17]. In addition the YDF can be, and indeed was, pumped from both ends, and this then opens up for a brightness enhancement of 492,000 with this particular fibre. Thus, brightness enhancements of over five orders of magnitude have been demonstrated experimentally, and six orders of magnitude look possible theoretically with YDFs [18]. An important part of my research is the development of CP Raman fibre devices that increase the brightness and beam quality, relative to that of the pump source.

2.4 Raman Scattering

2.4.1 Introduction

The first observation of spontaneous Raman scattering dates back to 1928. C. V. Raman noticed the change in the spectrum when focussed sunlight was scattered from different liquids and vapours [19]. However, the stimulated version, SRS generally requires much higher optical intensities than achievable with sunlight, and was demonstrated by Woodbury only in 1962 [20], following the advent of the laser. Whereas the Raman-scattered power is proportional to the pump power in case of spontaneous Raman scattering, it increases exponentially with pump power in case of SRS (in the undepleted pump regime). It can also be seeded, so SRS can be used to amplify a signal, with the input signal being proportional to the output signal (in the absence of pump depletion and in some other cases). In 1973, Stolen and Ippen demonstrated the first RFA [21]. In 2002, CP Raman fibre devices were proposed [8][22], and J. Nilsson and co-workers at the ORC for the first time demonstrated a CP RFA [8]. It was pulse-pumped and based

on a germanosilicate fibre. The output beam was diffraction-limited and reached a maximum average power of 50 mW.

Raman scattering is an inelastic nonlinear effect arising from the interaction between incident light and the vibrational states of materials [19]. During Raman scattering, a pump photon is scattered to longer wavelengths under the generation of an optical phonon in the medium. Generally, inelastic scattering to longer wavelengths is called Stokes scattering. The phonon's frequency is equal to the frequency difference between the incident and scattered photon. The vibrational levels of a medium determine the frequency shift and, in case of a Raman amplifier, the gain curve relative to the pump frequency. The Raman spectrum and the gain curve shape are independent of the pump frequency.

SRS is a nearly instantaneous process. Therefore, the signal and pump beams must overlap with each other to amplify the signal through SRS. Furthermore, since SRS can be viewed as a quite weak nonlinearity (especially in silica), it benefits from a strong interaction with intense beams over a significant length. As discussed in Chapter 1, this makes optical fibres particularly well suited for SRS.

For silica glass, its Raman gain spectrum is shown in Figure 2.1. The gain range is over 40 THz, and the frequency shift to the gain peak is about 13 THz.

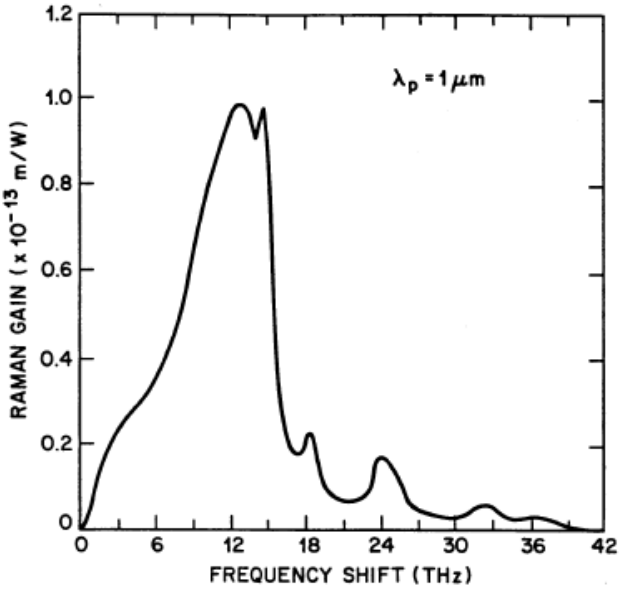

Figure 2.1: Raman-gain spectrum for fused silica at a pump wavelength λ_p = 1 μm [21].

2.4.2 SRS in singe-mode optical fibres

The following two coupled equations describe the evolution of the pump and Stokes (i.e., signal) intensity through SRS process along a length of a SMF in the CW or quasi-CW regime [11].

$$\frac{dI_s}{dz} = g_R I_P I_s - \alpha_s I_s . \tag{2.10}$$

$$\frac{dI_p}{dz} = -\frac{\omega_p}{\omega_s} g_R I_P I_s - \alpha_p I_p . \tag{2.11}$$

Here, both pump and signal are assumed to propagate in the positive direction of the longitudinal fibre coordinate z. The intensity is represented by I_i and the fibre propagation loss by α_i with subscripts $i = p$, s denoting the pump and Stokes beams. Furthermore, g_R is the Raman gain coefficient. The power propagating in a fibre can be found by integrating Eq. (2.10) and Eq. (2.11) in the transverse section [23],

$$\frac{dP_s}{dz} = g_R P_p P_s \frac{\iint I_P I_s dS}{\iint I_P dS \iint I_s dS} - \alpha_s P_s . \tag{2.12}$$

$$\frac{dP_p}{dz} = -\frac{\omega_p}{\omega_s} g_R P_p P_s \frac{\iint I_P I_s dS}{\iint I_P dS \iint I_s dS} - \alpha_p P_p . \tag{2.13}$$

Here, I have used $P = \iint I dS$. The intensity I is proportional to $C|E|^2$, where C is a constant related to the fibre materials and wavelength, and E is the electrical field amplitude. Furthermore, $|E|^2 = |F(x,y)|^2 |A|^2$, where, F is transverse mode field distribution and A is the slowly varying pulse amplitude. Thus,

$$\frac{\iint I_P I_s dS}{\iint I_P dS \iint I_s dS} = \frac{\iint \left|F_p(x,y)\right|^2 \left|F_s(x,y)\right|^2 dS}{\iint \left|F_p(x,y)\right|^2 dS \iint \left|F_s(x,y)\right|^2 dS} = (A_{eff})^{-1} \tag{2.14}$$

where A_{eff} is referred to as the effective area and its reverse is normally referred to as the overlap. Finally, Eq. (2.12) and Eq. (2.13) can be modified as below [23]:

$$\frac{dP_s}{dz} = g_R P_p P_s \frac{1}{A_{eff}} - \alpha_s P_s . \tag{2.15}$$

$$\frac{dP_p}{dz} = -\frac{\omega_p}{\omega_s} g_R P_p P_s \frac{1}{A_{eff}} - \alpha_p P_p . \tag{2.16}$$

If the signal power is small enough for the pump depletion to be negligible, i.e., the first RHS term is negligible in Eq. (2.16), then we can directly get an analytic

solution for the pump power P_p and subsequently the signal power P_s by substituting the pump evolution into Eq. (2.15):

$$P_s(z) = P_s(0)\exp(g_R \frac{1}{A_{eff}} \int_0^z P_p(u)du - \alpha_s z) = P_s(0)\exp(g_R \frac{P_p(0)}{A_{eff}} L_{eff} - \alpha_s z) \quad (2.17)$$

where $P_i(0)$ and $P_i(z)$ are the launched power and the power at a distance z from the launch point, respectively. The effective length L_{eff} is defined as follows [11]:

$$L_{eff} = \frac{\int_0^z P_p(l)dl}{P_p(0)} = \frac{1}{P_p(0)} \int_0^z P_p(0)\exp(-\alpha_p l)dl = \frac{1-\exp(-\alpha_p z)}{\alpha_p}. \quad (2.18)$$

The solution Eq. (2.17) shows that because of the background loss, the effective interaction length is reduced from the actual fibre L to effective length L_{eff}. If the fibre length is long enough, the effective length L_{eff} converges to α_p^{-1} according to Eq. (2.18). The small-signal net gain (i.e., the signal gain with an undepleted pump) can be straightforwardly deduced from Eq. (2.17):

$$G_{net} = 4.343\left(g_R \frac{P_p}{A_{eff}} L_{eff} - \alpha_s z\right). \quad (2.19)$$

The small signal net gain G_{net} is in dB. On-off gain is often used too, and is attractive because it is easy to measure. It is defined as the power ratio between the signal power at the output of the fibre when the pump is on and off and thus takes the signal background loss out of the equation above,

$$G_{on-off} = 4.343 g_R \frac{P_p}{A_{eff}} L_{eff}. \quad (2.20)$$

From both equations above, it is clear that by reducing the effective area, increasing the pump power or the effective fibre length, or using a fibre with a high Raman gain coefficient, a higher Raman gain can be obtained.

2.4.3 Raman critical power or threshold in fibres

Another important parameter for a Raman amplifier is the critical power, also called threshold. The critical power is defined as the input pump power at which the Stokes power equals the pump power at the output of the fibre. Smith has offered an approximate expression, for the case when the 1st Stokes is built up from the noise [24].

For forward SRS, i.e., with co-propagating pump and signal:

$$P_{critical}^{p} \approx 16\frac{A_{eff}}{g_R L_{eff}}. \tag{2.21}$$

For backward SRS, i.e., with counter-propagating pump and signal:

$$P_{critical}^{p} \approx 20\frac{A_{eff}}{g_R L_{eff}}. \tag{2.22}$$

The expression for the co-propagating case is valid both cw and pulsed (if walk-off is negligible), whereas the expression for the counter-propagating case only applies for cw light and for pulses that are long compared to the fibre. Another important assumption is that SRS occurs predominantly in the co- and counter-propagating direction, respectively, for Eq. (2.21) and Eq. (2.22). When the Stokes builds up from noise as assumed here, this will be the case for the co-propagating Stokes with pulsed pumping, but not otherwise. (This discards the possibility of some unidirectional effect such as an isolator or parametric gain overlapping with the Raman gain.) Rather, the local Raman gain at any one point is practically identical in all directions (in an isotropic material). Thus, in case of cw pump light, the forward and backward Raman gain will be the same, and the forward and backward Stokes wave will carry the same amount of power. However, in practice there are likely to be fluctuations in the pump power (when the pump coherence length is shorter than the fibre length), and this makes the forward-propagating Stokes power higher than the backward propagating power, although this effect is reduced by (co-propagating) walk-off between pump and signal.

Although often quoted, the counter-propagating case of Eq. (2.22) comes across as a theoretical abnormality, relying on assumptions that cannot be encountered in practice. The reason why the critical power is higher according to Eq. (2.22), although the forward and backward Raman gain is everywhere the same, is that a backward Stokes wave depletes the pump over a longer length of fibre than a forward Stokes wave does. Thus, a (seeded) backward-propagating Stokes wave is more effective in reducing the gain for itself as the seed power increases. In reality, however, due to the pump fluctuations mentioned above, the forward Stokes wave will build up before or at least not later than the backward Stokes wave, so the assumption of Eq. (2.22) of a dominating backward Stokes wave will not be realised in practice.

Despite these concerns, the critical power can be used to roughly estimate the pump power or fibre length needed for Raman conversion in many cases. It can also be

used to estimate when unwanted SRS starts to appear, e.g., in RE-doped fibre devices although the SRS tolerated in a RE-doped fibre may be much lower.

Note that the 1st-Stokes power can be amplified to the point when it starts to generate the next-order Stokes. The 1st Stokes acts as a pump for the 2nd Stokes, and its power starts to decrease when the 2nd-Stokes power starts to build up. The energy is then rapidly transferred to the 2nd-Stokes beam. The process can continue in a cascaded fashion, so that, even higher-order Stokes radiation can be generated, provided that the input pump power is sufficiently high. Carl Farrell has studied this experimentally [25], and found the following average pump powers at 1064 nm with 20% duty cycle to be required for the generation of Stokes orders 1 – 7 in 2 km of highly nonlinear germanosilicate fibre: 167, 285, 400, 581, 750, 1060, and 1510 mW. The power ratios relative to the 167 mW of power required for the 1st Stokes order become 1, 1.71, 2.40, 3.48, 4.49, 6.35, and 9.04. The peak wavelengths of the Stokes orders were 1116, 1172, 1236, 1306, 1384, 1475, and 1574 nm. These powers correspond to the point where essentially all the power is converted to a specific Stokes order, but this is only slightly higher than the critical power corresponding to Eq. (2.21).

2.4.4 SRS in MM fibres

In a MMF, SRS is similar but more complicated than that in a SMF, described by the equations given in section 2.4.2. The pump and / or signal beams are transported by several modes in a MMF. The power of each mode then creates an optical power distribution that generates a Raman gain in proportion to the local intensity. Thus, it is necessary to consider all modes involved in the SRS process [5]. In the CW or quasi-CW regime, the intensity evolution of each propagating mode at different wavelengths under Raman scattering can be modified from Eq. (2.10) and Eq. (2.11). Through integration across the transverse section similar as done in section 2.4.2, we can obtain:

$$\frac{dP(z,\lambda_i,l)}{dz} = -\alpha(\lambda_i,l)P(z,\lambda_i,l) + P(z,\lambda_i,l)\sum_{j=0}^{j=i-1}\left(\sum_{k=0}^{N_j}\left(P(z,\lambda_j,k)\frac{g_R(\lambda_j,\lambda_i)}{A_{eff}(\lambda_j,\lambda_i,k,l)}\right)\right) - P(z,\lambda_i,l)\sum_{j=i+1}^{j=M}\frac{\lambda_j}{\lambda_i}\left(\sum_{k=0}^{N_j}\left(P(z,\lambda_j,k)\frac{g_R(\lambda_i,\lambda_j)}{A_{eff}(\lambda_i,\lambda_j,l,k)}\right)\right). \quad (2.23)$$

Here, co-pumping is assumed and mode coupling is not considered, which means that the power of different modes (or quasi-modes) increases or decreases independently, in the incoherent regime. The variable $P(z, \lambda_i, l)$ represents the power of the mode l with

the wavelength λ_i at the distance z. The subscript index i stands for any arbitrary wavelength. Later, for simplicity, I will consider that the subscript index i (and j) is referred to as the (primary) pump ($i = 0$), 1st Stokes ($i = 1$), up to M^{th} Stokes ($i = M$). In addition, the wavelengths are arranged to increase with the subscription. The effective area $A_{eff}(\lambda_i, \lambda_j, l, k)$ corresponds to the interacting pump wavelength λ_i, signal wavelength λ_j with specific mode l and k respectively. The Raman gain coefficient $g_R(\lambda_i, \lambda_j)$, corresponding to the pump wavelength λ_i, signal wavelength λ_j, is determined by the material distribution and composition inside the transverse section S. The variable $\alpha(\lambda_i, l)$ is referred to as the background loss at wavelength λ_i with mode l. The background loss is supposed not to vary along the fibre. Finally, N_j is the number of modes that can be supported at the wavelength λ_j inside the fibre. In principle, this number can change along the fibre.

The beating between pump modes is neglected during SRS process. This may be justified by the fact that the SRS gain is small over a characteristic length given by the inverse of $k_{max} - k_{min}$, where k_{max} (k_{min}) is the largest (smallest) wave-vector of any pump mode at the pump wavelength. Assuming that $k_{max} - k_{min} \approx 2\pi / \lambda(n_{co} - n_{oc})$, the "coherence length" of the pump light in different modes is of the order of 10^{-3} m in the DCRFs used in this thesis. Very little happens over such distances in a Raman amplifier. Although other modes have propagation constants closer to each other, their beat length is still small compared to the Raman interaction length, and / or, the power carried by such modes can be expected to be small compared to the total power. Therefore, it is normally justified to neglect the interference of the pump modes, even when the coherence of the pump modes is maintained throughout the fibre, even more so with lower-coherence pumping.

Furthermore, the mode coupling between the core mode(s) and inner-cladding modes of a specific Stokers order can normally be neglected too in the DCRFs I have used. With a double-clad structure, the strong relative enhancement of the fundamental mode or lower order core mode(s) when seeded or when selected by a grating or by an aperture (e.g. by a SMF spliced to the DCRF), reduces modal interference.

Here, spontaneous Raman scattering and Rayleigh back-scattering are not considered. During my experiments, the CP RFAs are usually seeded with sufficient power to make stimulated Raman scattering dominate over spontaneous Raman

scattering everywhere in the fibre, and the lasers operate with sufficiently low gain for this to be true for theme as well. Furthermore, the influence of Rayleigh back-scattering is related to fibre length. See the example in Ref. [26]. In there, the total back-scattered power is smaller than 0.1% even with a fibre length of 100 km (several times the attenuation length), even when the loss is dominated by Rayleigh scattering. In my case, the fibres were typically much shorter than the attenuation length, and this reduces the backscattered power in proportion. While the backscattered power increases with the NA, the core-NAs of my fibres were comparable to that of the standard single-mode fibres used in Ref. [26]. Furthermore, as it comes to back-scattering, a loss dominated by Rayleigh-scattering is a worst-case scenario, and it is likely that other mechanisms contributed to the loss in my fibres. In addition, in the case of pulse pumping, the backward Raman gain is much less due to walk-off as discussed in section 2.2. Thus, Rayleigh scattering is not considered either.

Equation (2.23) can be simplified if the number of treated wavelengths is reduced. Specifically, in my work I often need to treat only the 1st and 2nd Stokes orders, together with the pump. If we only consider a single wavelength for each of them, we get the following equations.

$$\begin{aligned}\frac{dP(z,\lambda_0,l)}{dz} = &-\alpha(\lambda_0,l)P(z,\lambda_0,l) - P(z,\lambda_0,l)\frac{\lambda_1}{\lambda_0}\sum_{k=0}^{N_1}\left(P(z,\lambda_1,k)\frac{g_R(\lambda_0,\lambda_1)}{A_{eff}(\lambda_0,\lambda_1,l,k)}\right) \\ &- P(z,\lambda_0,l)\frac{\lambda_2}{\lambda_0}\sum_{k=0}^{N_2}\left(P(z,\lambda_2,k)\frac{g_R(\lambda_0,\lambda_2)}{A_{eff}(\lambda_0,\lambda_2,l,k)}\right)\end{aligned}. \quad (2.24)$$

$$\begin{aligned}\frac{dP(z,\lambda_1,m)}{dz} = &-\alpha(\lambda_1,m)P(z,\lambda_1,m) + P(z,\lambda_1,m)\sum_{k=0}^{N_0}\left(P(z,\lambda_0,k)\frac{g_R(\lambda_0,\lambda_1)}{A_{eff}(\lambda_0,\lambda_1,k,m)}\right) \\ &- P(z,\lambda_1,m)\frac{\lambda_2}{\lambda_1}\sum_{k=0}^{N_2}\left(P(z,\lambda_2,k)\frac{g_R(\lambda_1,\lambda_2)}{A_{eff}(\lambda_1,\lambda_2,m,k)}\right)\end{aligned}. \quad (2.25)$$

$$\begin{aligned}\frac{dP(z,\lambda_2,n)}{dz} = &-\alpha(\lambda_2,n)P(z,\lambda_2,n) + P(z,\lambda_2,n)\sum_{k=0}^{N_0}\left(P(z,\lambda_0,k)\frac{g_R(\lambda_0,\lambda_2)}{A_{eff}(\lambda_0,\lambda_2,k,n)}\right) \\ &+ P(z,\lambda_2,n)\sum_{k=0}^{N_1}\left(P(z,\lambda_1,k)\frac{g_R(\lambda_1,\lambda_2)}{A_{eff}(\lambda_1,\lambda_2,k,n)}\right)\end{aligned}. \quad (2.26)$$

Here, there are N_0, N_1, and N_2 modes, respectively, at pump wavelength λ_0, 1st-Stokes wavelength λ_1, and 2nd-Stokes wavelength λ_2. Equations (2.24) to (2.26) can be numerically solved with appropriate boundary conditions by commercial software such as MATLAB. For Raman fibre amplifiers, powers at the input are known, and the

equations above can be solved as an initial value problem. For Raman fibre lasers, another equation is needed to describe the propagation of the backward Stokes, which can be easily modified from Eq. (2.25) by changing the sign of the term on the LHS. At the cavity mirrors, the forward Stokes power and backward Stokes power are related to each other through the cavity reflectivities. Thus, the equations can be solved as a boundary value problem. In reality, however, it will be difficult to know the power in each excited mode, in particular when mode coupling is significant. Therefore, an approximate treatment that considers the power in several, or even all, modes of a particular Stokes order together is often better. Assume therefore that the ratio between a certain mode l and the total pump power $P_T(z, \lambda_0)$ at position z is $q_l(z)$. The power of the mode l can be described:

$$P(z,\lambda_0,l) = q_l(z)P_T(z,\lambda_0) \tag{2.27}$$

with $\sum_{l=0}^{N_0} q_l(z) = 1$. After replacing the pump power in a certain mode with Eq. (2.27) from Eq. (2.24) to Eq. (2.26) and summing the pump power in all modes together, we obtain:

$$\begin{aligned}\frac{dP_T(z,\lambda_0)}{dz} = &-P_T(z,\lambda_0)\sum_{l=0}^{N_0} q_l(z)\alpha(\lambda_0,l) \\ &- P_T(z,\lambda_0)\frac{\lambda_1}{\lambda_0}\sum_{k=0}^{N_1}\left(P(z,\lambda_1,k)\sum_{l=0}^{N_0} q_l(z)\frac{g_R(\lambda_0,\lambda_1)}{A_{eff}(\lambda_0,\lambda_1,l,k)}\right) \\ &- P_T(z,\lambda_0)\frac{\lambda_2}{\lambda_0}\sum_{k=0}^{N_2}\left(P(z,\lambda_2,k)\sum_{l=0}^{N_0} q_l(z)\frac{g_R(\lambda_0,\lambda_2)}{A_{eff}(\lambda_0,\lambda_1,l,k)}\right)\end{aligned} \tag{2.28}$$

$$\begin{aligned}\frac{dP(z,\lambda_1,m)}{dz} = &-\alpha(\lambda_1,m)P(z,\lambda_1,m) + P(z,\lambda_1,m)P_T(z,\lambda_0)\sum_{k=0}^{N_0}\left(\frac{q_k(z)g_R(\lambda_0,\lambda_1)}{A_{eff}(\lambda_0,\lambda_1,k,m)}\right) \\ &- P(z,\lambda_1,m)\frac{\lambda_2}{\lambda_1}\sum_{k=0}^{N_2}\left(P(z,\lambda_2,k)\frac{g_R(\lambda_1,\lambda_2)}{A_{eff}(\lambda_1,\lambda_2,m,k)}\right)\end{aligned} \tag{2.29}$$

$$\begin{aligned}\frac{dP(z,\lambda_2,n)}{dz} = &-\alpha(\lambda_2,n)P(z,\lambda_2,n) + P(z,\lambda_2,n)P_T(z,\lambda_0)\sum_{k=0}^{N_0}\left(\frac{q_k(z)g_R(\lambda_0,\lambda_2)}{A_{eff}(\lambda_0,\lambda_2,k,n)}\right) \\ &+ P(z,\lambda_2,n)\sum_{k=0}^{N_1}\left(P(z,\lambda_1,k)\frac{g_R(\lambda_1,\lambda_2)}{A_{eff}(\lambda_1,\lambda_2,k,n)}\right)\end{aligned} \tag{2.30}$$

Here, we can define a new parameter A'_{eff}, which I call the average effective area, to describe the effect on an individual Stokes mode k of the total pump power:

$$(A_{eff}^{'}(\lambda_0,\lambda_1,k))^{-1}=\sum_{l=0}^{N_0}\frac{q_l(z)}{A_{eff}(\lambda_0,\lambda_1,l,k)}. \tag{2.31}$$

It can be named as average effective area.

For CP Raman fibre devices, we are primarily interested in the operation of the fundamental mode (in the core in case of a DCRF) of the 1st Stokes. This corresponds, hopefully, to a diffraction-limited mode with highest possible efficiency, since emission at the 1st-Stokes wavelength minimizes the quantum defect. While Raman gain in a DCRF is induced wherever there is pump light, there are many ways to ensure that the Raman conversion occurs only in the core, to the fundamental mode. Besides the methods mentioned the section 2.1, the gain coefficient in the core is often higher than that in the inner cladding. For example, the core region can have a higher germanium concentration, which increases locally the Raman gain [27]. Note that there will also be some gain at the wavelength of the 2nd Stokes induced directly at the pump, since, in silica, there is still some Raman gain at twice the frequency shift of the gain peak [11]. However, the Raman gain coefficient is much smaller there. Furthermore, in the brightness-enhancing regime that we are interested in, the intensity of the signal in the core, averaged along the fibre, will be higher than that of the pump. Therefore, the second order Stokes gain is, essentially always, highest in the core and generated almost exclusively by the light at the 1st-Stokes wavelength. Hence, the direct contribution from the pump to the gain at the 2nd Stokes can be neglected. With Eq. (2.31), Eq. (2.28) – Eq. (2.30) can be modified as follows:

$$\frac{dP_T(z,\lambda_0)}{dz}=-\alpha(\lambda_0)P_T(z,\lambda_0)-P_T(z,\lambda_0)\frac{\lambda_1}{\lambda_0}P(z,\lambda_1)\frac{g_R(\lambda_0,\lambda_1)}{A_{eff}^{'}(\lambda_0,\lambda_1)}. \tag{2.32}$$

$$\begin{aligned}\frac{dP(z,\lambda_1)}{dz}=&-\alpha(\lambda_1)P(z,\lambda_1)+P(z,\lambda_1)P_T(z,\lambda_0)\frac{g_R(\lambda_0,\lambda_1)}{A_{eff}^{'}(\lambda_0,\lambda_1)}\\&-P(z,\lambda_1)\frac{\lambda_2}{\lambda_1}P(z,\lambda_2)\frac{g_R(\lambda_1,\lambda_2)}{A_{eff}(\lambda_1,\lambda_2)}.\end{aligned} \tag{2.33}$$

$$\frac{dP(z,\lambda_2)}{dz}=-\alpha(\lambda_2)P(z,\lambda_2)+P(z,\lambda_2,n)P(z,\lambda_1,k)\frac{g_R(\lambda_1,\lambda_2)}{A_{eff}(\lambda_1,\lambda_2)}. \tag{2.34}$$

Here, I assume that only a single (spatial) mode is excited at both 1st and 2nd Stokes orders. This is often the case, especially when the core of the DCRF is single-moded. For brevity, I remove the parameter for the mode in the different variables. Also, the background loss is assumed to be the same at a certain wavelength, independent of modes. Even though the loss in the core and inner cladding may well be different, this is

still a reasonable assumption, since the bulk of the pump power propagates in the inner cladding, and the Stokes power propagates in the core.

Above, Eq. (2.32) – Eq. (2.34) describes the evolution of the total pump power and the 1st- and 2nd-Stokes power (both in the fundamental core-mode), under the assumption that the power in the pump modes can be treated as a single quantity. For this to be reasonable even when the 1st-Stokes wave starts to deplete the different pump modes, the pump modes should either be sufficiently strongly coupled for the powers in different pump modes to maintain their relative values, or the (direct) depletion rate should be similar for all pump modes. Otherwise, the average effective index varies along the fibre. The equations can also be used to calculate the gain, if a Stokes wave is seeded.

In the case of strong mode-coupling of the pump modes, it is reasonable to assume that the pump is evenly distributed across the inner cladding. In this case, the effective area for SRS from the pump in the inner cladding to the 1st Stokes in the core is equal to the inner-cladding area A_{cl}. If the Stokes waves are evenly distributed in the core, the effective area for SRS from the 1st Stokes to the higher order Stokes is equal to the core area A_{co}. Still under the assumption of co-propagating, we can get the set of coupled equations for SRS in DCRFs [28]:

$$\frac{dP_T(z,\lambda_0)}{dz} = -\alpha(\lambda_0)P_T(z,\lambda_0) - \frac{\lambda_1}{\lambda_0}P_T(z,\lambda_0)P(z,\lambda_1)g_R^{'}(\lambda_0,\lambda_1)/A_{cl} \quad . \tag{2.35}$$

$$\begin{aligned}\frac{dP(z,\lambda_1)}{dz} &= -\alpha(\lambda_1)P(z,\lambda_1) + P(z,\lambda_1)P_T(z,\lambda_0)g_R^{'}(\lambda_0,\lambda_1)/A_{cl} \\ &- \frac{\lambda_2}{\lambda_1}P(z,\lambda_1)P(z,\lambda_2)g_R^{'}(\lambda_1,\lambda_2)/A_{co}\end{aligned} \quad . \tag{2.36}$$

$$\frac{dP(z,\lambda_2)}{dz} = -\alpha(\lambda_2)P(z,\lambda_2) + P(z,\lambda_2)P(z,\lambda_1)g_R^{'}(\lambda_1,\lambda_2)/A_{co} \, . \tag{2.37}$$

Here, the Raman gain coefficient g_R' is related to the core. I also treat the pump power in different modes as a single quality. The effective area for the pump and signal are kept constant along the fibre, which is not the necessary case for the average effective area given in the previous model under the assumption of weak mode coupling if different modes are depleted at different rates. The previous model is more suitable applied to devices utilising a short piece of fibre used in devices. Instead, if a relatively long piece is used, the model given here is more suitable. The key difference between

two models is the value of the average effective area between the pump and the 1st Stokes. It is critical to the SRS generation. The average effective area depends on the pump modes involved in the process. As discussed in section 2.1, we can excite lower order modes on purpose in different ways, and thus, get smaller average effective area.

I normally use both sets of simplified equations for most simulations of CP RFAs or RFLs in this thesis.

2.5 Simulation example on a CP RFA

In this section, I use Eq. (2.35) to Eq. (2.37) to simulate a single-stage co-pumped CP RFA. The amplifier consists of a 150 m long DCRF with parameters corresponding to the fibre F71-LF11 I used experimentally. The single-mode core diameter is 9 μm and the inner-cladding diameter is 21.6 μm. A 1 kW Raman pump beam at 1550 nm and a 50 mW 1st-Stokes beam at 1660 nm are launched into the fibre from the same end. The background loss is 3.1 dB/km in the core and 2.3 dB/km in the inner cladding. The Raman gain coefficients are 5.29×10^{-14} m/W, and 6.34×10^{-14} m/W, respectively, in the inner cladding and core. Through SRS, the power is transferred from the pump to the 1st Stokes, and the 1st-Stokes power is limited by the 2nd-Stokes generation. The power evolution of the pump, 1st Stokes, and 2nd Stokes along the fibre is given in Figure 2.2. It is clear that the fibre length must be carefully optimised to reach the maximum power of the 1st Stokes. With such length optimisation, thanks to the design of this fibre, the pump is essentially depleted at the point where the 2nd-Stokes power starts to grow. However, this will not be the case for inappropriate fibre designs, as I will discuss in more detail in the next chapter. The conversion efficiency into the 1st Stokes with respect to input pump power in a 76 m long piece of this DCRF (optimised fibre length in Figure 2.2) is also calculated, with as well as without considering background loss. Other parameters are the same. Figure 2.3 show the calculated results. The conversion efficiency increases initially with pump power but rolls over when the pump power is beyond 1 kW due to the 2nd-Stokes generation. With background loss, the highest conversion is 84.4%. This is lower than the quantum efficiency of 93.4%, which is shown by a red dashed line. However, the conversion efficiency into the 1st Stokes is also lower than the quantum efficiency even when the background loss is ignored. I will discuss this further in the next chapter.

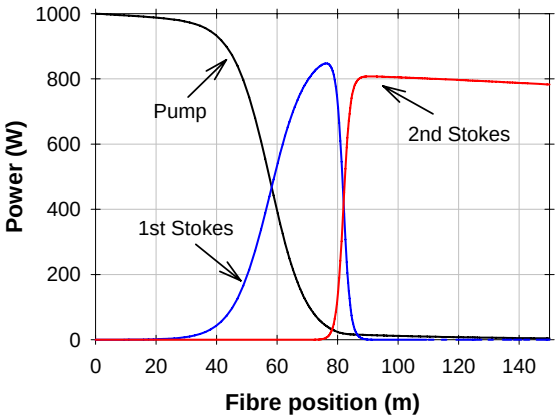

Figure 2.2: (Simulation) Simulation of a single-stage co-pumped CP RFA with a 9 µm diameter core and a 21.6 µm diameter inner cladding fibre. Raman pump (black curve) input power at 1550 nm: 1 kW; 1st-Stokes seed (blue curve) input power at 1660 nm: 50 mW; 2nd Stokes (red curve) builds from noise.

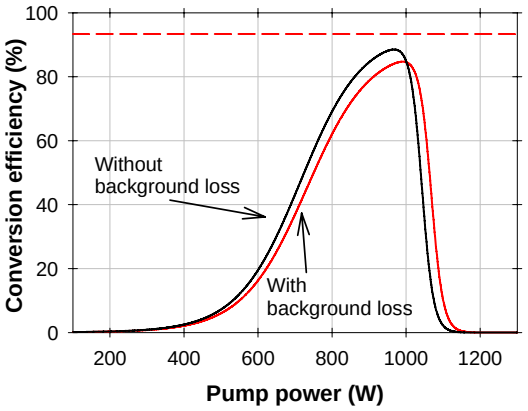

Figure 2.3: (Simulation) Simulation on the conversion efficiency into the 1st Stokes in a single-stage co-pumped CP RFA with a 76 m long piece under different input pump power with (red curve) and without background loss (black curve).

2.6 Summary

In this chapter, I have introduced background theory related to that work I present in this thesis. I have discussed mode selection, walk-off, beam quality, and Raman scattering. Equations are given to describe SRS both in SMFs and in MMFs in the CW and quasi-CW regime. Besides, I used the equations to simulate a single-stage co-pumped CP RFA. The simulation results show that the fibre length and background loss play a role for the conversion efficiency. I will discuss these factors and other limitations set on the conversion efficiency in detail in next two chapters.

2.7 Reference

[1] K. S. Chiang, "Stimulated Raman scattering in a multimode optical fiber: evolution of modes in Stokes waves", Opt. Lett., **17**(5), 352 (1992).

[2] J. -T. Horng, and D. C. Chang, "Coupling an elliptical Gaussian beam into a multimode step-index fiber", Appl. Optics, **22**(23), 3887 (1983).

[3] K. -Y. Lee, and W. -S. Wang, "Ray-optics analysis of the coupling efficiency from a Gaussian beam to a rectangular multimode embedded strip waveguide", Fiber Integrated Opt., **13**(3), 321 (1994).

[4] D. B. S. Soh, J. Nilsson, S. Baek, C. Codemard, Y. Jeong, and V. Philippov, "Modal power decomposition of beam intensity profiles into linearly polarized modes of multimode optical fibers", J. Opt. Soc. Am. A, **21**(7), 1241 (2004).

[5] F. Capasso and P. Di Porto, "Coupled-mode theory of Raman amplification in lossless optical fibers", J. Appl. Phys., **47**(4), 1472 (1976).

[6] A. V. Shmal'ko, "Mode excitation of optial strip waveguides and fibers by end-fire mutual coupling", Czech. J. Phys. B, **34**(6), 538 (1984).
[7] M. E. Fermann, "Single-mode excitation of multimode fibers with ultrashort pulses", Opt. Lett., **23**(1), 52 (1998).
[8] J. Nilsson, J. K. Sahu, J. N. Jang, R. Selvas, D. C. Hanna, and A. B. Grudinin, "Cladding-pumped Raman fiber amplifier", in Proc. of Optical Amplifiers and Their Applications (OAA 2002), Vancouver Canada 14-17 Jul. 2002, paper PD2-1/2/3 (Postdeadline).
[9] C. A. Codemard, P. Dupriez, Y. Jeong, J. K. Sahu, M. Ibsen, and J. Nilsson, "High-power continuous-wave cladding-pumped Raman fiber laser", Opt. Lett., **31**(15), 2290 (2006).
[10] R. H. Stolen and A. M. Johnson, "The effect of pulse walkoff on stimulated Raman scattering in fibres", IEEE J. Quantum Electron., **QE-22**(11), 2154 (1986).
[11] G. P. Agrawal, *Nonlinear Fiber Optics*, 4th Ed., Academic Press Inc, San Diego CA (2006).
[12] A. W. Snyder and J. D. Love, *Optical Waveguide Theory*, Kluwer Academic Publishers (2000).
[13] ISO Standard 11146, "Lasers and laser-related equipment — Test methods for laser beam widths, divergence angles and beam propagation ratios", (2005).
[14] http://en.wikipedia.org/wiki/Radiance.
[15] A. E. Siegman, *Lasers*, University Science Books, California (1986).
[16] Y. Jeong, A. J. Boyland, J. K. Sahu, S. Chung, J. Nilsson, and D. N. Payne, "Multi-kilowatt single-mode ytterbium-doped laser-core fiber laser", Journal of Optical Society of Korea, **13**(4), 416 (2009). (Invited paper)
[17] Private communication with Prof. Johan Nilsson.
[18] J. Nilsson, "High power fiber lasers and amplifiers", in Proc. of Advanced Solid-State Photonics (ASSP), San Diego USA 1-3 Feb. 2010, short course SC290.
[19] C. V. Raman and K. S. Krishnan, "A new type of secondary radiation", Nature, **121**(3048), 501 (1928).
[20] G. Eckhardt, R. W. Hellwarth, F. J. McClung, S. E. Schwarz, D. Weiner, and E. J. Woodbury, "Stimulated Raman scattering from organic liquids", Phys. Rev. Lett., **9**(11), 455 (1962).
[21] R. H. Stolen and E. P. Ippen, "Raman gain in glass optical waveguides", Appl. Phys. Lett., **22**(6), 276 (1973).
[22] R. Rice, "Multimode Raman fiber amplifier and method", US patent no. 6,353,087 (2002).
[23] C. Headley and G. P. Agrawal, *Raman Amplification in Fiber Optical Communication Systems*, Elsevier Academic Press, San Diego (2005)
[24] R. G. Smith, "Optical power handling capacity of low-loss optical fibers as determined by stimulated Raman and Brillouin scattering", Appl. Optics, **11**(11), 2489 (1972)
[25] C. Farrell, "Pulse-pumping of cascaded Raman fibre amplifiers", PhD Thesis, University of Southampton (2011).
[26] S. K. Turitsyn, S. A. Babin, A. E. El-Taher, P. Harper, D. V. Churkin, S. I. Kablukov, J. D. Ania-Castanón, V. Karalekas, and E. V. Podivilov, "Random distributed feedback fibre laser", Nature Photonics, **4**, 231 (2010).
[27] S. J. Davey, D. L. Williams, B. J. Ainslie, W. J. M. Rothwell, and B. Wakefield, "Optical gain spectrum of GeO_2-SiO_2 Raman fibre amplifiers", IEE proceedings, Part J. Optoelectronics, **136**(6), 301 (1989).

[28] J. Ji, C. A. Codemard, M. Ibsen, J. K. Sahu, and J. Nilsson, "Analysis of the conversion to the first stokes in cladding-pumped fiber Raman amplifiers", IEEE J. Sel. Top. Quantum Electron., **15**(1), 129 (2009).

Chapter 3 Brightness enhancement limits in pulsed CP RFAs

In this chapter, I theoretically analyse limitations on brightness enhancement when a multimode pump beam is converted into a diffraction-limited Stokes wave in an efficient pulsed CP RFA. There are many limiting factors. Firstly, there is unwanted cascaded SRS into the 2nd-Stokes order. If unchecked (e.g., in a step-index core), the 2nd-Stokes generation restricts the inner-cladding-to-core area ratio around eight. By designing a new DCRF with a W-type core, I manage to improve this limitation by nearly five times over that of a DCRF with a step-index core, according to model calculations. Other limits are also analysed such as those imposed by glass damage, propagation loss, and pump-signal pulse walk-off in MM fibres. I have found that the designed fibre allows for a pump-to-signal brightness improvement of over 1000 times for pulses longer than 40 ns and up to 3500 times in the CW regime in case of a propagation loss of 3.5 dB/km.

3.1 Introduction

A simple but important application of a DCRF is to convert the output of a MM laser into a diffraction-limited beam. Ideally, this can be achieved by simply adding a DCRF to a MM source [1]-[5]. However, the brightness enhancement achieved in the past has been limited to around 10, for a pump beam quality of $M^2 \sim 3$. This unattractively low value is incompatible with many MM lasers. Another paper [6] reports a brightness enhancement of 192 times in a pulsed CP RFA. Unfortunately, the energy conversion efficiency was poor, only ~ 6.6%. This illustrates the challenges of simultaneously achieving a high brightness enhancement and a high conversion efficiency. In contrast, the brightness can be improved by over five orders of magnitude in highly efficient CP YDF amplifiers and lasers as discussed in section 2.3. This is an exceptionally high number, which even allows for the damage threshold to be exceeded with state-of-the-

art diodes. Although such high numbers may not be necessary, it is important to establish the brightness enhancement that can be reached in CP Raman fibre devices while retaining a high conversion efficiency. This is the subject of this chapter. A new DCRF with a W-type core for improved brightness enhancement is designed and the achievable brightness enhancement is calculated. The calculated result shows that over a 1000-fold improvement of the brightness is possible with realistic parameters, compatible with a wide range of MM pump sources, including diodes.

3.2 Limitations on the area ratio and fibre design

3.2.1 Inner-cladding-to-core area ratio requirement

Figure 2.3 illustrated that the background loss limits the conversion efficiency into the 1st Stokes. However, even with a lossless fibre, the highest achievable conversion efficiency into the 1st Stokes is still lower than the quantum efficiency, as shown in the same plot. This is irrespective of pump power. Thus, whereas a RE-doped fibre laser would, to first approximation, allow for quantum-limited efficiency, in a lossless fibre if one operates sufficiently high above threshold, there must be other factors restricting the conversion efficiency besides the background loss in a DCRF. Figure 3.1 illustrates the impact of the inner-cladding-to-core area ratio on the conversion efficiency in a single-stage co-pumped CP RFA, as calculated with numerical simulations of Eq. (2.35) – Eq. (2.37) in the quasi-CW regime. For this, I consider DCRFs which have the same core size, 9 μm diameter (single-moded) and different inner-cladding sizes. The inner-cladding diameter is varied from 9 μm (the fibre becomes a SMF in this case) to 70 μm. The fibre length is carefully optimized for each inner-cladding size to reach highest possible conversion efficiency into the 1st Stokes. Background loss is not considered. Other parameters remain the same as the example in section 2.5. The red curve with circles shows the dependence of the conversion efficiencies on the inner-cladding diameters and corresponding inner-cladding-to-core area ratios. The red dashed line indicates the quantum efficiency. In the case of a SMF, the conversion efficiency into the 1st Stokes is practically identical to the quantum efficiency. By increasing the inner-cladding-to-core area ratio, the conversion efficiency drops off. When the area ratio between the inner cladding and core is larger than 8 (the case identified with a circle), the conversion efficiency is below 80%. This example shows that the inner-cladding-to-core area ratio also limits the conversion efficiency into the 1st Stokes.

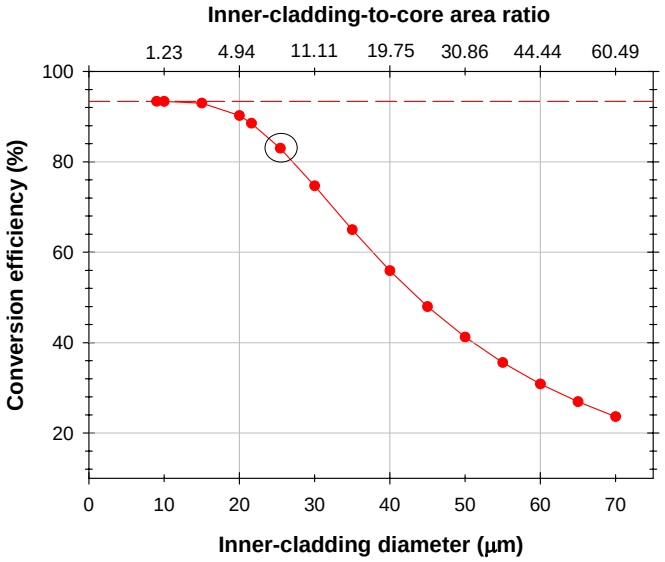

Figure 3.1: (Simulation) Simulation of a single-pass co-pumped CP RFA based on fibres with different inner-cladding sizes under 1 kW input pump power. Dashed line represents the quantum efficiency; Solid line: conversion efficiency into the 1st Stokes.

In the example above the inner-cladding-to-core area ratio should be no more than around eight for a high conversion efficiency into the 1st Stokes. This is actually a general result. In the following, I deduce the required area ratio between inner cladding and core for efficient CP RFAs based on fibres with basic step-index profiles. From Eq. (2.35) – Eq. (2.37), it follows that the SRS-induced nonlinear depletion of the pump by the 1st Stokes ζ_0, in nepers, is given by:

$$\zeta_0 = \frac{\lambda_1}{\lambda_0} \frac{g_R'(\lambda_0, \lambda_1)}{A_{cl}} \int_0^L P(z, \lambda_1) dz. \tag{3.1}$$

This quantifies the relative amount of pump power transferred to the 1st Stokes by SRS. Similarly to Eq. (3.1), disregarding background loss, the gain of the fundamental mode at the 2nd Stokes, induced by the 1st-Stokes wave in the core of the DCRF, is given by:

$$G_2 = \frac{g_R'(\lambda_1, \lambda_2)}{A_{co}} \int_0^L P(z, \lambda_1) dz \tag{3.2}$$

where G_2 is the gain, also in nepers. Note that here, I assume the pump and signal are uniformly distributed in the inner cladding and core, respectively. Thus, the effective area (as defined in Eq. (2.14)) between the pump and 1st Stokes equals the inner-cladding area while the effective area between the 1st Stokes and 2nd Stokes is equal to the core area.

The 2nd Stokes, building up from noise, will become important once its gain reaches about 16 nepers (~70 dB) [1], or earlier if there is any feedback. This is however unwanted since it depletes the 1st Stokes. Furthermore, in order to have an efficient conversion of the pump into the 1st Stokes, the nonlinear pump absorption should be in the region of 2 nepers (8.7 dB) or more. Thus, the ratio of the 2nd Stokes gain and the pump absorption must fulfil:

$$\frac{G_2}{\zeta_0} < 8. \tag{3.3}$$

Using Eq. (3.1) and Eq. (3.2) to replace G_2 and ζ_0 in Eq. (3.3), we obtain the following condition:

$$\frac{G_2}{\zeta_0} = \left(\frac{A_{cl}}{A_{co}}\right)\left(\frac{\lambda_0}{\lambda_1}\right)^2 = \left(\frac{D_{cl}\lambda_0}{d_{co}\lambda_1}\right)^2 < 8 \tag{3.4}$$

where D_{cl} and d_{co} are the cladding and core diameter, respectively, and where I have used that the Raman gain is approximately inversely proportional to the pump wavelength [1]. Equation (3.4) forms a basic rule for the area ratio required to avoid the 2nd Stokes, when losses are low and the nonlinear pump absorption is sufficiently large to allow for efficient conversion. This matches well the value given in Figure 3.1. Thus for a given core size, the inner-cladding area must be restricted to ensure that the pump power can be efficiently transferred to the 1st Stokes before the 2nd Stokes is generated. Otherwise, the 2nd Stokes will inevitably build up before the pump is transferred into the 1st Stokes. Equation (3.4) follows from the symmetry of SRS in terms of Raman gain on the Stokes side and nonlinear depletion on the anti-Stokes side of the 1st Stokes, and the effective area dependence (see Eq. (3.1) and Eq. (3.2)). Importantly, this equation also sets a limit to the brightness enhancement, when combined with achievable NAs of the pump and signal. Still, it is possible to relax this condition if the loss at the 2nd Stokes is increased to prevent the 2nd Stokes from building up. At the same time, to reach a high efficiency, the loss for the 1st Stokes and the pump must remain low.

Figure 3.2 illustrates how the powers of the pump and 1st and 2nd Stokes evolve, as calculated with Eq. (2.35) – Eq. (2.37) in a single-pass CP RFA based on DCRFs with inner-cladding-to-core area ratios of 5.8 and 11.1 respectively. For the fibre with the inner-cladding-to-core ratio at 5.8, the DCRF is exactly same as one in Figure 2.2, and the inequality (3.4) is satisfied. Thanks to the appropriate area ratio, the pump power is well depleted at the point where the 2nd Stokes at 1790 nm starts to grow. The

residual pump power is about 0.4% of the input Raman pump. By contrast, if the inner cladding diameter is 30 µm while the other parameters remain the same, a significant amount of pump power, over 10%, will not be converted into the 1st Stokes before the 2nd Stokes is generated. Here, the inner-cladding-to-core area ratio is 11.1, not meeting the inequality above. Furthermore, with even larger inner-cladding-to-core area ratio, the conversion efficiency becomes even worse, as for the case shown in Figure 3.1. Once the 1st-Stokes power has been converted into the 2nd Stokes, there is no longer any effective conversion of the pump, so a fraction of the power will remain in the low-brightness pump beam. This is seen in Figure 3.2, even with the relatively benign area ratio of 11.1. Eventually, a new 1st-Stokes wave can build up from the remaining pump, but only if the 1st-Stokes gain induced by the pump overcomes the 1st-Stokes depletion rate induced by the 2nd Stokes, as well as the fibre background loss.

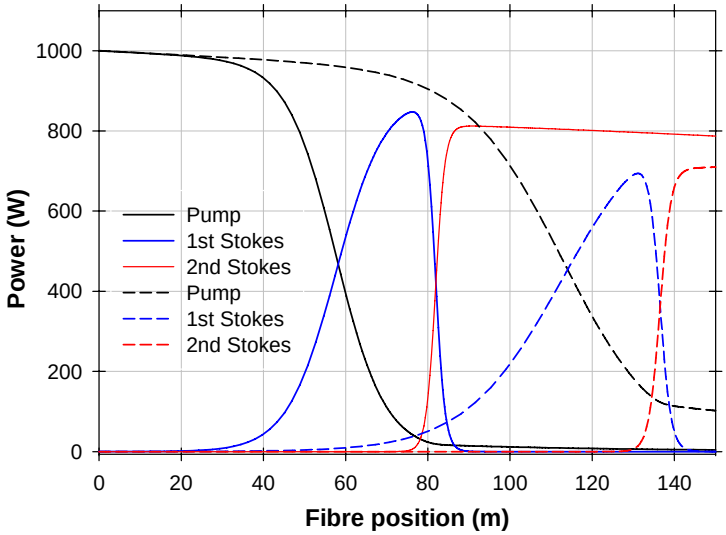

Figure 3.2: (Simulation) Simulation of single-stage co-pumped CP RFAs based on a fibre with a 9 µm diameter core. Solid lines: Area ratio 5.8 between the inner cladding and core; Dashed lines: Area ratio 11.1 between the inner cladding and core; Raman pump (black curves) input power at 1550 nm: 1 kW; 1st Stokes seed (blue curves) input power: 50 mW. Red curves present 2nd Stokes.

3.2.2 Loss required to suppress buildup of the 2nd-Stokes gain peak

It would be helpful to relax the restriction of the geometry described by Eq. (3.4), so that larger inner claddings and lower brightness pump sources can be employed. As mentioned above, this is possible if a loss at the 2nd-Stokes wavelength is introduced to prevent the growth of the 2nd-Stokes power through SRS process. A waveguide filter such as a W-type fibre [7], is one method for introducing a high loss at longer wavelengths (i.e., at the 2nd Stokes) while keeping the loss low at the 1st Stokes when

the W-type fibre is bended. The induced loss through bending is normally referred to as bendloss, and the bendloss spectrum depends on the fibre design and the bend radius, as well. With a waveguide filter, Eq. (3.4) should be modified as:

$$(G_2 - \alpha_2 L)/\zeta_0 < 8 \tag{3.5}$$

where α_2 is the loss per unit length at the 2nd Stokes and L is the fibre length. Again using Eq. (3.1) and Eq. (3.2), we get

$$\frac{A_{cl}}{A_{co}}\left(\frac{\lambda_0}{\lambda_1}\right)^2\left(1-\frac{\alpha_2 L}{\alpha_2 L+16}\right)=\left(\frac{a_{cl}}{a_{co}}\frac{\lambda_0}{\lambda_1}\right)^2\left(1-\frac{\alpha_2 L}{\alpha_2 L+16}\right)<8\,. \tag{3.6}$$

Here I have used that with loss, the condition for avoiding build-up of the 2nd Stokes becomes

$$G_2 - \alpha_2 L < 16\,. \tag{3.7}$$

Therefore, the area ratio condition in Eq. (3.4) is relaxed and the inner-cladding area can be increased for a given core size. The required loss can be deduced from Eq. (3.6):

$$\alpha_2 > \frac{A_{cl}}{A_{co}}\left(\frac{\lambda_0}{\lambda_1}\right)^2\frac{2}{L}-\frac{16}{L}. \tag{3.8}$$

If the background loss is negligible for both the 1st Stokes and Raman pump, and there is no power conversion to the 2nd Stokes, we have,

$$\zeta_0 = \frac{\lambda_1}{\lambda_0}\frac{g_R^{'}(\lambda_0,\lambda_1)}{A_{cl}}\int_0^L P_1(z)dz \tag{3.9}$$

and

$$G_1 = \frac{g_R^{'}(\lambda_0,\lambda_1)}{A_{cl}}\int_0^L P_0(z)dz\ . \tag{3.10}$$

Here, G_1 is the Raman gain at the 1st Stokes, $g_R^{'}(\lambda_0, \lambda_1)$ is the Raman gain coefficient in the core at the 1st-Stokes wavelength λ_1 with a pump at λ_0, and P_0 and P_1 are the powers at the pump and 1st Stokes respectively. Note further that in the absence of loss, the total number of photons is preserved. In case of co-propagating pump and 1st Stokes, the sum $(\lambda_1/\lambda_0)\,P_1 + P_0$ is then constant along z. Thus, add Eq. (3.9) can be added to Eq. (3.10) to obtain:

$$G_1 + \zeta_0 = P_0(0)g_R^{'}(\lambda_0,\lambda_1)L/A_{cl} \tag{3.11}$$

where $P_0(0)$ is the Raman pump power at the input. The initial power of the 1st Stokes, $P_1(0)$, is assumed to be negligible compared to that of the pump. Otherwise, this can be readily added to the right hand side of Eq. (3.11).

From Eq. (3.11), the fibre length can now be determined as:

$$L = A_{cl}\frac{G_1 + \zeta_0}{g_R'(\lambda_0,\lambda_1)P_0(0)}. \tag{3.12}$$

Substituting Eq. (3.12) into Eq. (3.8) yields,

$$\alpha_2 > \frac{2(A_{cl}/A_{co})(\lambda_0/\lambda_1)^2 - 16}{A_{cl}(G_1 + \zeta_0)/(P_0(0)g_R'(\lambda_0,\lambda_1))}. \tag{3.13}$$

As a representative numerical example, I suppose next that G_1 = 7 Np (i.e., 30.4 dB) and, as before, that ζ_0 = 2 Np. Then, equation (3.13) becomes:

$$\alpha_2 > \frac{P_0(0)g_R'(\lambda_0,\lambda_1)}{(2+7)A_{co}}\left[2\left(\frac{\lambda_0}{\lambda_1}\right)^2 - 16\frac{A_{co}}{A_{cl}}\right]. \tag{3.14}$$

This will be a reasonable approximation for the required 2nd Stokes loss for most realistic Raman gain values, say, between 3 and 12 Np.

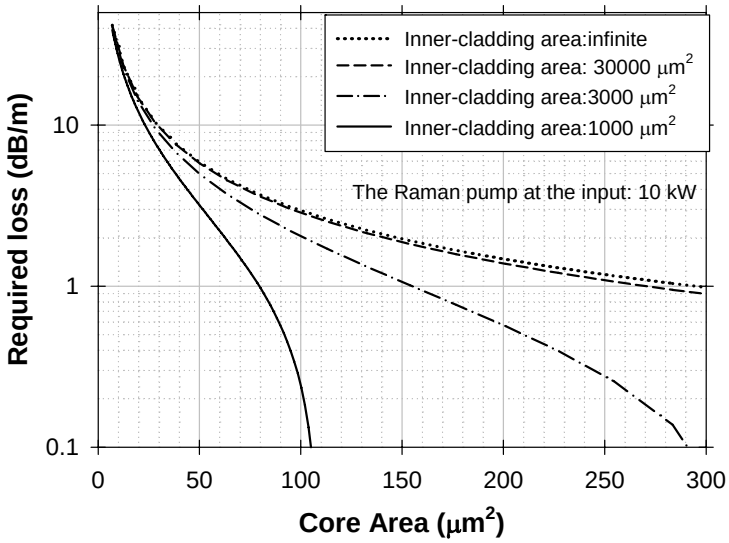

Figure 3.3: (Simulation) Loss required to suppress the generation of the 2nd Stokes in a germanosilicate fibre pumped at 1.55 μm with a pump power of 10 kW and a Raman gain coefficient of 0.35×10^{-13} m/W.

For a numerical illustration, I will next assume a pump wavelength of 1.55 μm and a power of 10 kW. This leads to a 1st-Stokes wavelength of 1.66 μm in a germanosilicate fibre, with a typical value of $g_R'(\lambda_0, \lambda_1)$ of 0.35×10^{-13} m/W. Figure 3.3 shows the resulting loss α_2 that is required to suppress the 2nd Stokes according to

Eq. (3.14) as a function of core area, for different inner-cladding areas. This assumes that the fibre length is chosen according to Eq. (3.12). When the inner-cladding-to-core area ratio is small enough, i.e., below 8, no loss is needed to suppress the 2nd Stokes in the core. The required loss is inversely proportional to the length, and therefore proportional to the pump, and can easily be scaled to other pump powers (when chosen according to Eq. (3.12)).

3.2.3 Spectral bendloss filtering and the influence of off-peak SRS on the area ratio limitation

Clearly, in a fibre that reaches the loss of Figure 3.3, the 2nd Stokes will not build up. However, even if it is possible to reach this loss at the 2nd-Stokes gain peak wavelength, it is not realistic to expect it to be reached across the entire 2nd-Stokes gain band, which extends all the way to the 1st-Stokes wavelength. Therefore, to determine if the 2nd Stokes is totally suppressed, one must consider all wavelengths within the 2nd-Stokes band, and the precise spectral dependence of the Raman gain and the bendloss within this region. Since the loss at the 1st-Stoke wavelength must be small, and since the attenuation increases only gradually from the 1st-Stokes wavelength (λ_1) to the 2nd-Stokes peak wavelength (λ_2), the loss for small Stokes shift will necessarily be small. At the same time, the Raman gain coefficient for the 2nd Stokes also increases gradually for wavelengths λ_i in the range $\lambda_1 \leq \lambda_i < \lambda_2$. Depending on which increases faster, and therefore on the filter sharpness, the net gain in the presence of the bendloss may then peak at the intrinsic Raman gain peak wavelength, or at some shorter wavelength. Mathematically, Eq. (3.6) should be modified as follows:

$$\left(\frac{A_{cl}}{A_{co}}\right)_{\lambda_i}\left(\frac{\lambda_0}{\lambda_1}\right)^2\left(1-\frac{\alpha_2(\lambda_i)L}{\alpha_2(\lambda_i)L+16}\right) < 8\times\frac{g'(\lambda_1,\lambda_2)}{g'(\lambda_1,\lambda_i)}. \qquad (3.15)$$

This condition must hold across the spectral range from λ_1 to λ_2, so the condition of Eq. (3.15) becomes wavelength-dependent. Figure 3.4(a) shows a bendloss spectrum for a representative W-type fibre and the spectrum of the Raman gain coefficient. The corresponding area ratio limitation is shown against wavelength in Figure 3.4(b) for a 100 m long fibre, which corresponds, for example, to a pump power of 10 kW and an inner-cladding area of 3889 μm^2. Without filtering, the most stringent area ratio limitation occurs for a 2nd Stokes at the intrinsic gain-peak wavelength λ_2 (1.79 μm), as expected. However, with bendloss, the limiting area ratio occurs for a smaller 2nd-

Stokes shift, at a wavelength of ~ 1.685 μm in this case. This wavelength corresponds to a hump in the silica Raman spectrum at ~ 80 cm^{-1}, which appears to be particularly difficult to suppress. For the calculations I neglect the gain induced directly by the pump at 2nd-Stokes wavelengths, which is acceptable given the limited gain induced by the pump even at the peak of the signal gain (7 Np).

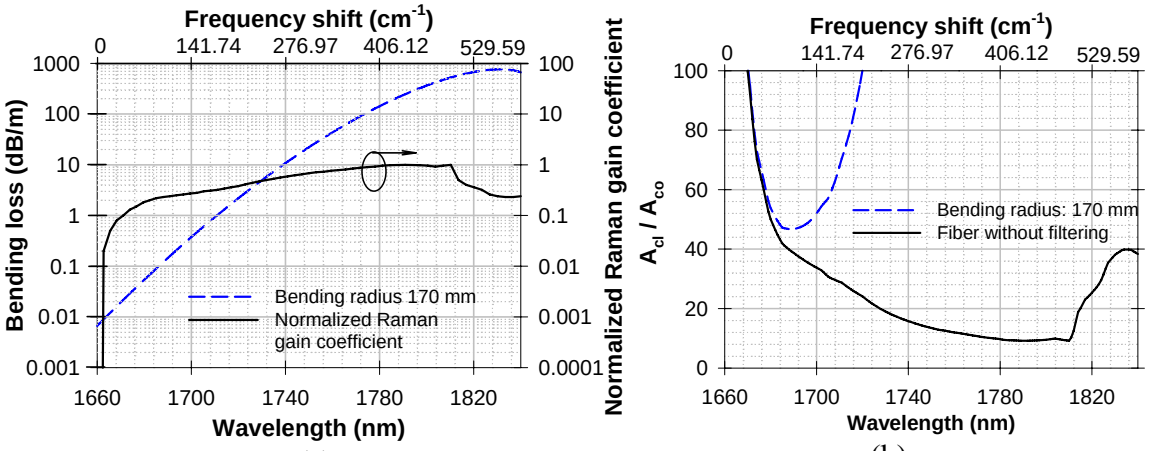

(a) (b)

Figure 3.4: (Simulation) (a) Bendloss spectrum and Raman gain coefficient spectrum; (b) maximum inner-cladding-to-core area ratio with 100 m long piece of fibre. Parameters of the W-type fibre: core radius a_{co} = 6 μm; depressed region radius a_{dp} = 15 μm; core refractive index n_{co} = 1.4654; depressed region refractive index n_{dp} = 1.44; cladding refractive index n_{cl} = 1.462; cut-off wavelength λ_c = 1.85 μm. Figure 3.6 clarifies the meaning of these parameters.

For a quantitative analysis of the effect of bendloss and filter sharpness on the area ratio, I introduce a simple model to fit fibre bendloss spectra as below:

$$\alpha(\Delta\lambda) = \alpha_1 \exp[p\Delta\lambda + p(-1.962\cdot10^{-3} + p6.772\cdot10^{-3})\Delta\lambda^2 + p(-2.753\cdot10^{-6} + p7.803\cdot10^{-6})\Delta\lambda^3] \quad . \tag{3.16}$$

Here, $\Delta\lambda = \lambda_i - \lambda_1$, α_1 equals the loss at the 1st Stokes, and p is the slope of the bendloss curve close to the 1st-Stokes wavelength on a logarithmic scale. The unit of α can either be Np/m or dB/m, according to the unit of α_1. This model is sufficiently accurate for different fibres and for different bending conditions, for the ranges of wavelengths and bendloss slopes of primary interest. I use it to investigate how the maximum area ratio depends on the bendloss slope p at the 1st Stokes for different values of the bendloss at the 1st Stokes, which, to repeat, must be kept small.

To proceed further with the analysis, I next set a specific value of the 1st-Stokes loss $\alpha_1 L$ of 1 dB, which is sufficiently low to allow for high conversion efficiency. This

allows us to calculate the spectrally resolved area ratio limit for different p-values by substituting Eq. (3.16) into Eq. (3.15). Figure 3.5 shows the results for a total 1st-Stokes loss. From Figure 3.5(b), the area ratio limit improves rapidly with p up to $p \approx 0.03$, but only slowly thereafter.

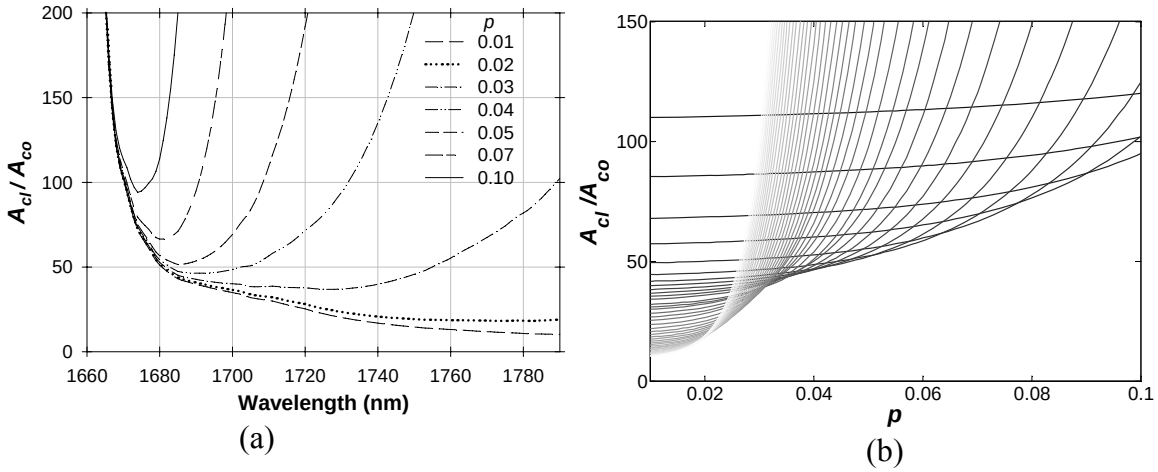

(a) (b)

Figure 3.5: (Simulation) (a) Area ratio limit for different p-value *vs.* wavelength. For p-values larger than ~ 0.03, the overall limit is set by Stokes shifts smaller than ~ 20 nm. For such small Stokes shift, the logarithmic bendloss curve will deviate only slightly from a straight line, and the approximation of Eq. (3.16) will be good. (b) Limiting area ratio *vs*. p. Each curve represents a single wavelength within the range λ_1 to λ_2, with the shallower-slope curves representing shorter wavelengths. The lower envelope of the curves represents the limiting area ratio across the whole spectral range.

It is difficult to combine the desired sharp bendloss characteristics (i.e., a large p-value) with a large core [7]. Therefore, a compromise must be found. I propose that the best point of operation may be at the knee around $p = 0.03$. A p-value above this value will only slowly increase the maximum area ratio, and given the smaller core that a higher p-value necessitates, the maximum inner-cladding area is likely to decrease. This is indeed found to be the case for W-type fibres, analysed in detail in the next section.

3.2.4 W-type fibre design

This section discusses in detail the design of a W-type fibre that best combines the requirements of a filter sharpness and a large core area. I choose to work with W-type fibres, because of their sharp bendloss characteristics [7]. Figure 3.6 shows the RIP of a W-type fibre. Under the assumption of weak guidance, the transverse distribution of LP-modes becomes [8]:

$$\begin{cases} \varphi_0 = A_0 J_m(ur/a_{co}), & r \le a_{co} \\ \varphi_1 = A_1 I_m(w'r/a_{dp}) + A_2 K_m(w'r/a_{dp}), & a_{co} < r < a_{dp} \\ \varphi_2 = A_3 K_m(wr/a_{dp}), & r \ge a_{dp} \end{cases} \tag{3.17}$$

where r is the radial coordinate, A_i (i = 0, 1, 2, 3) are constants, and J_m, K_m, and I_m represent Bessel functions, modified Bessel functions of the 1st kind, and modified Bessel functions of the 2nd kind, respectively. Other parameters are defined in Figure 3.6. Furthermore, $u = a_{co}\,k_0(n_{co}^2 - n_{eff}^2)^{0.5}$, $w' = a_{dp}\,k_0(n_{eff}^2 - n_{dp}^2)^{0.5}$, and $w = a_{dp}\,k_0(n_{eff}^2 - n_{cl}^2)^{0.5}$, with n_{eff} being the effective index of the mode and k_0 the wavenumber in vacuum. The effective index is determined by the characteristic equation, which follows from the boundary conditions, that is,

$$\frac{[\hat{J}_m(u) - \hat{K}_m(w'q)][\hat{K}_m(w) - \hat{I}_m(w')]}{[\hat{J}_m(u) + \hat{I}_m(w'q)][\hat{K}_m(w) - \hat{K}_m(w')]} = \frac{I_{m+1}(w'q)K_{m+1}(w')}{I_{m+1}(w')K_{m+1}(w'q)}. \tag{3.18}$$

Here, $\hat{Z}_m(x) = Z_m(x)/\{xZ_{m+1}(x)\}$, with Z representing Bessel functions, and $q = a_{co}/a_{dp}$. This then allows us to calculate the mode field distribution.

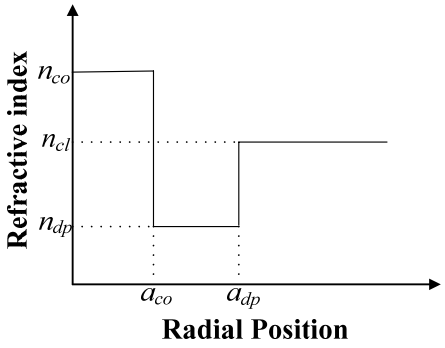

Figure 3.6: Schematic diagram of the RIP of a W-type fibre.

Because of the large number of parameters of a W-type fibre, some are fixed to simplify the analysis. To make a W-type fibre with a sharp cut-off, it helps to have the difference between the refractive index of the cladding and the depressed region as large as possible [9], although this difference is limited by the fabrication process for the low-loss silica fibres that are required. The refractive index of the pure silica is 1.445 at 1.55 μm. I assume that the refractive index can be reduced to 1.44, by the MCVD fabrication process. Therefore, n_{dp} is set at 1.44. Moreover, n_{cl} is set at 1.457, corresponding to a moderate up-doping of the cladding. This is typically done with germanium, and at the corresponding doping-level, machining of the preform is still relatively straightforward. The preform can be machined to make the inner cladding non-circular, as this improves the interaction between the signal in the core and the

pump in the inner cladding [10]. The radius of the depressed region (a_{dp}) is set to twice that of the core radius (a_{co}). This is a somewhat arbitrary choice, but I have found it to work well in our simulations.

The bendloss characteristics are then calculated for a range of different values of the core refractive index n_{co} and radius a_{co}, using Marcuse's bendloss model [11]. The fibre bend radius is adjusted to yield a specific, maximum tolerable, loss at the 1st-Stokes wavelength. I set this to be 0.01 dB/m, which leads to a loss of 1 dB in a 100 m long fibre. The fibre length is somehow arbitrary choice. However, I will prove later that the designed fibre optimised at this length works well at other lengths. Furthermore, the filter sharpness parameter p is determined by fitting the calculated bendloss spectrum to Eq. (3.16). This is done for each core design and bend radius. Several combinations of core parameters and bend radii can yield the same value for p. Of these, the best core designs (i.e., the design with the largest area) are typically such that they result in the maximum tolerable 1st-Stokes bendloss at the maximum tolerable bend radius, which was 20 cm in the case to allow for practical packaging. It seems likely that if larger bend radii are accepted, somewhat larger core areas can be used. I also determine the maximum allowable area ratio by using Eq. (3.15), and from that, calculate the maximum allowable inner-cladding area. These are plotted in Figure 3.7, as a function of the filter sharpness.

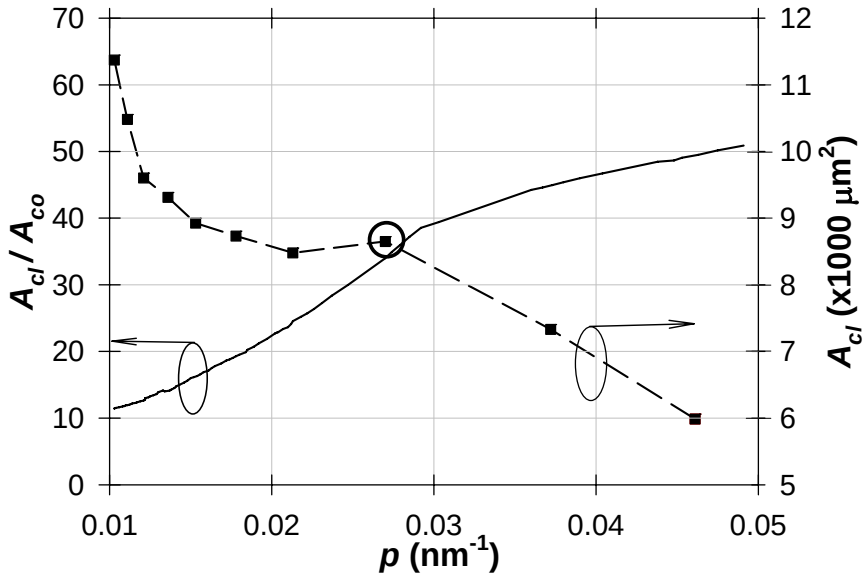

Figure 3.7: (Simulation) Inner-cladding-to-core area ratio and inner-cladding area *vs*. filter sharpness parameter p for W-type fibre with different cut-off wavelengths.

The area ratio limit with the numerically determined bendloss spectra (parameterized by the filter sharpness) in Figure 3.7 is nearly the same as the one in

Figure 3.5(b), using bendloss spectra according to Eq. (3.16). This is expected, given that Eq. (3.16) is a good approximation of the bendloss spectrum for all fibres, at the relatively small Stokes shifts that limit the area ratio (see Figure 3.5(a)). By contrast, the core areas, and therefore the inner-cladding areas, differ considerably between different core designs with the same filter sharpness. Figure 3.7 only includes data for the best core design, i.e., those that allow for the largest core area for a given filter sharpness, while designs falling below that have been discarded.

Figure 3.7 can be used to assess which filter sharpness is best. As suggested in conjunction with Figure 3.5(b), filter sharpnesses beyond $p = 0.027\ \mathrm{nm}^{-1}$ lead to a more stringent inner-cladding area limit. This is caused by the rapidly decreasing core sizes required for such sharp filters, in conjunction with the hump in the Raman spectrum at around $80\ \mathrm{cm}^{-1}$ (see Figure 3.4), which reduces the benefits of filters sharper than $p = 0.027\ \mathrm{nm}^{-1}$. For $p < 0.027\ \mathrm{nm}^{-1}$, the allowable inner-cladding area varies somewhat around an approximate value of $9000\ \mu\mathrm{m}^2$. In this regime, the core area is larger and the area ratio smaller than at $p = 0.027\ \mathrm{nm}^{-1}$. This regime can also be interesting, e.g., when optical damage necessitates a large core. However, micro-bending can be a concern with some core and inner-cladding parameters in the region $p < 0.027\ \mathrm{nm}^{-1}$. A thick glass structure and a small core help to reduce micro-bending. A thick fibre is possible irrespective of core and inner-cladding parameters in so-called jacketed air-clad fibres or rod-fibres [12]. However, they are much more difficult to fabricate than conventional DCFs with a polymer outer cladding. Amongst the fibres with inner-cladding areas of $\sim 9000\ \mu\mathrm{m}^2$ in Figure 3.7, the fibre with the highest area ratio, and therefore the smallest core, would fare best as it comes to micro-bending. Hence, I view the W-type fibre with $p = 0.027\ \mathrm{nm}^{-1}$, i.e., with the following parameters as being particularly interesting: $a_{co} = 9\ \mu\mathrm{m}$, $a_{dp} = 18\ \mu\mathrm{m}$, $a_{cl} = 52.5\ \mu\mathrm{m}$, $n_{co} = 1.4589$, $n_{dp} = 1.44$, $n_{cl} = 1.457$, and $\lambda_c = 2000\ \mathrm{nm}$. This core should be sufficiently small, and the inner cladding sufficiently large to make the fibre relatively immune to micro-bending [13] even when fabricated with a polymer outer-cladding. Furthermore, with an inner-cladding diameter of 105 μm and an area ratio of 34, it allows for considerable brightness enhancement and the use of pump sources of low beam quality.

While I have treated a specific fibre length, I have found that the designed fibre performs similarly with different lengths, provided that the pump intensity is adjusted appropriately. For example, with a pump intensity of $5\ \mathrm{W}/\mu\mathrm{m}^2$, a 57 m long fibre should

be chosen according to Eq. (3.12), and in case of a W-type core according to the design above, the inner-cladding-to-core area ratio could be 32 with 1 dB loss at the 1st Stokes, although now with 19 cm bend radius instead of 20 cm. With a 575 m long piece, as appropriate for a pump intensity of 0.5 W/μm^2, the same W-type core design allows for an area ratio of 39. This is even slightly better than for the design length of 100 m, although now with a 22 cm bend radius. Thus, the designed fibre works well for fibre lengths in the ranger 57 m to 575 m, which is the limit of what I considered.

Ideally, for best performance, if a length other than 100 m is targeted, the same procedure should be repeated to design a new fibre. However, for the cases I have considered, the improvement is small. For example, if a 1 km long fibre is targeted, again with a total 1st-Stokes loss of 1 dB, a similarly optimised fibre has a 1.4587 refractive index and 19.8 μm diameter core, a 112 μm diameter inner cladding, and a cut-off wavelength at 2100 nm. The inner-cladding-to-core area ratio is 32. Thus, the fibre dimensions and area ratio are very similar to the fibre optimised for 100 m.

I conclude that a W-type fibre optimised for one length works well also at other lengths, and that fibres optimised for different lengths are similar, with small differences in performance.

3.3 Core damage limitation

Core damage can also limit the area ratio, since a high pump intensity combined with a large area ratio may well lead to a 1st-Stokes intensity in the core that exceeds the material damage threshold. Thus, if a pump of intensity I_0 is launched into the inner cladding of a fibre, the area ratio must fulfil the following relation:

$$\frac{A_{cl}}{A_{co}} \leq \frac{I_1^{Max}(\tau)}{I_0 \eta}. \tag{3.19}$$

where $I_1^{\max}$ is the damage intensity (for the signal) at pulse duration τ, and η is the conversion efficiency.

The conversion efficiency may be as high as ~ 80% in lossless DCRF; here I will assume a value of 68.7%. This corresponds to a pump depletion of 2 Np (86.5%) and a total background loss of 1 dB (20.6%) for the whole DCRF. The damage threshold is assumed to be 500 W/μm^2 for 1 ns pulses, which is a value commonly adopted for bulk fused silica [14]. Furthermore, the dependence of the damage threshold on the pulse

duration is assumed to follow a square-root intensity law [15]-[16]. Thus, the area ratio limit depends on the pulse duration, too. This is shown in Figure 3.8, for different pump intensities, which correspond to different conversion (i.e., fibre) lengths, according to Eq. (3.12). The area ratio limit (= 34) resulting from the 2nd-Stokes generation for the W-type fibre designed in section 3.2.4 is shown as well. Therefore, Figure 3.8 indicates that for this fibre, it is the damage threshold rather than the 2nd Stokes that limits the area ratio for pulses longer than 20 ns with a pump intensity of 5 W/μm^2. This pump intensity allows for a maximum propagation loss of 17.5 dB/km over the resulting conversion length (57 m), if efficient operation is to be maintained (i.e., if the total propagation loss is to remain below 1 dB). If the propagation loss is higher than this, shorter fibres and higher pump intensities are required, which further limit the area ratio. For a pulse duration of 625 ns, the damage threshold for pulses reaches the commonly accepted CW damage threshold of 20 W/μm^2 [17], according to the damage equation used here. Therefore, data for 625 ns pulses, i.e., the longest duration shown in Figure 3.8, actually correspond to the CW regime.

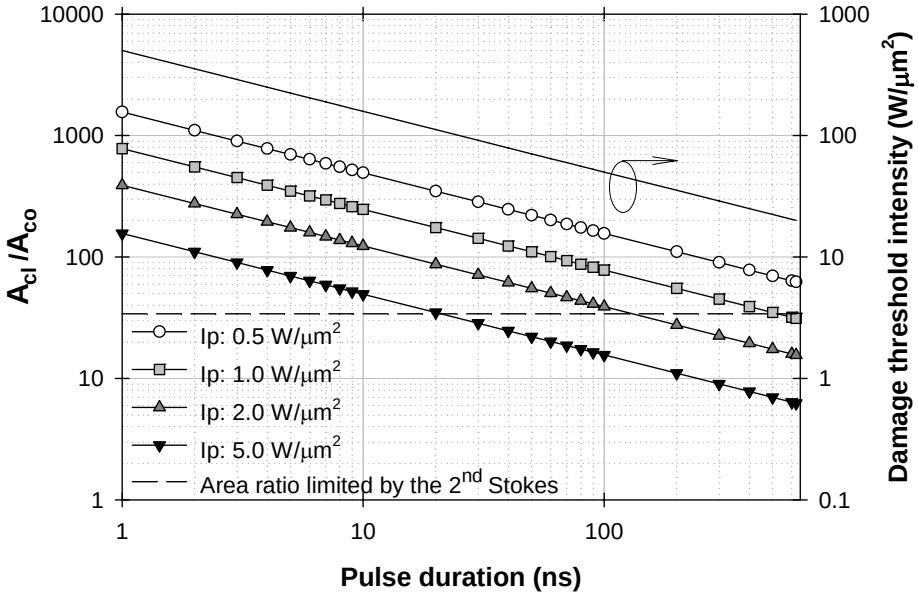

Figure 3.8: (Simulation) Area ratio limit set by damage threshold for pump intensities of 0.5 W/μm^2 (solid line with dots), 1 W/μm^2 (solid line with squares), 2 W/μm^2 (solid line with up-triangles), and 5 W/μm^2 (solid line with down-triangles). The curves are calculated according to Eq. (3.19), under the assumption of 1 dB of total loss at the 1st Stokes. This implies a maximum propagation loss of 1.7 dB/km, 3.5 dB/km, 7.0 dB/km and 17.5 dB/km for the for different pump intensities, and fibre length of 575 m, 287 m, 143 m, and 57 m. The area ratio limit of 34 set by the 2nd Stokes in a W-type fibre is shown too, (dashed line), together with the damage threshold intensity (solid line, right axis).

3.4 Pump-signal pulse walk-off limitation

We must also consider the walk-off that takes place between pulses at different wavelengths and in different modes in multimode fibres. In a CP RFA, this is important since the energy is directly transferred from the pump to the Stokes waves, so these must coincide for efficient operation. In addition, the pump and signal pulses can experience temporal broadening. These effects limit the brightness enhancement by limiting the pump-NA that can be used. The pump – signal walk-off depends on the differences in group velocities between the signal mode in the core and the pump modes in the cladding, which in turn depend on the fibre design, the material dispersion, the wavelengths, and which pump modes are excited. If the walk-off length is shorter than the fibre length needed for pump-to-signal energy transfer in the CP RFA, it will reduce the energy conversion efficiency. Here, I will only attempt an approximate analysis of this effect. For this, I consider the pulse broadening of light propagating in a multimode step-index fibre, i.e., the pump light in the cladding in our example. I will assume that the signal and pump pulses are initially temporally matched. Note that experimentally, configurations in which the signal pulses build up from a CW seed signal (or noise) are often used. Then, the pump pulses and amplified signal pulses do coincide temporally. Furthermore, since the signal is assumed to be in a single mode, I neglect dispersion of the signal pulse. For the designed DCRF, the chromatic dispersion was calculated using OptiFiber (a commercial software product). It is 30 ps/km/nm at 1660 nm. For a 3 ns pulse, the walk-off length due to chromatic dispersion is around 1 km. This is much longer than the fibre length that I am interested in. By contrast, the multimode pump pulse does broaden, through modal dispersion. The pump pulse as a whole may also walk away from the signal. However, I assume that the signal remains within the envelope of the pump pulse, i.e., that there are pump modes with higher as well as lower group velocity than the signal mode. This is typically the case. Nevertheless, the broadening of the pump pulse leads to a decrease in the pump intensity, which is assumed to be inversely proportional to the pulse duration. As before, I stipulate that for efficient conversion, this decrease should be no more than 1 dB (20%) over the length of the fibre, and thus that the pulse should broaden by no more than 25%. In a multimode step-index fibre, the pulse broadening is given by [18]:

$$\Delta\tau \approx \frac{n_{co}}{c}\left[\frac{n_{co}}{(n_{co}^2 - NA_{cl}^{\ 2})^{0.5}} - 1\right]L \tag{3.20}$$

where c is the speed of light in vacuum, and L is the device length.

From this, it is possible to solve the maximum allowable pump-NA for which the pump broadening $\Delta\tau = \tau/4$. This depends on the fibre length as well as the pulse duration. We get,

$$NA_{cl}(\tau) \approx n_{co}\sqrt{1 - \frac{1}{\left(1 + \tau\, c/(4L\, n_{co})\right)^2}}\,. \tag{3.21}$$

Note that even if the inner cladding supports a larger NA than that, it is still possible to operate with a lower pump-NA by under-filling the inner cladding.

As before, the fibre length L can be calculated according to Eq. (3.12) for different pump intensities. Equation (3.21) then limits the inner-cladding NA that can be used effectively in a pulsed cladding-pumped fibre Raman amplifier. This depends on the fibre length, and therefore, according to Eq. (3.12), on the pump intensity.

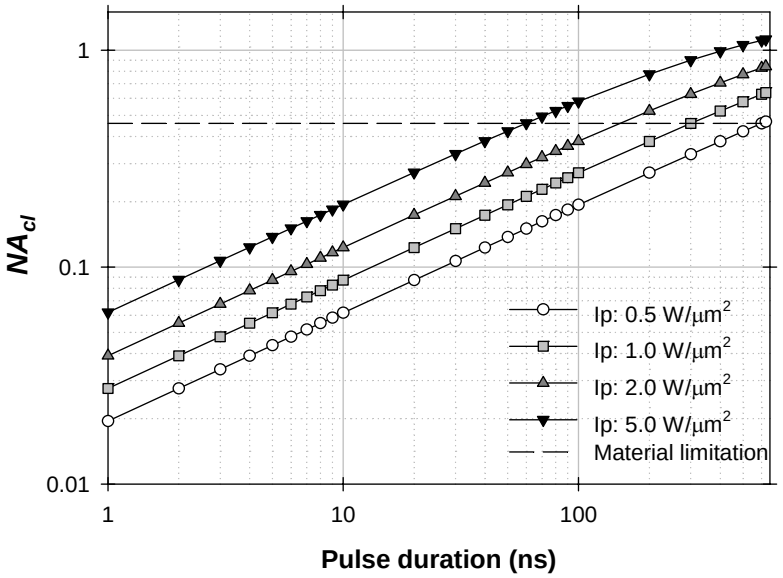

Figure 3.9: (Simulation) Pump-NA limit set by signal – pump walk-off for pump intensities of 0.5 W/μm^2 (solid line with dots), 1 W/μm^2 (solid line with squares), 2 W/μm^2 (solid line with up-triangles), and 5 W/μm^2 (solid line with down-triangles). The curves are calculated according to Eq. (3.21), under the assumption of 1 dB decrease in the pump intensity caused by pump-pulse broadening. The pump intensities correspond to fibre lengths of 575 m, 287 m, 143 m, and 57 m. The dashed line is the maximum NA of 0.46 set by typical fibre materials.

Based on this analysis, one can plot the maximum pump-NA *vs.* pulse duration for different pump intensities. See Figure 3.9. At the same time, also the refractive indices of the used materials limit the inner-cladding NA that one can use. This is also plotted

in Figure 3.9, with a value of 0.46 corresponding to the inner-cladding NA typically obtained with a pure silica inner cladding and a fluorinated-polymer outer cladding.

I have not attempted to precisely calculate the reduction in conversion efficiency that a 25% broadening corresponds to. This is complicated and depends on many factors such as the details of the shape of the pump pulse, which will vary along the fibre in the presence of modal dispersion. Furthermore, as shown in the next chapter, the impact on the conversion efficiency of the pulse shape depends on the area ratio.

3.5 Brightness enhancement limits

The limits on the area ratio set by the parasitic 2nd Stokes and by optical damage, combined with the limit on the inner cladding NA set by materials and walk-off, determine the brightness enhancement one can achieve. This can be expressed as below,

$$\frac{B_{out}}{B_{in}} = \frac{P_1(L)/(\pi NA_{co}^2 A_{co})}{P_0(0)/(\pi NA_{cl}^2 A_{cl})} \approx \eta\left(\frac{A_{cl}}{A_{co}}\right)\left(\frac{NA_{cl}}{NA_{co}}\right)^2 = \eta\left(\frac{\lambda_0}{\lambda_1}\frac{V_{cl}}{V_{co}}\right)^2 \tag{3.22}$$

where B_{out} and B_{in} are the signal output and pump input brightnesses, respectively, and $P_1(L)$ is the signal output power in the core (1st-Stokes power), while the input pump power $P_0(0)$ is launched into the core and inner cladding. Furthermore, V_{cl} and V_{co} are the V-numbers of the inner cladding and core. If the signal is assumed to be always single-moded, equation (3.22) can be simplified as below,

$$\frac{B_{out}}{B_{in}} \approx \eta\left(\frac{\lambda_0}{\lambda_1}\right)^2 \frac{4}{\pi^2} V_{cl}^{\ 2}. \tag{3.23}$$

Here, I have used that the number of pump modes guided by a step index fibre is given approximately by $4V^2/\pi^2$ [19]. Note that this approximation is valid for large V-number. Thus, the brightness calculated by Eq. (3.23) will be slightly different from the result by Eq. (3.22). For the example given in section 2.3, the brightness enhancement is 354,000 instead of 246,000 for the YDFL. For the W-type fibre with 18 μm core diameter treated in section 3.2.4, one can now calculate the maximum brightness enhancement achievable in a pulsed CP RFA based on Eq. (3.1) – Eq. (3.23). This is plotted in Figure 3.10, against the pulse duration under different pump intensities for three different inner-cladding NAs. In Figure 3.10(a), the inner-cladding NA is 0.22, which is typical for low loss all-glass fibre. In Figure 3.10(b) the inner-cladding NA is 0.46, which is typical in case of a low-index polymer outer cladding. Finally, in Figure 3.10(c) the

inner-cladding NA is 0.82, which can be achieved with jacketed air-clad fibres [20]. For shorter pulse duration, pulse walk-off limits the brightness enhancement, while for longer pulses duration core damage sets the limit. In Figure 3.10(a), with a material-limited pump-NA of 0.22, the central flat section occurs when the 2nd-Stokes generation rather than damage, limits the area ratio and the fibre materials rather than walk-off limit the pump-NA. With the higher NAs treated in Figure 3.10(b), this limit is never reached. Thus for well-design DCRF with 0.46 inner-cladding NA and background loss of f 3.5 dB/km, I find a maximum brightness enhancement factor of 2000. For jacketed air-clad fibres, the brightness enhancement factor can be as high as 3500.

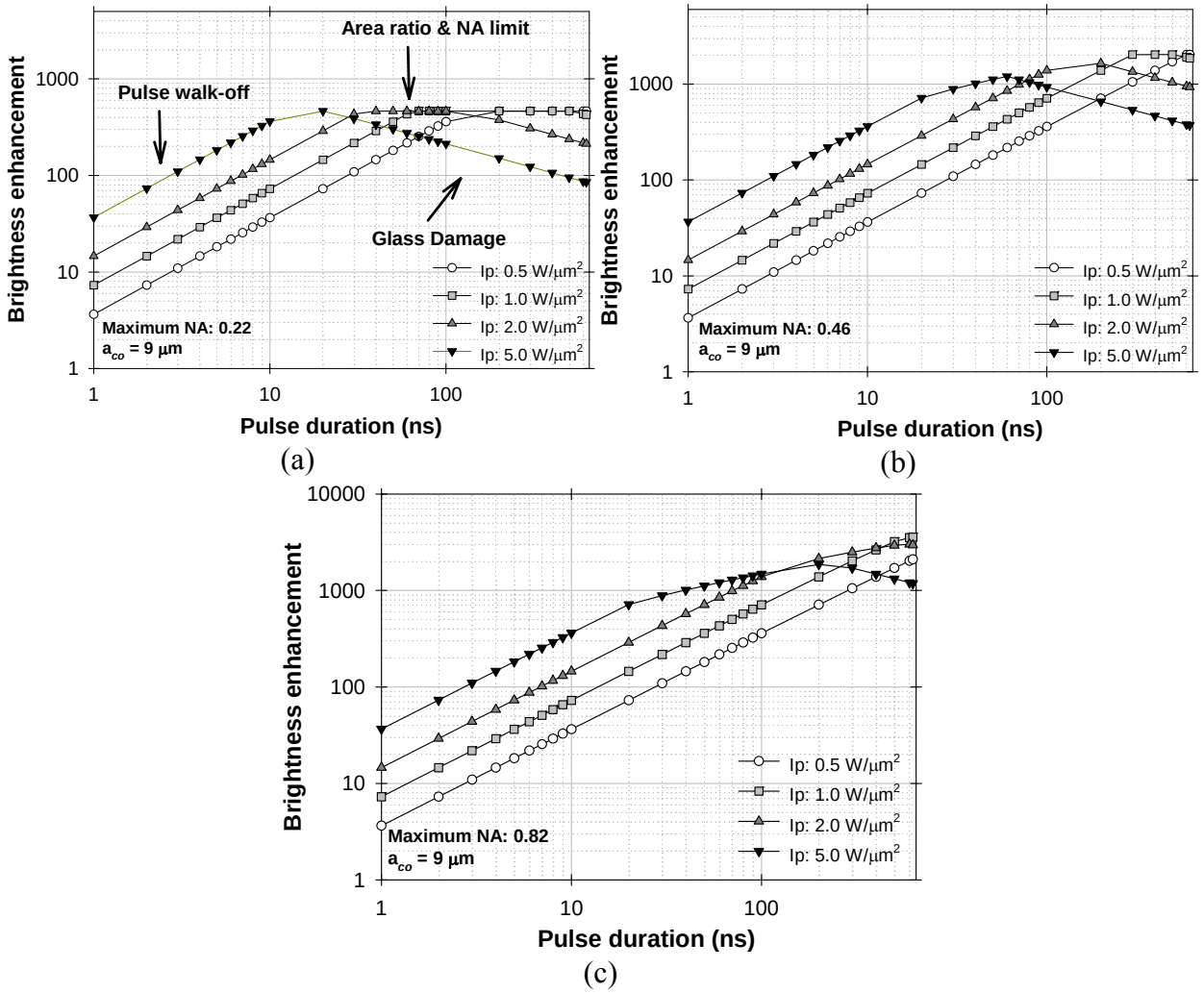

Figure 3.10: (Simulation) Limits on brightness enhancement *vs*. pulse duration for fibres with pump-NAs (as determined by the fibre materials) of 0.22 (a), 0.46 (b), and 0.82 (c). The fibre has an optimized W-type core of 18 μm diameter. Four different pump intensities are considered: 0.5 W/μm^2 (solid line with dots), 1 W/μm^2 (solid line with squares), 2 W/μm^2 (solid line with up-triangles, and 5 W/μm^2 (solid line with down-triangles).

3.6 Summary

In this chapter, I have analysed limits on brightness enhancement in efficient cladding-pumped fibre Raman amplifiers. One limit arises from the appearance of the 2nd Stokes, if the inner-cladding-to-core area ratio is too large. I propose a fibre design with a W-type core, which provides a spectrally sharp bend loss that helps to suppress the 2nd Stokes. The designed fibre has an 18 μm diameter core and a 105 μm diameter inner cladding, corresponding to an inner-cladding-to-core area ratio of 34. This should allow for the use of pump sources with relatively poor beam quality (e.g., $M^2 = 12$ in case of an all-glass fibre and pump wavelength at 1550 nm). Most types of pump lasers would have beam qualities better than that, with the exception of low-brightness diode lasers.

I have also analysed the limit induced by optical damage in the pulsed regime, and relate it to the propagation loss of the Raman fibre. Again, this limits the area ratio that can be used. Finally, I considered the effect of walk-off between the pump modes and the signal mode, and show that this is the dominant limitation factor in the short-pulse regime (i.e., 10 ns or less).

The brightness enhancement achieved is considerably better than experimental results for efficient CP FRA, and points to the potential for significant further improvements with the right pump source matched to the right fibre.

3.7 Reference

[1] G. P. Agrawal, *Nonlinear Fiber Optics*, 3rd Ed., Academic Press Inc, San Diego CA (2001).

[2] J. Nilsson, J. K. Sahu, J. N. Jang, R. Selvas, D. C. Hanna, and A. B. Grudinin, "Cladding-pumped Raman fiber amplifier," in Proc. of Optical Amplifiers and Their Applications (OAA 2002) Vancouver, Canada 14-17 Jul. 2002, paper PD2-1/2/3 (Postdeadline).

[3] C. A. Codemard, J. K. Sahu, and J. Nilsson, "Cladding-pumped Raman fiber amplifier for high-gain high-energy single-stage amplification", in Proc. of OFC, Anaheim, CA, USA 6-11 March 2005, paper OutF5.

[4] J. Ji, C. A. Codemard, M. Ibsen, J. K. Sahu, and J. Nilsson, "Analysis of the conversion to the first stokes in cladding-pumped fiber Raman amplifiers", IEEE J. Sel. Top. Quan., **15**(1), 129 (2009).

[5] A. Shirakawa, C. A. Codemard, J. Ji, K. K. Chen, A. Malinowski, D. J. Richardson, J. K. Sahu, and J. Nilsson, "High-brightness 210 micron J pulsed Raman fiber source", in Proc. of Conf. Lasers and Electro-Optics /QELS, San Jose 4-9 May 2008, paper CTuL1.

[6] A. K. Sridharan, J. E. Heebner, M. J. Messerly, J. W. Dawson, R. J. Beach, and C. P. J. Barty, "Brightness enhancement in a high-peak-power cladding-pumped Raman fiber amplifier", Opt. Lett., **34**(4), 2234 (2009).
[7] J. Kim, P. Dupriez, C. Codemard, J. Nilsson, and J. K. Sahu, "Suppression of stimulated Raman scattering in a high power Yb-doped fiber amplifier using a W-type core with fundamental mode cut-off", Opt. Express, **14**(12), 5103 (2006).
[8] M. Monerie, "Propagation in doubly clad single-mode fibers", IEEE Trans. Microw. Theory Tech., **30**(4), 381 (1982)
[9] L. G. Cohen, D. Marcuse, W. L. Mammel, "Radiating leaky-mode losses in single-mode lightguides with depressed-index claddings", IEEE Trans. Microw. Theory Tech., **30**(10), 1455 (1982).
[10] P. Even, D. Pureur, "High power double clad fiber lasers: a review", in Proc. of SPIE, 4638, 1 (2002).
[11] D. Marcuse, "Influence of curvature on the losses of doubly clad fiber", Appl. Optics, **21**(23), 4208 (1982)
[12] J. Limpert, N. Deguil-Robin, I. Manek-Hönninger, F. Salin, F. Röser, A. Liem, T. Schreiber, S. Nolte, H. Zellmer, A. Tünnermann, J. Broeng, A, Petersson, and C. Jacobsen, "High power rod-type photonic crystal fiber laser", Opt. Express, **13**(4), 1055 (2005).
[13] M. E. Fermann, "Single-mode excitation of multimode fibers with ultrashort pulses", Opt. Lett., **23**(1), 52 (1998).
[14] M. Y. Cheng, Y. C. Chang, A. Galvanauskas, P. Mamidipudi, R. Changkakoti, and P. Gatchell, "High-energy and high-peak-power nanosecond pulse generation with beam quality control in 200-μm core highly multimode Yb-doped fiber amplifiers", Opt. Lett., **30**(4),358 (2005).
[15] A.-C. Tien, S. Backus, H. Kapteyn, M. Murnane, and G. Mourou, "Short-pulse laser damage in transparent materials as a function of pulse duration", Phys. Rev. Lett., **82**(19), 3884 (1999).
[16] B. C. Stuart, M. D. Feit, S. Herman, A. M. Rubenchik, B. W. Shore, and M. D. Perry, "Nanosecond-to-femtosecond laser-induced breakdown in dielectrics", Phys. Rev. B, **53**(4), 1749 (1996).
[17] J. Nilsson, J. K. Sahu, Y. Jeong, W. A. Clarkson, R. Selvas, A. B. Grudinin, and S-U, Alam, "High power fiber lasers: new developments", in Proc. of SPIE, 4974, 50 (2003).
[18] A. W. Snyder and J. D. Love, *Optical Waveguide Theory*, Kluwer Academic Publishers (2000).
[19] B. E. A. Saleh and M. C. Teich, *Fundamentals of Photonics*, Wiley & Sons, Inc. (2007).
[20] J. K. Sahu, C. C. Renaud, K. Furusawa, R. Selvas, J. A. Alvarez-Chavez, D. J. Richardson, and J. Nilsson, "Jacketed air-clad cladding pumped ytterbium-doped fibre laser with wide tuning range", Electron. Lett., **37**(18), 1116 (2001).

Chapter 4 High conversion efficiency CP RFA

The efficiency is a concern for any laser and amplifier. While it is important throughout this thesis, for example through its link with brightness enhancement and pump beam quality requirements as discussed in chapter 3, this chapter presents work which explicitly targeted a high efficiency CP RFA. For this I used F71-LF11 (the same fibre as considered in section 2.5) as the DCRF and a multimode Er:Yb co-doped fibre MOPA generating pulses of 20 ns duration at around 1.55 μm as the Raman pump source. A fibre Raman ring laser emitting at around 1.66 μm acted as a Raman seed, which was then amplified in the DCRF. A peak power conversion into the 1st Stokes of over 75% was obtained, while the pulse energy conversion efficiency exceeded 60%. I will also consider the limitations on the conversion efficiency into the 1st Stokes and options for improving the performance of such devices, based partly on the discussions in chapter 3.

4.1 Introduction

For a CP RFA working in the pulsed regime, the average power or energy conversion efficiency into the 1st Stokes is limited by several factors, such as background loss, pulse shape, and walk-off. For example, in [1]-[2], the average power conversion efficiency obtained in the fibre F71-LF11 from the pump at around 1550 nm to the 1st Stokes was ~ 36%. This is because a relatively long piece, ~ 900 m, was utilised in the experiments. Such a long piece led to a relatively high total background loss, which limits the conversion efficiency. This can be improved by using a shorter fibre with lower total loss. In later work by me and my colleagues [3]-[4], with the same fibre, the energy conversion was higher than 50% since the fibre length in these experiments was one order of magnitude shorter than that in [1]-[2]. The simulations shown in Figure 2.3 also illustrate that the background loss in a DCRF limits the power conversion efficiency from the pump into the 1st Stokes. In another experiment [5], the energy conversion efficiency into the 1st Stokes was only 6.6%. The fibre used in this

experiment was a commercial fibre with an inner-cladding-to-core area ratio ~ 32. Such a large area ratio limits the conversion efficiency from the pump to the 1st Stoke due to the 2nd-Stokes generation [3]. As I discussed in section 3.2, inner-cladding-to-core area ratios larger than eight degrade the conversion efficiency into the 1st Stokes in the absence of a spectral filter.

In this chapter, these issues are discussed in detail, in conjunction with experiments on a pulse-pumped CP RFA. Special attention is paid to the conversion efficiency from the Raman pump to the 1st Stokes.

4.2 Double-clad Raman fibre: F71-LF11

The DCRF F71-LF11 is used in experiments in both this and the next chapter. It was also used in several publications, e.g., [1]-[4], [6]-[8]. The fibre was fabricated by Dr. Jayanta Sahu in the Silica Fibre Fabrication group at ORC through the MCVD process. A careful investigation of the fibre properties is needed to understand how it works as a CP Raman fibre converter. Next I will describe the details of this fibre.

4.2.1 Refractive index profile

This fibre comprises a pure-silica outer cladding and germanium-doped silica inner cladding and core. They are circularly shaped and concentric. Outside the outer cladding, there is a polymer coating to protect the fibre. The coating has a high refractive index so that the outer cladding does not guide light. Thus the fibre F71-LF11 has a so-called all-glass structure for guiding light, with neither pump nor Stokes wave in contact with the polymer coating. The NAs are 0.22 for the inner cladding (relative to the outer cladding) and 0.14 for the core (relative to the inner cladding). A picture and an idealised RIP of this DCRF are shown in Figure 4.1. In this, the core and inner- and outer-cladding diameters are 9 μm, 21.6 μm, and ~ 100 μm, respectively. However, the diameters vary along the length of the fibre. The fibre used in this chapter has a 7.7 μm diameter core and an 18.6 μm diameter inner cladding.

The refractive index has a dip in the centre due to the evaporation of germanium during preform collapse. This can be seen in Figure 4.2, which shows the RIP of the fibre F71-LF11 as measured by Mr. Robert Standish in ORC's Silica Fibre Fabrication group. The dip does affect the mode distribution, but not the principle of CP Raman fibre devices. The beam quality of the fundamental mode may be degraded due to the

existence of the dip. The M2 of the fundamental mode in the core was calculated to be 1.18 at 1660 nm. Besides, the Raman gain coefficient is lower in the fibre centre. This may affect the performance of devices based on this fibre. However, I found that this fibre worked well in my experiments, and generally I believe that the effects of the dip would be difficult to discern experimentally. Although there is a degree of subjectivity due to the gradual transition from core to inner cladding, the cut-off wavelength is estimated to 1645 nm for the core. Therefore, the fibre core will be slightly multimoded at a pump wavelength of around 1550 nm, but single-moded at the 1st-Stokes wavelength.

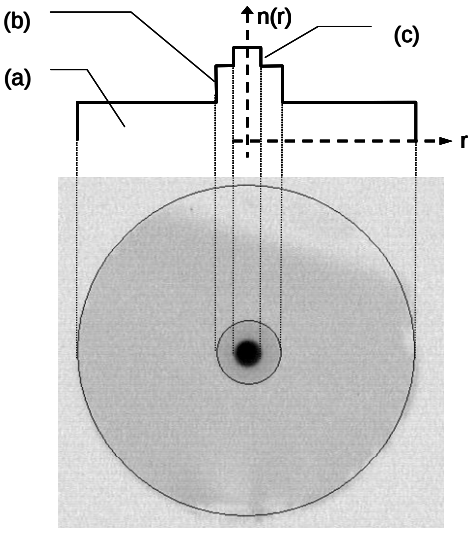

Figure 4.1: Image of cross-section of DCRF F71-LF11 with idealized RIP and cross-section: (a) outer cladding (silica); (b) inner cladding (germanium-doped silica); (c) core (germanium-doped silica).

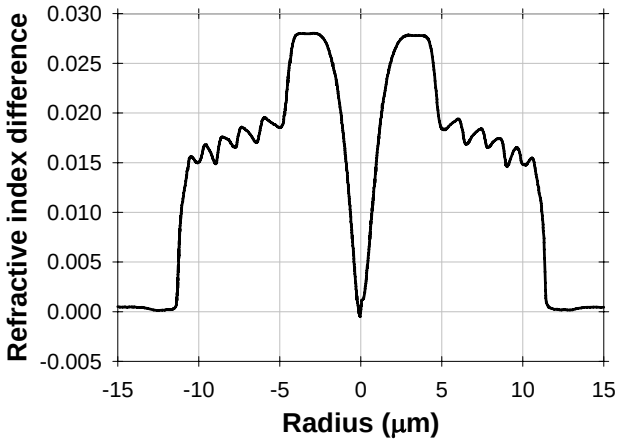

Figure 4.2: Measured refractive index profile of F71-LF11.

4.2.2 Background loss

The background loss of a 484.5 m long piece of this fibre was characterised with a conventional cutback measurement that employed a white light source (WLS) and an ANDO optical spectrum analyser (OSA). When the background loss in the core was measured, a 1 m long SMF was spliced to the one end of the DCRF. The other end of the DCRF was connected to the OSA. The cut-off wavelength of the SMF is around 1200 nm. For longer wavelengths for which the SMF only supports one spatial mode, with careful splicing, primarily the fundamental core-mode will be excited. However at

shorter wavelengths, there will be more power in higher-order modes, although primarily within the core of the DCRF.

Interference becomes an issue when multiple modes are excited. Multimode interference effects can be detected by moving the fibre around and watching for power drifts or by looking for beats in the transmission spectrum. They can be avoided by using a sufficiently large optical bandwidth for the measurement. In case of F71-LF11, the effective-index spacing between modes is typically 0.001, which leads to an optical pass difference (OPD) of 484.5 mm in a 484.5 m long fibre and beating with a wavelength periodicity of 0.8 pm at 1550 nm. That is below the resolution of an OSA but above the linewidth of a conventional tuneable laser diode. For shorter fibres, e.g., after the fibre is cut back, the periodicity will be much greater and may well be resolvable by an OSA. The WLS beam was free-space launched into the SMF. The transmission spectra from the output of DCRF were recorded by the OSA both before and after the DCRF was cut back to a length of 1.5 m. By comparing the two spectra, the background loss spectrum in the core can be obtained. Figure 4.3 shows the result. We see also that there is no beating in the spectrum. By repeating the cut-back method without the SMF, the background loss for light propagating within the inner cladding (including the core) was measured as the black curve in Figure 4.3. The background losses at 1550 nm are 1.61 dB/km in the core and 1.39 dB/km in the inner cladding. Based on the RIP of this fibre, the germanium concentration is estimated to be 25% to 30% (mol). The reported background loss in 30% (mol) GeO_2-doped fibre is around 1.33 dB/km at 1550 nm [9]-[10]. The background loss measured in our fibre is very close to the reported value. It is also lower than what was previously reported for this fibre [1]-[2], for unknown reasons.

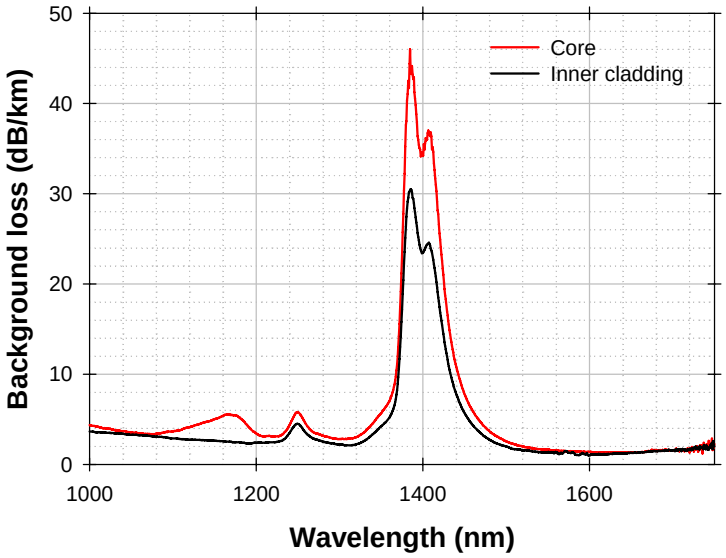

Figure 4.3: Background loss spectra in the core (red curve) and inner cladding (black curve) of DCRF F71-LF11.

4.2.3 Raman gain coefficient

We can estimate the Raman gain coefficient based on the refractive index difference shown in Figure 4.2 between the pure-silica outer cladding and GeO_2-doped inner cladding and core [11]-[13]. At 1550 nm, the Raman gain coefficient is estimated to 5.29×10^{-14} m/W in the inner cladding and 6.34×10^{-14} m/W in the core for unpolarised light.

4.2.4 Mode excitation

Based on the RIP in Figure 4.2, the effective index was calculated for different modes at different wavelengths using commercial software (OptiFiber™ from Optiwave™). The RIP was scaled to match the size of the fibre used here. At 1545 nm, there are 12 linearly polarised (LP) fibre modes in this fibre, two of which are core-modes. These modes are split into 2 or 4 modes if polarisation-degenerate and sine and cosine modes are considered. The effective indexes of all modes at 1545 nm are shown in Figure 4.4.

The mode distributions at 1545 nm were calculated with the same software. From these distributions, the overlaps between different modes have been obtained according to Eq. (2.14). The result is shown in Figure 4.5. Note that higher-order modes with non-circularly symmetry, e.g., $LP_{l,m}$ modes with $l\neq0$, can be degenerate with a sine and cosine mode. Here, the degenerate modes are supposed to be equally excited. The overlap is taken as the average of both cases. Maybe other treatments of the degeneracy

are possible, but the approach used here is correct for the calculations in this thesis. Depending on the involved modes, the overlap varies and is in general larger for low-order modes than for high-order modes. Later, the overlaps between pump modes and signal modes are approximated by the values given here. The signal wavelength is very close to the pump wavelength, and thus, the signal mode distribution is slightly different from pump mode distribution.

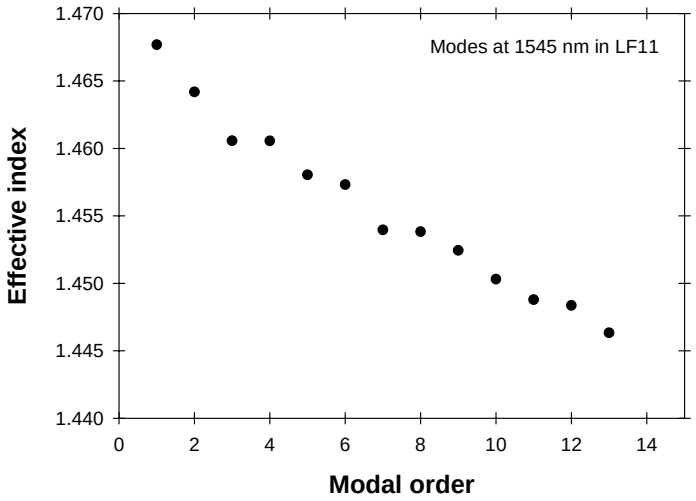

Figure 4.4: (Simulation) Effective index of modes at 1545 nm in the DCRF F71-LF11.

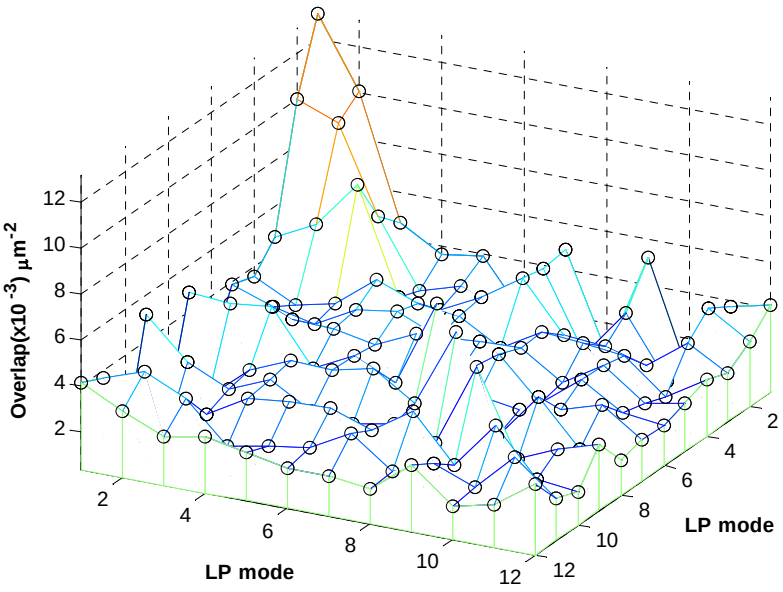

Figure 4.5: (Simulation) Overlaps between various modes at 1545 nm.

A modelling example of a single-stage CP RFA is given in Figure 4.6 to illustrate how a multimode Raman pump is converted into a diffraction-limited Raman signal through a DCRF converter. This is similar to the example in section 2.5 and

section 3.2.1, except that this now treats the pump and signal power in different modes, and no longer assumes that the pump power is evenly distributed across the inner cladding in each transverse cross-section of the DCRF. A Raman seed beam at 1660 nm and a pump beam at 1545 nm are launched into the same end of a 100 m DCRF F71-LF11 and propagate in the same direction along the fibre. The total Raman seed power is set to 25 mW. To demonstrate how the fundamental core-mode can get amplified and extract most pump power than high-order modes do, two modes LP_{01} and LP_{02} at the 1st-Stokes wavelength are supposed to be equally excited at the input. The total launched Raman pump power is assumed to be 1 kW. All pump modes are supposed to be equally excited. The resulting power ratio between different pump modes is listed in Table 4.1, taking the degeneracy of the modes into account. Note that the overlap values given in Table 4.1 were calculated between various modes at the pump wavelength. Nonetheless, they are only slightly different from the overlaps between pump modes and signal modes since their wavelengths are quite close to each other. Furthermore, the pump and Stokes mode coupling mechanisms are not taken into account. Walk-off is assumed not important either in this case. Besides, only Stokes with orders below the 2nd order is considered.

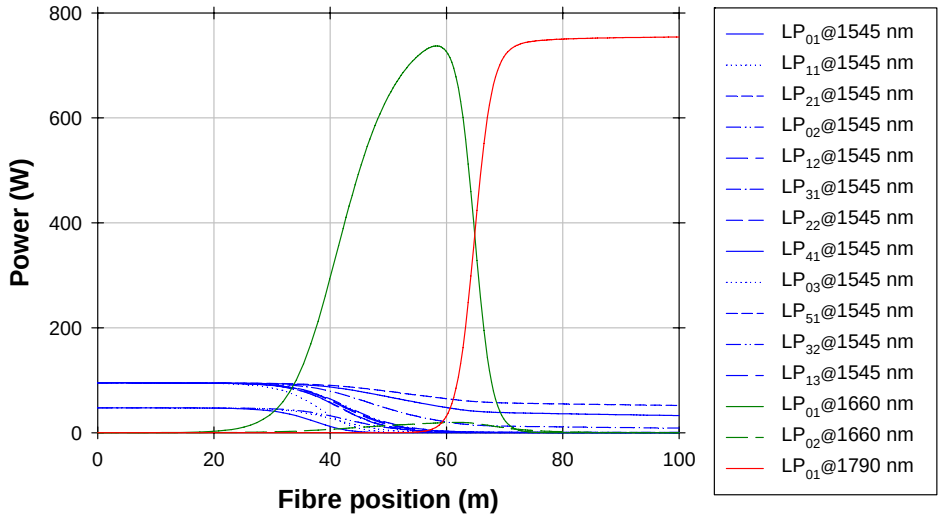

Figure 4.6: (Simulation) Simulation of a single-stage co-pumped CP RFA with a 100 m long DCRF F71-LF11. Blue curves: pump wave; Green curves: 1st Stokes; Red curve: 2nd Stokes.

Table 4.1: Overlaps between interacting modes and relative power among pump modes.

	Relative power	LP_{01} ($\times 10^{-3}$ μm^{-2})	LP_{02} ($\times 10^{-3}$ μm^{-2})
LP_{01}	1	13.17	3.61
LP_{11}	2	10.06	2.72

LP_{21}	2	4.69	3.07
LP_{02}	1	3.61	4.46
LP_{12}	2	3.88	3.78
LP_{31}	2	1.59	3.59
LP_{22}	2	4.83	2.53
LP_{41}	2	0.66	3.51
LP_{03}	1	5.16	3.37
LP_{51}	2	0.34	3.18
LP_{32}	2	3.68	1.71
LP_{13}	2	4.11	2.78

Based on the overlaps and initial conditions given above, the equations Eq. (2.24) – Eq. (2.26) can be numerically solved and Figure 4.6 shows the calculated results. First of all, we see that almost all of the pump power is effectively converted into the 1st Stokes despite the variation in overlap between different pump modes and the Stokes modes. Besides, the pump modes are converted into the 1st Stokes at approximately the same position, i.e., where the 1st-Stokes power reaches levels for depletion to occur. Thus, if a fibre length is well chosen, a high efficiency such device will be achievable. The conversion efficiency of 74% at the optimum length can be compared to the 84% obtained in section 2.5. Furthermore, the LP_{01} mode sees a higher Raman gain at the 1st Stokes than the LP_{02} modes does, and converts most of pump power along the fibre. In contrast, the power of LP_{02} mode remains low all along the fibre. Therefore, at the output, the signal beam is (nearly) diffraction limited. A key reason why most of pump power is Raman-scattered into the LP_{01} mode is that the LP_{01} mode has a smaller average effective area with the pump modes (234 μm^2) than the LP_{02} mode (322 μm^2). The other reason is that the higher Raman gain coefficient in the core area favours the generation of the core-modes. Thus, the simulations suggest that this fibre can automatically select the fundamental mode at the Stokes wavelength. In addition, if even better mode selection is required, one can ensure that only core-modes (or only the fundamental mode) at the Stokes wavelength are excited at the fibre input, through careful adjustment of the launch.

Also, the pump launch and the resulting pump power distribution are important since they determine the transverse Raman gain profile. While all pump modes are assumed to be equally excited in Figure 4.6, pump modes that cannot effectively transferred energy into the 1st Stokes, e.g., LP_{41} and LP_{51}, can be less excited by adjusting the pump launch, if the pump beam quality is sufficiently good for selective pump-mode excitation. This can further improve the conversion efficiency.

The simulation presented here shows theoretically that a DCRF can work efficiently as a CP Raman converter and transfer power into the diffraction-limited signal from a multimode pump source, even when some pump modes have much weaker overlap with the core than others, and even though coupling of pump modes was neglected. This is a worst-case scenario in that coupling of pump modes will negate the differences between the pump modes and therefore increase the efficiency. Next, I will present experimental results on a high efficiency CP RFA.

4.3 High efficiency CP RFA

4.3.1 Multimode Raman pump

For these experiments, the pump source was a three-stage MOPA (master oscillator – power amplifier) system as shown in Figure 4.7. The oscillator was a Tunics Plus tuneable laser source (TLS) directly modulated by shaped pulses from a dual-channel arbitrary waveform generator (AWG, Tektronix AFG 3102). The pulse duration from the AWG was 20 ns and the PRF was fixed at 100 kHz. The pulses were then first amplified in a core-pumped EDFA. An acousto-optic modulator (AOM) was inserted at the output of the first amplifier to suppress unwanted amplified spontaneous emission between pulses. The AOM was also controlled by the AWG and synchronized with the oscillator modulation. Then two cladding-pumped Er:Yb co-doped fibre amplifiers (EYDFAs) were used to further increase the peak power of the pump pulses. The first EYDFA was an early prototype amplifier from SPI Lasers capable of delivering 1 W of average power. The final amplification stage was a custom-built end-pumped EYDFA based on a 7.5 m long D-shaped DCF made in house with fibre number F402-LF122.

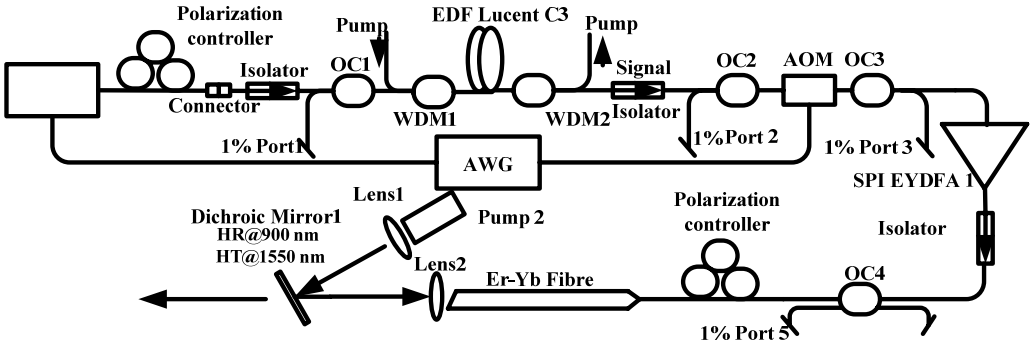

Figure 4.7: Experimental setup of pulsed MOPA emitting at 1550 nm acting as the Raman pump.

The fibre has a 27 μm diameter core with a numerical aperture of 0.22. Therefore with a V-value of ~ 12 at 1550 nm the fibre is multimoded. The beam propagation factor (M^2) was measured to 3.5 at the output of the pump source. The average output power was 1.27 W, corresponding to about 670 W peak power as shown in Figure 4.8. The inset of this plot shows the output spectrum at 1.27 W average output power. The conversion efficiency was low for the last stage of the pump MOPA since this was not optimised for high conversion efficiency. Especially the wavelength of the 3rd-stage pump diode was below 900 nm. This leads to insufficient pump absorption even in this 7.5 m long fibre. The pump absorption is ~ 0.55 dB/m at 900 nm in the fibre F402-LF122. Several 1% taps were used in the setup to monitor signal between amplifiers and the overall MOPA performance. The peak output power was limited by stimulated Brillouin scattering (SBS). SBS can be avoided with shorter pulse duration, and is generally considered to be completely suppressed for pulses shorter than a few nanoseconds. Unfortunately, I did not have an AWG with sufficient bandwidth for shaping of such short pulses, and the bandwidth of the TLS and the rest of the circuitry may well have been insufficient for shorter pulses, too. The oscillator pulses were shaped in order to obtain nearly rectangular pulses at the output of the pump MOPA, even in the presence of some distortion from gain compression [14]. Since SRS is a nearly instantaneous process which depends on the instantaneous power, rectangular pulses make the Raman conversion more efficient [15]. Figure 4.9 illustrates the pulse evolution along the MOPA at 0.56 W average output power. The output pulses of the Raman pump are nearly rectangular, and remain so even for the lowest (0.37 W) and highest output power (1.27 W) later used for Raman pumping. The power variation across the pulse top was smaller than ±5%.

This formed the multimode pulsed pump source.

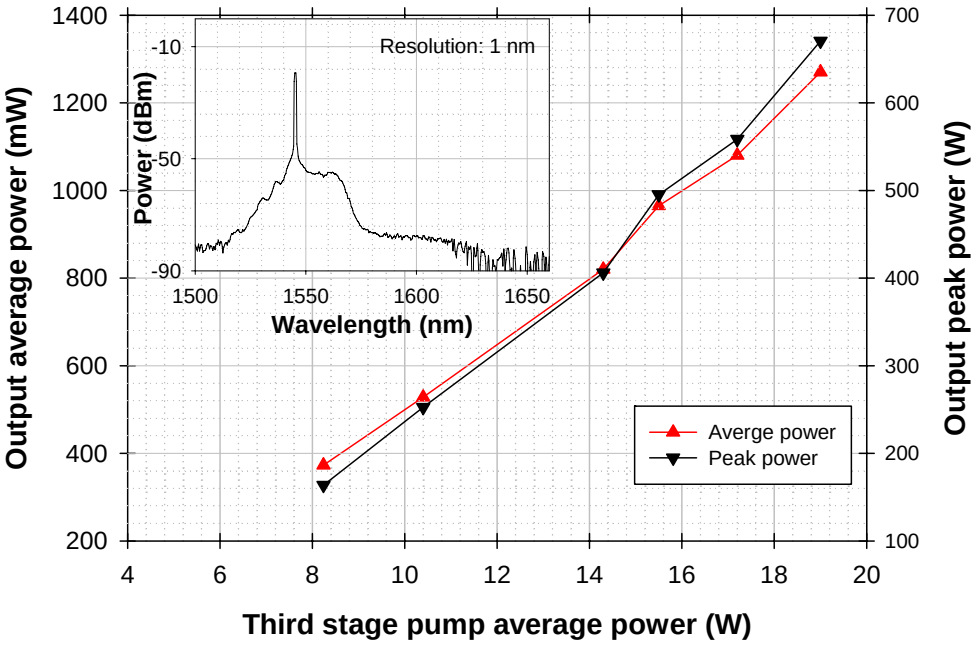

Figure 4.8: Output average (red curve) and peak powers (black curve) of the Raman pump MOPA *vs*. the 3rd-stage pump average power. Inset: output spectrum at 1.27 W output average power.

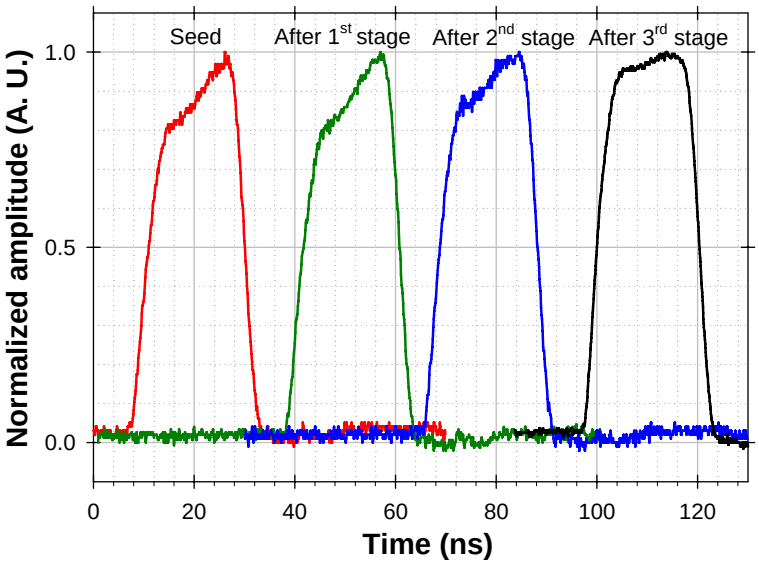

Figure 4.9: The evolution of the Raman pump pulse shapes along the MOPA at 0.56 W output average power.

4.3.2 Diffraction-limited CW Raman seed laser

I constructed a CW ring-cavity RFL at 1.66 μm to be used as a seed for the RFA. Figure 4.10 shows the setup. The 1.66 μm Raman seed laser was pumped by a CW EYDFL, also in a ring-cavity configuration and tuned to emit at 1.55 μm. The output from the 1.55 μm EYDFL was launched into a 2 km long highly nonlinear fibre (HNLF) from

Sumitomo (Part number: HNRAC-2) via a wavelength division multiplexer (WDM). The residual pump exited the Raman laser cavity through another WDM. This prevented the pump light from reaching an isolator inserted into the cavity. This isolator designed for wavelengths around 1550 nm, ensured uni-directional signal propagation in the opposite direction of the pump. Finally, the generated light at 1.66 μm was out-coupled by a 3 dB coupler. Another 1550 nm isolator at the laser output helped to stabilise the 1.66 μm seed laser, by isolating the Raman laser from the CP RFA. The operating wavelength of the 1.66 μm Raman seed could be tuned by changing its pump wavelength which was determined by a filter (JDS Uniphase TB9266) in the EYDFL. The tuning range of this filter was from 1.46 μm to 1.57 μm and the 3-dB bandwidth is 0.55 nm. During my experiments, it was normally set around 1.55 μm in order to make the Raman seed laser operate at 1.66 μm.

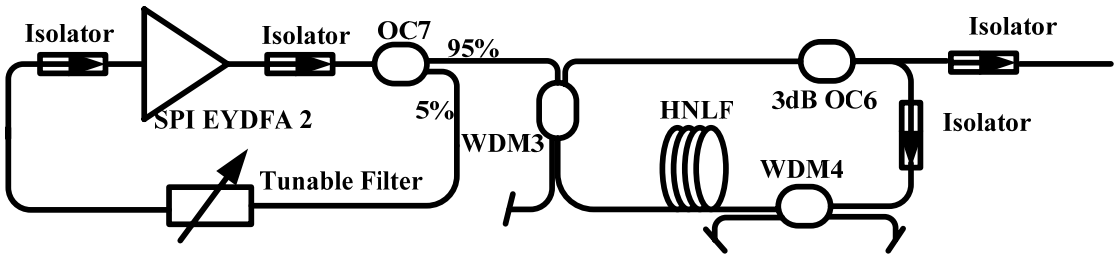

Figure 4.10: Experimental setup of the 1660 nm diffraction-limited CW Raman seed laser. OC: optical coupler; WDM: wavelength division multiplexer.

Figure 4.11 shows the dependence of the output power of the 1.66 μm Raman seed laser on the pump power. The output spectrum is also shown in the inset at a pump power of 690 mW. During this characterisation, the tuneable filter was set to 1548 nm. As shown in Figure 4.11, the threshold was about 130 mW for the Raman ring-cavity laser. The Raman gain coefficient (g_{co}) / effective area (A_{eff}) product and transmission loss were 6 km^{-1} W^{-1} and 0.6 dB/km, respectively, according to the manufacturer's data. The cavity loss was estimated to about 5 dB based on the splice, component, and fibre loss. The threshold should be:

$$P_{threshold} = \frac{L_{cavity}}{4.343(g_{co} / A_{eff})L_{eff}} \qquad (4.1)$$

where L_{cavity} is the cavity loss in decibels, and L_{eff} is the effective length. The calculated threshold is about 110 mW, in good agreement with the measured threshold. The maximum 1st-Stokes output power from the Raman ring-cavity laser was 483 mW, which was limited by the available pump power. From the black curve in Figure 4.11,

the conversion efficiency into the 1st Stokes decreased with pump power over 700 mW. One possibility is that the 2nd Stokes was generated and caused the roll-off. This would not necessarily be seen at the output, depending on the spectral characteristics of the WDMs and isolators, although the insertion loss of the isolator was not measured. A high 2nd-Stokes insertion loss also leads to the higher threshold for the 2nd Stokes according to Eq. (4.1). In simulations, no 2nd Stokes was generated, and the simulation results matched the experimental ones for pump powers below 700 mW. The simulations are given in a red curve in Figure 4.11. It is not clear why the experimental output power is lower than the simulated one for pump powers over 700 mW, but this is of no practical importance. The laser linewidth broadening which occurred for pump powers over 700 mW (See inset of Figure 4.11.) could be more important. This may be induced by self-phase modulation (SPM). The nonlinear coefficient γ is about 10 W^{-1} km^{-1} at 1550 nm for the HNLF, which leads to a nonlinear length of 2 km at the output signal power of 100 mW. This is estimated under the assumption that the signal power increases linearly with propagation distance inside the laser cavity. Above this power, SPM becomes increasingly important and gradually roadens the linewidth. However, during my experiments, the Raman seed power was always below 300 mW, which made the linewidth broadening unimportant, according to Figure 4.11.

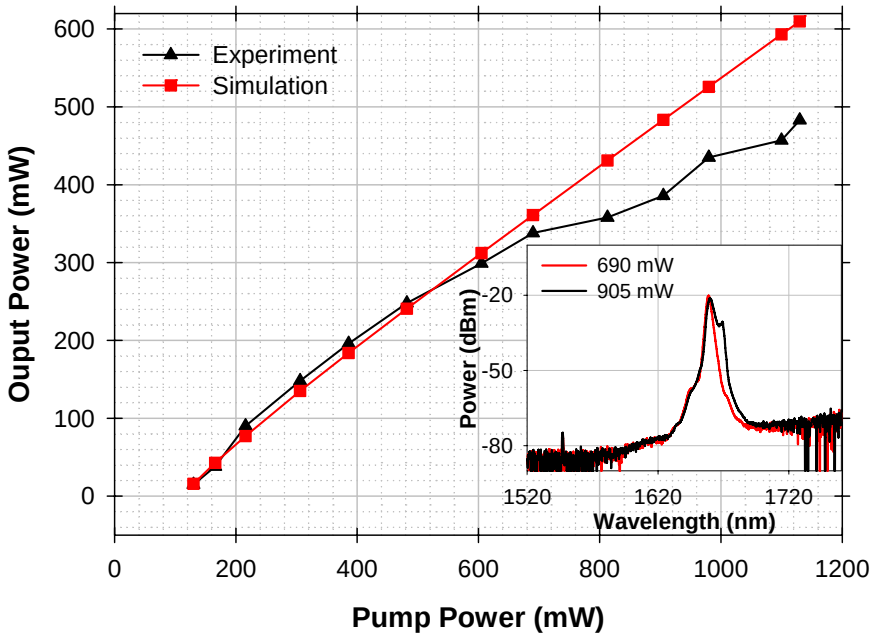

Figure 4.11: Output power at around 1.66 μm from the Raman seed laser according to simulations (red curve with squares) and experiments (black curve with triangles) *vs*. pump power. Inset: Optical output spectrum for a pump power of 690 mW and 905 mW. The OSA resolution was set to 1 nm.

4.3.3 Experiments and discussion

I used the Raman pump and seed lasers together with the DCRF for cladding-pumped Raman amplification experiments. A schematic of the experimental setup is shown in Figure 4.12. The DCRF was 89 m long. One end was spliced to another section of the DCRF of negligible length with a FBG written in it at ORC by Dr. Morten Ibsen. The FBG is highly reflective at 1660 nm for light in the core. The Raman pump laser was tuned to 1545 nm. The pulsed multimode pump beam was free-space launched into the DCRF via dichroic mirrors (DMs) and lenses. From the fibre details and pulse duration, the pulse walk-off length was estimated to around 200 m for the pump mode with the largest group velocity difference to the 1st-Stokes wave in the fundamental mode according to Eq. (2.3). This was much longer than the fibre, and furthermore most pump modes have group velocities closer to the Stokes mode. Thus the effect of walk-off was expected to be small. The launch efficiency of the Raman pump was 69%. At the opposite end of the DCRF, the 1660 nm CW seed light was injected into the core of the DCRF through a spliced 3 dB coupler. This light was then reflected at the pump launch end by the FBG. After the reflection, the Stokes seed co-propagated with the pump pulses. Thus, the part of the 1660 nm seed which temporally overlapped with the pump pulses, experienced the amplification through SRS process. Although the launched seed was CW, it was modulated by the pump after the amplification and therefore the output at the 1st Stokes was pulsed with a weak, unamplified, CW background. WDM couplers were used to separate the residual pump in the core, the 1st Stokes, and the 2nd Stokes at the output of the amplifier. Any remaining pump light or any other light in the cladding of the DCRF was lost in the WDM couplers, since these do not transmit any cladding-modes. I took the power at the DCRF end, just after the splice to the 3 dB coupler, to be the signal output power from the amplifier. For the input seed power, I used the power reflected by the FBG. The linewidth of the pump source and of the Raman seed laser were measured to be 0.15 nm and 2.8 nm respectively. This is sufficiently wide to suppress SBS, and this was indeed not observed in the RFA. Both pump and Stokes pulses were temporally stable.

Figure 4.13 shows the 1st-Stokes output peak power of the CP RFA and corresponding peak power conversion with respect to the launched pump peak power. The 1st-Stokes input power was 25 mW at 1660 nm. At the optimum, i.e., highest conversion efficiency, the peak pump power was 280 W while the peak power of the

output 1st Stokes was 211 W for a peak power conversion of 75%. The high peak power conversion indicates that a high power conversion efficiency is achievable in CW regime with this fibre.

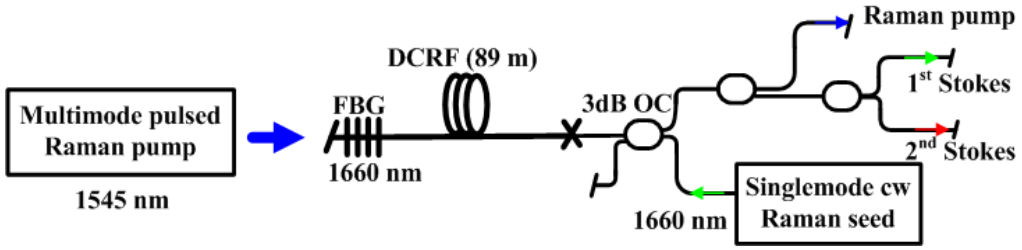

Figure 4.12: Experimental setup of the pulsed CP RFA. Blue arrow: pump; green arrow: 1st Stokes; red arrow: 2nd Stokes.

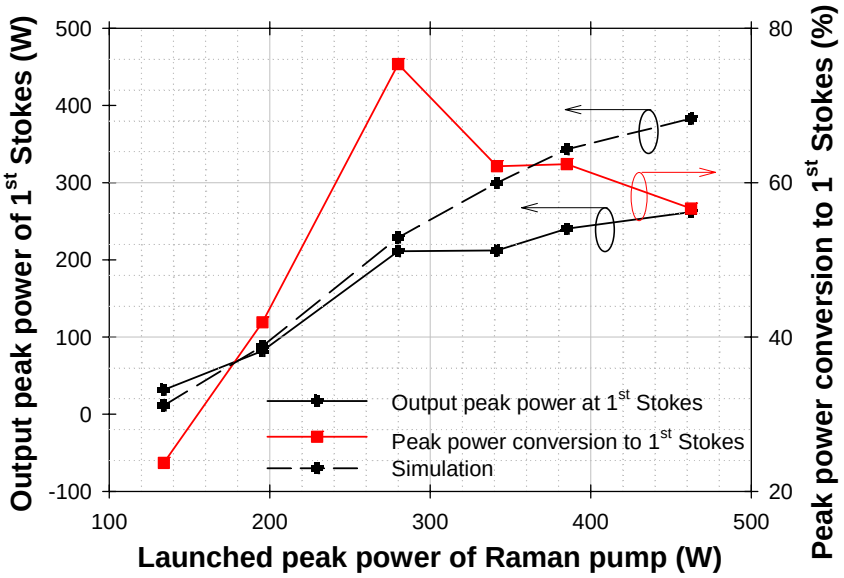

Figure 4.13: Output peak power (black solid curve: experimental results; black dashed curve: simulation results) and corresponding conversion efficiency (red curve) *vs*. launched pump peak power.

The dashed line in Figure 4.13 is the result of a simulation using the same model as for the earlier simulation in section 4.2.4. For the 1st and 2nd Stokes, only the LP_{01} mode was considered. The pump modal decomposition used in this simulation is given in Table 4.2. This was calculated by the software OptiFiber™ with the assumption that the incident pump was a diffraction-limited Gaussian beam with a 24 μm beam width (FWHM) centred on at a 3°incident angle. This determined the excited pump modes inside the fibre and the corresponding power ratios as listed in Table 4.2. Although the launch details were somewhat arbitrarily chosen, the calculated launch efficiency of 68% is in good agreement with the experimental launch efficiency, which was 69%. There are certainly other launch conditions that lead to a 69% launch efficiency but with a different modal power distribution. However, the simulation

results fit the experimental data well when the launched pump peak power was below 280 W. Above 280 W, the 1st-Stokes power kept growing with increasing pump power in the simulations, with negligible power Raman-scattered to the 2nd Stokes, while experimentally, the 1st-Stokes peak power was saturated and depleted by cascaded SRS to the 2nd Stokes. There are many possible explanations for the earlier appearance of the 2nd Stokes in the experiments, such as spikes in the pump pulses (leading to variations in peak pump power), polarisation effects, modulation instability [16], and pump-mode coupling and indeed excitation. There is also the influence of the 3-dB coupler and WDMs at the output, in which the 1st Stokes could be further converted into the 2nd Stokes. The simulation did not take this into account.

Table 4.2: Power ratio between excited pump modes at 1545 nm.

Mode	LP_{01}	LP_{11}	LP_{21}	LP_{02}	LP_{12}	LP_{31}	LP_{22}	LP_{32}	LP_{13}
Power ratio	22	14.5	3.5	3.2	16.5	0.5	3.1	1	4.6

Figure 4.14 shows the 1st-Stokes average output power and average power conversion efficiency into the 1st Stokes with respect to the launched Raman pump average power, for a Raman seed power of 25 mW. The highest average pump conversion to the 1st Stokes obtained was 60.5% at 565 mW of average pump power. The average power conversion efficiency was lower than the peak power conversion since there are other limiting factors on the average power conversion, e.g., pulse shape.

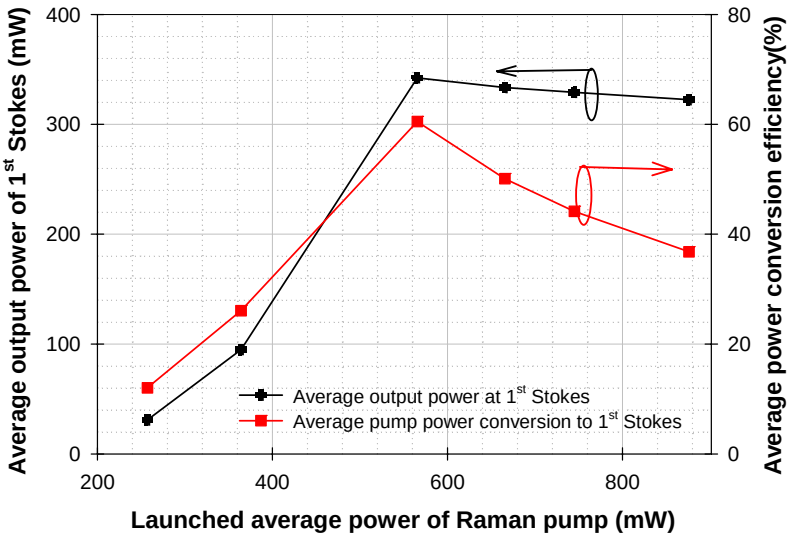

Figure 4.14: Average output power (black curve) and conversion efficiency (red curve) *vs*. launched pump average power

Figure 4.15 show pulse shapes of the launched pump, overlaid with traces of the 1st Stokes and residual Raman pump in the core at the output or the 2nd Stokes, at the

optimal pump power of 565 mW and at the maximum pump powers, respectively. In Figure 4.15(a), the residual 1545 nm pump power was low, but there were peaks at the edges of the pulse corresponding to pump power not efficiently transferred to the 1st Stokes. This reduced the conversion efficiency into the 1st Stokes. The reason for this is that the instantaneous pump power in the edges was not high enough for efficient conversion. The steepness of the pulse edges was determined by the speed of the AWG, and I believe that a higher conversion efficiency is possible with readily available faster generators. Note that to a CW CP Raman fibre device, the pulse shape will not be a limiting factor on the conversion efficiency. At the same time, the high symmetry of the output pulse shapes suggests that walk-off was not important for this pulse duration. Figure 4.15(b) shows the depletion of the 1st Stokes by the generation of the 2nd Stokes at the maximum pump power. The power of the 2nd Stokes is not scaled since I did not characterise the couplers and WDMs at this wavelength. The energy conversion to the 1st Stokes dropped to ~ 37%. The higher-order Stokes generation can be avoided with a shorter fibre. The Stokes pulses were noisy. This might be caused or enhanced by modulation instability because the 1545 nm pump and the signal were operating in the anomalous dispersion regime of this fibre [16]. Figure 4.16 shows output spectra at the optimal pump power. The solid line is the residual Raman pump measured at the 1550 nm port of the WDMs and the dashed line is the amplified Raman signal measured at the 1660 nm port.

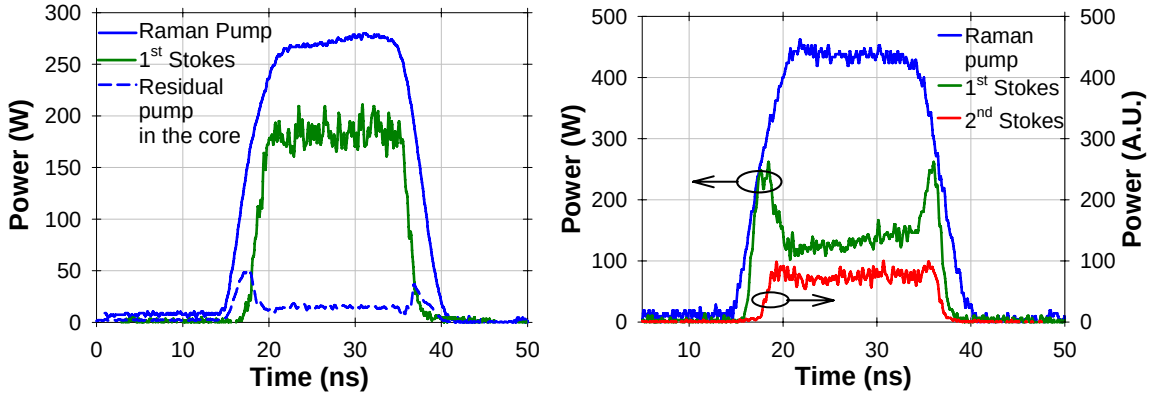

(a) (b)

Figure 4.15: Pulse shapes of input Raman pump (solid blue curve), 1st Stokes (green curve), 2nd Stokes (red curve), residual pump in the core (dashed blue curve) at the launched average pump power of (a) 565 mW; (b) 876 mW.

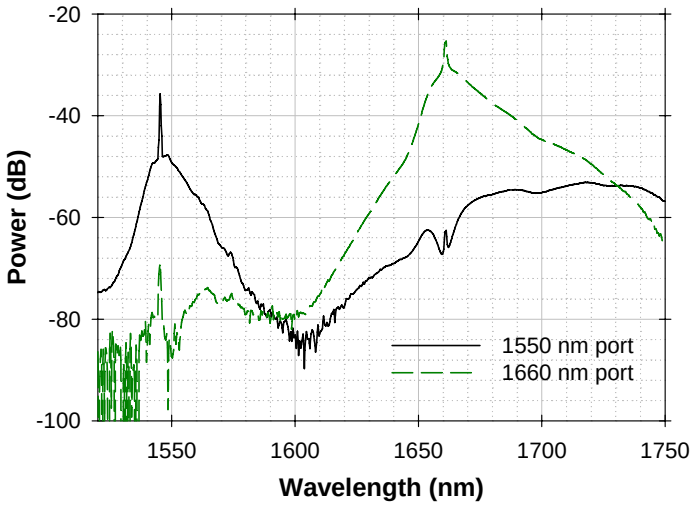

Figure 4.16: Output spectra at 565 mW launched average pump power.

Regarding brightness enhancement, the beam quality of the launched pump was not measured. Nevertheless, we still can estimate the maximum brightness enhancement obtained with this setup based on Eq. (2.8) according to:

$$\eta_B = \frac{B_s}{B_p} \approx \frac{P_s}{P_p}\left(\frac{\pi N A_{cl} a_{cl}}{\lambda_s M_s^2}\right)^2 . \tag{4.2}$$

Since the signal was emitted from the SMF, M_s^2 is set to 1. Given the geometry of this fibre and the maximum power conversion I obtained experimentally, the maximum brightness enhancement would be 8.7.

To better understand the conversion process and the limits, it is useful to measure the spatial distribution of the transmitted pump at the output of the DCRF. For this, the splice at the output of the DCRF was broken and lenses were used to couple the 1660 nm seed into the DCRF. A 4%-reflecting silica wedge was inserted to sample the residual 1545 nm pump. A camera (Electrophysics 7290A) imaged the output beam. A DM was used to reflect longer wavelengths and ensure that only the residual 1545 nm pump light reached the camera. The Rayleigh resolution limit of the imaging system became 5 μm with an NA of 0.2. This can be used as an estimate of the resolution. Figure 4.17 shows the images of the residual Raman pump at different input powers of the Raman seed. Here, the launched average Raman pump power was about 510 mW. The SRS in absence of a Raman seed was negligible, so Figure 4.17(d) corresponds to the undepleted pump distribution.

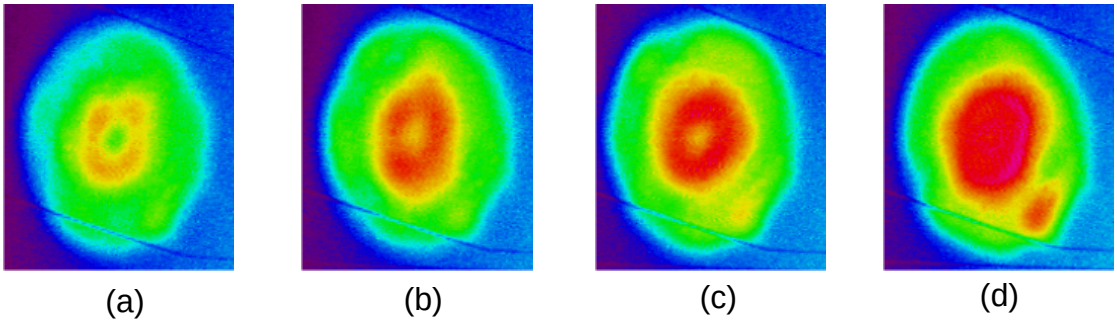

Figure 4.17: Residual pump power distribution at the output of the DCRF with Raman seed powers at: (a) 20.2 mW; (b) 1.9 mW; (c) 0.48 mW; (d) 0 mW.

We see from Figure 4.17(d) that the power in the centre could be converted efficiently into the 1st Stokes. However, there was still some remaining pump power around the edge of the inner cladding. The camera was also used to image the output at the 1st Stokes, in this case together with another DM. See the inset of Figure 4.18. The 1st Stokes was in the fundamental mode, which was diffraction limited. Its beam propagation factor (M^2) was 1.02, measured by a Gentec P7 beam scope and analysed with a Gaussian-beam fit (Figure 4.18). Therefore, it was truly single-moded. The measured beam quality of the fundamental mode is slightly better than the calculated one, i.e., 1.18. One of the possibilities is that the RIP of the piece used in my experiment is different from the one in Figure 4.2. The central dip is not so deep. Another possibility is that this is measurement error.

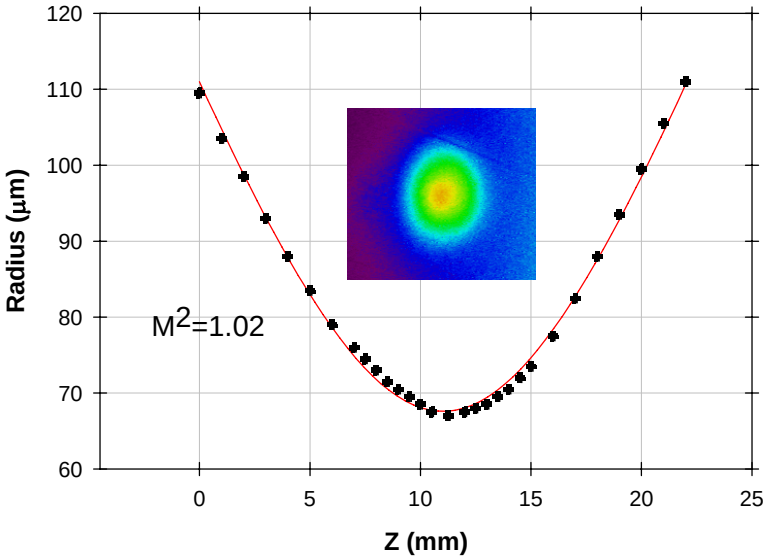

Figure 4.18: M^2 and fit. Inset: the image of the 1st stokes sampled by the wedge. The launched pump average power was 510 mW and the input Raman seed was 20.2 mW.

The beam intensity of the residual Raman pump along the fibre radius is shown in Figure 4.19. In the scaling of the figure, the core radius was around 619 µm and the

inner-cladding radius was about 1375 μm. The pump light in the centre of the fibre core was efficiently Raman-scattered to the 1st Stokes. However, the SRS efficiency of the pump distributed around the core edge was relatively poor. Considering the refractive index profile of the fibre, one of the possible modes for the Raman pump was a ring mode as shown in Figure 4.17. The overlap is poor between it and the 1st Stokes, which was localized to the core. To improve the conversion of the pump around the inner-cladding edge, a D-shaped inner cladding can be adopted to improve the interaction of the modes with the core [17].

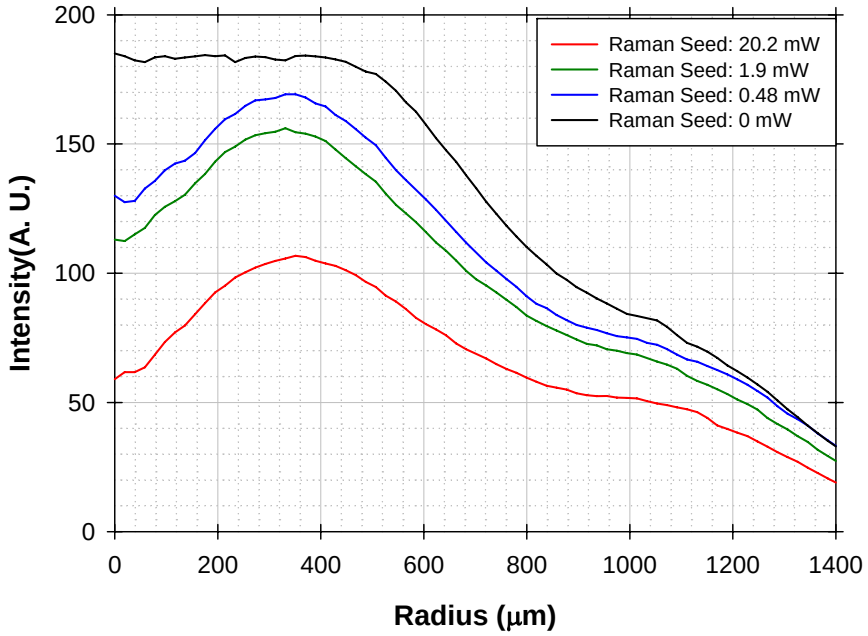

Figure 4.19: Intensity distribution of the residual Raman pump along the fibre radius under different input Raman seed powers.

I also characterised the residual 1545 nm pump beam by scanning a piece of standard SMF across the image, in the image-plane, instead of using the camera. One end of the fibre was mounted on a translation stage and the other end was sequentially connected to a HP 8153A power meter, a 2.5 GHz Tektronix oscilloscope with a 5 GHz Thorlabs detector, and an Ando OSA, to spatially resolve the power, pulse shape, and spectrum. Here, the input 1660 nm seed power was 18 mW and the launched 1545 nm average pump power was around 525 mW. Figure 4.20 depicts pulse shapes of the residual 1545 nm pump at different distances from the centre. Most of the Raman pump in the fibre core was converted into the 1st Stokes, although also in this case the power conversion was limited in the leading and trailing edges of the pulses. The dotted circle

stands for the $1/e^2$ intensity radius of the 1st Stokes based on the 1st-Stokes distribution shown in the inset of Figure 4.18 and the radius was calculated to be ~ 770 μm.

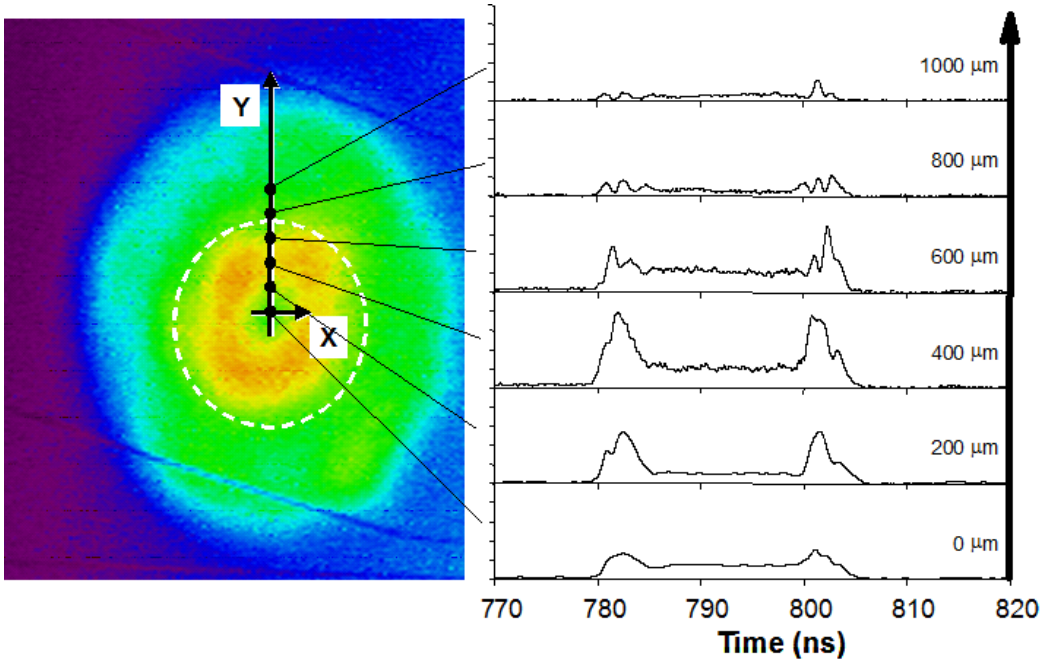

Figure 4.20: Pulses shapes of residual pump in transverse section.

4.3.4 Conversion efficiency limited by pulse shape

The pump pulse shape is very critical for the conversion efficiency into the 1st Stokes in the experiments above. The pre-pulse shaping adopted here allows for a high conversion efficiency with the nearly rectangular pump pulses. However, pulses necessarily have instantaneous powers ranging from the peak power down to zero (or some low minimum value), and the edges of the pulses did degrade the efficiency somewhat in the experiments. Below, I will analyse the effect of the pulse shape on the conversion efficiency in DCRFs with different inner-cladding-to-core area ratios. The instantaneous power can be treated as a constant power if dispersion is not important and if counter-propagating waves are discarded. Thus, let us first quantify effect of a mismatched pump power on the conversion efficiency in the CW regime for different inner-cladding-to-core area rations. The simplified model (Eq. (2.35) – Eq. (2.37)) is numerically solved in the (quasi-) CW regime for a CP RFA with co-propagating pump and Stokes waves, pumped at 1550 nm and seeded by 1 mW at 1660 nm. The Raman gain coefficient is taken to be 6.34×10^{-14} and 5.29×10^{-14} m/W, respectively, in the core and inner cladding. The Raman gain coefficient $g_R(\lambda_0, \lambda_2,)$ is set to $g_R(\lambda_0, \lambda_1) / 8$. The core diameter is 9 μm. Both walk-off and background loss are ignored. The power is

assumed to be below the damage threshold. For each area ratio, the fibre length is optimised to yield the highest possible 1st-Stokes output power for an input pump power of 1 kW. Figure 4.21(a) shows the dependence of the 1st-Stokes power on the input pump power for different area ratios. For an excessive area ratio of 12, the 1st-Stokes power decreases sharply above the optimal 1 kW pump power. The same is true for an area ratio of eight, although this does allow for a high conversion efficiency at the optimal power. For smaller area ratios, however, and in particular for unity area ratio, the 1st-Stokes power continues to grow even beyond the 1 kW of pump power that yields the highest conversion efficiency. This is because as the area ratio increases, any 2nd-Stokes power becomes progressively more effective in depleting the 1st-Stokes power, relative to the ability of the pump to amplify it. Therefore, excessive pump power leads to the buildup of the 2nd Stokes, which at high area ratios very rapidly depletes the 1st-Stokes power for a specific fibre length. In Figure 4.21(b), the data has been recalculated to directly show the conversion efficiency to the 1st Stokes. Clearly, a fibre with smaller area ratio can remain efficient over a wide pump-power range. For example, with an inner-cladding-to-core area ratio of one, the conversion efficiency drops by less than 10% if the pump power remains within ±40% of the optimum. However, higher area ratios require a better control of the pump power for efficient conversion into the 1st Stokes. With an inner-cladding-to-core area ratio of eight, the input pump power can only range from -5% to +2% of the optimal value, if the conversion efficiency is to remain within 10% of the maximum. This example also illustrates that pump power fluctuations will affect the conversion efficiency for both pulsed and CW Raman fibre devices. For DCRFs with large inner-cladding-to-core area ratios, pump stability becomes more important for high conversion efficiency.

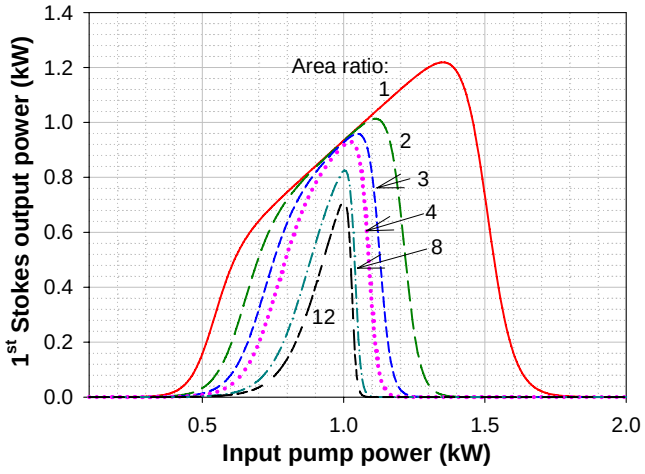

(a)

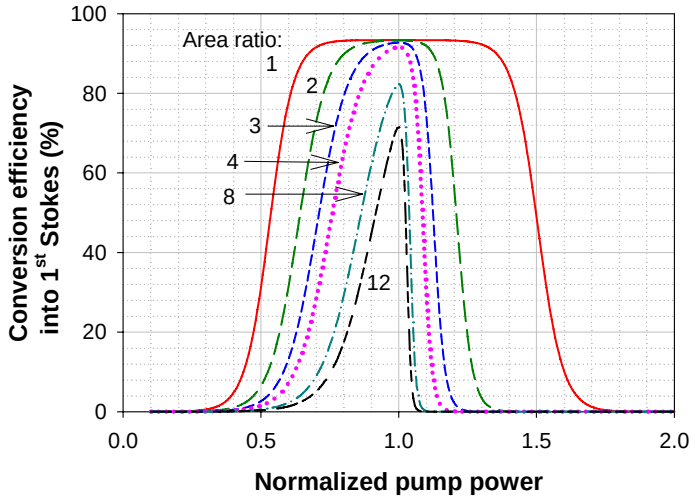

(b)

Figure 4.21: (Simulation) (a) 1st Stokes output power *vs*. input pump power; (b) Conversion efficiency to 1st Stokes *vs*. input pump power normalized to 1 kW. CW / quasi-CW regime in absence of counter-propagating waves.

The instantaneity of SRS and the sensitively of the conversion efficiency to the pump power is a problem for pulses because of the variations in instantaneous power. Figure 4.22 shows how the energy is distributed across the instantaneous power for Gaussian, 2nd and 4th order super-Gaussian, square pulses and a representative pulse of the Raman pump used experimentally in this chapter, which is the pulse given in Figure 4.9. Insofar as it is valid to use a quasi-CW treatment, it is possible to calculate the conversion efficiency for each instantaneous power of a pulse using the data of Figure 4.21, and from that together with the instantaneous-power distribution, the total conversion efficiency of a pulse. For example, for a Gaussian pulse, about 24% of the total energy resides in the leading and trailing edges of the pulse with instantaneous power smaller than half of the peak power. Given the narrow range of powers for efficient conversion at high area ratios, and the precipitous drop in efficiency at too high powers in Figure 4.21(b), the peak power can only slightly overshoot the optimal CW power level. Consequently, the central part of a pulse will be converted relatively efficiently, while a large fraction of the leading and trailing edges of the pump pulse, in fact more than 24% of the total pump energy, remains unconverted. However, the fraction of energy with instantaneous power less than half of the peak value is reduced to 12% and 5% for a 2nd and 4th super-Gaussian pulse, respectively. Ideally, although not realisable in practice due to bandwidth limitations, a square pulse would be perfect as a Raman pump since all energy then has the same instantaneous power. Therefore, rectangular pulses can eliminate the pulse-shape penalty. For the pump pulse shape used

experimentally in this chapter, almost 80% of the energy resides in the central part of the pulse with instantaneous power of over 80% of the peak power. This is achieved in this case in pulses of relatively low bandwidth, with pulses being pre-shaped to compensate for the gain-shaping that is typical for long pulses of high peak power. This helps in achieving high energy conversion efficiency.

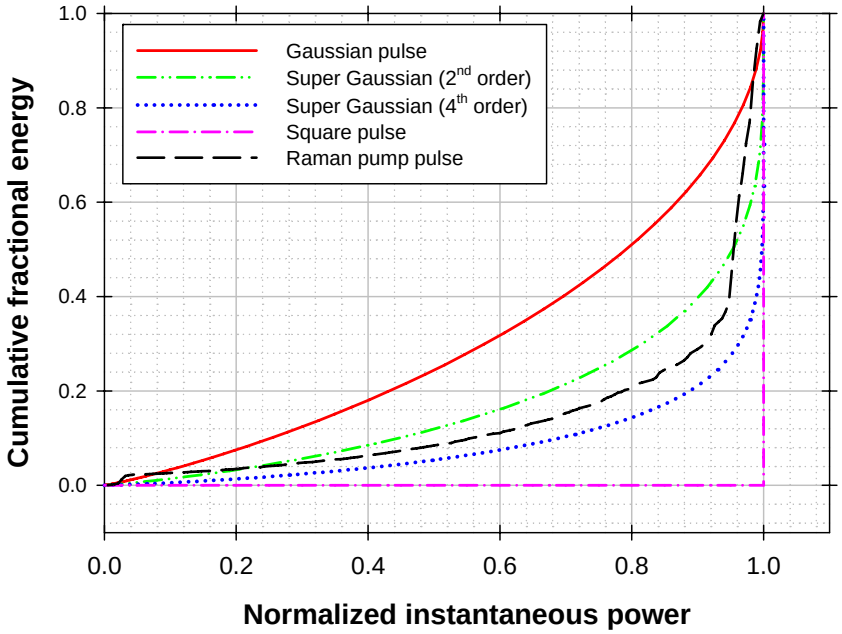

Figure 4.22: (Simulation) Cumulative fractional energy *vs*. instantaneous power for pulses of different shapes.

Figure 4.23 shows how the energy conversion efficiency of a quasi-CW Gaussian pulse and the Raman pump pulse (black curve in Figure 4.9) vary with the peak power, relative to the optimal instantaneous (or CW) power (i.e., 1 kW), at different area ratios. This was calculated from the dependence on the efficiency on the pump power and the energy distribution as described above. We can see that the optimal peak power exceeds the optimal CW value, but indeed only by a small amount at large area ratios. For Gaussian pulses at unity area ratio, the peak power is be nearly 40% higher than the optimal CW value, but this drops to 2% for an area ratio of eight. It is the same for the Raman pump pulse used in this chapter. For a larger area ratio, e.g., 8, Furthermore, with Gaussian pulses, while the efficiency only drops from the CW value of 93.4% to 76.9% at optimal peak power for unity area ratio, the drop from 84.7% to 38.6% for an area ratio of eight is much more significant. For the Raman pump pulses used experimentally, the energy conversion efficiency is improved to 87% with unity area ratio while it is improved to 62.9% for an area ratio of eight. For the DCRF F71-LF11,

the inner-cladding-to-core area ratio is 5.76. From the Figure 4.23(b), the highest energy conversion could be 70%. In the experiment, the achieved energy conversion was 60%, which is reasonably close to the theoretical value (which neglects loss and other effects).

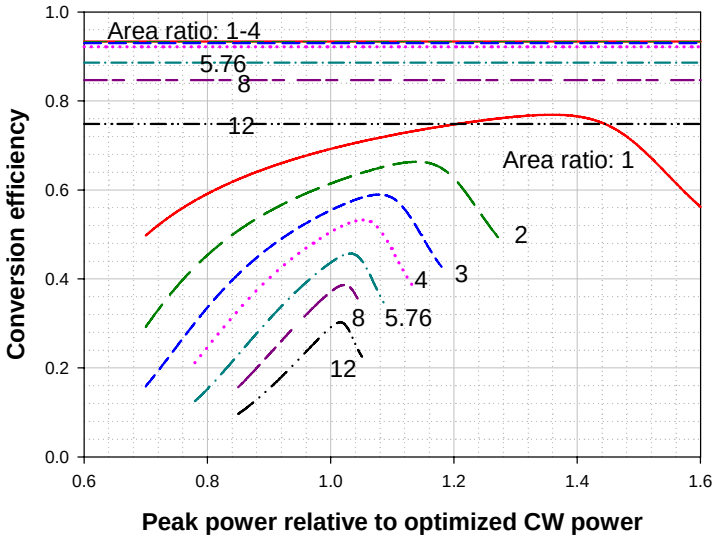

(a)

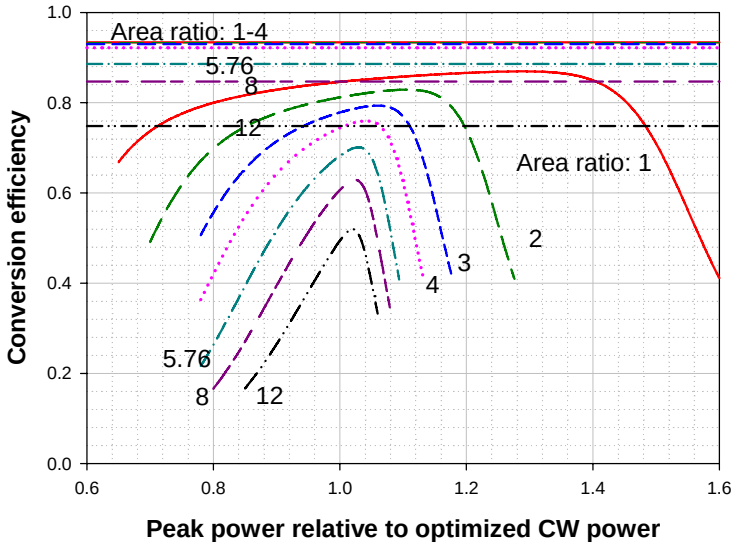

(b)

Figure 4.23: (Simulation) Energy conversion efficiency into 1st Stokes for quasi-CW (a) Gaussian pulses (b) Raman pump pulses (black curve in Figure 4.9) *vs*. peak power relative to optimal CW power with different inner-cladding-to-core area ratio, as marked in the graph. Straight lines: CW conversion efficiencies. The highest CW conversion efficiency is essentially the same as the quantum limit.

The analysis above suggests that it is necessary to use rectangular pulses, with all energy at a single instantaneous power, to reach a high conversion efficiency in a DCRF. Alternatively, a CW pump may be used, although the power requirements will be prohibitive in many practical cases. Nonetheless, the high peak power conversion obtained in the experiments indicates that high overall pump conversion can be feasible

for high power CW-pumped RFAs. In addition, although this fibre is well designed according to Eq. (3.4), some of the Raman pump might not be efficiently absorbed because of the circular symmetry of the inner cladding. This leads to pump modes with low overlap with the core (Table 4.1.), making it difficult to convert the power in them to the core-mode of the first Stokes. This is similar to RE-doped fibre and the pump conversion is expected to improve with a D-shaped inner cladding (e.g. [17]). These limitations together with the background loss may explain the lower energy conversion efficiency obtained in the experiment relative to the theoretical one in Figure 4.23(b).

4.4 Summary

In this chapter, I demonstrated a high efficiency pulse-pumped CP RFA based on the DCRF F71-LF11. The peak power conversion was as high as 75% while the obtained energy conversion efficiency was 60%. The experimental results require attention to the following factors: Firstly, a well-chosen area ratio of this DCRF allows for a high conversion efficiency into the 1st Stokes. Specifically, the inner-cladding-to-core area ratio should be smaller than eight since otherwise, the 2nd Stokes will inevitably grow before most the pump power is transferred into the 1st Stokes as discussed in chapter 3. Secondly, the fibre was sufficiently short to reduce the background loss and avoided walk-off. This requires a sufficiently high pump peak power. Finally, the Raman pump pulse was pre-shaped and the resulting nearly rectangular pulse shape promoted a high energy conversion efficiency to the 1st Stokes. With a asymmetrical inner cladding and more closely rectangular pump pulse, even better conversion efficiency should be possible. In the pulsed regime, the pump pulse shape is critical since the (instantaneous) conversion efficiency depends strongly on the instantaneous power. While ideal square pulses are unphysical, the pulse shape will not be an issue for a CW CP Raman fibre device. The achievable instantaneous conversion efficiency can be approximated by the peak power conversion into the 1st Stokes, and the 75% achieved here indicate that very high conversion efficiencies are achievable in CW regime with the same fibre. However, for CW pumping, if there are power fluctuations at sufficiently low frequencies, the fluctuation can be passed to the cw seed, and the seed becomes more noise after Raman amplification. Furthermore, the conversion efficiency can be degraded just like it is with pulses. If the power fluctuation frequency is high enough, the seed cannot respond and sees a constant Raman gain, which allows for an improved conversion efficiency. In

cases when the output beam is counter-directional to the pump beam, even relatively low-frequency fluctuations are averaged out in this way [12], which helps to make counter-pumped devices more efficient. In the next chapter, I will demonstrate a high power CW CP RFL with diffraction-limited output, with a focus on the counter-pumped configuration.

4.5 Reference

[1] J. Nilsson, J. K. Sahu, J. N. Jang, R. Selvas, D. C. Hanna, and A. B. Grudinin, "Cladding-pumped Raman fiber amplifier", in Proc. of Optical Amplifiers and Their Applications (OAA 2002) Vancouver, Canada 14-17 Jul. 2002, paper PD2-1/2/3 (Postdeadline).

[2] C. A. Codemard, J. K. Sahu, and J. Nilsson, "Cladding-pumped Raman fiber amplifier for high-gain high-energy single-stage amplification", in Proc. of OFC, Anaheim, CA, USA 6-11 March 2005, paper OutF5.

[3] J. Ji, C. A. Codemard, M. Ibsen, J. K. Sahu, and J. Nilsson, "Analysis of the conversion to the first stokes in cladding-pumped fiber Raman amplifiers", IEEE J. Sel. Top. Quantum Electron., **15**(1), 129 (2009).

[4] A. Shirakawa, C. A. Codemard, J. Ji, K. K. Chen, A. Malinowski, D. J. Richardson, J. K. Sahu, and J. Nilsson, "High-brightness 210 μJ pulsed Raman fiber source", in Proc. of Conf. Lasers and Electro-Optics /QELS, San Jose 4-9 May 2008, paper CTuL1.

[5] A. K. Sridharan, J. E. Heebner, M. J. Messerly, J. W. Dawson, R. J. Beach, and C. P. J. Barty, "Brightness enhancement in a high-peak-power cladding-pumped Raman fiber amplifier", Opt. Lett., **34**(4), 2234 (2009).

[6] J. Jang, Y. Jeong, J. K. Sahu, M. Ibsen, C. A. Codemard, R. Selvas, D. C. Hanna, and J. Nilsson, "Cladding-pumped continuous-wave Raman fiber laser", in Proc. of Conf. Lasers and Electro-Optics/QELS, Baltimore 3-5 Jun 2003, paper CWL1.

[7] C. A. Codemard, P. Dupriez, Y. Jeong, J. K. Sahu, M. Ibsen, and J. Nilsson, "High-power continuous-wave cladding-pumped Raman fiber laser", Opt. Lett., **31**(15), 2290 (2006).

[8] C. A. Codemard, J. K. Sahu, and J. Nilsson, "High-brightness pulsed cladding-pumped Raman fiber source at 1660 nm", in Proc. Conf. Lasers and Electro-Optics /QELS, Baltimore 6-11 May 2007, paper CTuN3.

[9] M. M. Bubnov, S. L. Semjonov, M. E. Likhachev, E. M. Dianov, V. E. Khopin, M. Y. Salganskii, A. N. Guryanov, J. C. Fajardo, D. V. Kuksenkov, J. Koh, and P. Mazumder, "On the origin of excess loss in highly GeO_2-doped single-mode MCVD fibers", IEEE Photonics Technol. Lett., **16**(8), 1870 (2004).

[10] E. M. Dianov, "Advances in Raman fibers", J. Lightwave Technol., **20**(8), 1457 (2002).

[11] S. T. Davey, D. L. Williams, B. J. Ainslie, W. J. M. Rothwell, and B. Wakefield, "Optical gain spectrum of GeO_2-SiO_2 Raman fiber amplifiers", in Proc. of Inst. Elect. Eng., **136**(6), 301 (1989).

[12] J. Bromage, K. Rottwitt, and M. E. Lines, "A Method to predict the Raman gain Spectra of germanosilicate fibers with arbitrary index profiles", IEEE Photonics Technol. Lett., **14**(1), 24 (2002).

[13] C. Fukai, K. Nakajima, J. Zhou, K. Tajima, K. Kurokawa, and I. Sankawa, "Effective Raman gain characteristics in germanium- and fluorine-doped optical fibers", Opt. Lett., **29**(6), 545 (2004).
[14] K. T. Vu, A. Malinowski, D. J. Richardson, F. Ghiringhelli, L. M. B. Hickey, and M. N. Zervas, "Adaptive pulse shape control in a diode-seeded nanosecond fiber MOPA system", Opt. Express, **14**(23), 10996 (2006).
[15] A. Malinowski, K. T. Vu, K. K. Chen, P. Horak, D. J. Richardson, "Selective generation of individual Raman Stokes wavelengths using shaped optical pulses", in Proc. of OFC, San Diego 24-28 Feb 2008, paper OTuB3.
[16] G. Millot, P. Tchofo Dinda, E. Seve, and S. Wabnitz, "Modulational instability and stimulated Raman scattering in normally dispersive highly birefringent fibers", Opt. Fiber Technol., **7**(3), 170 (2001).
[17] P. Leproux, S. Fevrier, V. Doya, P. Roy, and D. Pagnoux, "Modeling and optimization of double-clad fiber amplifiers using chaotic propagation of pump", Opt. Fiber Technol., **6**(4), 324 (2001).
[18] C. Headley and G. P. Agrawal, *Raman amplification in fiber optical communications systems*, Elsevier Academic Press (2005).

Chapter 5 High-power operation of continuous-wave CP RFLs

In the previous chapter, I discussed limitations on the power conversion efficiency from the Raman pump to the 1st Stokes in a pulse-pumped CP RFA. One limitation stems from the inherent variation in instantaneous power of all realistic pulses. Walk-off is an issue as well (see section 3.4). However, these problems can be avoided in the case of CW pumping. Thus, the conversion efficiency obtainable in a CW CP RFL should be comparable to the peak power conversion efficiency obtained from the pulse-pumped CP RFA. In this sense, CW operation is easier, but the large instantaneous power required is more difficult to obtain. This on the other hand, also makes it attractive for scaling to high average power. In this chapter, I will discuss the particulars of CW pumping, largely based on my experimental work on a 100 W CW CP RFL with diffraction-limited output at 1 μm but also on other devices. First, I will describe the progress in output power from Raman fibre sources. After that, factors limiting the output power will be analysed and the achievable output from CW CP RFAs will be considered. This is followed by descriptions of experiments and discussions. The same DCRF is used in this chapter as in the previous one, i.e., F71-LF11. The experiments were carried out by Dr. C. A. Codemard and me.

5.1 Power scalability of the Raman fibre sources

The power from Raman fibre sources has been growing rapidly in recent years. Figure 5.1 shows the output powers from record-breaking Raman fibre sources reported in the last eight years. These are all CW, with the exception of a pulsed CP Raman fibre source [1] identified by a circle in Figure 5.1. Among various options for Raman fibre sources, SMFs have relatively small core size, which benefits the generation of SRS. They are also easy to splice, and compatible components are widely available, at least at some wavelengths. Substantial amounts of Raman research have been carried out with SMFs. On the other hand, small cores require pump sources with

good beam quality. Compared to multimode pump sources, single-mode pump sources with high average power are more difficult to realise. The power from Raman fibre sources based on SMFs increased steadily but at a comparatively low level of about 10 W in 2003 to 80 W in 2009, as shown in Figure 5.1 [2]-[4]. Then, the output power increased to 150 W [5]. This was an all-fibre system, making it a very impressive achievement. However, it would be very challenging to obtain even higher output power, in particular as it comes to the pump launch. Furthermore, as it comes to spatial brightness, this can only be degraded in single-mode-, single-end-pumped Raman fibre sources. By contrast, Raman fibre sources based on both MMFs and DCRFs can transfer multimode pump beams into nearly diffraction-limited signal beams, and improve the brightness. However, the highest power reported from MM fibre approach is only 5.8 W with M^2 of 3.5 at the Stokes wavelength [6]. Thus, compared to core-pumping, the power that has been achieved is lower and the beam quality is worse. Although one can expect that the performance of MM fibres for high-power, high-brightness Raman sources would increase significantly with more research, DCRFs still seem more promising. The output power from DCRFs has increased nearly exponentially since the first CW CP RFL was demonstrated in 2003 [7]. See the blue circles in Figure 5.1. Three years later, the power was further improved to 10 W from 3.4 W [8]. Recently, it reached 100 W with nearly diffraction-limited beam [9].

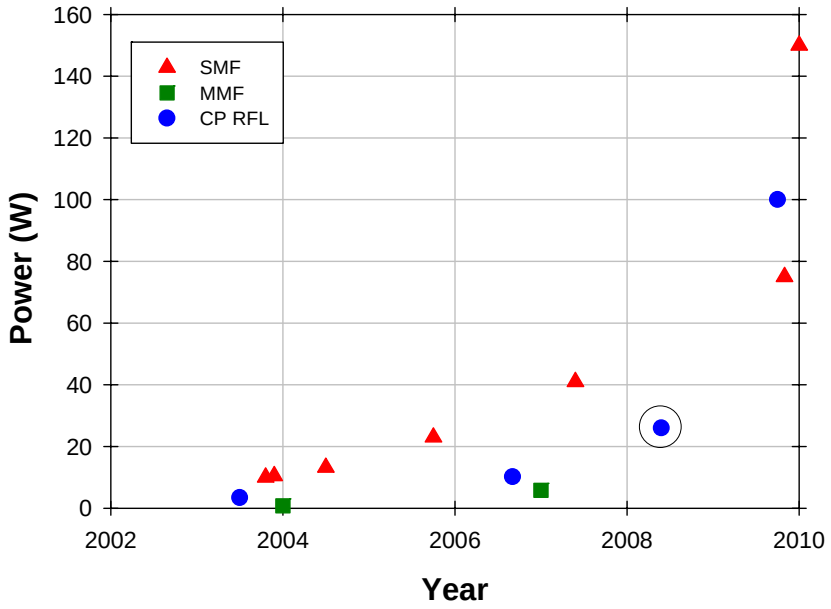

Figure 5.1: Power evolution of CW Raman fibre sources in recent years.

Despite the recent rapid progress, and while CP RFLs also benefit from wavelength agility, the power is still much lower than the record levels reported from

RE-doped fibres at specific wavelengths. For example, at 1 μm, a nearly single-mode YDF source with 10 kW output power has been reported [10], and at 2 μm, a diffraction-limited thulium-doped fibre (TDF) source with 1 kW output power was demonstrated recently [11]. However, it is clear that CP RFLs should be scalable to much higher powers, possibly even to the multi-kW level achieved by RE-doped fibre lasers. Therefore, I will next analyse the power scalability of high-efficiency Raman fibre sources in a similar way as previously done for diffraction-limited RE-doped fibre devices [12]-[13]. Only CW high power RFAs with broad bandwidth and diffraction-limited output are considered. In this case SBS [14] is not a factor, nor is SPM. Four-wave mixing (FWM) is also ignored, leaving SRS as the only nonlinearity that is considered. Other limiting factors that I take into account below are as described in [12] and [13], using similar but appropriately modified equations. For more information, e.g., on the physics behind the equations, please see [12]-[13] and references therein.

(1) Thermal fracture

The heat power deposited in a piece of fibre of length L, can cause thermal fracture at a level ($P_{rapture}$) given by [15]:

$$P_{rupture} / L = 4\pi R_m / (1 - a_{co}^2 / 2a_{cl}^2) . \tag{5.1}$$

The rupture modulus of the glass R_m is 2460 W/m in silica [16]. In a co-pumping CP RFA, the maximum heat generation in per unit length is estimated as below [17],

$$(P_{thermal} / L)_{\max} \approx (\nu_0 - \nu_1) / \nu_0 \times P_0^2(0) g_R(\lambda_0, \lambda_1) / (4A_{co}) \tag{5.2}$$

where ν_0 and ν_1 represent the frequency of the pump and 1st Stokes respectively, and $P_0(0)$ is the pump power at the input. To protect the fibre, $(P_{thermal} / L)_{\max}$ should be no more than $(P_{rapture} / L)$. This leads to,

$$P_0(0) < \left[\frac{4\pi R_m}{1 - a_{co}^2 / 2a_{cl}^2} \times \frac{4A_{co}\nu_0}{g_R(\lambda_0, \lambda_1)(\nu_0 - \nu_1)} \right]^{1/2} . \tag{5.3}$$

According to this, the input pump power should be no more than 47 kW at 1064 nm in a fibre with a core diameter of 10 μm and inner-cladding-to-core area ratio of 8. The corresponding limited output power can be obtained by multiplying by the optical-to-optical power conversion efficiency η_{laser}, and is given by [12]-[13]:

$$P_{rupture}^{out} = \eta_{laser} \left[\frac{4\pi R_m}{1 - a_{co}^2 / 2a_{cl}^2} \times \frac{4A_{co}\nu_0}{g_R(\lambda_0, \lambda_1)(\nu_0 - \nu_1)} \right]^{1/2} . \tag{5.4}$$

(2) Melting of the core

The heat power deposited per unit length, which leads to melting of the fibre core, is given in a similar form as Eq. (5.4) [15]:

$$P_{melting} / L = \frac{4\pi k(T_m - T_c)}{1 + 2k/(a_{cl}h) + 2\ln(a_{cl}/a_{co})}. \tag{5.5}$$

For numerical evaluation, the thermal conductivity k of silica is 1.3 W/(m-K) while the melting temperature T_m and the coolant temperature T_c are 1983 K and 300 K respectively [18]. Depending on the cooling mechanism, the convective film coefficient h can vary significantly [19], and here is assumed to be 10,000 W/(m^2 K) in the case of forced flow of a liquid coolant. In a similar fashion, to meet the requirement $(P_{thermal}/L)_{\max} < (P_{melting}/L)$ and with conversion efficiency η_{laser}, the output power limited by the melting effect can be given by:

$$P_{melting}^{out} = \eta_{laser}\left[\frac{4\pi k(T_m - T_c)}{1 + 2k/(a_{cl}h) + 2\ln(a_{cl}/a_{co})} \times \frac{4A_{co}\nu_0}{g_R(\lambda_0, \lambda_1)(\nu_0 - \nu_1)}\right]^{1/2}. \tag{5.6}$$

(3) Thermal lens

The heating induces a temperature gradient in the fibre core, and creates a thermal lens. The strength of this becomes comparable to the index guiding from the fibre core, at a thermal load given by [12]:

$$P_{lens} / L = \frac{\pi k \lambda_1^2}{2a_{co}^2 \frac{dn}{dT}}. \tag{5.7}$$

The change in index with the core temperature dn/dT is 11.8×10^{-6} K^{-1} in silica [18]. To meet the requirement $(P_{thermal}/L)_{\max} < (P_{lens}/L)$, the output power as limited by thermal lens is given by:

$$P_{lens}^{out} = \eta_{laser}\left[\frac{\pi k \lambda_1^2}{2a_{co}^2 \frac{dn}{dT}} \times \frac{4A_{co}\nu_0}{g_R(\lambda_0, \lambda_1)(\nu_0 - \nu_1)}\right]^{1/2}. \tag{5.8}$$

(4) Damage limitations

As discussed in section 3.3, a high pump intensity combined with a large area ratio may well lead to a 1st-Stokes intensity in the core that exceeds the material damage threshold. Although the peak intensity of the fundamental mode can be more than twice the average intensity across the core, I will here for simplicity assume that the mode is uniformly distributed in the core. The output power limited by the material damage threshold is given by:

$$P_{damage}^{out} = I_1^{\max} A_{co} . \tag{5.9}$$

The material damage intensity $I_1^{\max}$ is assumed to be 20 W/μm^2 for CW beams in silica [20]. Note that this neglects the contribution of the pump to the damage, which is a reasonable approximation in case of cladding-pumping, even at relatively small area ratios.

(5) Pump power limitations

Unlike RE-doped fibre sources, Raman fibre sources should be pumped by relatively bright sources since SRS is proportional to the pump intensity. Together with the fibre size and NA, the pump beam brightness determines how much pump light can be coupled into the fibre, and further limits the output power as [12]:

$$P_{pump-\lim ited}^{out} = \eta_{laser} B_{pump} (\pi a_{cl}^2)(\pi NA_{cl}^2) \tag{5.10}$$

where $P_{pump-\lim ited}^{out}$ is the output power limit due to the pump light, in case of single-ended pumping. I will consider both direct diode-pumping and pumping with fibre lasers. For direct diode-pumping, the pump brightness B_{pump} is taken to be 0.021 W/(μm^2 sr). Such bright laser diodes are commonly available [21]. For pumping with fibre lasers, I will use a brightness of 33 W/(μm^2 sr). At 1064 nm, this corresponds to a power of 54 W in a single mode, which is readily available. The inner-cladding NA is assumed to be 0.46. Furthermore, to achieve the high conversion efficiency to the 1st Stokes without the build-up of 2nd Stokes, the inner-cladding-to-core area ratio is assumed to be 8 without spectral filtering for 2nd-Stokes suppression and 34 with spectral 2nd-Stokes suppression, e.g., as provided by the W-type fibre designed in Chapter 3 (with 18 μm core diameter). Meanwhile, the fibre length is assumed to be chosen to avoid 2nd-Stokes generation. Note that this also means that in contrast to [12]-[13], limits from unwanted SRS do not have to be considered explicitly (cf., e.g., Eq. (8)

in [13]). Furthermore, background loss is ignored. At such high power-levels, relatively short fibres can be used, so that background loss can be negligible.

Thus, for any given core size, the corresponding maximum output power determined by different factors can be calculated by Eq. (5.4) (thermal fracture), Eq. (5.6) (melting), Eq. (5.8) (thermal lensing), Eq. (5.9) (optical damage), and Eq. (5.10) (limited pump power). The lowest of these power limits will be the actual limit on output power. In the calculations, the fraction of the pump power converted to the signal η_{laser} is assumed to be 70%. The Raman gain coefficient is assumed to be 5×10^{-14} m/W with a pump wavelength λ_0 at 1064 nm and a signal wavelength λ_1 at 1116 nm. Figure 5.2 shows the calculated results. First of all, to achieve the maximum output power, fibre size is key. If DCRFs are pumped by sources of sufficient brightness, optical damage limits the output power from fibres with small cores, e.g., core radius no more than 19 μm for the inner-cladding-to-core area ratio at 8. The output power due to the optical damage remains the same for fibres with different area ratios. With large cores, the output power is determined by the thermal lensing instead, reaching a core-size-independent limit of 23.8 kW. Secondly, the beam quality of the pump source is important since it determines the available pump power inside the fibre. We note that a pump brightness of 5.37 W/(μm^2 sr) (or 5.4 W in a single mode at 1064 nm) makes the glass damage and the available pump power limit coincide in case of an area ration of 8, so this is really the highest useful pump brightness according to these equations. For an area ratio of 34, the corresponding brightness is 1.26 W/(μm^2 sr). Note also that the output power limited by the thermal lensing depends on the square of the working wavelength according to Eq. (5.8). Thus, if the 1st-Stokes wavelength is at 2 μm, the corresponding output power will be nearly four times higher. Besides, the double-clad structure of a DCRF allows us to launch more pump power into the fibre than a SMF does if cores sizes are the same, when pumping with the same brightness. For example, if a commercial SMF with a 9 μm diameter core and 0.12 NA is pumped by the Raman pump fibre source with brightness of 33 W μm^{-2} sr^{-1} (54 W in a single mode at 1064 nm) used later in this chapter, the output power will be limited to 76 W by the available pump power, with 80% conversion efficiency. In contrast, for a DCRF with the same core size and area ratio of 8, the output power will be up to 1.27 kW limited by the optical damage. Therefore, DCRFs are more promising to generate high power sources with moderate brightness pump sources since such pump sources can be

launched more efficiently into DCRFs than into SMFs. In theory, it is possible to achieve output power from Raman fibre sources as high as that from RE-doped fibre sources, or even higher.

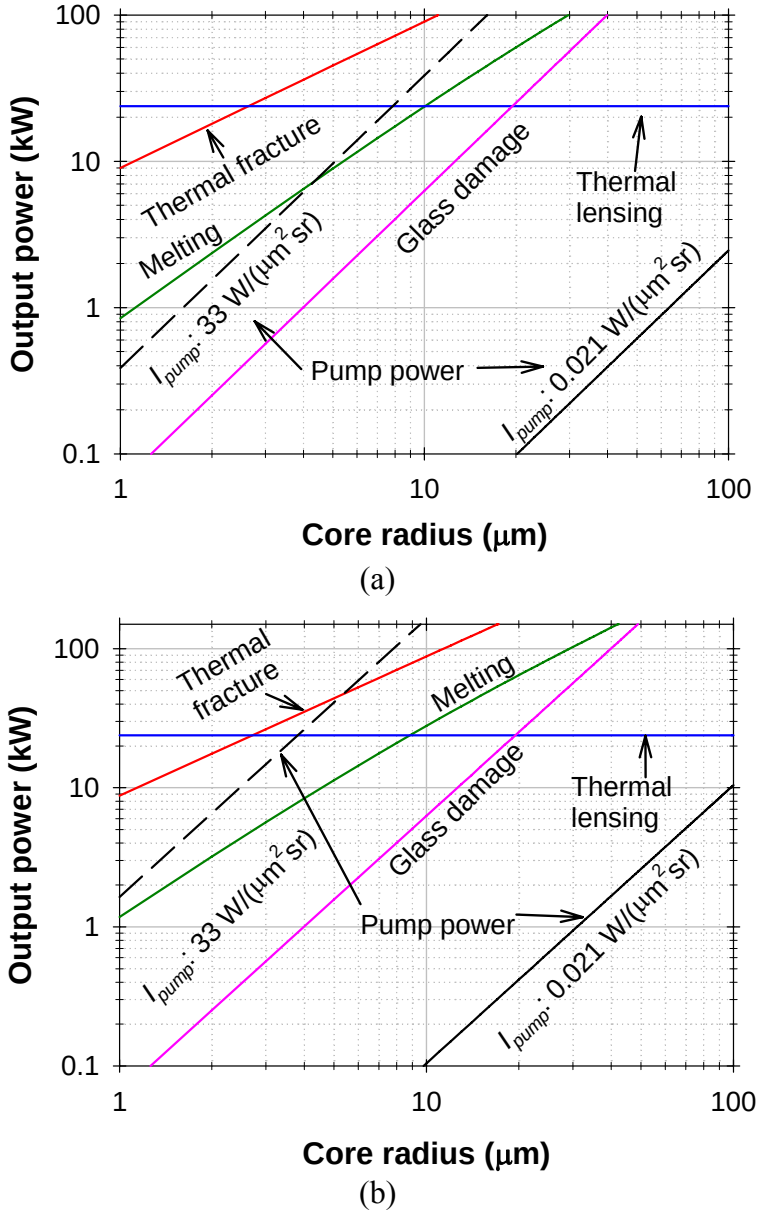

Figure 5.2: (Simulation) Maximum output power achievable from DCRFs with inner-cladding-to-core area of: (a) 8; (b) 34.

5.2 Experiments and discussions

Though the experimental demonstrations are over two orders of magnitude lower in power than the theoretical limits, the powers are still useful and progress has been fast. Next, I will describe my experiments on high power CW CP RFLs based on the DCRF

F71-LF11. The highest obtained output power of 100 W is close to a tenfold improvement over previous results. These were also obtained with the same DCRFs.

In the experiments, an YDF MOPA built by Dr. C. A. Codemard and capable of delivering up to 150 W of power at 1064 nm in a beam with $M^2 \approx 2$, was used as the Raman pump source. Thus this fibre source is slightly multimoded, and is well suited to pumping the DCRF F71-LF11, even though it has a relatively small inner-cladding diameter (~ 21 μm) and NA (~ 0.22). The high beam quality of the pump source led to a high launch efficiency of 84% into the DCRF. The pump launch end of the DCRF was held in a water-cooled metallic V-groove that is designed to prevent thermal damage to the fibre coating by any non-guided pump power or by the heat generated in the laser cycle itself. Finally, the stability of the pump source was monitored by measuring light reflected from wedges which were inserted into the beam path of the pump MOPA.

5.2.1 Characteristics of DCRF F71-LF11 at 1 μm

The DCRF F71-LF11 was used in the last chapter and details such as its geometry have been given in section 4.2. To understand better how it works at 1 μm, it is necessary to also details the specifics in this wavelength regime. First of all, the background losses at 1064 nm are 3.4 and 3.2 dB/km, respectively, in the core and inner cladding according to a cut-back measurement, the results of which were presented in Figure 4.3. Secondly, the Raman gain coefficients are estimated to be 9.2×10^{-14} and 7.7×10^{-14} m/W, respectively, in the core and inner cladding [22]-[24] based on the RIP in Figure 4.2. The higher Raman gain coefficient around 1 μm benefits SRS. Thirdly, there are 26 LP fibre modes not counting degeneracies, three of which are core-modes, i.e., with effective index higher than the inner-cladding index. The effective indexes of all modes calculated by OptiFiber™ at the pump wavelength are given in Figure 5.3. The overlaps between different modes are important, too. Therefore, the mode distributions at 1064 nm were calculated by the same software. From these, the overlaps between different modes have been obtained according to Eq. (2.14). The result is shown in Figure 5.4. Here, the overlaps of degenerate sine and cosine modes are treated the same way as in section 4.2.4.

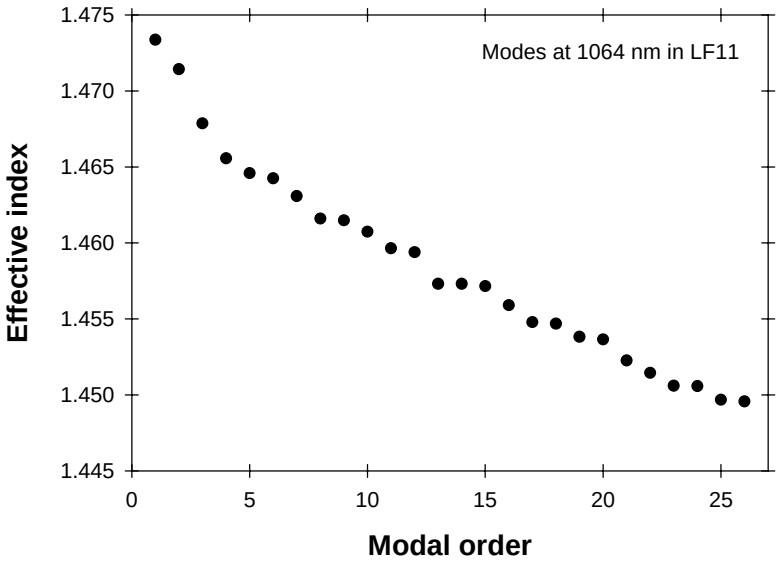

Figure 5.3: (Simulation) Effective index of modes at 1064 nm in the DCRF F71-LF11.

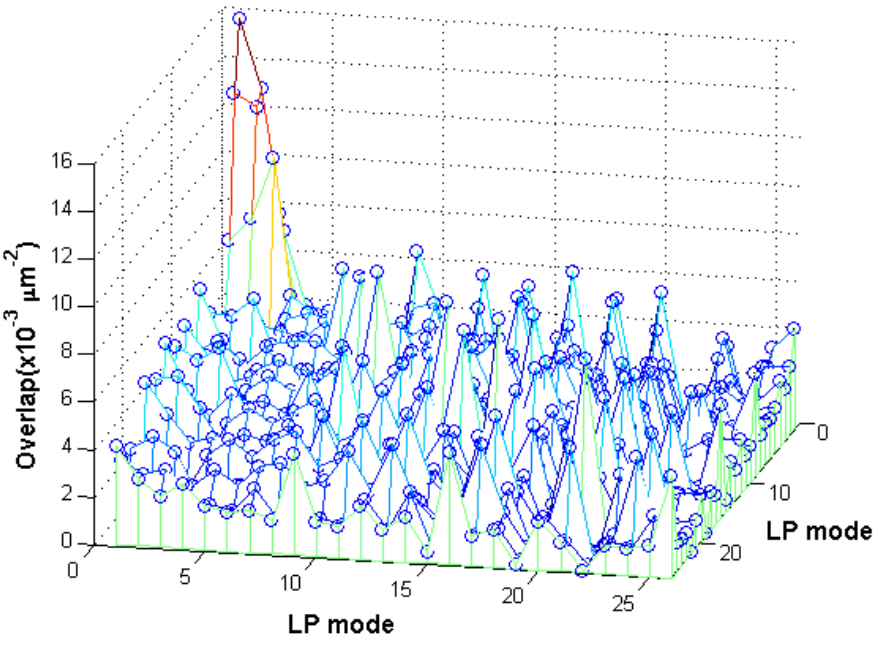

Figure 5.4: (Simulation) Overlaps between various modes at 1064 nm in the DCRF F71-LF11.

5.2.2 CP RFL in a 4% - 100% linear cavity

5.2.2.1 Experimental setup

One of the cavity configurations investigated experimentally was a 4% - 100% linear cavity, as shown schematically in Figure 5.5. The multimode pump beam was free-space launched into an 85 m long piece of the DCRF F71-LF11. The fibre facet at the pump-launch end was flat-cleaved and acted as one cavity mirror of the linear cavity.

The other end of the fibre was angle-cleaved to suppress Fresnel-reflection feedback. Instead, the cavity mirror comprised a lens-coupled dichroic mirror (DM4) with high reflection at the signal wavelength. Between the DM4 and the angled-cleaved fibre end, two mirrors, DM2 and DM3, were inserted to remove the residual pump power and any 2nd-Stokes light from the laser cavity. Another dichroic mirror, DM1, separated the pump and signal beam paths at the pump launch end. To protect the YDF MOPA from any reflection originating in the RFL, a free-space isolator was inserted between the RFL and the Raman pump MOPA.

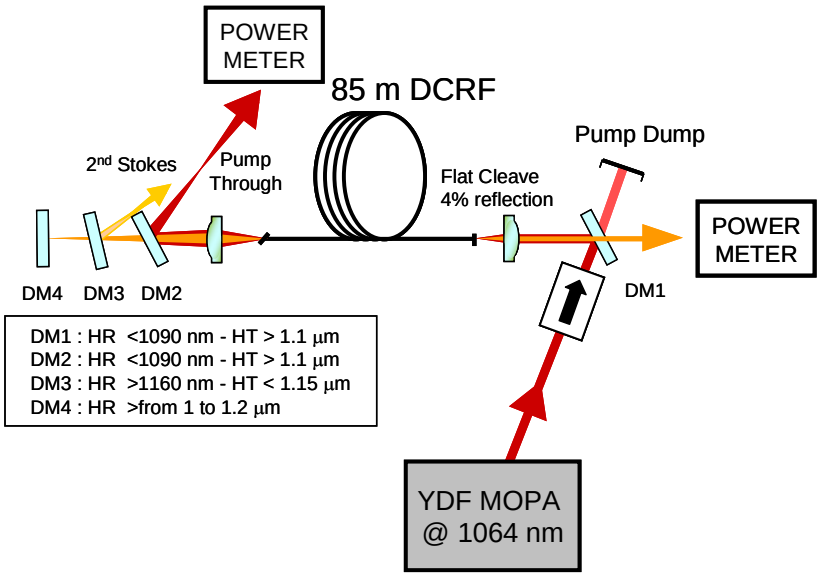

Figure 5.5: Experimental setup of the CP RFL in a 4% - 100% linear cavity.

5.2.2.2 Experimental results

Figure 5.6 shows the dependence of the output power of the RFL on the launched pump power. The residual pump power reflected by the DM2 is also plotted against the launched pump power. As shown in Figure 5.6, the threshold was about 28.8 W for the linear-cavity CP RFL. Above the laser threshold, the output power increased linearly with the increase of the launched pump power. The maximum signal output power was 102.5 W at 165 W of launched pump power. The laser output power rolled off for higher pump powers. The output power was not limited by the 2nd-Stokes generation. Figure 5.7 shows the measured spectrum at the maximum signal output power. The 2nd Stokes was not seen. One possible explanation of the roll-off is thermal lensing in the free-space isolator at high power. This was observed to degrade the pump beam quality and modify the pump-launch efficiency. Figure 5.7 shows that the CP RFL was lasing at

1120 nm and the output spectrum was very clean with an extinction ratio over 40 dB at 2 nm resolution bandwidth.

The RFL slope efficiency was 71% with respect to the launched pump power. See the dashed fitting curve in Figure 5.6. This is comparable to typical ytterbium-doped fibre lasers. Discounting the leakage of un-converted pump power, we obtain a slope efficiency of 80% with respect to the lost pump power. Though quite high, it is still lower than the quantum defect would allow for. The excess loss, beyond the quantum defect, was dominated by the insertion losses induced by the DMs placed at the angle-cleaved fibre end. This was confirmed by removing these DMs and operating the same fibre in a 4% - 4% linear-cavity laser, leading to a better slope efficiency. Those results will be shown in the next section.

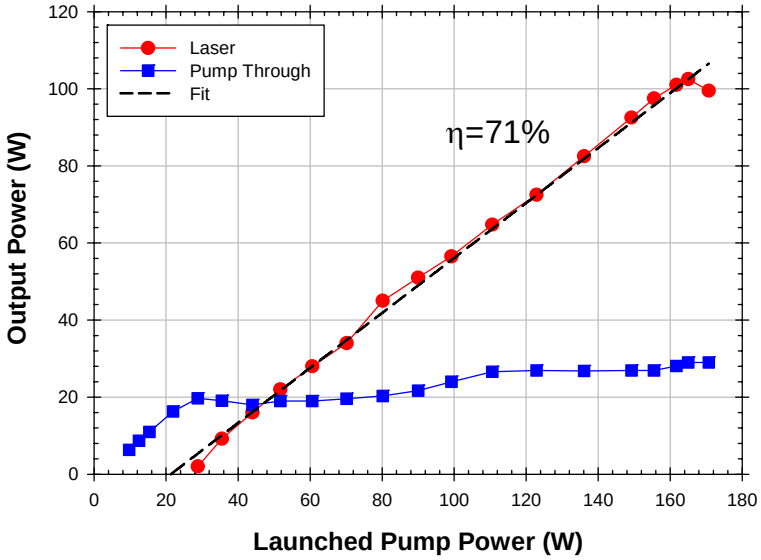

Figure 5.6: Output Power (red curve) and pump throughput (blue curve) *vs*. launched pump power.

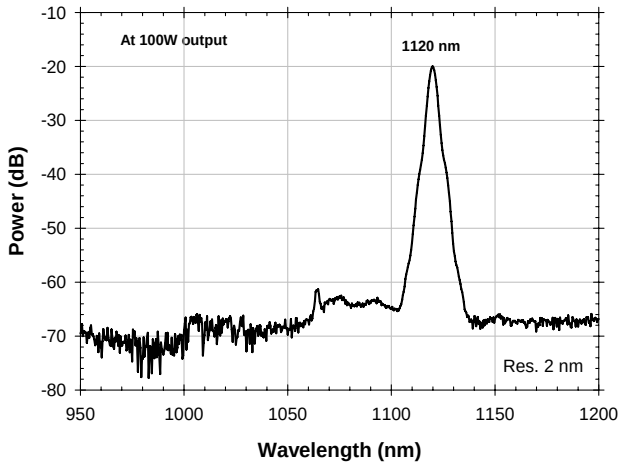

Figure 5.7: Output spectrum at 100 W output power.

Furthermore, the output beam quality was measured at different powers. Just above laser threshold, the beam propagation factor (M^2) was measured to be 1.35 as shown in Figure 5.8(a). This is comparable to the theoretical value of 1.21 for the fundamental mode at this wavelength obtained from this fibre's RIP [25]-[26]. At 80 W of laser output power, the beam quality of the signal was slightly degraded. The beam propagation factor (M^2) was determined to be 1.63, from the measured data shown in Figure 5.8(b). It indicates that part of the pump power was transferred into higher-order modes. It should be possible to improve the beam quality of the laser output light by inserting spatial mode filters into the laser cavity. Nonetheless, the beam quality is perfectly acceptable for many applications.

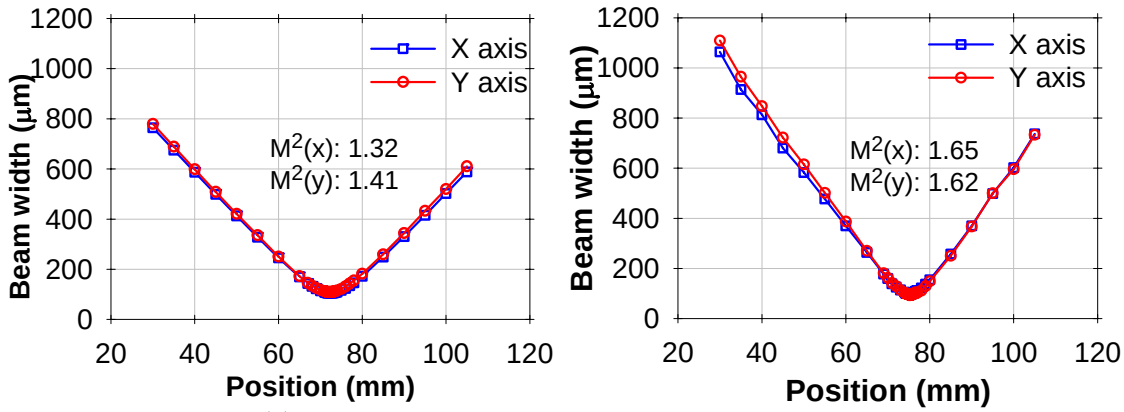

Figure 5.8: M^2 measurement of the 1st Stokes at output power of: (a) 2 W; (b) 80 W.

5.2.3 CP RFL in a 4% - 4% linear cavity

5.2.3.1 Experimental setup

The laser characteristics were also studied in a 4% - 4% linear cavity, which is illustrated in Figure 5.9. The Raman pump beam was free-space launched into a 75 m long piece of DCRF F71-LF11. Both fibre ends were flat cleaved and worked as cavity mirrors by using the 4% Fresnel reflection. DMs were put at both fibre ends to separate Raman pump beam paths from output signal beam paths. The free-spaced isolator was still placed between the Raman laser and the YDF MOPA, for protection.

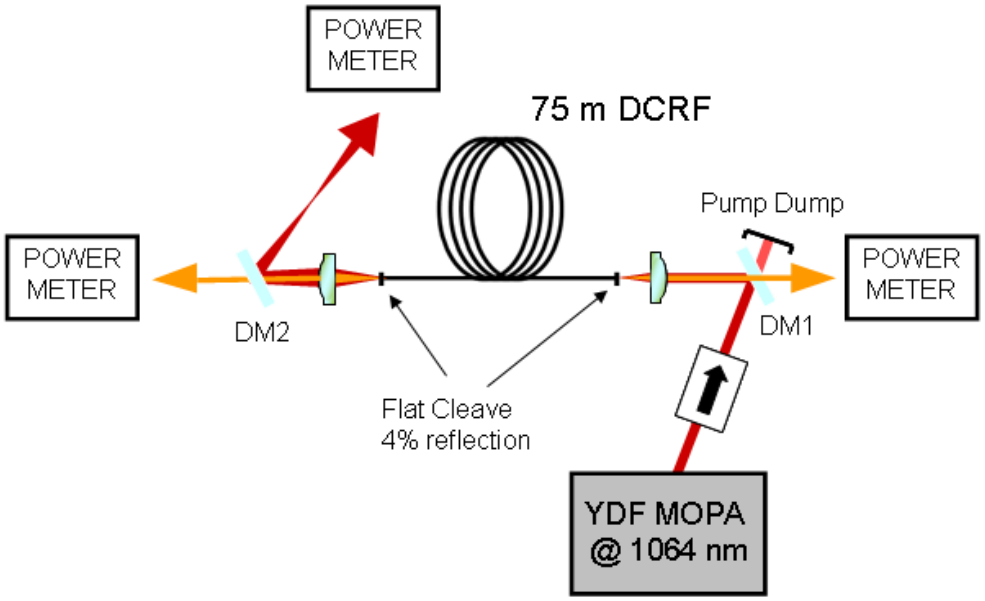

Figure 5.9: Experimental setup of CP RFL in a 4% - 4% linear cavity.

5.2.3.2 Experimental result

Figure 5.10 shows the dependence of the total laser output power out-coupled from both ends on the launched pump power. The leaked pump power is shown, as well. The laser threshold increased to about 43 W, as estimated from Figure 5.9. The maximum laser output power was 111 W, obtained at 158 W of launched pump power. Here, the output power includes some 2^{nd}-Stokes power. However, the 2^{nd} Stokes just started to appear at the highest pump power and its power was negligible compared to the 1^{st}-Stokes power. Figure 5.11 shows output spectra near the threshold and at 110 W output power, at which point the 2^{nd} Stokes can be clearly seen. The slope efficiency was 86% with respect to the launched pump power and as high as 91% with respect to the lost pump power. Given the losses in the mirror, this number is very close to the quantum-defect limited efficiency of 95%. The difference is largely explained by the fibre propagation loss, while all other loss sources appear to be negligible.

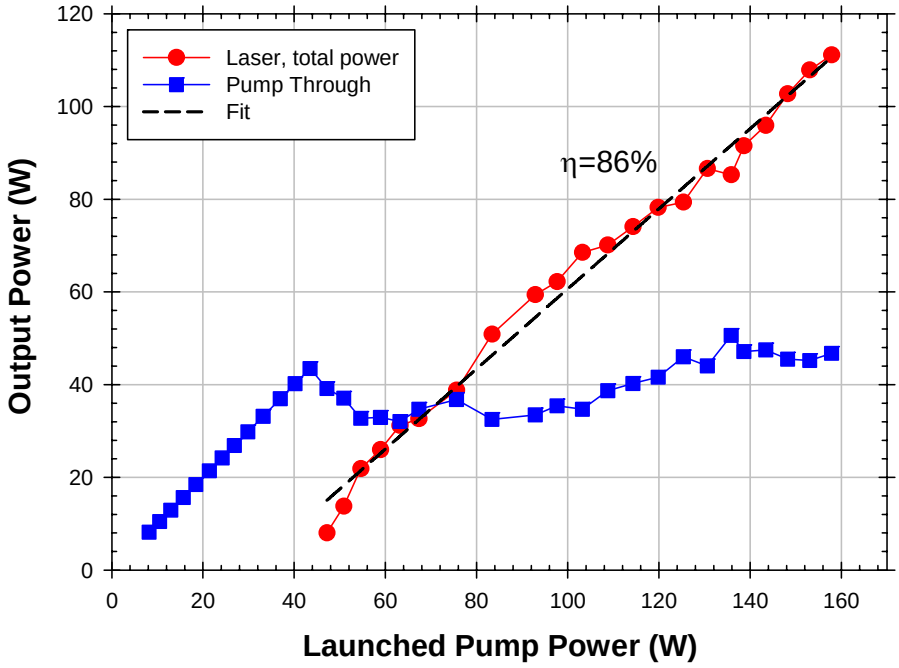

Figure 5.10: Output power (red curve) and residual pump power (blue curve) *vs.* launched pump power.

The propagation factor M^2 was measured to be 1.36 when the output power was low. Unfortunately, it was not measured at high output power. However, the beam quality should be comparable to that obtained with single-ended output.

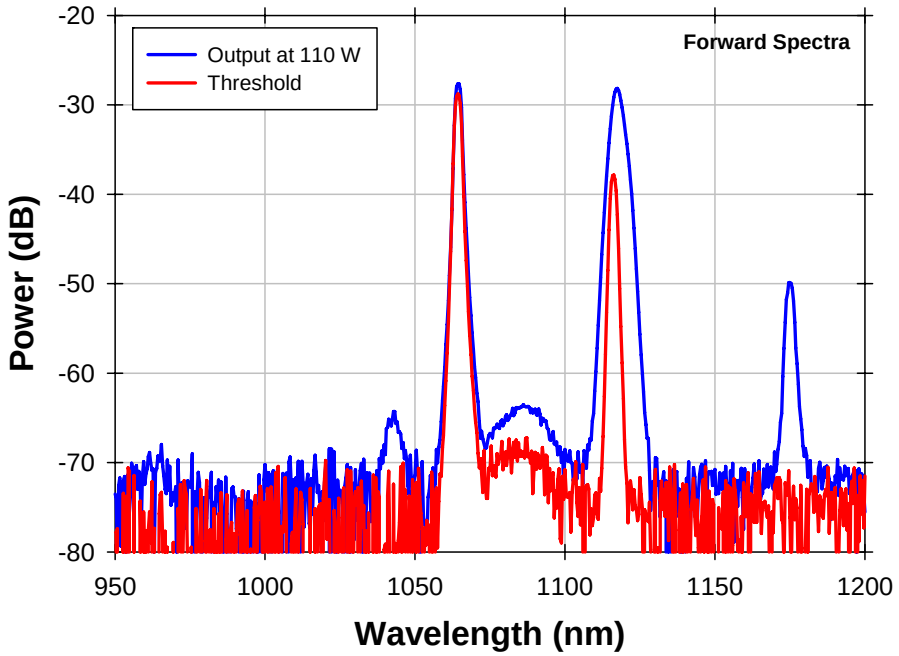

Figure 5.11: Output spectra at the threshold (red curve) and at 110 W output power (blue curve).

5.3 Simulations

I numerically solved Eq. (2.32) – Eq. (2.34) with appropriate parameters and boundary conditions in order to calculate the output power of the 4% - 4% linear-cavity CP RFL described above, and compare experimental and model data. All parameters needed for the simulation are known except for the average effective areas, $A_{eff}(\lambda_0, \lambda_1)$ for SRS from pump to 1st Stokes and $A_{eff}(\lambda_1, \lambda_2)$ for SRS from 1st to 2nd Stokes. Given the high beam quality obtained experimentally it seems reasonable to assume that the 1st Stokes builds up primarily in the fundamental mode. This creates gain primarily for the fundamental mode at the 2nd-Stokes wavelength. Therefore, although there will be some power in other modes, $A_{eff}(\lambda_1, \lambda_2)$ can be approximated by the effective area for SRS from the fundamental mode at the 1st Stokes to the fundamental mode at the 2nd Stokes, which is about 63 μm^2. With reference to Eq. (4.1), the effective area $A_{eff}(\lambda_0, \lambda_1)$ can be obtained from the laser threshold, which is determined as:

$$P_{threshold} = \frac{L_{cavity}}{4.343(2L_{eff})g_{co}} A_{eff}(\lambda_0, \lambda_1). \tag{5.11}$$

Here, L_{cavity} is the cavity loss in dB. The threshold $P_{threshold}$ was ~ 43 W in the experiment, from which the average effective area $A_{eff}(\lambda_0, \lambda_1)$ is calculated to 95 μm^2. Figure 5.12 shows the calculated and experimental output power with respect to the launched pump power. The simulated 1st-Stokes output power agrees well with the experimental results when the launched pump power is below 100 W. When the pump power is further increased, the 2nd Stokes starts to build up and deplete the 1st-Stokes power in the simulation. However, the 2nd Stokes was not seen during the experiment until the pump power reached the maximum, and even then, the 2nd-Stokes power was only 0.5% of the 1st-Stokes power. This discrepancy is tentatively attributed to an increase in effective area as the pump power increases. Considering first the gradual roll-over in the experimental curve seen in Figure 5.12, there are two reasons why the effective area for this process (SRS from pump to Stokes) increases at higher pump power. One is that the pump beam quality degrades, e.g., because of thermal lensing in the isolator. At low pump power a significant fraction of the pump power may actually be launched into the core, or have a stronger overlap with the core than the fibre geometry suggests. Note here that the 11 μm diameter of the effective area $A_{eff}(\lambda_0, \lambda_1)$, evaluated at low pump power is much smaller than the geometric diameter of 21 μm as

shown in Figure 4.2. In addition, power in pump modes with high overlap with the signal mode depletes quicker than other modes, which implies that the pump – signal overlap decreases at higher pump depletion. At the highest pump power in Figure 5.12, the pump depletion exceeds 70%. If the effective area is adjusted to match the high-power characteristics rather than the threshold it becomes 178 μm^2. See Figure 5.13. As it comes to the onset of the 2nd Stokes, this occurs at ~ 45% higher 1st-Stokes power experimentally (110 W) than it does in the model calculations (76 W). This may be due to 1st-Stokes power in higher-order modes, and the corresponding increase in effective area. For the 4% - 100% cavity, the beam quality (M^2) degraded from 1.35 at low power to 1.63 at high power. If this attributed to an increased beam area, it corresponds to an increase of 41%. While Figure 5.8 appears to suggest that it is the beam divergence rather than the beam area that increased when the beam quality decreased, this is not necessarily so since the optical alignment used when measuring the beam quality at those two powers is likely to have been different.

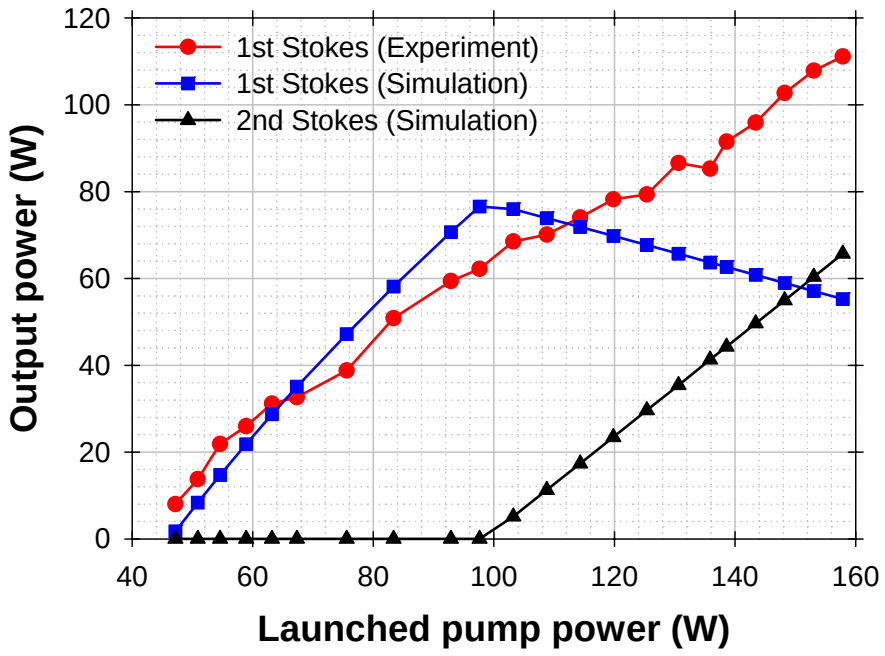

Figure 5.12: Simulations and experimental results of laser output power *vs.* launched pump power in the case of 4% – 4% linear-cavity CP RFL. $A_{eff}(\lambda_0, \lambda_1)$: $\pi(11/2)^2 \approx$ 95 μm^2; $A_{eff}(\lambda_1, \lambda_2)$: $\pi(8.95/2)^2 \approx 63$ μm^2.

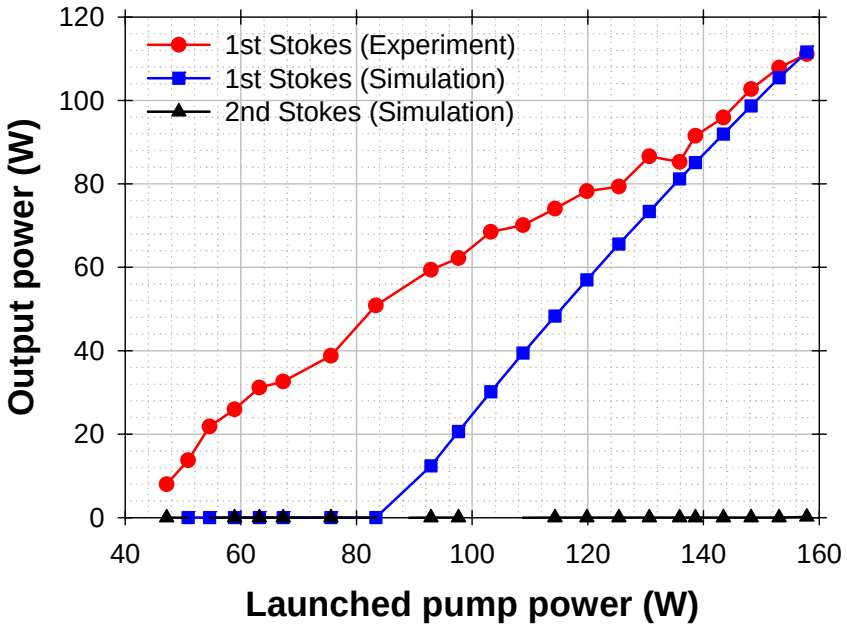

Figure 5.13: Simulations (blue curve) and experimental results (red curve) *vs.* the launched pump power in the case of 4% – 4% linear-cavity CP RFL. $A_{eff}(\lambda_0, \lambda_1)$: $\pi(15/2)^2 \approx 178$ μm^2; $A_{eff}(\lambda_1, \lambda_2)$: $\pi(10.5/2)^2 \approx 86.6$ μm^2.

5.4 Summary

In this chapter, I have described experiments on high-power CW CP RFL in 4% – 100% and 4% – 4% linear cavities. The output was nearly diffraction limited with both schemes, and reached over 100 W of output power at 1120 nm. This is the highest output power obtained from a CP Raman fibre device so far. The experimental slope efficiency was high, reaching 80% and 91% with respect to absorbed pump power in the 4% – 100% and 4% – 4% laser cavity configurations, respectively. The output beam is slightly multimoded at high power since the core of this fibre is not single-moded at the emitting wavelength. Even higher powers should be possible through this approach. In the experiments, thermal lensing in the isolator was the principal obstacle to scaling to higher powers. While an isolator may be necessary during experimental work, it is quite possible that a finalised configuration can work without an isolator, if pump feedback is minimised by angle-cleaving the ends of the DCRF.

The power scalability of CW CP Raman fibre devices with broad linewidth was analysed theoretically by considering the limiting factors, e.g., thermal effect, optical damage, and pump brightness. If a DCRF is pumped by the source with the same intensity as that of the YDF MOPA used in this chapter, the ultimate power can be as high as 23.8 kW for inner-cladding-to-core area ratios of both 8 and 34. This is limited

by thermal lensing, and requires very large cores. For smaller cores, the output power is limited by the material damage. Thus, a large core is critical for high-power operation. The relatively small core size of the DCRF F71-LF11 would be a hurdle for power-scaling to very high levels. In the next chapter I will introduce new DCRFs with large-mode areas. Although those were only investigated in the pulsed regime, they should be scalable to the multi-kW regime in the cw regime.

5.5 Reference

[1] A. Shirakawa, C. A. Codemard, J. Ji, K. K. Chen, A. Malinowski, D. J. Richardson, J. K. Sahu, and J. Nilsson, "High-brightness 210 μJ pulsed Raman fiber source", in Proc. of Conf. Lasers and Electro-Optics /QELS, San Jose 4-9 May 2008, paper CTuL1.

[2] S. Huang, Y. Feng, A. Shirakawa, K. Ueda, "Generation of 10.5 W, 1178 nm laser based on phosphosilicate Raman fiber laser", Jpn. J. App. Phys. **42**(part 2, 12A), L1439 (2003).

[3] Z. Xiong, N. Moore, Z. G. Li, and G. C. Lim, "10-W Raman fiber lasers at 1248 nm using phosphosilicate fibers", J. Lightwave Technol., **21**(10), 2377 (2003).

[4] Y. Feng, L. R. Taylor, and D. B. Calia, "25 W CW Raman-fiber-amplifier-based 589 nm source for laser guide star", Opt. Express, **17**(21), 19021 (2009).

[5] Y. Feng, L. R. Taylor, and D. B. Calia, "150 W highly-efficient Raman fiber laser", Opt. Express, **17**(26), 23678 (2009).

[6] N. B. Terry, K. T. Engel, T. G. Alley, and T. H. Russell, "Use of a continuous wave Raman fiber laser in graded index multimode fiber for SRS beam combination", Opt. Express, **15**(2), 602 (2007).

[7] J. Jang, Y. Jeong, J. K. Sahu, M. Ibsen, C. A. Codemard, R. Selvas, D. C. Hanna, and J. Nilsson, "Cladding-pumped continuous-wave Raman fiber laser", in Proc. of Conf. Lasers and Electro-Optics/QELS, Baltimore 3-5 Jun 2003, paper CWL1.

[8] C. A. Codemard, P. Dupriez, Y. Jeong, J. K. Sahu, M. Ibsen, and J. Nilsson, "High-power continuous-wave cladding-pumped Raman fiber laser", Opt. Lett., **31**(15), 2290 (2006).

[9] C. A. Codemard, J. Ji, J. K. Sahu, and J. Nilsson, "100 W CW cladding-pumped Raman fiber laser at 1120 nm", in Proc. of SPIE Photonics West, San Francisco Jan. 2010, paper 7950-58.

[10] E. Stiles, "New developments in IPG fiber laser technology", in Proc. of 5th Int. Workshop Fiber Lasers, Dresden Germany October 2009.

[11] T. Ehrenreich, R. Leveille, I. Majid, K. Tankala, G. A. Rines, and P. F. Moulton, "1-kW, all glass Tm:fiber laser", in Proc. of SPIE Photonics West, San Francisco Jan. 2010 (Postdeadline).

[12] J. Nilsson, "High power fiber lasers and amplifiers", in Proc. of OFC, San Diego March 2009, Short course SC290.

[13] J. W. Dawson, M. J. Messerly, R. J. Beach, M. Y. Shverdin, E. A. Stappaerts, A. K. Sridharan, P. H. Rax, J. E. Heebner, C. W. Siders, and C. P. J. Barty, "Analysis of the scalability of diffraction-limited fiber lasers and amplifiers to high average power", Opt. Express, **16**(17), 13240 (2008).

[14] G. P. Agrawal, *Nonlinear Fiber Optics*, 3rd Ed., Academic Press Inc, San Diego CA (2001).
[15] D. Brown and H. J. Hoffman, "Thermal, stress, and thermo-optic effects in high average power double-clad fiber lasers", IEEE J. Sel. Top. Quantum Electron., **37**(2), 207 (2001).
[16] W. Krupke, M. D. Shinn, J. E. Marion, J. A. Caird, and S. E. Stokowski, "Spectroscopic, optical, and thermomechanical properties of neodymium- and chromium-doped gadolinium scandium gallium garnet", J. Opt. Soc. Am. B, **3**(1), 102 (1986).
[17] Private discussion with Prof. Johan Nilsson.
[18] D. E. Gray, *American Institute of Physics Handbook*, 3rd Ed., McGraw-Hill (1972).
[19] W. Koechner, *Solid State Laser Engineering*, 6th Ed., Springer (2006).
[20] J. Nilsson, J. K. Sahu, Y. Jeong, W. A. Clarkson, R. Selvas, A. B. Grudinin, and S-U, Alam, "High power fiber lasers: new developments", Proc. SPIE 4974, 50 (2003).
[21] Information on the recent diode laser brightness capabilities can be referred to manufacturers such as JDS Uniphase, nLight, Jenoptik, IPG Photonics and others.
[22] S. T. Davey, D. L. Williams, B. J. Ainslie, W. J. M. Rothwell, and B. Wakefield, "Optical gain spectrum of GeO_2-SiO_2 Raman fiber amplifiers", in Proc. of Inst. Elect. Eng., **136**(6), 301 (1989).
[23] J. Bromage, K. Rottwitt, and M. E. Lines, "A Method to predict the Raman gain Spectra of germanosilicate fibers with arbitrary index profiles", IEEE Photonics Technol. Lett., **14**(1), 24 (2002).
[24] C. Fukai, K. Nakajima, J. Zhou, K. Tajima, K. Kurokawa, and I. Sankawa, "Effective Raman gain characteristics in germanium- and fluorine-doped optical fibers", Opt. Lett., **29**(6), 545 (2004).
[25] H. Yoda, P. Polynkin, and M. Mansuripur, "Beam quality factor of higher order modes in a step-index fiber", J. Lightwave Technol., **24**(3), 1350 (2006).
[26] Z. Jiang, and J. R. Marciante, "Impact of transverse spatial-hole burning on beam quality in large-mode-area Yb-doped fibers", J. Opt. Soc. Am. B, **25**(2), 247 (2008).

Chapter 6 DCRFs with large-mode areas

The only DCRF used in my experiments presented so far in this thesis is F71-LF11. Several good results have been obtained, demonstrating the versatility of DCRFs and this fibre in particular. For example, a high conversion efficiency pulse-pumped CP RFA was described in Chapter 4. The peak power conversion was more than 75% while the energy conversion efficiency exceeded 60%. In Chapter 5, a 100 W CW CP RFL was described. Besides, this fibre was also used as a cladding-pumped Raman converter, generating nearly diffraction-limited pulses with 210 μJ output energy [1]. In spite of these results, the comparatively small size of this fibre restricts its applications. Firstly, the core dimension is critical for the power scalability of CP Raman fibre devices as discussed in the previous chapter. The relatively small core (about 9 μm diameter) leads to a relatively low core damage threshold, and further limits the achievable power and energy from this fibre. Secondly, because of its small inner cladding (~ 21.6 μm diameter) together with its small inner-cladding NA (~ 0.22), the fibre has to be pumped by sources with relatively good beam quality. Thirdly, as discussed in Chapter 3, a small area ratio between inner cladding and core is required for high conversion efficiency into the 1st Stokes. According to Eq. (3.4), the inner-cladding-to-core area ratio should be no more than eight. However, the area ratio of this fibre is even more restricted, just 5.76. Thus, these geometrical factors ultimately limit the brightness enhancement that this fibre can provide. The brightness enhancement obtained in the experiments with this fibre was limited to ~ 10 [1]-[8].

To overcome the limitations set by the fibre geometry, we have recently introduced new DCRFs with large-mode areas [9]-[11]. These new fibres with fibre number T0340, T0342 and T0343 allow sources with relatively poor beam quality to be used as Raman pumps, and thus achieve better brightness enhancement. Furthermore, they are more promising for high-power or high-energy sources with good beam quality compared to the old fibre F71-LF11. More details of the new fibres will be given in this chapter, in conjunction with the experiments carried out with these three large-mode-area DCRFs. Firstly, section 6.1 presents the characteristics of the new fibres.

Subsequently, section 6.2 describes pulse-pumped CP RFAs that were built with these new fibres and pumped by a multimode fibre source. The experimental results show that the DCRFs T0340, T0342 and T0343 can work as efficiently as the old fibre F71-LF11. The peak power conversion into the 1st Stokes was above 60% obtained for all three new fibres. The highest output peak power of 2.72 kW was obtained at 4.88 kW input pump peak power in the DCRF T0343. The brightness gain (degree of brightness enhancement) was also improved by these new fibres compared to that of the old fibre.

Then, a simple and effective approach is proposed for SC-generation based on CP Raman fibre converters. Its principle and benefits in comparison with the normal methods are given in section 6.3. A 19 W average power SC ranging from 1 μm to beyond 1.75 μm was generated in 100 m of DCRF T0340. Section 6.4 reports a 1 mJ energy source based on a piece of DCRF T0343, pumped by a Q-switched Nd:YAG laser. The output energy was restricted by fibre facet damage. To my knowledge, this is the highest energy ever achieved from a Raman fibre device. I also discuss the performances of the Raman fibre converters pumped by temporally spiky pulses, which is exactly the case of the Nd:YAG laser used in this chapter. Finally, section 6.5 summarises the chapter.

6.1 Double-clad Raman fibres with large-mode areas

The new DCRFs with large-mode areas, T0340, T0342, and T0343, were fabricated through the MCVD process by Mr. Andrew Web and Mr. Robert Standish in the Silica Fibre Fabrication group at ORC. These fibres were drawn from the same preform (preform number: L30199) into three different sizes. Thus, they have almost the same area ratio between the inner cladding and the core. The fibres were carefully investigated and their details are as follows.

6.1.1 Refractive index profile

All three fibres comprise a germanium-doped silica core and a pure-silica inner cladding. Outside the inner cladding, there is a layer of fluorine-doped silica glass to confine the inner-cladding modes. The fluorine-doped silica layer is surrounded by another layer of pure-silica to make the fibre sufficiently thick to avoid micro-bending [12] as well as a polymer coating for protection. Thus, like the fibre F71-LF11, these new fibres also

have an all-glass-structure for guiding light. Note that the pure-silica layer next to the coating can guide the light too since the coating has a low index, so caution is required to make sure the light is launched into the core or inner cladding rather than this outside region, which is optically isolated from the core at the NAs I use. The dimensions of these three fibres are summarised in Table 6.1. The largest fibre, T0343, has a 40 μm diameter core and 107 μm diameter inner cladding, which is almost five times larger than for the fibre F71-LF11. The inner-cladding-to-core area ratio is around 7.2 for the new DCRFs, which is also larger than that of F71-LF11, but still meets the requirement set on the area ratio given by Eq. (3.4) in order to obtain high conversion efficiency into the 1st Stokes.

Table 6.1: Geometrical characteristics of DCRFs with large-mode areas.

Fibre number	T0340	T0342	T0343
Core diameter (μm)	18.4	31	40
Inner-cladding diameter (μm)	49.1	83.4	107
Outer-cladding diameter (μm)	160	275	350
Area ratio between the inner cladding and core	7.1	7.2	7.2

A picture and an idealized RIP of the fibre T0340 are shown in Figure 6.1(a). During the preform preparation, unwanted air bubbles were generated around the inner cladding. This is caused by the difference of the volatility between pure silica and fluorine-doped silica glass [13]. Air bubbles appear inside the fibres T0342 and T0343 too. The existence of the air bubbles makes the new fibres more fragile than normal fibres. Thus, special cautions are required when handling these new fibres, e.g., in fibre facet preparation. Another issue brought by the air bubbles is the background loss. Loss measurements (described in the next section) show that the air bubbles do induce extra loss, but the background loss is still acceptable for a CP RFA, and the fibres are still useful. The undesirable air bubbles could well change the inner-cladding NA too, but did not in reality. I measured the inner-cladding NA of the three fibres, and they are all around 0.2, which matches the NA expected from the refractive index of the glasses. The core NA (relative to the inner cladding) is estimated to be 0.066 from the RIP in Figure 6.1(b). It was directly measured on the preform by Mr. Robert Standish, scaled to match the size of the fibre. Similar as the fibre F71-LF11, the refractive index has a dip in the centre due to the evaporation of germanium during preform collapse. It changes the mode distribution but not the principle of the CP Raman converters. The V-numbers

of the cores are about 3.8, 6.4, and 8.3, respectively, for the fibre T0340, T0342, and T0343 at a wavelength of 1 μm, making them all slightly multimoded. The cut-off wavelength is estimated to around 1.7 μm for the DCRF T0340. It will be even longer for the other two, in proportion to their V-values.

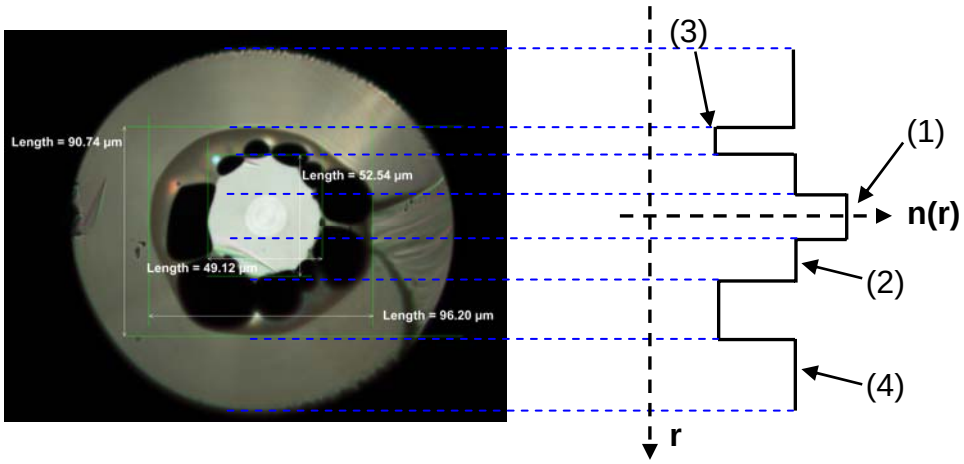

(a)

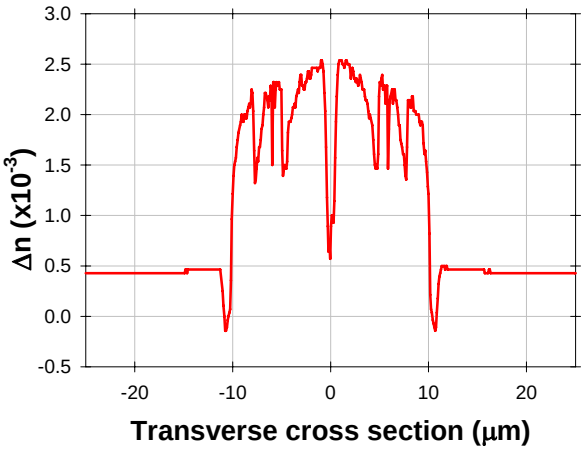

(b)

Figure 6.1: (a) Image of cross-section of DCRF T0340 with idealised RIP: (1) germanium-doped silica core; (2) pure-silica inner cladding; (3) fluorine-doped silica layer with air-bubbles; (4) pure-silica outer cladding; (b) Measured RIP of preform L30199, scaled to match the core size of DCRF T0340.

6.1.2 Background loss

The air bubbles might induce unacceptable loss for my SRS experiments. Therefore, the transmission spectrum of a 709 m long piece of DCRF T0340 was characterised with a WLS and an ANDO OSA. The fibre was then cut back to a length of 1.5 m and the transmission spectrum re-measured so that the background loss of the inner cladding could be determined according to the conventional cut-back method. The WLS beam was free-space-coupled to the fibre. The recorded transmission spectra are shown as red

and blue curves in Figure 6.2, together with the background loss for the inner cladding, as determined from the two. The background loss at 1 μm is around 7 dB/km in the inner cladding. The background loss in the core was measured with a single-mode fibre source at 1116 nm. The light from the fibre source was launched into the core of a 100 m long DCRF T0340 by careful alignment. The beam quality at the output was monitored to ensure that the light was guided inside the core. After cutting back the fibre, the background loss was obtained, ~ 2.4 dB/km. Thus, for wavelengths around 1 μm, the propagation loss is much higher in the inner cladding than in the core, presumably because of the air bubbles. The high background loss will affect the conversion efficiency for long fibres, but not for sufficiently short ones. Since the other two fibres T0342 and T0343 were drawn from the same preform, their background losses are assumed to be similar to that of the DCRF T0340. Compared to the background loss of the fibre F71-LF11 (3.4 dB/km and 3.2 dB/km in the core and inner cladding, respectively), the loss in the core of this fibre is slightly lower, perhaps because the germanium concentration in the core is lower in this fibre while its inner-cladding loss is higher, probably because of the air bubbles.

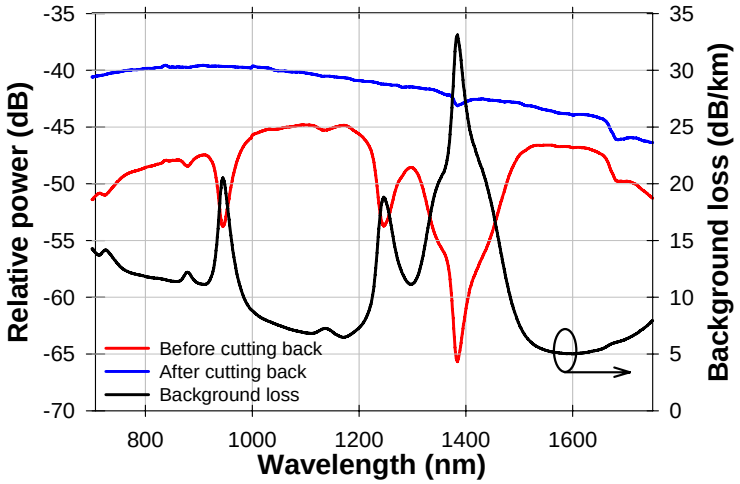

Figure 6.2: Inner-cladding background loss spectrum of DCRF T0340.

6.1.3 Raman gain coefficient

Since the inner cladding is pure silica, the Raman gain coefficient is 5×10^{-14} m/W for unpolarised light at 1 μm. Based on the RIP of this fibre, the germanium concentration in the core is estimated to be around 1.2% (mol). With such low concentration of germanium, the Raman gain coefficient in the core remains almost the same as in the inner cladding [14]-[16]. Due to the high germanium concentration, the Raman gain

coefficients are higher in the fibre F71-LF11. Furthermore, in F71-LF11, the Raman gain coefficient is higher in the core than in the inner cladding, which favours SRS into the core modes. The less favourable situation in the new fibres calls for special attention.

6.1.4 Modes

Based on the RIP in Figure 6.1, the effective index was calculated for the modes in the new fibres at a wavelength of 1064 nm with OptiFiber™. The RIP measured on the preform was scaled to match the real size of these fibres. Furthermore, circularly symmetric RIPs approximated the actual RIPs for these calculations. The number of modes increases with increasing fibre size as shown in Figure 6.3. There are 118, 261, 460 LP fibre modes, respectively, inside the fibre T0340, T0342, and T0343. In contrast, there are only 26 LP fibre modes inside the fibre F71-LF11 at 1 μm. These numbers do not include the sine / cosine mode multiplicity of modes with azimuthal dependence. The black horizontal line in the plot marks the inner-cladding refractive index. At 1064 nm, there are four, six, and ten core-modes, respectively, in T0340, T0342, and T0343. The fibre F71-LF11 has three core modes. More core modes make it more difficult to obtain good beam quality.

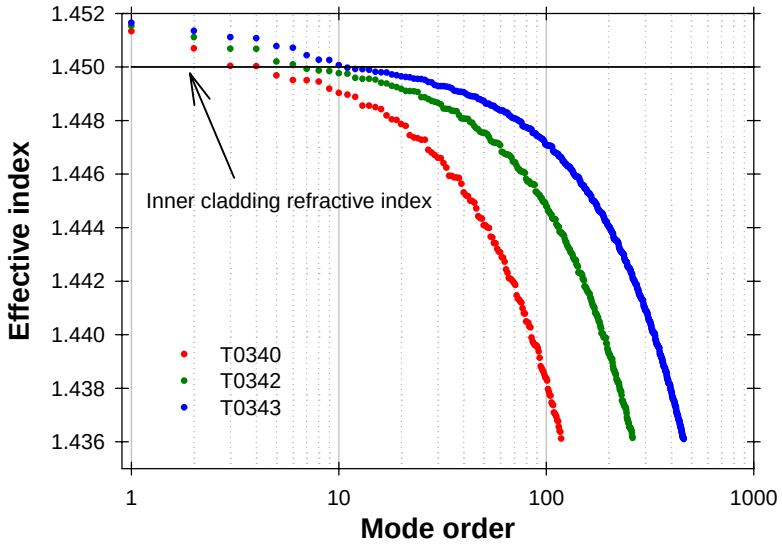

Figure 6.3: (Simulation) Effective index of modes at 1064 nm in the new DCRFs, from left to right, T0340 (red dots), T0342 (green dots), and T0343 (blue dots).

6.2 Pulse-pumped CP RFAs with DCRFs T0340, T0342, and T0343

In this section, I describe the Raman amplifier experiments performed with the new fibres T0340, T0342, and T0343. As discussed in the previous section, a short fibre is

preferred for high conversion efficiency due to the relatively high inner-cladding background loss. Together with the large inner-cladding areas, this leads to a high Raman threshold. Thus, a pulse-pumping is chosen for these experiments. The DCRFs were set up as CP RFAs, pumped by a commercial multimode pulsed fibre source and seeded by a diffraction-limited CW fibre source built in-house, as described below.

6.2.1 Multimode Raman pump

An industrial pulsed fibre source from SPI Laser Inc. (SP-30P-0031-000 "G3") was used as the Raman pump. It is a diode-seeded two-stage YDF MOPA system at 1064 nm with tuneable pulse duration and PRF. It can produce up to 16 kW peak power at 30 kHz PRF. Unfortunately, the pulse shape is less suitable for efficient Raman conversion and well-controlled experimentation than was the case for the in-house EYDF pump MOPA used in chapter 4. There is a spike in the leading edge of the pulse, followed by a long tail. By increasing the PRF, the pulse becomes more square-like at the price of the output peak power. At 150 kHz PRF, the output peak power is lowered to 10 kW. The output pulses are of a more suitable super-Gaussian-like shape. Figure 6.4 shows the pulse shapes at different peak powers. As a compromise between the pulse shape and the peak power, the PRF was fixed at 150 kHz during the experiments. At this PRF, the pulse duration is around 23 ns (FWHM). The beam quality (M^2) is around 3.2. The inset shows the corresponding output spectra. It broadens with the increase of the peak power due to SPM.

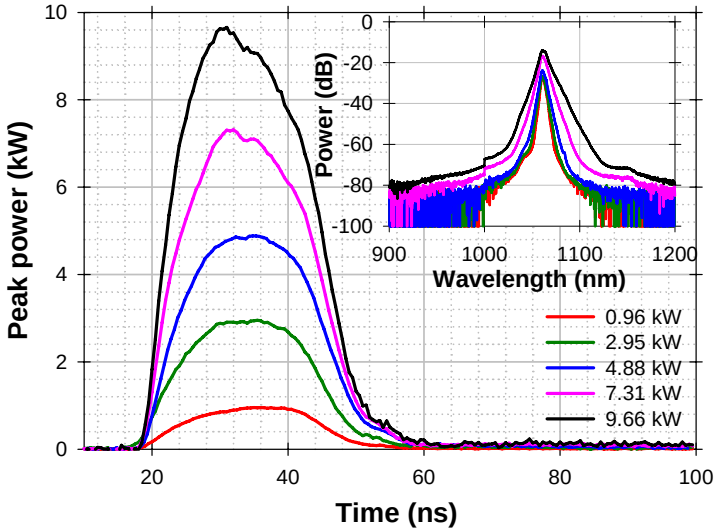

Figure 6.4: Raman pump pulse shapes under different output peak power at 150 kHz PRF. Inset: corresponding output spectra.

6.2.2 Diffraction-limited CW Raman seed laser

A CW core-pumped RFL at 1116 nm in a linear cavity was constructed to be used as a seed laser for the CP RFA. Figure 6.5 shows the configuration. The seed laser itself was pumped by a linear-cavity YDFL at 1064 nm. The YDFL consists of a piece of GTwave™ fibre, a 10 W, 915 nm laser diode, and two FBGs acting as cavity mirrors with 99.9% and 14.5% reflections at 1064.5 nm. The output end of the YDFL was spliced to a 2 kW long piece of Pirelli Freelight™ fibre. This, together with two FBGs serving as cavity mirrors, formed the RFL at 1116 nm. The FBG reflectivities were 99.9% and 15% at 1116 nm. At the output of the RFL, a WDM from Lightel Technologies Inc was used to separate the residual pump at 1064 nm from the signal at 1116 nm. The pigtails of all the FBGs and the WDM are Hi1060 fibre. Thus, although the Freelight™ fibre is not single-moded at 1 μm, the output beam from the CW Raman seed was truly single-moded and very close to diffraction-limited.

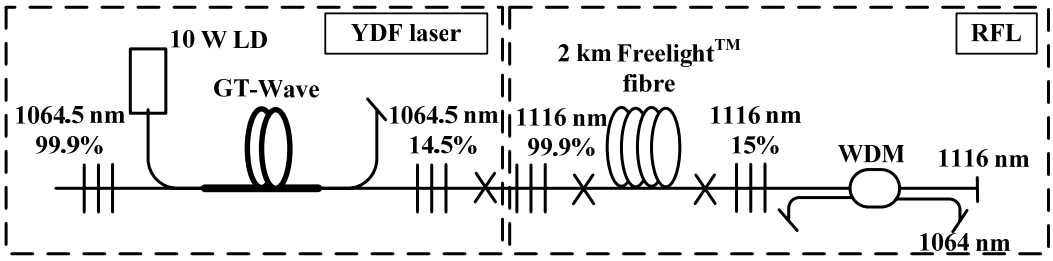

Figure 6.5: Experimental setup of the diffraction-limited CW Raman seed laser at 1116 nm.

Figure 6.6 shows the output power and spectra (inset) of the seed laser at 1116 nm after the WDM against its pump power. The black curve in the plot shows experimental data while the red curve shows the simulation results. Based on the experimental data, the threshold was estimated to be about 360 mW for the RFL. The Raman gain coefficient g_R is about 6.22×10^{-14} m/W at 1116 nm, from calculations based on the RIP of the Freelight™ fibre. The calculated effective area A_{eff} was 31.4 μm^2 for the fundamental mode based on the mode distribution obtained through the software OptiFiber™. The total cavity loss L_{cavity} was around 10 dB. The threshold in a linear-cavity Raman laser should be:

$$P_{threshold} = \frac{L_{cavity}}{4.343(g_{co} / A_{eff})(2L_{eff})}. \qquad (6.1)$$

The calculated threshold is about 349 mW, in good agreement with the experimental result. The slope efficiency was 64.6% with respect to the pump power. The maximum

signal power obtained is 1.12 W, limited by the available pump power. The corresponding conversion efficiency was 54% with respect to the pump power. However, there was also some power in the 2nd Stokes, which can be seen from the inset of Figure 6.6. The simulation also shows that the 2nd Stokes starts to appear at the maximum pump power. The simulation results of the RFL fit the experimental value well. In the simulation, the total background loss was assumed to be 1.8 dB including the fibre background loss and the insertion loss of the WDM.

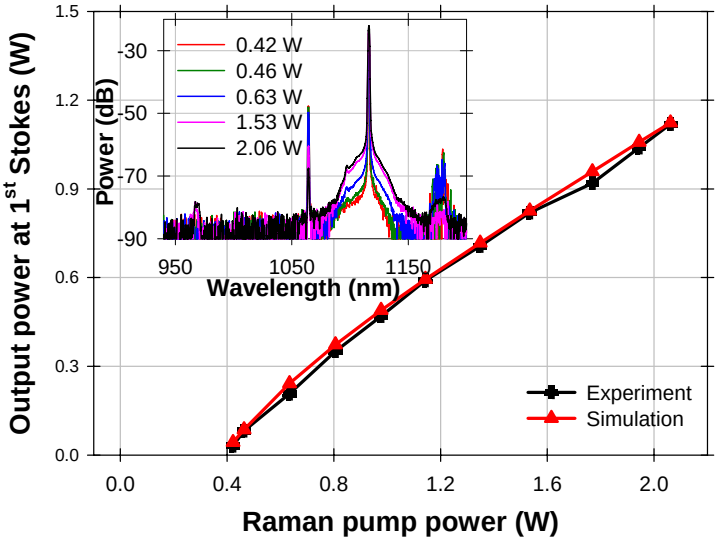

Figure 6.6: Output power at the 1st Stokes *vs*. pump power. Black curve: experimental data; Red curve: simulation result. Inset: Output spectra after the WDM under different pump powers.

6.2.3 CP RFA configuration

I used the multimode Raman pump and the diffraction-limited seed laser together with the new DCRFs T0340, T0342, and T0343 for CP Raman amplification experiments. Figure 6.7 illustrates the experimental setup. In this scheme, both the pulsed Raman pump beam and the CW Raman seed beam were free-space launched into the same end of the DCRF via DMs and focusing lenses. The lenses were carefully chosen so that the CW Raman seed beam was launched into the DCRF core and excited the core modes. At the same time, the Raman pump beam was launched into the core and inner cladding. The seed travelled in the same direction as the Raman pump along the fibre. As before in section 4.3.3, the part of the seed that overlapped in time with the Raman pump pulses experienced Raman gain, which strongly modulated the amplified signal output. At the output, several DMs were utilized to separate the residual pump, and 1st Stokes

and 2nd Stokes beams. Finally, a polarisation-independent free-space isolator was used to protect the pulsed Raman pump laser from back-reflections from the Raman amplifier.

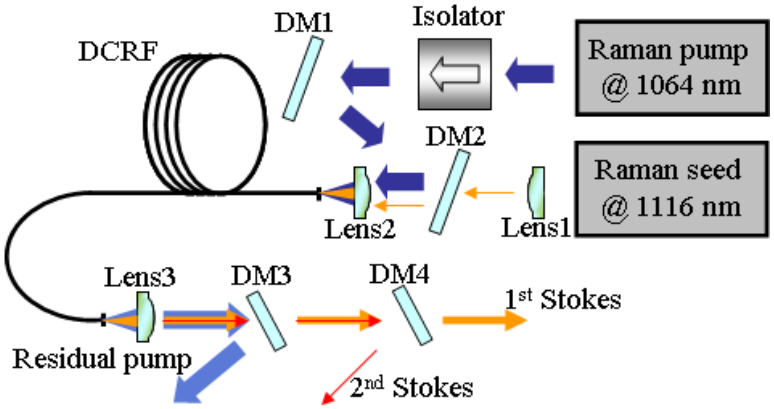

Figure 6.7: Experimental setup of pulsed CP RFAs. DM1, DM2, DM3: HR@1064 nm, HT@1116 nm and 1178 nm; DM4: HR@1178 nm, HT@1116 nm.

6.2.4 Experimental results and discussion

First, to investigate the effect on the conversion efficiency of the background loss, a relative long piece of DCRF T0340, around 700 m, was used in the pulse-pumped Raman fibre amplifier. The launch efficiencies of the Raman pump and the Raman seed were 86% and 90%, respectively, with a small fraction of the seed and most of the pump propagating in the inner cladding. The background losses in this piece were measured and found to be 4.9 dB and 2.2 dB for the pump and seed, respectively. During the experiment, the launched Raman seed power was kept constant at 180 mW while the Raman pump power was varied.

Figure 6.8 shows the output peak power against the peak power of the launched Raman pump. At the optimum, i.e., highest relative conversion into the 1st Stokes, the 1st-Stokes output peak power was 296 W, and the launched pump peak power was 1.0 kW. The corresponding conversion into the 1st Stokes was 30% with respect to the launched pump peak power. The slope was 65% with respect to the launched pump power. The 1st-Stokes power was limited by the generation of the 2nd Stokes. The 2nd Stokes depleted the 1st-Stokes power and increased in a 249% slope relative to the launched pump peak power. This fast growth can be explained by the difference between the effective area for the pump-to-1st-Stokes energy transfer, which was about the size of the inner-cladding area (depending on the launch conditions and modal excitations), and the effective area for the 1st-to-2nd-Stokes transfer, which was about the core size [2]. Since the Raman gain is inversely proportional to the effective area, the

nonlinear growth of the 2nd Stokes was faster than that of the 1st Stokes. Also note that with Raman fibre amplifiers, the slopes can exceed 100% over a limited power range, due to increased pump depletion at higher powers. This is true for SRS from the pump to the 1st Stokes, and even more so for cascaded SRS in a CP RFA.

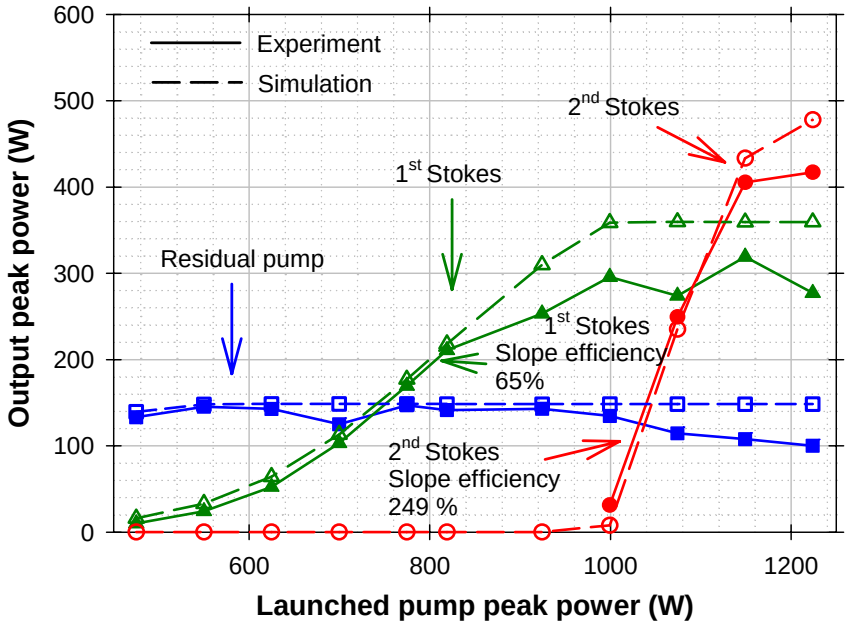

Figure 6.8: Output peak power of the residual pump (blue curve), 1st Stokes (green curve), and 2nd Stokes (red curve) *vs*. launched pump peak power in a 700 m long DCRF T0340. Solid lines: experimental results; Dashed lines: simulation results.

In the measurements of Figure 6.8, the peak power of the residual pump was almost constant at ~130 W regardless of the launched pump power. In the absence of walk-off between pump and signal modes, this can be understood as follows. There is an instantaneous launched pump power that leads to the highest transmitted instantaneous pump power. Beyond this launched power, the transmitted pump power decreases due to increased depletion. However once the launched peak power exceeds this level, the level will always be reached somewhere within the pulse. This then clamps the transmitted peak power of the residual pump. A similar clamping was found in Figure 4.13 in section 4.3.3.

Figure 6.9 shows the average powers of the 1st Stokes, 2nd Stokes, and residual pump with respect to the average power of the launched pump. From 2.2 W to 3.5 W, the Raman pump power was converted into the 1st Stokes with a slope efficiency of 59%. The highest average power of the 1st Stokes obtained was 890 mW at 3.48 W average launched pump power. At higher pump power, the 2nd Stokes quickly built up from the 1st Stokes with a 103% slope with respect to the average launched pump power.

The highest conversion efficiency into the 1st Stokes was 26% relative to the launched pump power. The corresponding pump power was also 3.48 W. The average power conversion was lower than the peak power conversion, mainly due at least partly to the imperfect pump pulse shape as discussed in section 4.3.4. Since the power between pulses is small, the pulse energy can be found by simply dividing the average power in Figure 6.9 by the PRF.

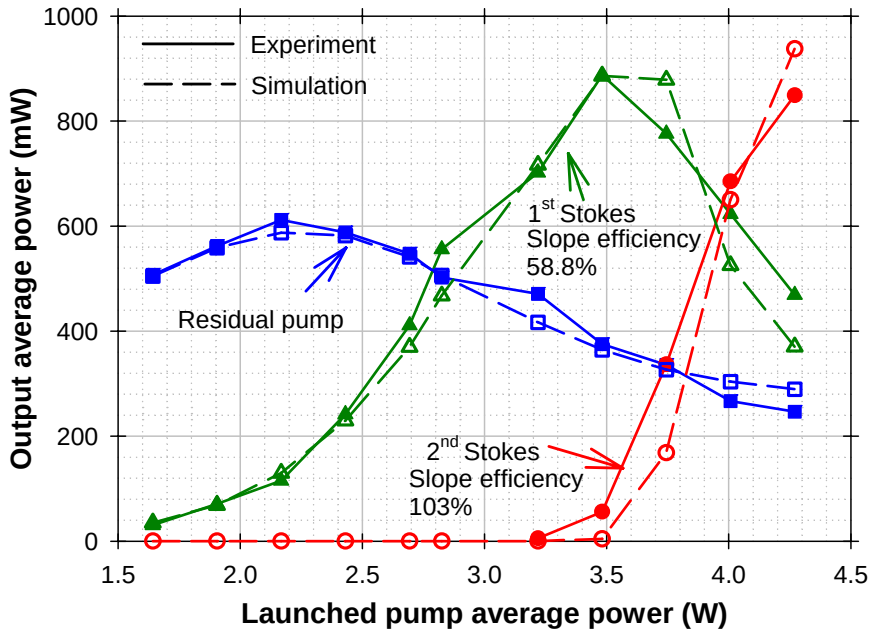

Figure 6.9: Output average power of the residual pump (blue curve), 1st Stokes (green curve), and 2nd Stokes (red curve) *vs*. launched pump average power in a 700 m long DCRF T0340. Solid lines: experimental results; Dashed lines: simulation results.

The simulation results in Figure 6.8 and Figure 6.9 were obtained by numerically solving Eq. (2.32) – Eq. (2.34) with appropriate initial conditions. In the simulation, SRS to the 2nd Stokes directly from the Raman pump was also included, at a rate corresponding to $g_R(\lambda_0, \lambda_1) / 8 \approx 0.625\times10^{-14}$ m/W. The average effective areas $A_{eff}(\lambda_0, \lambda_1)$ and $A_{eff}(\lambda_0, \lambda_2)$ were assumed to be 1960 μm^2, corresponding to a disc of 50 μm diameter and close to the actual inner-cladding size A_{cl} of 1893 μm^2. The average effective area $A_{eff}(\lambda_1, \lambda_2)$ was assumed to be 346 μm^2, corresponding to a disc of 10.5 μm diameter, and close to the core area A_{co} of 266 μm^2. It is difficult to know exactly the effective area, with which waves interact, but these areas are reasonable and the simulation results were in good agreement with the experimental results for both the peak powers and average power.

As mentioned in section 6.1, there are more modes in the new large-mode-area cores than previously with fibre F71-LF11. It is not straightforward to ensure a high beam quality of the amplified output signal since the fundamental mode may not dominate the Raman amplification. I measured the M^2-parameter of the 1st Stokes and the 2nd Stokes at 1.0 kW peak power of the launched pump with a beam profiler (Thorlabs model number BP104-IR). The measured M^2 was 2.7 and 1.4, respectively, for the 1st- and 2nd-Stokes beam. The 1st-Stokes beam quality was slightly worse than the results obtained from the fibre F71-LF11. However, the beam quality of the 2nd Stokes was better and close to the beam quality of the fundamental core mode, calculated to 1.01 based on the RIP [17]-[18]. Also as mentioned in the last section, better pump-to-signal brightness enhancement should be possible with the new fibres than with F71-LF11. According to the Eq. (4.2), the brightness enhancement obtained here was 6.7 at 3.48 W average power of the launched Raman pump, which is actually slightly worse than that obtained in the pulse-pumped CP RFL with F71-LF11 in Chapter 4. The worse pump-to-signal brightness enhancement was partly caused by the high brightness of the pump source, which did not make the most of the inner cladding of T0340. Other contributing factors were the low average-power conversion into the 1st Stokes, only 25%, and the limited 1st-Stokes beam quality. The low conversion efficiency was caused mainly by the relatively high background loss in the long fibre used in the experiment, and also by the imperfect pulse shape.

In order to improve the conversion efficiency and the brightness enhancement, I shortened the fibre to 100 m. This time, the measured launched efficiencies for the Raman pump and Raman seed were 89% and 92.5%, respectively. The launched Raman seed power was now fixed at 88 mW while the Raman pump power was varied during the experiment.

Figure 6.10 shows the dependence of the output peak power of the 1st Stokes, 2nd Stokes, and the residual pump on the peak power of the launched Raman pump. The peak power conversion into the 1st Stokes was improved to 77% from the 35% obtained with the 700 m long piece. The corresponding launched pump peak power was 2.81 kW. At the same pump power, the highest peak power of the 1st Stokes was achieved, which was around 2.15 kW. The 1st-Stokes power was limited by the generation of the 2nd Stokes.

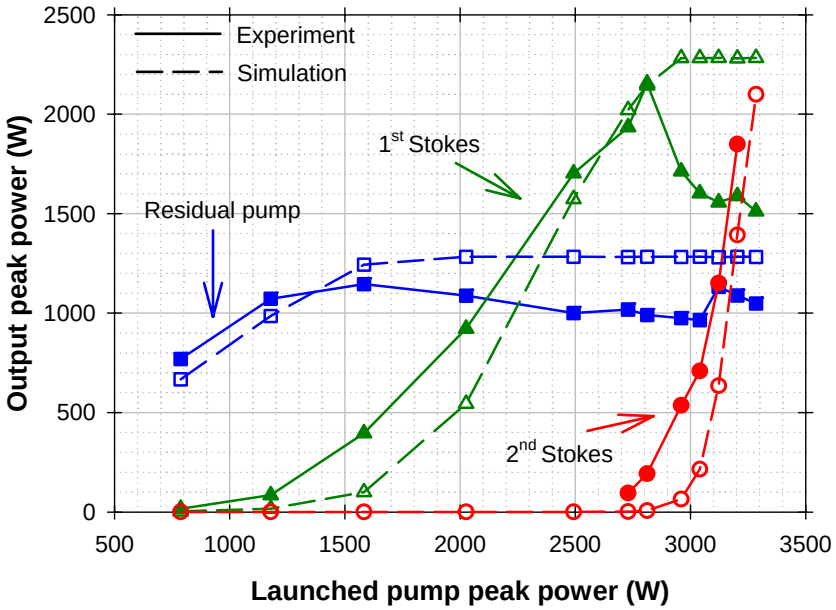

Figure 6.10: Output peak power of the residual pump (blue curve), 1st Stokes (green curve), and 2nd Stokes (red curve) *vs*. launched pump peak power in a 100 m long DCRF T0340. Solid lines: experimental results; Dashed lines: simulation results.

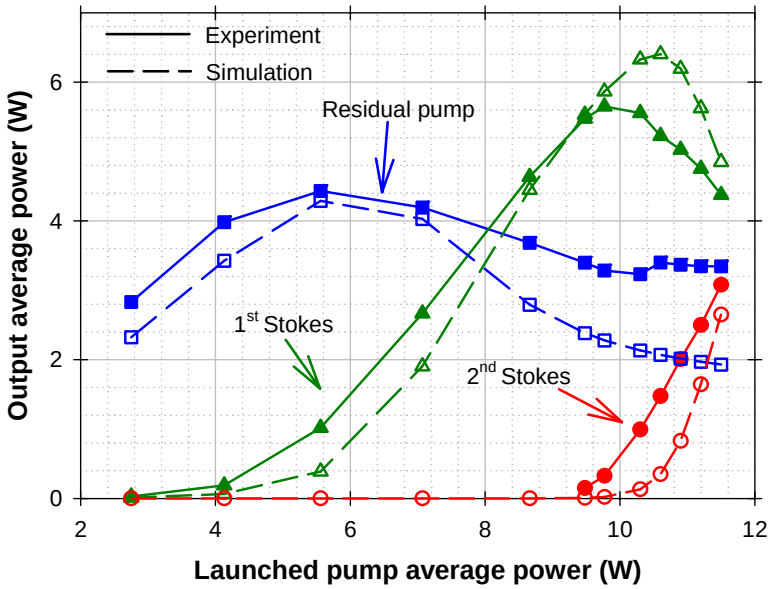

Figure 6.11: Average output power of the residual pump (blue curve), 1st Stokes (green curve), and 2nd Stokes (red curve) *vs*. launched pump average power in a 100 m DCRF T0340. Solid lines: experimental results; Dashed lines: simulation results.

The average output powers of the 1st Stokes, 2nd Stokes, and the residual pump against the average power of the launched pump are given in Figure 6.11. The average power conversion efficiency into the 1st Stokes was improved from 26% to 58%, obtained at 9.77 W launched pump power. At the same pump power, the 1st-Stokes reached its maximum average power of 5.65 W. This was limited by the 2nd Stokes

generation. The 1st Stokes increased with a 112% slope with respect to the launched pump power before the 2nd Stokes built up, increasing with a 149% slope. With an even shorter piece of this fibre pumped by the same pump source, additional, but smaller improvements in the 1st-Stokes power are expected.

The same model as used for simulating the 700-m length RFA was used again to produce the simulation results shown in Figure 6.10 and Figure 6.11. All parameters were kept the same except that the average effective areas $A_{eff}(\lambda_0, \lambda_1)$ and $A_{eff}(\lambda_1, \lambda_2)$ were replaced by 908 μm^2 and 314 μm^2 respectively. However, the simulation results do not match the experimental results as well as for the 700 m fibre. The numerical model used here is a simplified one that ignores many factors, e.g., mode coupling. The effect of pump mode coupling can often be simplified as one of two extreme cases: weak and strong mode coupling [19]. In the case of strong mode coupling, the pump power is distributed equally over the strongly coupled modes, which are then depleted at the same rate by SRS. In other words, the mode coupling is stronger than the SRS. Thus, an average effective area can be used to describe the power evolution of all pump modes. This seems to be the case for the 700 m piece. On the other hand, if there is no mode coupling, or if the mode coupling is weaker than the SRS, then the pump modes are depleted at different rates. See the example given in section 4.2.4. The situation becomes more complicated. Usually, the average effective area then varies along the fibre. This seems to be the case for the 100 m piece. Thus, the simple model used here cannot match the experimental results very well.

Walk-off has been neglected and this needs to be justified. According to Eq. (2.3), the walk-off length of this fibre is 450 m. This justifies the neglect of walk-off for the 100 m long fibre, but it may be an issue for the 700 m fibre. Nevertheless, although walk-off was neglected, the simulation results still match the experimental data well. Thus, it seems that walk-off is not a concern for the 700 m long fibre either. As I discussed in section 2.2, since a relatively high brightness pump source was used in this experiment, it is possible that predominantly lower-order pump modes were excited inside the fibre. The walk-off of these from the 1st-Stokes core modes is slower, and will for some modes lead to a walk-off length that exceeds 700 m.

Figure 6.12 shows the output pulse shapes of the residual pump, the 1st Stokes, and the 2nd Stokes at the output for different pump powers. Temporal pulse shapes were measured by a detector with 0.1 ns rise time (Thorlabs D400FC) and an oscilloscope

with 6 GHz bandwidth (Agilent 54855A). As discussed in Chapter 4, the pulse shape is critical for the conversion efficiency into the 1st Stokes. Here, the measured pulse shapes proved this once again, and again, this can be improved by using square-shape pulses [20]. Furthermore, in Figure 6.12, some of the pump power remained in the middle of the pulses even at high pump power where one might expect complete depletion. Besides, there was a spike in the middle of the pulse of the residual pump in Figure 6.12(d). The limited depletion is tentatively attributed to pump modes with poor spatial overlap with the 1st-Stokes core modes. However, this can be mitigated by non-circular inner-cladding designs, e.g. D-shape ones [21].

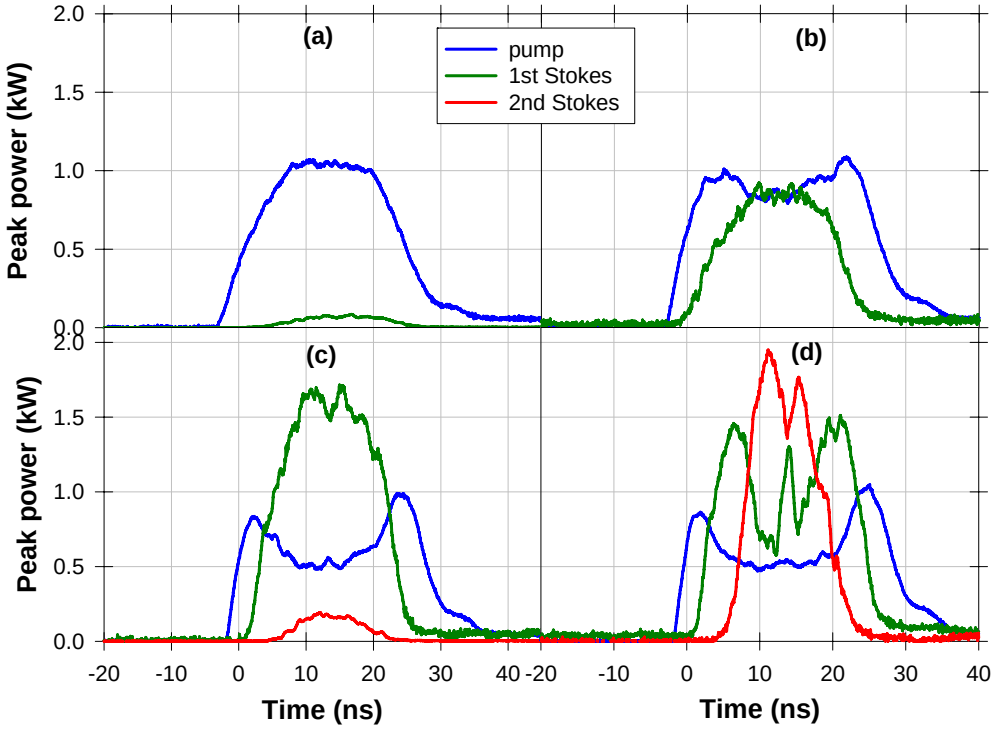

Figure 6.12: Output pulses shapes of the residual Raman pump (blue curves), 1st Stokes (green curves), and 2nd Stokes (red curves) under the peak power of the launched Raman pump: (a) 1.18 kW; (b) 2.03 kW; (c) 2.81 kW; (d) 3.28 kW.

Figure 6.13 shows output spectra corresponding to different pump powers. The spectra were measured by an OSA (Ando AQ-6315E). At the highest of these pump powers, there is significant power in the second Stokes, while the power in the third Stokes remains negligible.

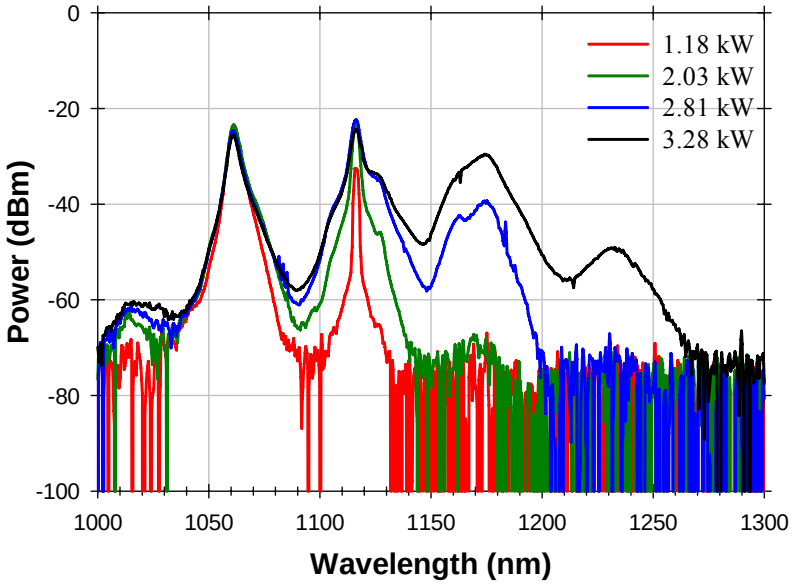

Figure 6.13: Output spectra of Raman pump peak power at: (a) 1.18 kW; (b) 2.03 kW; (c) 2.81 kW; (d) 3.28 kW.

I measured the beam quality of the seed at the 1st Stokes at the output of the DCRF T0340 in absence of the pump. Its M^2 was around 2.2, which indicates that the seed power propagating in the inner cladding was low and several core modes were excited. The beam quality of the 1st Stokes improved when the pump was turned on, i.e., through the Raman amplification. The measured M^2 was around 1.69 at 2.5 kW of launched pump power. The measured beam propagation is depicted in Figure 6.14. This implies that in the amplification process, the pump power was transferred primarily into the core modes of lower orders. After further increasing the pump power to 3.1 kW, the M^2 of the 2nd Stokes was measured, and was about 1.54. According to the Eq. (4.2), the pump-to-signal brightness enhancement was calculated to 40.6. As before, this was calculated based on the fibre geometry since the beam quality of the launched pump was not measured (but was much better than the beam quality corresponding to a completely filled inner cladding). Compared to that obtained in the 700 m piece, the brightness gain is now nearly seven times higher.

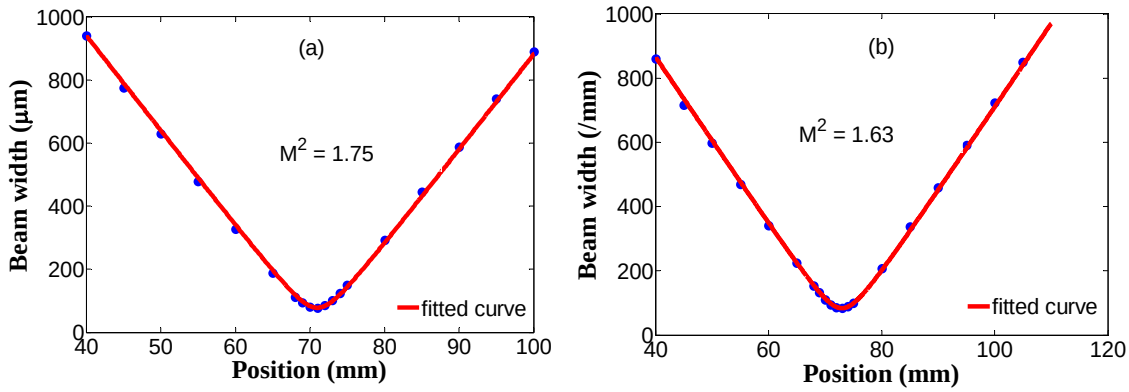

Figure 6.14: Beam quality measurement data for the 1st Stokes with 2.5 kW peak power of the launched Raman pump: (a) x-axis data; (b) y-axis data.

Then, with the same setup, the fibre T0340 was replaced by the other two fibres, T0342 and T0343. The fibre parameters as well as the experimental results of the pulse-pumped CP RFAs are summarised and compared in Table 4.1.

Table 6.2: Results of CP FRAs with DCRF T0340, T0342, and T0343.

Fibre number	**T0340**		**T0342**	**T0343**
Core diameter (μm)	18		31	40
Inner-cladding diameter (μm)	49		83	107
Area ratio between the inner cladding and core	7.4		7.2	7.2
Beam diameter of the effective area $A_{eff}(\lambda_1, \lambda_2)$ with both Stokes beams in the fundamental core-mode (μm)	16.0		19.3	22.0
Area ratio between the inner cladding and the effective area $A_{eff}(\lambda_1, \lambda_2)$ above	9.5		18.7	23.6
Fibre length (m)	700	100	100	160
Input seed power (mW)	200	95	95	80
Pump launch efficiency (%)	86	89	92	92*
Seed launch efficiency (%)	90	92	93	93*
1st-Stokes threshold (peak power) (kW)**	0.74	2.10	2.90	3.72
Maximum 1st-Stokes average power (W)	0.89	5.65	7.15	6.99
Maximum 1st-Stokes peak power (kW)	0.3	2.1	2.5	2.7
Maximum average power conversion efficiency into 1st Stokes (%)	25	58	54	43
Maximum peak power conversion efficiency into 1st Stokes (%)	30	77	68	60
Transmitted seed M^2 (unamplified)	NA	2.2	5.0	8.2
Amplified 1st-Stokes M^2	2.7	1.6	2.5	2.2
2nd-Stokes M^2	1.4	1.5	1.9	1.5
Brightness enhancement***	6.7	40.6	47.9	79.7

* This value was not measured, but was assumed to be the same as for T0342.

** The threshold definition here is the launched pump power at which the 1st Stokes output peak power equals the residual pump peak power.
*** Brightness enhancement was calculated according to Eq. (4.2).

My experimental results prove that with the new fibres T0340, T0342, and T0343, high-efficiency CP Raman fibre devices can be made, provided that the power is sufficient to keep the fibre reasonably short. The achieved peak power conversion into the 1st Stokes was over 60% for all three fibres. The highest 1st-Stokes peak power obtained was 2.7 kW from the 160 m long DCRF T0343. It was limited by the build-up of the 2nd Stokes. With the current Raman pump sources, higher peak power can be expected in even shorter fibres. The average power conversion efficiencies into the 1st Stokes were around 50% for three fibres. Here, this is restricted by several factors, e.g., pump pulse shapes, background loss, inner-cladding shapes, and inner-cladding-to-core area ratio.

My results also show that both the peak power and average power conversion into the 1st Stokes decreased when the fibre size increased although the area ratio between the inner cladding and core is almost the same, 7.2, for these new fibres. In order to assess the effect of the pulse shape on the conversion efficiency into the 1st Stokes, the process previously done for Figure 4.23 was repeated for the new fibres with the shape of the real pump pulse used here. Background losses were ignored. The calculated maximum energy conversion is about 59% for all three fibres regardless of fibre sizes. The calculated energy conversion efficiency is close to the experimental value obtained with 100 m of T0340, but much higher than that of T0343. In the calculation, the average effective area for 1st-to-2nd-order conversion, $A_{eff}(\lambda_1, \lambda_2)$, is assumed equal to the core size, which, for example, is valid if the signal is uniformly distributed over the cross-section of the core. However this is typically not the case. If both the 1st and 2nd Stokes are in the fundamental mode in the core, the effective area $A_{eff}(\lambda_1, \lambda_2)$ becomes different for the three fibres as shown in the table above. The calculated maximum conversion efficiencies become 52, 35, and 30, respectively, for T0340, T0342, and T0343, in the absence of background loss. The theoretical conversion efficiencies thus decrease with increasing fibre size and are, with the assumptions implicit in the calculations, even lower than the corresponding ones obtained experimentally. One reason is that the 1st-Stokes power did not build up only in the fundamental mode. This is clear from the beam quality of the amplified signals, which is larger than that

calculated theoretically for the fundamental mode. Another possibility is that the inner cladding was not fully filled in the experiments so that the real average effective area for pump-to-1st-Stokes conversion, $A_{eff}(\lambda_0, \lambda_1)$, was smaller than the inner-cladding area, which was used in the calculations. Both possibilities decrease the area ratio between $A_{eff}(\lambda_0, \lambda_1)$ and $A_{eff}(\lambda_1, \lambda_2)$, which in turn increases the achievable conversion efficiency.

Thirdly, my experiments show that thanks to the large size and good beam quality of the signal, the pump-to-signal brightness enhancement obtainable in the new fibres is much better than those reported for the fibre F71-LF11.

In conclusion, the new DCRFs with large-mode areas work well experimentally and largely as expected.

6.3 Beam quality improvement through cascaded SRS and SC source based on CP Raman converters

6.3.1 Beam quality improvement through cascaded SRS

The seed beam was not diffraction-limited at the DCRF output in the absence of SRS. Thus, when seed light was launched into the core, it excited higher-order modes as well as the fundamental mode. The beam quality of the transmitted seed degraded with increasing core V-number. While the seed M^2 was as good as 2.2 after 100 m of fibre T0340, it degraded to 8.2 at the output of the 160 m fibre T0343. However, with Raman amplification (SRS), the beam quality of the amplified 1st Stokes improved. For example, at the output of the 160 m fibre T0343, the beam propagation factor (M^2) of the amplified 1st-Stokes wave improved to 2.22. This is a variant of so-called "beam cleanup" [22]. Also, see the simulation example given in Figure 4.6, which shows cleanup in fibre F71-LF11.

The beam quality of the 2nd Stokes was further improved and better than that of the 1st Stokes shown in the Table 6.2. This is another example of beam clean-up, in this case through SRS from 1st to 2nd Stokes. For instance, the M^2-factor of the 2nd Stokes was measured to ~ 1.48 at the output of the 160 m fibre T0343. This is an improvement, and further improvements may still be possible with further SRS to even higher Stokes orders. I investigated this using a 700 m long piece of T0340. The experimental conditions and setup (Figure 6.7) were the same as for my previous experiments with the same length of this fibre, but the pump power was increased to generate higher-

order SRS. Furthermore, another DM was added at the output to separate the 2nd and 3rd Stokes. At 1.23 kW of launched pump power, the M^2 of the 3rd Stokes was measured to about 1.35, which is better than that of both the amplified 1st Stokes and 2nd Stokes. However, the improvement is small, even smaller, relatively, than the change in wavelength. Therefore, the beam parameter product did not improve, and this rules out an improvement in brightness even at 100% conversion efficiency.

The M^2 of the LP_{01} and LP_{11} mode were calculated to 1.01 and 2.01, respectively, at the 3rd-Stokes wavelength according to the RIP of this fibre [17]-[18]. The beam qualities of other core modes are worse. Thus, most of the 3rd-Stokes power was distributed between the LP_{01} and lower order core-modes, e.g., LP_{11} mode.

Figure 6.15 compares the measured beam qualities of the residual pump, 1st Stokes, 2nd Stokes, and 3rd Stokes. The pump source with poor beam quality was converted into a signal with much better beam quality at the output, then through cascaded SRS, the beam quality of the output signal at longer wavelength was further improved and became nearly diffraction limited. However, the BPP did not improve from the 2nd to the 3rd Stokes. Unfortunately, I did not have a DM to separate the 3rd Stokes from higher order Stokes and could therefore not measure the beam quality of the 4th Stokes (nor that of the 3rd Stokes at higher pump power).

The spectral content is interesting, too, and will be detailed in the following section, in terms of a novel method for SC generation.

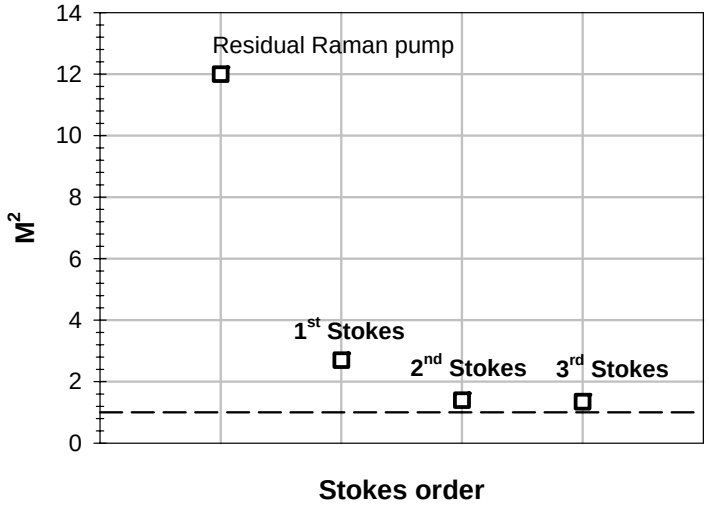

Figure 6.15: M^2 at the output of the CP RFA for the signals. The dashed line indicates the diffraction-limit.

6.3.2 SC source based on CP RFAs

The spectral output shown in Figure 6.13 begs the question how well cladding-pumped DCRFs may work for supercontinuum generation. SC generation has been widely reported and intensely studied since it was discovered by Alfano and Shapiro [23]. With the development of ultra-short pulse diffraction-limited pump lasers, fibres with novel geometries and new materials, SC sources can now cover wavelength from the mid-IR region, e.g., in soft glass [24], to the UV region, e.g., in silica, by tailoring the dispersion [25]. Notwithstanding this success, power-scaling of diffraction-limited pulsed pump sources, especially ultra-fast sources widely used in the SC generation [26]-[28], is challenging, and this restricts the SC power. However, nowadays the intensities needed for the nonlinear process can be reached readily also by CW pump sources. These are easier to power-scale, and the record average output power reported from SC sources is 50 W, pumped by a single mode CW 400 W industrial fibre laser [29]. Still, this approach presents many challenges, e.g., the pump launch efficiency into a small-core fibre, and altogether, the power conversion efficiency was only 13% from the pump into the SC source.

Based on the experiment above in section 6.3.1, a cladding-pumped DCRF is proposed as a simple and effective approach for high-power SC sources, with excellent power scalability also in the pulsed regime. First, a pulsed multimode pump beam is launched into a DCRF. Next, a 1st-Stokes wave is generated primarily in the core through SRS, which can be seeded. By further increasing the pump power, higher order Stokes waves with good beam quality are generated through cascaded SRS in the core as described in the previous section until the Stokes light reaches or exceeds the zero dispersion wavelengths (ZDW) of the generated core-modes. Then, a broad SC builds up, growing in spectral width and power as the pump power increases. The SC beam quality is largely determined by the core RIP. However, for efficient Raman conversion efficiency, the inner-cladding-to-core area ratio must largely meet the basic rule given by Eq. (3.4). Otherwise, significant power may remain in the pump even as the Raman cascade progresses, as illustrated in Figure 3.2. There is some room for the 1st Stokes to build up anew from the partly depleted pump, after the initial 1st-Stokes wave has cascaded to the 3rd order, but the subsequent cascading and broadening occurs too quickly for this to be efficient in most cases. Other limitations on the conversion efficiency were also discussed in the previous chapters.

The experimental setup of the SC source was the same as the one shown in Figure 6.7 except that a 100 m long piece of DCRF T0340 was used. The launch efficiencies for the pump and the seed were 89% and 92%, respectively. In the experiments, the launched seed power was kept at 90 mW while the pump power was varied.

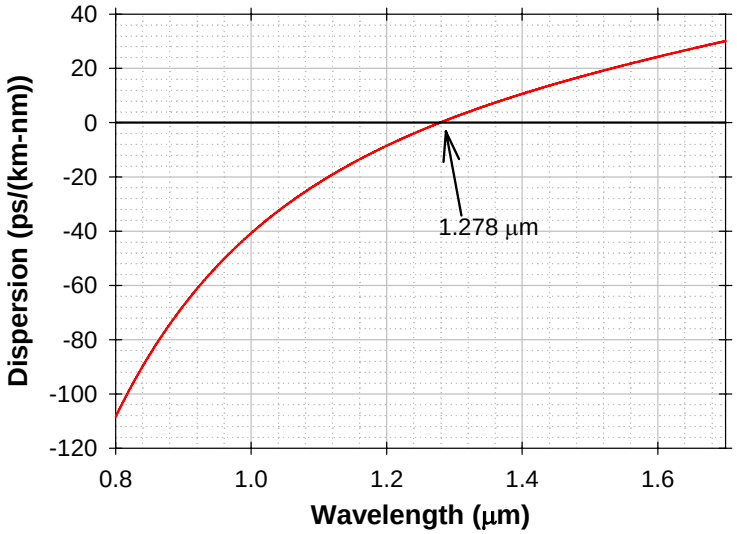

Figure 6.16: (Simulation) Dispersion curve of the fundamental core mode.

As discussed in section 6.3.1, I found experimentally that most of the higher-order Stokes power is distributed in the fundamental mode in the core. Since dispersion is very important for SC generation, I calculated the dispersion curve of the fundamental core-mode using the commercial software Optifiber^{TM} together with the RIP of the fibre. Figure 6.16 shows the calculated results. The ZDW of the fundamental core mode is at about 1.28 μm. The SC is expected to start when the Stokes wave has Raman-scattered to around this wavelength.

This is indeed the case. Figure 6.17 shows experimental output spectra, generated at different pump powers in this 100 m long piece of fibre T0340. For low powers, an increasing number of discrete Raman Stokes orders were generated as the power increased, up to the 3rd Stokes, at about 1230 nm, which is still below the ZDW of the fundamental core mode. The 4th Raman Stokes order is at 1300 nm but cannot be resolved. It is in the anomalous dispersion regime in which the spectrum broadens quickly and continuously through various nonlinear effects, primarily to longer but also to shorter wavelengths. In this region, the output spectrum was getting flatter and flatter as the pump power increased. At the maximum launched pump power of 8.05 kW, the spectrum was much flatter than at lower pump powers, and extended beyond 1.75 μm,

which was outside the measurement range of the ANDO OSA (model number AQ-6315E) used here.

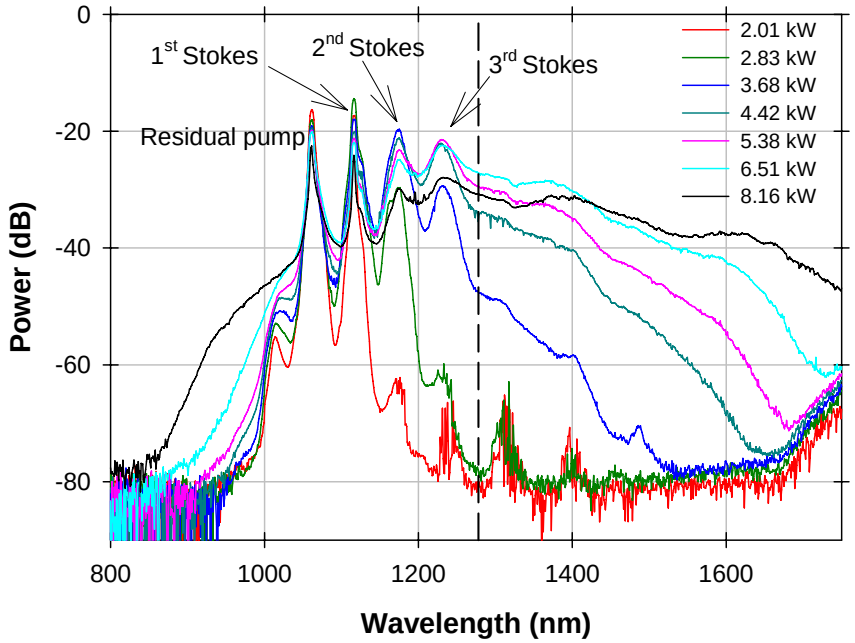

Figure 6.17: Output spectra for different launched pump powers. The dashed vertical line is at the ZDW of the fundamental core-mode.

In addition to this 100 m piece, a 700 m long fibre T0340 was also used to generate SC. Figure 6.18 compares the output spectra from both lengths of fibre at the maximum launched pump power of 8.05 kW. For the 100 m long piece, the power density was over 40 mW/nm around 1400 nm. This value is close to the record power density of 50 mW/nm reported in [29]. In the case of the 700 m long piece, the SC extended to longer wavelengths although the conversion efficiency was lower because of the higher total background loss. The part of the SC spectrum extending beyond 1750 nm could not be accurately measured. However, by using an Agilent 86140B OSA, capable of uncalibrated measurements to 2 μm, I verified that the SC extended out to 2 μm. See the inset of Figure 6.18. The pink curve in the plot shows the noise level while the dashed black curve is the measured SC from a 700 m long fibre. Unfortunately, the output spectrum from the 100 m long fibre was not measured with the Agilent OSA.

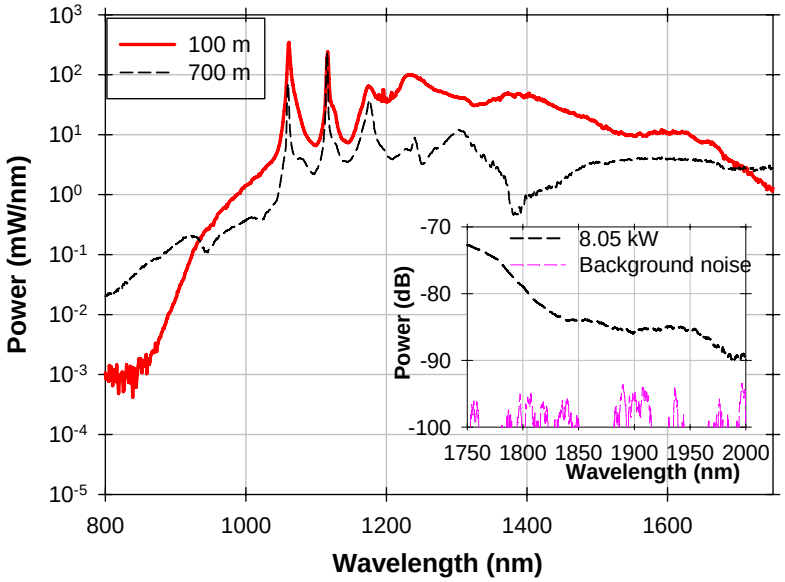

Figure 6.18: Power spectra at maximum launched pump power (8.05 kW peak power, 27.2 W average power) with 100 m (red curve) and 700 m (black curves) lengths of DCRF T0340. Inset: Spectrum measured by un-calibrated OSA for the 700 m length.

Figure 6.19 shows the dependence of the average output power on the average power of the launched pump. The slope efficiency with respect to the launched pump power was over 70%, excluding the power remaining in the pump.. The highest conversion efficiency with respect to the launched pump power was 75%, obtained at 20.4 W of launched pump power. At the maximum pump power, the conversion efficiency was 70.5% with respect to the launched pump power. The maximum SC power was 19 W, excluding the residual pump power, obtained with the 100 m long fibre.

For the 700 m long piece, the output power saturated very quickly. Once the pump power exceeded 8.4 W, the SC spectrum extended over 2 μm. The high loss at wavelengths longer than 2 μm in silica fibres limited the output power of the SC source. Also, the background loss in such long fibre resulted in a relatively low conversion efficiency also for pump powers too low for long wavelengths to be reached.

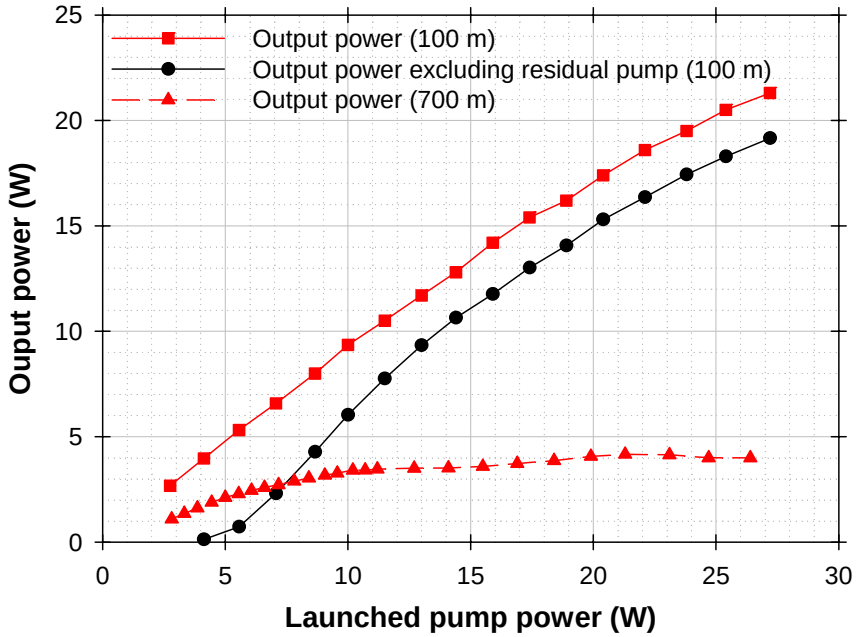

Figure 6.19: Average output power from a 100 m long DCRF T0340 including (red curve with squares) and excluding residual pump power (black curve with squares) as well as from a 700 m long piece of the same fibre (red curve with triangles) *vs*. average launched pump power.

In order to measure the beam quality at wavelengths beyond the 3rd Stokes, a filter sampled the SC from the 100 m long DCRF at 1539 nm for 6.51 kW of launched pump power. The measured M^2-factor at this wavelength was 1.57, which again can be considered to be nearly diffraction limited. A Thorlabs D400FC detector with 0.1 ns rise time and an Agilent 54855A oscilloscope with 6 GHz bandwidth were used to measure the pulse shape at this wavelength. Figure 6.20 shows the resulting pulse shape together with that of the launched pump at 6.51 kW of peak power, scaled to similar heights. The pulse duration at 1539 nm was about 10 ns, which is shorter than the pump pulse duration of around 23 ns. This is because the instantaneous power at the edges of the pump pulse cannot be effectively nonlinearly converted to 1539 nm. A similar situation is shown in Figure 6.12. In Figure 6.12(c), the 1st-Stokes pulse duration was about 17.5 ns while the 2nd-Stokes pulse duration was shortened to about 10.8 ns as shown in Figure 6.12(d).

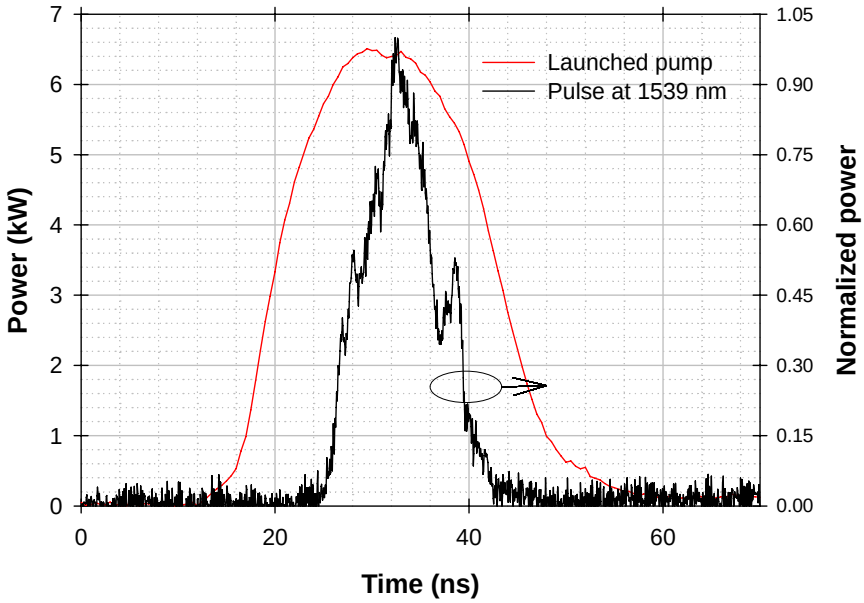

Figure 6.20: Normalized pulse shape of the beam at 1539 nm (black curve) and pulse shape of the launched pump with the 6.51 kW peak power (red curve).

I conclude that the DCRF represents a new, simple and effective approach to SC-generation that opens up for substantial further power-scaling even in the pulsed regime. Firstly, multimode fibre sources with nanosecond pulse durations are adopted as pumps. Such sources are cheaper and easier to build in comparison to the ultra-fast fibre sources with diffraction-limited output that are conventionally used for pumping. Secondly, due to the large inner-cladding diameter (e.g., 50 μm), the pump launch efficiency was nearly 90% even with a multimode pump source. Besides, large cores, e.g., with 20 μm diameter as used in the experiment, will be helpful for power scalability. Thirdly, a high conversion efficiency can be achieved, e.g., 75% as obtained in the experiment. Furthermore, the generated SC can be nearly diffraction limited. Thus, a 19 W average power, pulsed, nearly diffraction-limited SC was generated in a 100 m length of the fibre T0340. The fibres T0342 and T0343 with even larger cores are believed to work as efficiently as this fibre, and should be scalable to higher powers. With a CW multimode pump source used as a pump instead, I believe this approach is scalable beyond a kW of average power and even higher conversion efficiencies may be possible if the effect of the varying instantaneous power of the pulse shapes that I used is eliminated. The same method should be applicable to other types of material such as soft glass fibres which exhibit large nonlinear coefficients and wide transmission windows [30]. The generated SC is still narrower and less flat than what is possible with single-mode fibres. It is unclear if the double-clad fibres can be dispersion-engineered to allow for SC spectra of comparable width and flatness.

6.4 High-energy pulse conversion

In the past, the fibre F71-LF11 was used with high-energy pulses [1]-[2], [6]-[7], and those experiments show the brightness-enhancement capability of CP Raman fibres also in this regime. Reference [1] reported a CP Raman fibre converter producing record-breaking pulse energies of 210 μJ. The nearly diffraction-limited Stokes pulses were generated in a 50 m long F71-LF11 pumped by a slightly multimode YDF MOPA. When I introduced the new DCRFs with large-mode areas in section 6.1, I described them as being promising for (nearly) diffraction-limited high-energy sources. This section confirms this, based on experiments on a piece of DCRF T0343 with a 40 μm diameter core. It was pumped by a spatially and longitudinally multimode Nd:YAG laser producing temporally spiky pulses. With this, I managed to produce high-brightness pulses with over 1 mJ of energy. To my knowledge, this is the highest energy so far from any Raman fibre device.

6.4.1 Raman pump: Nd:YAG laser

A Q-switched Nd:YAG laser (Spectron Laser System SL400/SL800) was used as the Raman pump. Figure 6.21 shows the characteristics of this laser. The Nd:YAG laser is capable of delivering output energies of up to 23 mJ as shown in Figure 4.2(a) in linearly polarised pulses. The pulse energy was measured by an Ophir energy meter (model number PE10-SH). During the experiment, the PRF was fixed at 29 Hz. Although the laser can produce diffraction-limited pulses, it was not well aligned at that time, so the output beam was slightly multimoded and the beam quality was measured to $M^2 \approx 3.5$. The beam quality is assumed to have remained constant for the duration of these experiments. The output spectrum was measured by an ANDO 6315E OSA. The wavelength was 1064 nm with 0.096 nm linewidth as shown in Figure 6.21(b). Figure 6.21(c) illustrates a representative pulse trace for the Nd:YAG laser, as measured with a 20 GHz oscilloscope (Tektronix DSA72004B) and a 22.6 GHz detector (Discovery DSC30S). The figure also shows a fit of a Gaussian pulse of 14 ns FWHM. The pulses from the Nd:YAG laser contained very sharp spikes within the Gaussian envelope. Such behaviour is well-know for longitudinally multimode Nd:YAG lasers such as the one used here. The peak power in the spikes can be much higher than that of the approximately Gaussian envelope. In addition, neither the temporal shape nor energy of the output pulses was stable. Figure 6.19(d) shows three representative pulse traces at

the output. Because of the laser instabilities, the pulse energy varied by up to 3 dB. Together with the spikes inside the pulse envelope, these variations will certainly affect the Raman scattering and the conversion efficiency into the 1st Stokes.

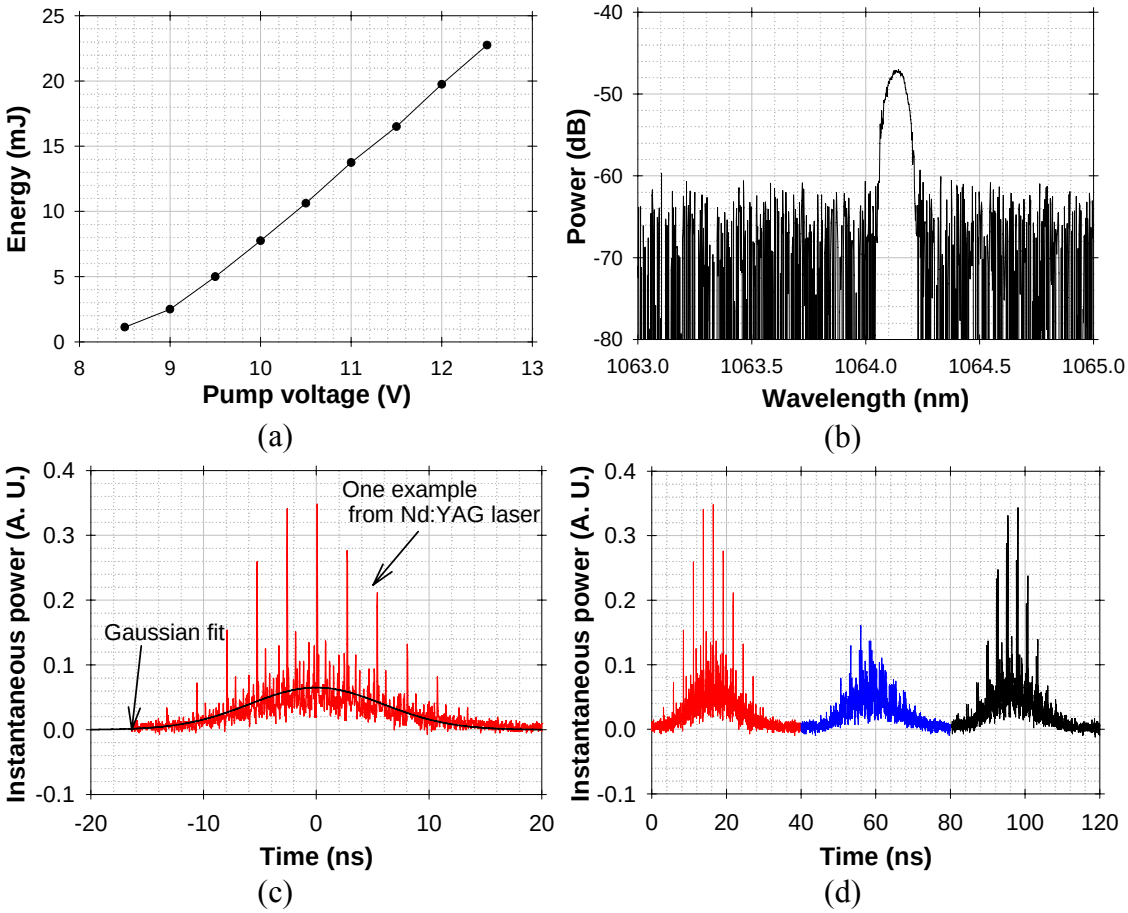

Figure 6.21: Characteristics of the Nd:YAG laser: (a) Output energy *vs*. pump voltage (with which the pulse energy is controlled); (b) Output spectrum; (c) A representative temporal pulse trace (red curve) and a Gaussian fit (black curve) with 14 ns FWHM; (d) Examples of three pulses at the output. Spectrum and pulse shapes were measured at 10 V pump voltage.

6.4.2 Experimental setup

The experimental schematic is shown in Figure 6.22. The free-space output of the Nd:YAG laser was launched through a focusing lens into a 40 m long piece of DCRF T0343. This is a quite simple configuration, without any seeding of the 1st Stokes. In order not to change the operating conditions of the Nd:YAG laser, and thus (systematically) change, e.g., pulse duration or pulse shape (beyond the significant random fluctuations) during the experiment, a half-wave plate and a polarizer were used as a variable optical attenuator between the Nd:YAG laser and fibre T0343. The output end of the DCRF was angle-cleaved to suppress feedback, which can otherwise induce

back-propagating SRS at high pulse energies [1]. DMs were used to separate the residual pump, 1st Stokes, and longer wavelengths in the output beam.

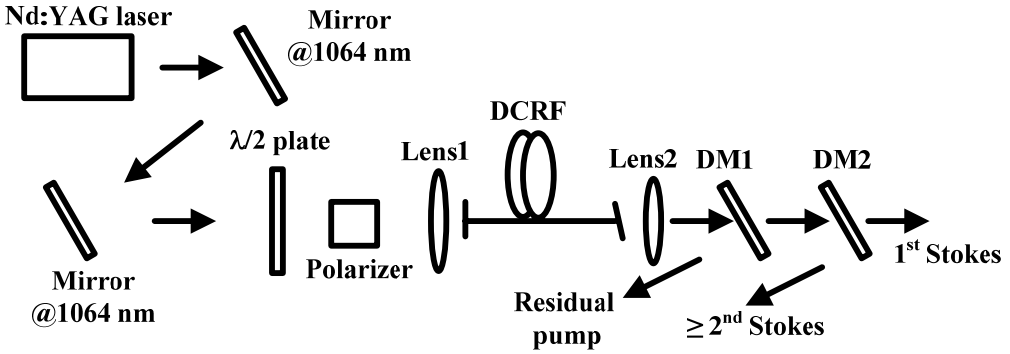

Figure 6.22: Experimental schematic. DM1: HR@ < 1064 nm, HT@ > 1116 nm; DM2: HR@ >1178 nm, HT@1116 nm.

6.4.3 Experimental results and discussion

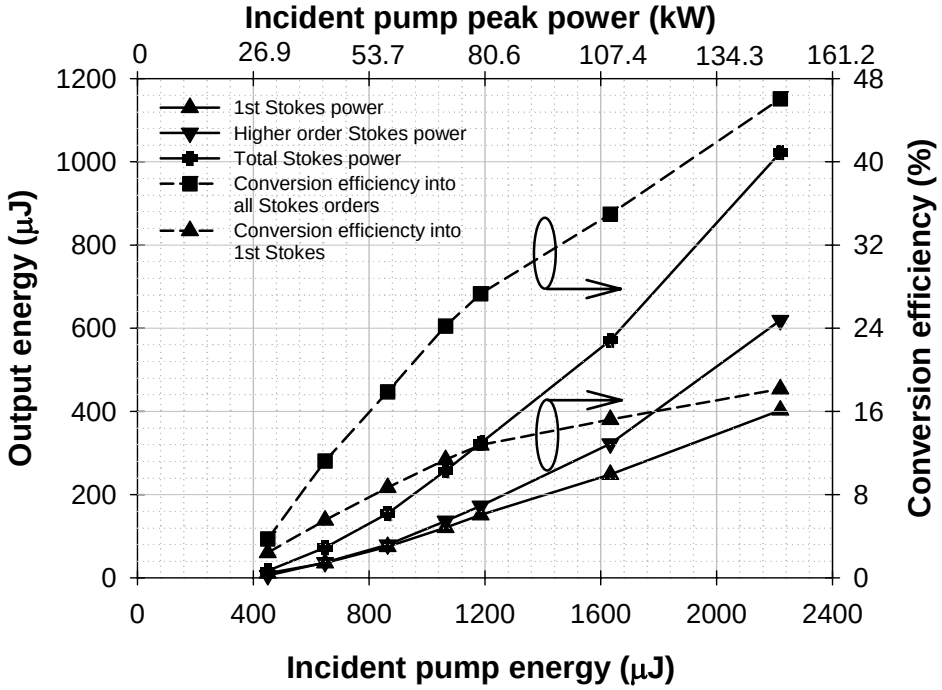

Figure 6.23: Output energy *vs*. pump energy incident on the DCRF. The upper scale shows the corresponding peak power, under the assumption of an ideal Gaussian pulse of 14 ns duration (full width at half maximum). Solid curve with up-triangles: energy in the 1st-Stokes; solid curve with down-triangles: energy in higher-order Stokes; solid curve with circles: energy in all Stokes order; dashed curve with up-triangles: conversion efficiency into the 1st Stokes; dashed curve with squares: conversion efficiency into all Stokes orders.

Figure 6.23 plots the output pulse energies in the 1st Stokes, higher Stokes order, and in all Stokes order together against the pump energy incident on the DCRF. The conversion efficiencies into the 1st Stokes and all Stokes order with respect to the incident pump energy are also given in Figure 6.23. The maximum Raman-converted

output energy was 1.02 mJ, distributed across all present Stokes orders. The highest conversion efficiency into all Stokes orders was ~ 46% relative to incident pump energy, obtained at a pump energy of 2.22 mJ. Of this, up to 400 μJ was in the 1st Stokes. The launch efficiency was not measured, but it was high, and estimated to 92% in this case. Figure 6.24 shows the output spectrum after transmission through DM1 and reflection in DM2, out to a wavelength of 1750 nm for a pump energy of 2.22 mJ. In stark contrast to the spectra given in Figure 6.13 and similar to the spectra in Figure 6.18, the spectrum clearly extended beyond 1750 nm. The broad output spectrum complicated the measurements. Shorter wavelengths than the 2nd Stokes were rejected by DM1 (reflected) and DM2 (transmitted), while 1750 nm was the upper wavelength limit of the OSA used here. Furthermore, DM1 also rejected some power at wavelengths over 1700 nm. These imperfections affected the measured spectrum as well as the pulse energy. Thus, at high pump energies, for which wavelengths above 1700 nm were reached, the total energy in all Stokes orders was actually somewhat higher than shown in Figure 6.23. There was also some energy leaking through DM2 at wavelengths over 1500 nm. DM2 was meant to separate the 1st Stokes from higher Stokes orders, but at 1 mJ of output energy across all Stokes orders, approximately 10% of the higher-order Stokes energy leaked through DM2 and added to the 1st-Stokes energy. Neither of these effects was compensated for in Figure 6.23.

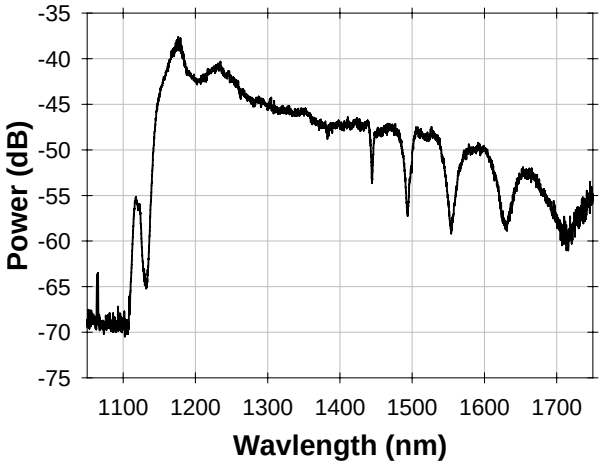

Figure 6.24: Output spectrum at 2.22 mJ incident pump energy following reflection in DM2. The structure in the spectrum was caused by DM1 and DM2.

The M^2-factor of the 1st Stokes was 1.37. Although the beam quality at longer wavelength was not measured, the beam quality of higher order Stokes is normally improved through cascaded SRS, as demonstrated experimentally in section 6.3. I therefore expect a comparable, or better, beam quality for all Stokes orders.

The pulse energy was limited by facet damage at the launch end. An endcap should increase the damage threshold, as should thermal treatment of the cleaved end-facet [31], and allow us to reach even higher energies with nearly diffraction-limited output. For example, assuming an effective area of 1000 μm^2, the damage threshold for 14 ns pulses should exceed 1.5 mJ. However, the damage location at the input is somewhat surprising given that the intensity should be relatively low across the inner cladding at launch. Therefore, the details of the damage are not clear, e.g., what the effective area is for the damage, and this makes it difficult to predict what pulse energies can be reached. The temporal variations add to this difficulty.

As it comes to the 1st-Stokes energy, this was primarily limited by the rapid rise of higher-order SRS. The 2nd Stokes was generated almost directly when the 1st Stokes appeared, at around 846 μJ of incident pump energy and 58 kW of nominal peak power, i.e., for a Gaussian pulse with 14 ns duration (FWHM). Scaled with the fibre length, the pump threshold was 2.1 MW×m for both 1st and 2nd Stokes. Note however the large fluctuations in instantaneous power, which may greatly change the nominal peak power at which threshold is reached, and that the actual pump as well as Stokes peak power were unknown. With these caveats, these thresholds can still be compared to the 0.31 MW×m and 0.62 MW×m of scaled threshold (launched pump peak power × fibre length) for the 1st and 2nd Stokes, respectively, in case of the 160 m long T0343 pumped by the temporally much cleaner SPI fibre laser in section 6.2. For this, the threshold Stokes power is taken as that at which the 1st Stokes reaches 10% of the launched pump power. For example, this corresponds to 240 mW of average Stokes power in Figure 6.9. At 0.31 MW×m, the Raman gain can be calculated to approximately 7.5 dB if the pump is distributed evenly over the inner cladding (area 9000 μm^2). However, given that the seed power was only 81 mW, the gain would have to be three or four times higher than that, before the 1st-Stokes power becomes noticeable relative to the pump power. I conclude tentatively that the reason is that pump overlapped better with the core than if the pump would be distributed evenly over the inner cladding. Generally this can be expected, for example if a relatively large fraction of the pump power is launched into the core because of a high beam quality of the pump. Even if we disregard the pump power guided in the core, a spatially Gaussian beam with high beam quality launched into the centre of the inner cladding, thus exciting primarily modes without azimuthal dependence, tends to maintain a central peak when propagating down the fibre [32]. I

conclude that a higher central pump intensity may well explain the relatively low pump threshold obtained with fibre laser pumping.

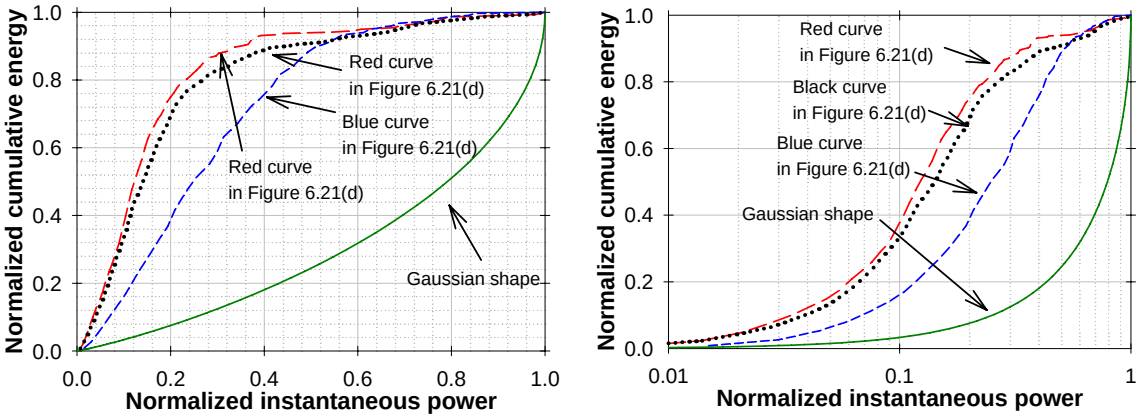

(a) (b)

Figure 6.25: (Simulation) Pulse instantaneous power *vs*. cumulative energy for pulse shapes in Figure 6.21(d) together with a Gaussian pulse shape with 14 ns FWHM in (a) linear scale; (b) logarithmic scale.

In case of Nd:YAG laser pumping, the scaled threshold (launched pump peak power × fibre length) is higher, but the gain requirements are considerably higher, too, given that the 1st Stokes builds up from noise in a short pulse. We estimate the gain at threshold to between 90 and 100 dB, which would require a pumping of around 4 MW×m. This is again almost twice higher than the experimental value, so one could attribute this to a pump power distribution that peaks in the center of the fibre, this time too. However, also the generation of 2nd and higher Stokes orders was much different, with rapid SC generation that warrants further consideration. The similar threshold for the 1st and 2nd Stokes cannot be explained by a pump distribution centered on the core, since the reduction in effective area ratio that this implies if anything would increase the relative difference between the 1st and 2nd-Stokes thresholds rather than decrease it. Rather, we attribute this to variations in the instantaneous power of the pump pulses, which rule out operation within the narrow range of instantaneous power that allows for efficient 1st-Stokes generation (See section 6.4.1). In addition to the variations intrinsic to a Gaussian pulse, there are the pulse-to-pulse energy variations by up to 3 dB due to laser instabilities, as well as the sharp spikes. See Figure 6.21(d). The peak power in the spikes is up to six times higher than that of the envelope, which is approximately Gaussian. The spikes (See Figure 6.21(d)) result in an energy distribution which is considerably worse than that of a Gaussian. This is a concern with core-pumped fibre Raman amplifiers [33]-[34], and even more so with a DCRF. Figure 6.25 shows how

the energy of three different pulses from the Nd:YAG laser is distributed over the instantaneous power. The distribution of a Gaussian pulse is shown as well. The range of powers that allow for efficient conversion into the 1st Stokes is only around 10% for an area ratio of eight, but the relatively wide and flat peak of a Gaussian pulse, with 35% of the energy falling within the center of the pulse with instantaneous powers of over 90% of the peak, still allows for relatively efficient conversion into the 1st Stokes. This concentration of energy to the highest instantaneous powers allows for a sharp threshold for the 1st Stokes, with significant margin to the onset of the 2nd Stokes (approximately 2.5 dB for CW pumping, for an area ratio of eight, in the absence of seeding).

The spiky Nd:YAG pulses create distinctly different characteristics. The energy distribution is such that the instantaneous power varies by around 3 dB for the 10% of the energy that has the highest instantaneous power. Thus, the highest-power spikes reach the 2nd-Stokes threshold before the instantaneous power of most of the pulse energy reaches the 1st-Stokes threshold, in a quasi-CW approximation. This leads to thresholds for 1st and 2nd Stokes quite close to each other.

Even if we disregard the relatively low fraction of energy in the spikes (around 10% according to Figure 6.25) the distribution of the remaining energy remains unfavorable, without the concentration of the (remaining) energy to the highest (remaining) instantaneous power (or any other power) that Gaussian pulses exhibit. Rather, the energy is distributed relatively evenly, i.e., close to a straight line in Figure 6.25, from the origin to 80 – 90% of the total energy. With this unfavorably energy distribution, a large fraction of the energy will inevitably Raman-scatter to high Stokes orders before the less intense parts of the pulse is converted to the 1st Stokes. This, in a quasi-CW approximation, explains why we see such rapid broadening of the spectrum.

However, the quasi-CW approximation is not necessarily valid, as the spike duration of around 0.1 ns makes them sufficiently short to be affected by dispersion and walk-off even in our relatively short fibre. In our case, with an inner-cladding NA of 0.2, the modal dispersion becomes 46 ps/m and the dispersion length becomes 2.2 m for 0.1 ns spike duration. This follows from Eq. (2.3), if we assume that the dispersion $\Delta\tau$ should equal the duration τ, (the best choice here depends on the shape of the spike, which is unknown). In a dispersion-limited case, the critical power for SRS P_{cr} becomes [35]:

$$P_{cr} = \frac{16A_{eff}}{g_R L_D} = \frac{16A_{eff}}{g_R}\frac{n_{ic}}{n_{oc}}\frac{n_{ic}-n_{oc}}{c\tau}. \tag{6.2}$$

Here, A_{eff} is the effective area for the interaction, g_R is the Raman gain coefficient, and L_D is the dispersion length. Furthermore, we have used the conventional factor of 16 for the gain (in nepers) required to amplify the 1st Stokes, from noise, to the point where it depletes the pump. However, at the kW power-level, a gain of around 20 Np may well be required. Since the Raman conversion length is inversely proportional to the peak power of a spike, and the dispersion length is proportional to the duration of the spike, it is actually the energy of a spike that determines if it, by itself, generates significant SRS before walk-off smears out the interaction. There is thus a critical energy E_{cr}, given by:

$$E_{cr} = P_{cr}\tau = \frac{16A_{eff}}{g_R L_D}\tau = \frac{16A_{eff}}{g_R}\frac{n_{ic}}{n_{oc}}\frac{n_{ic}-n_{oc}}{c}. \tag{6.3}$$

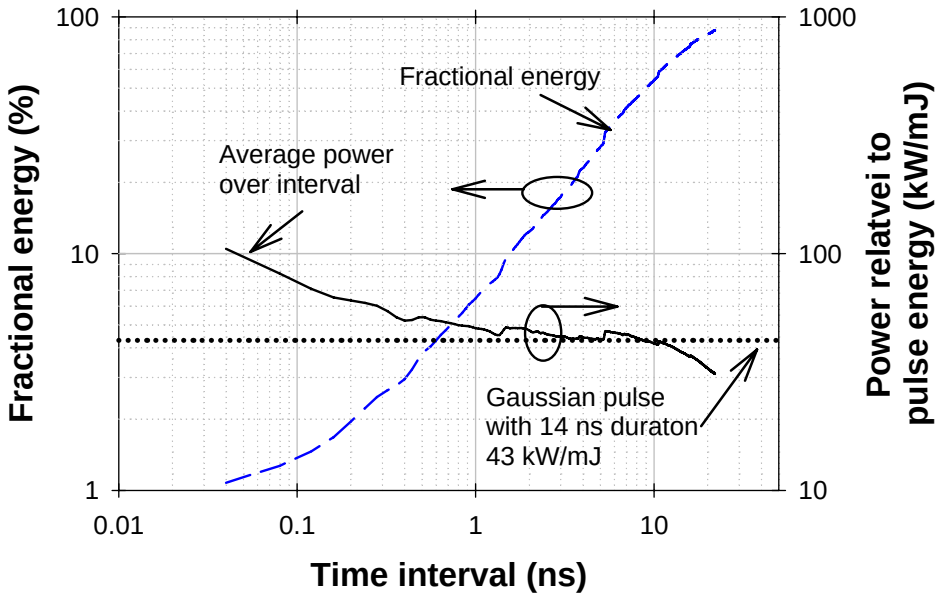

Figure 6.26: Fractional energy and average power *vs*. length of time interval of the pulse shown in Figure 6.21(c). The peak power of a gaussian pulse with 14 ns pulse duration is also included. The total launched pulse energy is 778 μJ.

With our parameters, with the inner-cladding area used for the effective area, I calculate a critical energy of 131 μJ. This energy would require a peak power of 1.31 MW in a 0.1 ns long spike or 2.62 MW in a 0.05 ns spike, which exceeds our maximum spike power, estimated to 0.8 MW in 0.05 ns at our highest pump pulse energy of 2.2 mJ. These characteristics suggest that the spikes disperse temporally before SRS can build up, and it is largely the average envelope of the pulse that matters. To further consider this, Figure 6.26 plots the maximum energy within a time interval

anywhere along the pulse, *vs*. the length of the time interval, for the pulse shown in Figure 6.21(c). The average power within the time interval is plotted, too, together with the peak power of a best-fit Gaussian pulse (FWHM 14 ns). This can be compared to the measured threshold energy in Figure 6.23 of 846 μJ incident or 778 μJ launched, for which the 1st-Stokes energy was 75 μJ. If we use this energy to scale the energy in Figure 6.26, the critical energy of 131 μJ (which would lead to a 1st-Stokes energy of around 65 μJ) requires a time interval of 2.88 ns. However, 2.88 ns exceeds the total dispersion in 40 m of our fibre, which is 1.8 ns. This actually sets an upper limit on the time interval that we should consider: only energy that falls within 1.8 ns can contribute to the Raman gain of a signal pulse at a given point in (retarded) time. The energy within 1.8 ns is 12% of the total, or 93 μJ, which is somewhat lower than 131 μJ.

For this particular pulse, the average power within the 2.88 ns becomes 44 kW, which is similar to the 43 kW peak power of a matching Gaussian pulse. The maximum average power over 1.8 ns is slightly higher, at 48 kW, so again similar and around 43 kW. Using the 46 kW, the power × length product becomes 1.8 MW×m at the experimental threshold of 778 μJ. This is less than our previous quasi-CW theoretical estimate of 4 MW×m. On the other hand, it is very close to the experimental result of 2.1 MW×m. This thus suggests that the experimentally measured threshold can be understood in terms of a spiky energy distribution. Still, numerical simulations with representative pulse shapes are needed to confirm agreement between theory and experiments. Simulations are also needed to confirm that the spikes explain qualitatively and quantitatively the low threshold for the 2nd Stokes, which is difficult to assess analytically in a dispersion-limited case. However, detailed simulations of a DCRF with dispersion of spiky pulses have yet to be reported. The challenges are many, and exacerbated by additional effects that may be important. Thus, though measurements show that the spikes in the pump pulses do broaden upon transmission through 40 m of the DCRF at powers sufficiently low to avoid SRS, the broadening was smaller than suggested by Eq. (2.3). This may be partly explained by an under-filled NA, but it is also possible that some spikes excited a subset of fibre modes with relatively low dispersion.

I conclude that the conversion of spiky pump pulses in a DCRF is a very complicated and challenging problem. My data do not contradict what can be expected, but more precise data and models are required to establish the degree of agreement

between theory and experiments. I will also point out that the dispersion and walk-off in a DCRF allows for some engineering of the effective frequency response of the Raman gain, which could be used favorably to eliminate the spikes.

Finally, I conducted these experiments late in my PhD, with an oscilloscope and a detector that allowed for measurements with 20 GHz bandwidth. It is possible that the spikes in the pulses would not have been resolved with the equipment used earlier in the thesis. One may think that likewise, this high bandwidth might have revealed spikes in pulses used in earlier work in earlier chapters. However, the peak powers and energies used in those chapters were much lower, and the fibres much longer. Thus, the frequency bandwidth of the pump-to-signal transfer was lower than the 6 GHz bandwidth equipment used in those chapters, so even if there were spikes they should not have made any difference.

6.5 Summary

In conclusion, this chapter has described several experiments with new large-mode-area DCRFs (T0340, T0342, T0343). Compared to the relatively small fibre F71-LF11 used in previous chapters, the much larger sizes of these new fibres, e.g. with 18.4, 31, and 40 μm diameter cores, make them more promising for high peak power and high energy operation. In addition, thanks to the large inner cladding, pump sources with relatively poor beam quality can be used to pump these fibres, and this opens up for considerable brightness enhancement. This was verified by the pulse-pumped CP RFAs based on the new fibres as shown in section 6.2. Besides, the experimental results show that the new DCRFs can work as efficiently as F71-LF11. Despite of these advantages brought by the increased geometric sizes, the experimental results also show that the conversion efficiency into the 1st Stokes becomes slightly worse with the increase of the fibre size.

In the pulsed regime, a 1 mJ energy source with high brightness was demonstrated in section 6.4. A 40 m length of DCRF T0343 was used as a Raman converter, which cladding-pumped by a Q-switched Nd:YAG laser and operating on several Raman orders. The output energy was limited by end-facet damage at the launch, which can be mitigated by end-capping. I believe this is the highest pulse energy reported from a Raman fibre device reported to date.

A novel application of the DCRFs was introduced in section 6.3, namely SC generation. A multimode pump wave is Raman-scattered into a 1st-Stokes wave propagating in the core of the DCRF. Following cascaded SRS to higher Raman orders, broadband SC generation commences when the Raman cascade reaches or exceeds the zero dispersion wavelength of the excited core mode(s). A 19 W SC source was realised using a 100 m long fibre T0340 with 75% conversion efficiency with respect to the launched pump power. The generated SC extended beyond 1.8 μm. This is a new, simple and efficient way to obtain a high-power pulsed SC.

6.6 Reference

[1] A. Shirakawa, C. A. Codemard, J. Ji, K. K. Chen, A. Malinowski, D. J. Richardson, J. K. Sahu, and J. Nilsson, "High-brightness 210 μJ pulsed Raman fiber source", in Proc. of, Conf. Lasers and Electro-Optics /QELS, San Jose 4-9 May 2008, paper CTuL1.

[2] J. Nilsson, J. K. Sahu, J. N. Jang, R. Selvas, D. C. Hanna, and A. B. Grudinin, "Cladding-pumped Raman fiber amplifier", in Proc. of Optical Amplifiers and Their Applications (OAA 2002), Vancouver 14-17 Jul. 2002, paper PD2-1/2/3 (Postdeadline).

[3] J. Jang, Y. Jeong, J. K. Sahu, M. Ibsen, C. A. Codemard, R. Selvas, D. C. Hanna, and J. Nilsson, "Cladding-pumped continuous-wave Raman fiber laser", in Proc. of Conf. Lasers and Electro-Optics/QELS, Baltimore 3-5 Jun 2003, paper CWL1.

[4] C. A. Codemard, J. K. Sahu, and J. Nilsson, "Cladding-pumped Raman fiber amplifier for high-gain high-energy single-stage amplification", in Proc. of OFC (2005), Anaheim 6-11 March 2005, paper OutF5.

[5] C. A. Codemard, P. Dupriez, Y. Jeong, J. K. Sahu, M. Ibsen, and J. Nilsson, "High-power continuous-wave cladding-pumped Raman fiber laser", Opt. Lett., 31(15), 2290 (2006).

[6] C. A. Codemard, J. K. Sahu, and J. Nilsson, "High-brightness pulsed cladding-pumped Raman fiber source at 1660 nm", in Proc. Conf. Lasers and Electro-Optics /QELS 2007, Baltimore 6-11 May 2007, paper CTuN3.

[7] J. Ji, C. A. Codemard, M. Ibsen, J. K. Sahu, and J. Nilsson, "Analysis of the conversion to the first stokes in cladding-pumped fiber Raman amplifiers", IEEE J. Sel. Top. Quan. Electron., **15**(1), 129 (2009).

[8] C. A. Codemard, J. Ji, J. K. Sahu, and J. Nilsson, "100 W CW cladding-pumped Raman fiber laser at 1120 nm", in Proc. of SPIE Photonics West, San Francisco Jan. 2010, paper 7580-58.

[9] J. Ji, C. A. Codemard, J. K. Sahu, and J. Nilsson, "Pulsed cladding-pumped large mode area fiber Raman amplifier", in Proc. of Photonics West, San Francisco Jan. 2010, paper 7580-47.

[10] J. Ji, C. A. Codemard, A. Boyland, J. K. Sahu, and J. Nilsson, "Beam quality and spectral evolution in large-core cladding-pumped cascaded-Raman fiber converter", in Proc. of Advanced Solid-State Photonics, San Diego Feb. 2010, paper AMB3.

[11] J. Ji., C. A. Codemard, A. S. Webb, J. K. Sahu, and J. Nilsson, "Near-diffraction-limited supercontinuum generation in a cladding-pumped nonlinear fiber

converter", in Proc. of Conf. Lasers and Electro-Optics /QELS, San Jose 16-21 May 2010, paper CMMM5.
[12] M. E. Fermann, "Single-mode excitation of multimode fibers with ultrashort pulses", Opt. Lett., **23**(1), 52 (1998).
[13] Information is available on http://www.heraeus-quarzglas.com/.
[14] S. T. Davey, D. L. Williams, B. J. Ainslie, W. J. M. Rothwell, and B. Wakefield, "Optical gain spectrum of GeO_2-SiO_2 Raman fiber amplifiers", in Proc. of Inst. Elect. Eng., **136**(6), 301 (1989).
[15] J. Bromage, K. Rottwitt, and M. E. Lines, "A Method to predict the Raman gain Spectra of germanosilicate fibers with arbitrary index profiles", IEEE Photonic Tech. Lett., **14**(1), 24 (2002).
[16] C. Fukai, K. Nakajima, J. Zhou, K. Tajima, K. Kurokawa, and I. Sankawa, "Effective Raman gain characteristics in germanium- and fluorine-doped optical fibers", Opt. Lett., **29**(6), 545 (2004).
[17] H. Yoda, P. Polynkin, and M. Mansuripur, "Beam quality factor of higher order modes in a step-index fiber", J. Light. Tech., **24**(3), 1350 (2006).
[18] Z. Jiang, and J. R. Marciante, "Impact of transverse spatial-hole burning on beam quality in large-mode-area Yb-doped fibers", J. Opt. Soc. Am. B, **25**(2), 247 (2008).
[19] F. Capasso and P. Di Porto, "Coupled-mode theory of Raman amplification in lossless optical fibers", J. Appl. Phys., **47**(4), 1472 (1976).
[20] A. Malinowski, K. T. Vu, K. K. Chen, P. Horak, D. J. Richardson, "Selective generation of individual Raman Stokes wavelengths using shaped optical pulses", in Proc. of OFC, San Diego 24-28 Feb 2008, paper OTuB3.
[21] P. Leproux, S. Fevrier, V. Doya, P. Roy, and D. Pagnoux, "Modeling and optimization of double-clad fiber amplifiers using chaotic propagation of pump", Opt. Fiber Technol., **6**(4), 324 (2001).
[22] K. S. Chiang, "Stimulated Raman scattering in a multimode optical fiber: evolution of modes in Stokes waves", Opt. Lett., **17**(5), 352 (1992).
[23] R. R. Alfano and S. L. Shapiro, "Observation of self-phase modulation and small-scale filaments in crystals and glasses", Phys. Rev. Lett., **24**(11), 592 (1970).
[24] J. H. V. Price, T. M. Monro, H. Ebendorff-Heidepriem, F. Poletti, P. Horak, V. Finazzi, J. Y. Y. Leong, P. Petropoulos, J. C. Flanagan, G. Brambilla, X. Feng, and D. J. Richardson, "Mid-IR supercontinuum generation from nonsilica microstructured optical fibers", IEEE J. Sel. Top. Quantum Electron., **13**(3), 738 (2007)
[25] J. H. V. Price, T. M. Monro, K. Furusawa, W. Belardi, J. C. Baggett, S. Coyle, C. Netti, J. J. Baumberg, R. Paschotta, and D. J. Richardson, "UV generation in a pure-silica holey fiber", App. Phys. B, **77**(2-3), 291 (2003).
[26] T. A. Birks, W. J. Wadsworth, and P. St. J. Russell, "Supercontinuum generation in tapered fibers", Opt. Lett., **25**(19), 1415 (2000).
[27] C. J. S. Matos, R. E. Kennedy, S. V. Popov, and J. R. Taylor, "20-kW peak power all-fiber 1.57-m source based on compression in air-core photonic bandgap fiber, its frequency doubling, and broadband generation from 430 to 1450 nm", Opt. Lett., **30**(4), 436 (2005).
[28] K. K. Chen, S. Alam, J. H. V. Price, J. R. Hayes, D. Lin, A. Malinowski, C. A. Codemard, D. Ghosh, M. Pal, S. K. Bhadra, and D. J. Richardson, "Picosecond fiber MOPA pumped supercontinuum source with 39 W output power", Opt. Express, **18**(6), 5426 (2010).

[29] J. C. Travers, A. B. Rulkov, R. A. Cumberland, S. V. Popov, and J. R. Taylor, "Visible supercontinuum generation in photonic crystal fibers with a 400 W continuous wave fiber laser", Opt. Express, **16**(19), 14435 (2008).
[30] M. J. F. Digonnet, *Rare-Earth Doped Fiber Lasers and Amplifiers*, Chapter 9 Rare earth doped infrared-transmitting glass fibers, 2nd Ed., New York: Marcel Dekker (2001).
[31] A. Kuhn, P. French, D. P. Hand, I. J. Blewett, M. Richmond, and J. D. C. Jones, "Preparation of fiber optics for the delivery of high-energy high-beam-quality Nd:YAG laser pulses", Appl. Opt., **39**(33), 6136 (2000).
[32] D. Su, A. A. Boechat, and J. D. C. Jones, "Beam delivery by large-core fibers: effect of launching conditions on near-field output profile", Appl. Opt., **31**(27), 5816 (1992).
[33] R. H. Stolen and C. Lee, "Development of the stimulated Raman spectrum in single-mode silica fiber", J. Opt. Soc. Am. B, **1**(4), 652 (1984).
[34] L. Garcia, A. Jalili, Y. Lee, N. Poole, K. Salit, P. Sidereas, C. G. Goedde, and J. R. Thompson, "Effects of pump pulsed temporal structure on long-pulse multi-order stimulated Raman scattering in optical fiber", Opt. Commun., **193**(1-6), 289 (2001).
[35] A. W. Snyder and J. D. Love, *Optical Waveguide Theory*, Kluwer Academic Publishers (2000).

Chapter 7 Summary and future work

In this chapter, I will summarise the work presented in this thesis and suggest possible improvements and future research direction on CP Raman fibre devices.

7.1 Summary

This thesis presents my research on cladding-pumped Raman fibre amplifiers and lasers. This is a new concept to obtain Raman gain and power conversion in a single- or few-moded core, whilst allowing for multimode pumping. This approach combines many attractions of the hugely successful cladding-pumped RE-doped fibres with the versatility and flexibility of Raman gain. Such devices are potential alternatives to RE-doped fibre devices, which are currently used in many applications. Since the first demonstration of cladding-pumped Raman fibre amplifiers [1], various work has been carried out in our group in the CW [2]-[3] and pulsed regime [4]-[6] both at around 1 μm and 1.5 μm. Based on these results, this thesis further investigated such novel fibre devices in various respects as described below.

- In Chapter 3, I theoretically investigated the achievable brightness enhancement in pulsed CP RFAs. I analysed several factors that can limit on the brightness enhancement. One of the limits is from the 2nd-Stokes generation. It leads to a limited inner-cladding-to-core area ratio if high conversion efficiency into the 1st Stokes is required. To solve this, I designed a new DCRF with a W-type core, which relaxes the restriction on the area ratio and improves it from 8 to 34 by suppressing the 2nd-Stokes build-up. The designed DCRF will allow pump sources with poorer beam quality to be used and further achieve higher brightness enhancement. Besides the 2nd Stokes, the material damage also limits the area ratio. Moreover, walk-off is also critical for the brightness enhancement in the short pulse regime in that it restricts the inner-cladding NA that can be used. The NA value depends on the material too. By combining all of these factors, I calculated

the maximum achievable brightness enhancement to be around 3000 for the W-type fibre I designed, although this depends both on the duration of the pump pulses and their peak intensity. This theoretically achievable brightness gain is much better than any results obtained from any efficient CP RFA so far. It points to the potential for significant further improvements with the right pump source matched to the right fibre.

- In Chapter 4, I focussed on the conversion efficiency of CP Raman fibre devices. A high-efficiency CP RFA with diffraction-limited output was demonstrated with the DCRF F71-LF11, which has a good design for this purpose. I experimentally obtained a peak power conversion from the pump to the 1st Stokes of 75% and a pulse energy conversion efficiency of 60%, both with respect to the launched pump. In the experiment, I paid attention to various factors limiting the conversion efficiency. Without careful attention, such good results cannot be obtained. Firstly, DCRF F71-LF11 has an inner-cladding-to-core area ratio of 5.8, which ensures that the 1st Stokes can deplete most of the pump before the 2nd Stokes is generated. Secondly, a short fibre was used to reduce the total background loss, e.g., to 0.14 dB in one experiment. Thirdly, the pump pulse shape was nearly rectangular thanks to the use of a MOPA with pre-shaped seed pulses. I theoretically analysed the effect of the pump pulse shape on the conversion efficiency in fibres with various inner-cladding-to-core area ratios. The results show that with an area ratio of eight, high conversion efficiency is possible. However, the pulse shape is critical, and rectangular-pulse (or CW) pumping will work best. Other limitations, e.g., inner-cladding shape, were also discussed. Finally, I experimentally obtained a brightness enhancement of 8.7.
- In Chapter 5, I concentrated on high-power CW CP Raman fibre devices. Firstly, I theoretically analysed their power scalability by considering factors such as thermal effects, optical damage, pump brightness, and 2nd-Stokes generation. With sufficient pump brightness (and enough pump power), the core damage turns out to be a critical factor in determining the achievable power when fibre core diameter is less than 38 μm. Thus, a large core is the key to high power, similarly as for RE-doped fibre devices. When the core is large enough, the ultimate power is decided by thermal lensing. The achievable power can be as high as 23 kW for the inner-cladding-to-core area ratio of both 8 and 34 (although less bright pumps can be

used in the latter case). Experimentally, a 100 W CP RFL based on F71-LF11 was demonstrated at 1.1 μm with nearly diffraction-limited output. Compared to previously published results of 10 W [3], from a CW CP RFL, this is a significantly improved, and this is the highest output power of CP Raman devices demonstrated to date, as far as I am aware. The achievable brightness enhancement here was estimated to be 11.5.

- In Chapter 6, three new DCRFs with large-mode areas were introduced. The new fibres were drawn from the same preform and had similar inner-cladding-to-core area ratios, ~ 7.2. Their core diameters are 18.4, 31, and 40 μm, respectively, for the fibre T0340, T0342, and T0343. Thanks to their large sizes, the new fibres are promising for high energy and high power sources. In addition, sources with relatively poor beam quality can be used to pump the new fibres, leading to better brightness enhancement. This is confirmed experimentally in pulsed CP RFAs incorporating the new fibres. The achievable brightness enhancement was 40, 48, and 80 from the fibre T0340, T0342, and T0343, respectively. The experimental results also show that the new fibres can work as efficiently as the previous fibre F71-LF11. In terms of high-energy Raman sources, a Q-switched Nd:YAG laser was used to cladding-pump 40 m of T0343, which was then able to turn out pulses with up to 1 mJ of energy, distributed over several Stokes orders. This is a significant improvement over the previous record of 210 μJ [6], obtained with the fibre F71-LF11. The output energy was restricted by fibre facet damage at the input end. A simple endcap should allow for higher output energy. Besides, I also discussed the issues brought about by the spiky and unstable Nd:YAG pump source I used, and proposed possible solutions. Still, further studies are needed to understand the very complex behaviour of CP Raman devices with such pump sources. Furthermore, as a novel application of a DCRF, I also demonstrated a cladding-pumped supercontinuum source using 100 m of T0340 in a simple, cheap and efficient configuration. The obtained SC had an output power of up to 19 W and extended beyond 1750 nm, which was the limit of the OSA measurement range. The power density achieved around 1400 nm exceeded 40 mW/nm, close to the record power density of 50 mW/nm reported in [7]. Overall, these new DCRFs with large-mode areas once again experimentally prove that cladding-pumping technology is an elegant solution for creating high-power and high-energy

nonlinear fibre sources with good beam quality and attractive properties. The potential for future scaling of power and energy should be significant with these new DCRFs.

7.2 Future work

In this section, I describe some aspects of cladding-pumped Raman fibre devices that remain unexplored and are worth investigation in the future in my view.

- **High efficiency and high brightness**

  1. 2^{nd}-order Stokes suppression: By suppressing the 2^{nd}-Stokes generation, the limitation set on the area ratio between inner cladding and core can be relaxed, so fibres with larger area ratios and pumps with relative poor beam quality can be used. Furthermore, the range of pump powers that allow for efficient conversion is also limited by the 2^{nd} Stokes. While I designed such fibres, they have yet to be fabricated and proven experimentally.

  1.1 Experimental demonstration: While I designed such fibres in section 3.2, they have not yet been fabricated and proven experimentally.

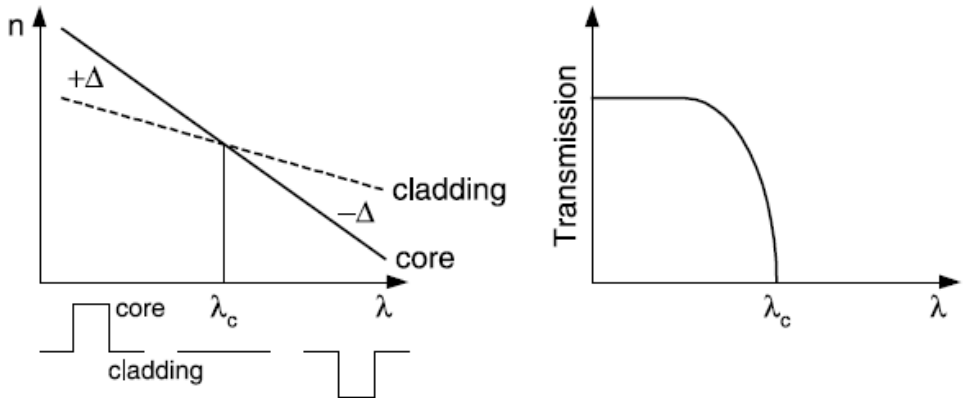

Figure 7.1: Schematic of the principle of the filter based on material dispersions [9].

  1.2 Improved W-type fibres: Fibre waveguide filters that use two dispersive materials have been demonstrated [8]-[9]. In [9], an optical fibre with borosilicate core and fluorosilicate cladding was experimentally demonstrated to work as a short-pass filter. Its principle is illustrated in Figure 7.1. Thanks to the different dispersion of the cladding and the core, a cut-off wavelength exits where the core refractive index equals to the cladding refractive index. Beyond the cut-off wavelength, light cannot be guided in the fibre core. Such materials

can also be used in combination with a W-type waveguide filter, allowing for a sharper cutoff of the 2nd Stokes and larger area ratios than I could reach (=34) without using such dispersive materials..

1.3 Other approaches to suppress the 2nd Stokes: Besides a W-type fibre and material dispersion, there are other options to suppress the 2nd Stokes, such as the recently demonstrated photonic bandgap fibre [10]-[11]. In addition, RE ion absorbers have been used to suppress the Raman scattering in the past [12]. Furthermore, depressed-clad hollow optical fibres have been demonstrated as alternative to W-type fibre, with the advantage that they allow for larger core sizes [13]. This facilitates brightness enhancement as well as scaling of both power and energy.

- **High power and high energy sources:** When it comes to the power scalability, the core size is a critical factor as discussed in Chapter 5. Thus, it will be interesting to fabricate fibres with large single-mode cores.

  1. Enlarged core size: As it comes to core size, there are a large number of methods proposed for core area scaling, for example, leakage channel fibres [14], chirally coupled cores [15], and high-order-mode operation [16]. Although these approaches are originally proposed for RE-doped and passive fibres, it is still reasonable to expect that different area-scaling approaches will bring advantages for DCRFs that are comparable to those for RE-doped fibres (if any). Meanwhile, if the core size is increased, the inner-cladding size can be enlarged accordingly. Better brightness enhancement can then be expected.

  2. Experimentally, we have demonstrated a CW CP RFL with a record-breading 100 W of output power with a piece of DCRF F71-LF11. I believe significant further power-scaling should be relatively straightforward. Firstly, new efficient DCRFs with large-mode areas have already been realised. Secondly, we will soon have a multi-kW thin disk laser (Triumph) in our lab. The prospect of demonstrating a diffraction-limited CP RFL with kW-level output power based on the large-mode-area DCRFs and the thin disk laser looks very promising. In the pulsed regime, we have realised a 1 mJ of pulse energy distributed over several Stokes orders by pumping a piece of DCRF T0343 with an Nd:YAG laser. Although the conversion efficiency into the 1st Stokes is limited due to the

characteristics of this pump laser, it should still be possible to further improve the conversion efficiency into the 1st Stokes and obtain high energy sources at the 1st Stokes. One option is to launch the Nd:YAG laser beam into a passive fibre with suitable length and remove the spikes through Raman scattering process at the beginning. The resulting spike-free beam can then be used to pump a CP RFA. Another option is to smear out the spikes by dispersion. This can be achieved by launching the Nd:YAG laser beam into a passive fibre with large NA. Alternatively, multimode high energy fibre MOPA sources [17] can be used to pump Raman fibre converters. For example, one YDF MOPA produced 82 mJ pulses with $M^2 = 25$ [17].

- **Directly diode-pumped CP Raman fibre devices:** The brightness of high-power laser diodes has improved rapidly in recent years. In this thesis, I have used them to pump RE-doped fibres, which in turn pumped the CP Raman fibre devices. Such tow-stage pumping generally makes a system more complex and reduces the electrical-to-optical conversion efficiency. Thus, it would be interesting to directly cladding-pump DCRFs. With laser diode. Such an arrangement also benefits from the wide range of wavelengths available from LDs, including relatively short wavelength such as 800 nm. The Raman gain of the core mode in the DCRF in the un-depleted regime can be expressed as:

$$G = 4.343 g_R L_{eff} \frac{P}{A_{cl}}. \tag{7.1}$$

Here, the Raman gain is in dB, and we assume that the pump is uniformly distributed transversely across the inner cladding. State-of-the-art laser diodes can deliver 100 W in a 105 μm diameter delivery fibre with 0.12 NA for a brightness of 0.25 W/(Sr×μm^2). The power from this LD can be efficiently launched into a DCRF with inner-cladding diameter as small as 27 μm if the inner-cladding NA is 0.48. Suppose that two such LDs pump the fibre from both ends with 90% launching efficiency and Raman gain coefficient of 10^{-13} m/W. We can then calculate the achievable Raman gain per meter as a function of the inner-cladding diameter. This is shown in Figure 7.2.

Fibres with smaller inner cladding see higher Raman gain, for example, that the Raman gain becomes 0.1 dB/m for a fibre with a 31 μm diameter inner

cladding. This is a small, but not unrealistic, diameter. For a DCRF with a 105 μm diameter inner cladding, the Raman gain is only 0.009 dB/m. However, through tapered fibre bundles (TFBs) [18], the power from several laser diodes can be combined and launched into the DCRF. Assume that the power coming from six 100-W LDs is combined through a TFB with six pump ports at 90% launching efficiency into a DCRF with 105 μm diameter, 0.48 NA inner cladding. The Raman gain can then be 54 dB/km, if one such TFB is used in each end of the DCRF. This gain is low, but should be sufficiently for a, say, 250 m long fibre. Meanwhile, various methods can be utilised to enable the core size to meet the area ratio requirement for efficient conversion. Thus, it looks possible to build an efficient all-fiberised CP Raman converter directly pumped by LDs.

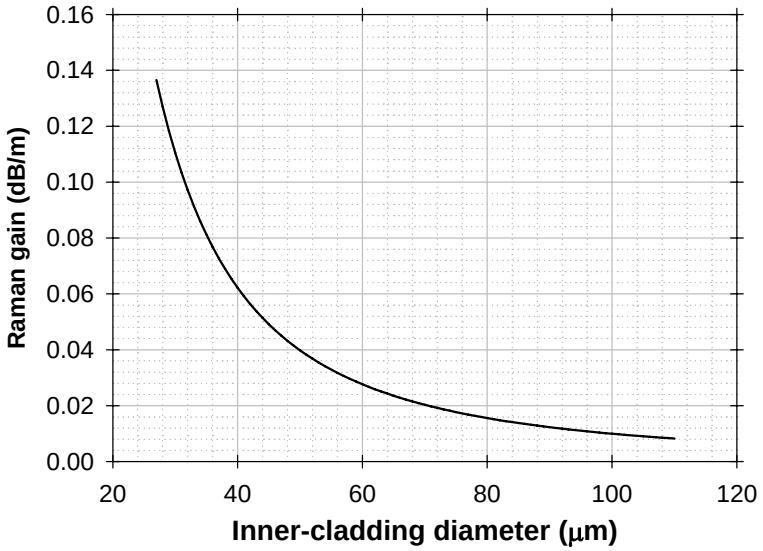

Figure 7.2: (Simulation) Raman gain *vs*. different inner-cladding size with 200 W pump and Raman gain coefficient of 10^{-13} m/W.

- **Other fibre hosts**: Raman gain can be generated at any wavelength determined by the pump wavelength and transparency window of fibre materials. In this thesis, I only used silica fibres. These are only transparent up to around 2 μm [19]. However, cladding-pumped Raman devices are also possible with other fibre hosts, e.g. soft glasses, which can be transparent at longer wavelengths [20]. Furthermore, a mid-IR SC light source has applications in a variety of areas [21]-[22]. Our approach to generate SC light source can also be used in the mid-IR in appropriate soft-glass fibres.

7.3 Reference

[1] J. Nilsson, J. K. Sahu, J. N. Jang, R. Selvas, D. C. Hanna, and A. B. Grudinin, "Cladding-pumped Raman fiber amplifier", in Proc. of Optical Amplifiers and Their Applications (OAA 2002), Vancouver Canada 14-17 Jul. 2002, paper PD2-1/2/3 (Postdeadline).

[2] J. Jang, Y. Jeong, J. K. Sahu, M. Ibsen, C. A. Codemard, R. Selvas, D. C. Hanna, and J. Nilsson, "Cladding-pumped continuous-wave Raman fiber laser", in Proc. of Conf. Lasers and Electro-Optics/QELS, Baltimore 3-5 Jun 2003, paper CWL1.

[3] C. A. Codemard, P. Dupriez, Y. Jeong, J. K. Sahu, M. Ibsen, and J. Nilsson, "High-power continuous-wave cladding-pumped Raman fiber laser", Opt. Lett., **31**(15), 2290 (2006).

[4] C. A. Codemard, J. K. Sahu, and J. Nilsson, "High-brightness pulsed cladding-pumped Raman fiber source at 1660 nm", in Proc. of Conf. Lasers and Electro-Optics /QELS, Baltimore 6-11 May 2007, paper CTuN3.

[5] C. A. Codemard, J. K. Sahu, and J. Nilsson, "Cladding-pumped Raman fiber amplifier for high-gain high-energy single-stage amplification", in Proc. of OFC, Anaheim 6-11 March 2005, paper OutF5.

[6] A. Shirakawa, C. A. Codemard, J. Ji, K. K. Chen, A. Malinowski, D. J. Richardson, J. K. Sahu, and J. Nilsson, "High-brightness 210 μJ pulsed Raman fiber source", in Proc. of Conf. Lasers and Electro-Optics /QELS, San Jose 4-9 May 2008, paper CTuL1.

[7] J. C. Travers, A. B. Rulkov, B. A. Cumberland, S. V. Popov, and J. R. Tayler, "Visible supercontinuum generation in photonic crystal fibers with a 400 W continuous wave fiber laser", Opt. Express, **16**(19), 14435 (2008).

[8] K. Morishita, M. S. Yataki, and W. A. Gambling, "In-line optical fibre filters using dispersive materials", Elect. Lett., **23**(7), 319 (1987).

[9] J. W. Yu, K. Oh, "New in-line fiber band pass filters using high silica dispersive optical fibers", Optics Communications, **204**(1-6), 111 (2002)

[10] A. Wang, A. K. George, and J. C. Knight, "Three-level neodymium fiber laser incorporating photonic bandgap fiber", Opt. Lett., **31**(10), 1388 (2006).

[11] E. M. Dianov, M. E. Likhachev, and S. Férier, "Solid-core photonic bandgap fibers for high-power fiber lasers", IEEE. J. Sel. Top. Quant. Electron., **26**(12), 20 (2009). (Invited paper)

[12] M. C. Farries, J. E. Townsend, "Suppression and modification of stimulated Raman scattering in otpical fibres by rare-earth doping", in Proc. of International conference on Nonlinear Optical Phenomena, Ireland May 1988.

[13] J. Kim, P. Dupriez, D. B. S. Soh, J. Nilsson, and J. K. Sahu, "Core area scaling of Nd:Al-doped silica depressed clad hollow optical fiber and Q-switched laser operation at 0.9 μm", Opt. Lett., **31**(9), 2833 (2006).

[14] L. Dong, X. Peng, and J. Li, "Leakage channel optical fibers with large effective area", J. Opt. Soc. Am. B, **24**(8), 1689 (2007).

[15] C.-H. Liu, G. Chang, N. Litchinitser, D. Gertin, N. Jacobsen, K. Tankala, and A. Galvanauskas, "Chirally coupled core fibers at 1550 nm and 1064 nm for effective single-mode core size scaling", in Proc. of Conf. on Lasers and Electro-Optics/QELS, Baltimore 2007, paper CTuBB3.

[16] S. Ramachandran, J. W. Nicholson, S. Ghalmi, M. F. Yan, P. Wisk, E. Monberg, and F. V. Dimarcello, "Light propagation with ultralarge modal areas in optical fibers", Opt. Lett., **31**(12), 1797 (2006).

[17] M. Y. Cheng, Y. C. Chang, and A. Galvanauskas, "High-energy and high-peak-power nanosecond pulse generation with beam quality control in 200- m core highly multimode Yb-doped fiber amplifiers", Opt. Lett., **30**(4), 358 (2005).
[18] D. J. DiGiovanni and A. J. Stentz, "Tapered fiber bundles for coupling light into and out of cladding-pumped devices", US patent no. 5,864,644.
[19] O. Humbach, H. Fabian, U. Grzesik, U. Haken, and Heitmann, "Analysis of OH absorption bands in synthetic silica", Journal of Non-Crystalline Solids, 203, 19 (1996).
[20] M. J. F. Digonnet, *Rare-earth-doped fiber lasers and amplifiers*, 2nd Edition, Marcel Dekker Inc. (2001).
[21] J. D. Monnier, "Optical interferometry in astronomy", Rep. Prog. Phys., **66**(5), 789 (2003)
[22] B. Guo, Y. Wang, C. Peng, H. L. Zhang, G. P. Luo, H. Q. Le, C. Gmachl, D. L. Sivco, M. L. Peabody, and A. Y. Cho, "Laser-based mid-infrared reflectance imaging of biological tissues", Opt. Express, **12**(1), 208 (2004).

Appendix I: List of publications

This appendix contains the list of published work during my PhD time at the ORC.

Journals publications

- **J. Ji**, C. A. Codemard, J. K. Sahu, and J. Nilsson, "Design, performance and limitations of fibers for cladding-pumped Raman lasers", Opt. Fiber Technol., **16**(6), 428-441, 2010, invited paper.
- **J. Ji**, C. A. Codemard, and J. Nilsson, "Analysis of spectral bendloss filtering in a cladding-pumped W-type fiber Raman amplifier", J. Lightwave Technol., **28**(15), 2179-2186, 2010.
- **J. Ji**, C. A. Codemard, J. K. Sahu, M. Ibsen, and J. Nilsson, "Analysis of the conversion to the first Stokes in cladding-pumped fiber Raman amplifiers", IEEE J. Sel. Top. Quant. Electron., **15**(1), 129-139, 2009.

Conferences

- J. Nilsson, **J. Ji**, C. A. Codemard, and J. K. Sahu, "Design, performance, and limitations of fibers for cladding-pumped Raman lasers", in Proc. of IEEE Winter Topicals, Keystone, Colorado, Jan. 2011, invited paper.
- Y. Jeong, C. A. Codemard, **J. Ji**, L. A. Vazquez-Zuniga, G. van der Westhuizen, S. Yoo, A. J. Boyland, M. N. Petrovich, F. Poletti, G. Ponzo, J. K. Sahu, J. Nilsson, D. J. Richardson, and D. N. Payne, "Novel fibre technology for high-power lasers", in Proc. of Asia Communications and Photonics Conference and Exhibition (ACP), Shanghai, China, Dec. 2010, invited paper.
- Y. Jeong, C. A. Codemard, **J. Ji**, L. A. Vazquez-Zuniga, G. van der Westhuizen, S. Yoo, A. J. Boyland, M. N. Petrovich, F. Poletti, J. K. Sahu, J. Nilsson, D. J. Richardson, and D. N. Payne, "Recent changes in high power optical fibers", in Proc. of ICOOPMA, Budapest, Hungry, 2010, invited paper.
- **J. Ji**, C. A. Codemard, A. S. Webb, J. K. Sahu, and J. Nilsson, "Near-diffraction-limited supercontinuum generation in a cladding-pumped nonlinear fiber converter", in Proc. of Conference on Lasers and Electro-Optics (CLEO), San Jose, US, 2010, paper CMMM5.
- **J. Ji**, C. A. Codemard, A. Boyland, J. K. Sahu, and J. Nilsson, "Beam quality and spectral evolution in large-core cladding-pumped cascaded-Raman fiber converter", in Proc. of Advanced Solid-State Photonics (ASSP), San Diego, US, 2010, paper AMB3.

- C. A. Codemard, **J. Ji**, J. K. Sahu, and J. Nilsson, "100 W CW cladding-pumped Raman fiber laser at 1120 nm", in Proc. of Photonics West, San Francisco, US, 2010, paper 7580-58.
- **J. Ji**, C. A. Codemard, J. K. Sahu, and J. Nilsson, "Pulsed cladding-pumped large mode area fiber Raman amplifier", in Proc. of Photonics West, San Francisco, US, 2010, paper 7598-47.
- **J. Ji**, C. A. Codemard, and J. Nilsson, "Brightness enhancement limits in pulsed cladding-pumped fiber Raman amplifiers", in Proc. of Photonics West, San Francisco, US, 2010, paper 7580-56.
- **J. Ji**, C. A. Codemard, and J. Nilsson, "Cladding-pumped Raman fiber with a W-type core design for power scaling", in Proc. of Conference on Lasers and Electro-Optics/Pacific Rim (CLEO/PR), Shanghai, China, 2009, paper TuD1_3.
- J. Nilsson, Y. Jeong, C. A. Codemard, C. Farrell, L. Vasquez, **J. Ji**, M. S. Z. Abidin, G. van der Westhuizen, S. Yoo, and J. K. Sahu, "High power fibre lasers: Exploitation of unique properties", in Proc. of The European Conference on Lasers and Electro-Optics (CLEO/Europe), Munich, Germany, 2009, paper TF2_2.
- J. Nilsson, S. Yoo, P. Dupriez, C. Farrell, M. S. Z. Abidin, **J. Ji**, J.-N. Maran, C. A. Codemard, Y. Jeong, J. K. Sahu, D. J. Richardson, and D. N. Payne, "Fiber MOPAs with high control and high power", in Proc. of Asia Optical Fiber Communication and Optoelectronic Exposition and Conference (AOE), Shanghai, China, 2008, paper SaB2, invited paper.
- **J. Ji**, C. A. Codemard, J. K. Sahu, M. Ibsen, and J. Nilsson, "High peak power conversion and high gain in pulsed cladding-pumped fiber Raman amplifier", in Proc. of Asia Optical Fiber Communication and Optoelectronic Exposition and Conference (AOE), Shanghai, China, 2008, paper SaB3.
- A. Shirakawa, C. A. Codemard, **J. Ji**, K. K. Chen, A. Malinowski, D. J. Richardson, J. K. Sahu, and J. Nilsson, "Brightness-enhancement of pulsed fiber source by double-clad Raman fiber", in Proc. of The 69th Autumn Meeting of JAP, Nagoya, Japan, 2008, paper 2a-ZA-7.
- J. Nilsson, Y. Jeong, C. A. Codemard, J.-N. Maran, C. Farrell, **J. Ji**, S. Yoo, J. K. Sahu, D. J. Richardson, and D. N. Payne, "High power fiber sources", in Proc. of Conference on Optoelectronics and Optical Communications (COOC), Busan, Korea, 2008, Plenary presentation.
- A. Shirakawa, C. A. Codemard, **J. Ji**, K. K. Chen, A. Malinowski, D. J. Richardson, J. K. Sahu, and J. Nilsson, "High-brightness 210 μJ pulsed Raman fiber source", in Proc. of Conference on Lasers and Electro-Optics (CLEO), San Jose, US, 2008, paper CTuL1.